UNIVERSIDAD DE
MEDELLÍN IN
COLLABORATION WITH
TOULOUSE INSTITUTE OF FLUID MECHANICS
AND PONTIFICIA UNIVERSIDAD JAVERIANA

Numerical simulation framework for water quality in tropical water systems.

Author:
Juliana ALZATE

Advisors:
Dr. Hélène ROUX
Dr. Carlos PIEDRAHITA,
Dr. Jorge ESCOBAR,
Dr. Luis Javier MONTOYA

Pontificia Universidad
JAVERIANA
Bogotá

A thesis submitted in fulfillment of the requirements for the degree of Doctor of Philosophy in
Modeling and Scientific Computing

December 15, 2023

"For of him, and through him, and unto him, are all things. To him be the glory for ever. Amen."

Romans 11:36

Contents

List of Figures

List of Tables

Acknowledgements

I would like to express my sincere gratitude to all the people and organizations that have contributed to the publication of this research work.

First and foremost, I would like to thank Almighty God for giving me the opportunity to undertake this research work and to persevere and complete it successfully. Without his blessing, this achievement would not have been possible.

I would also like to especially thank my supervisors, Professor Hélène Roux, and professors Ludovic Cassan, Thomas Bonometti and Jorge Escobar, for their invaluable guidance and support throughout the research process. Their expertise and insight were instrumental in shaping the direction and focus of my research. I am also grateful to the Institut de Mécanique des Fluides de Toulouse and the University of Medellin for providing me with the resources and support necessary to complete this project.

We would also like to thank Professors Luis Javier Montoya and Carlos Piedrahita for their feedback and support throughout the research process. In particular, for their valuable ideas and suggestions.

Finally, I would like to thank all the participants in this study for their time and willingness to share their experiences. Their contributions have been invaluable in helping me to understand the subject and draw meaningful conclusions.

Abstract

Water quality modeling plays an important role in understanding the severity and differential impacts of tropical hydrological systems. Changes in environmental flow concepts in human-modified lentic ecosystems can affect hydrodynamics, sediment transport, hydrology, and thus water quality. Understanding the dynamics of water quality in tropical systems is important because there are many issues in the energy-water-food nexus and water quality is a key determinant of these processes.

In this sense, representing very complex hydrodynamic systems requires the development of integrated multi-spatiotemporally coupled approach water quality models that effectively and accurately simulate flow, water quality parameters and dynamics at different scales in tropical ecosystems. Some of the shortcomings of the approaches currently adopted in many non-integrated studies, where not hybrid approach when studying the water quality-environment relationship across spatial scales and temporal periods, show the need for a more integrated conceptual approach.

The research presented proposes a multi-spatiotemporal coupled approach that simultaneously integrates hydrodynamics, hydrology, and water quality and applies it to multiple case studies.

This proposal shows that by using an ensemble model based on a realistic representation of all relevant processes, better or similar accuracy than traditional water quality approximations can be achieved. The robustness of the model provides greater confidence in the predicted results.
Regarding relationship between water quality and hydrometeorological variables in tropical reservoirs the results show that, for all monitoring stations, the water quality variables associated with the DO process are COD, BOD, and PO_4. Likewise, precipitation and flow discharge were the hydrometeorological parameters that had the most significant impact in water quality. Also, the principal component analysis (PCA) allowed us to identify that the strength of the relationships between water quality and hydrometeorology changes depending on the location of the monitoring site. Finally, the implementation of a VAR model showed good performance metrics for dissolved oxygen predictions based on all analyses.

On the issue analysis of air-water exchange in a Colombian tropical reservoir the analysis shows that the most crucial parameter for a correct representation of the observed temperature behavior are the heat exchange coefficient and the wind. The different approaches tested all have limitations, but they can reproduce reservoir temperature trends at different depths with a maximum standard deviation ranging from 3°C to 8°C.

The implementation of an integrated model for the specific case of a tropical river using

short-term field data to develop a mechanistic model of periphyton biomass-nutrient interactions. The results show that was possible to calibrate the model with experimental data, and calculated nutrients, space requirements, and losses due to detachment and friction velocity. And this study demonstrates the necessity to model nutrients, hydrological factors, and friction velocities to estimate detachment to accurately simulate periphyton.
Finally, a discussion about the need for this type of integrated tool to represent complex real systems and its potential for decision-making is presented.

Resumen

La modelación de la calidad del agua desempeña un papel importante en la comprensión de la gravedad y los impactos diferenciales de los sistemas hidrológicos tropicales. Los cambios en los conceptos de flujo ambiental en ecosistemas lénticos modificados por el hombre pueden afectar a la hidrodinámica, el transporte de sedimentos, la hidrología y, por ende, la calidad del agua. Comprender la dinámica de la calidad del agua en los sistemas tropicales es importante porque hay muchos problemas en el nexo energía-agua-alimentación y la calidad del agua es un determinante clave de estos procesos.

En este sentido, la representación de sistemas hidrodinámicos muy complejos requiere el desarrollo de modelos integrados de calidad del agua con un enfoque multi espacio-temporal acoplado que simulen con eficacia y precisión el flujo, los parámetros de calidad del agua y la dinámica a diferentes escalas en los ecosistemas tropicales. Algunas de las deficiencias de los enfoques adoptados actualmente en muchos estudios no integrados, en los que no se adopta un enfoque híbrido al estudiar la relación calidad del agua-medio ambiente a través de escalas espaciales y periodos temporales, muestran la necesidad de un enfoque conceptual más integrado.

La investigación presentada propone un enfoque multi espacio-temporal acoplado que integra simultáneamente la hidrodinámica, la hidrología y la calidad del agua y lo aplica a múltiples casos de estudio.

Esta propuesta demuestra que, utilizando un modelo de conjunto basado en una representación realista de todos los procesos relevantes, se puede conseguir una precisión mejor o similar a la de las aproximaciones tradicionales de la calidad del agua. La robustez del modelo proporciona una mayor confianza en los resultados previstos.

En cuanto a las relaciones entre la calidad del agua y las variables hidrometeorológicas en embalses tropicales, los resultados muestran que, para todas las estaciones de monitoreo analizadas, las variables de calidad del agua asociadas al proceso de OD son DQO, DBO y PO_4. Asimismo, la precipitación y el caudal fueron los parámetros hidrometeorológicos que tuvieron mayor impacto en la calidad del agua. Además, el análisis de componentes principales (ACP) nos permitió identificar que la fuerza de las relaciones entre la calidad del agua y la hidrometeorología cambia dependiendo de la ubicación del sitio de monitoreo. Finalmente, la implementación de un modelo VAR mostró buenas métricas de

rendimiento para las predicciones de oxígeno disuelto basadas en todos los análisis.

En el tema del análisis del intercambio aire-agua en un embalse tropical colombiano, el análisis muestra que los parámetros más cruciales para una correcta representación del comportamiento de la temperatura observado son el coeficiente de intercambio de calor y el viento. Todos los diferentes enfoques probados tienen limitaciones, pero pueden reproducir las tendencias de temperatura del embalse a diferentes profundidades con una desviación estándar máxima que oscila entre 3°C y 8°C.
En cuanto a la implementación de un modelo integrado para el caso específico de un río tropical utilizando datos de campo a corto plazo para desarrollar un modelo mecanicista de interacciones biomasa-nutrientes del perifiton. Los resultados muestran que fue posible calibrar el modelo con datos experimentales y calcular nutrientes, requerimientos de espacio y pérdidas por desprendimiento y velocidad de fricción. Y este estudio demuestra la necesidad de modelar nutrientes, factores hidrológicos y velocidades de fricción para estimar el desprendimiento y simular con precisión el perifiton.

Finalmente, se presenta una discusión sobre la necesidad de este tipo de herramientas integradas para representar sistemas reales complejos y su potencial para la toma de decisiones.

Introduction

The growing demand for food, energy, and water is causing major changes in our planet's water systems, especially local ecosystems. The high human population growth rate is driving the exploitation of resources on Earth (United Nations, 2019). Water is one of the most important resources for our life and, thus, exploiting our tropical water systems exposes the biosphere to significant risks. We can find tropical conditions in Latin American countries; this investigation focuses on the Colombian tropical system.

The impact on reservoir water quality is currently a major concern in ecological management, with problems as eutrophication or sedimentation. Life-quality is highly constrained by the quality of water, which in turn is affected by the quality of reservoirs built for hydroelectric projects, water supply, among others. This is particularly important for many Latin-American countries, where most of the electric supply comes from hydropower. In Colombia, hydroelectric projects are one of the most important sources of energy, about 65% and the electric demand is supplied for this source (annual report XM, 2017).

Reservoirs have been built in almost all of the hydrographic basins of Colombia. Their purposes include water supply for cities, irrigation and mainly, generation of electricity. These reservoirs favor local and regional economic development, but they also bring serious and irreversible alterations in the natural hydrologic regime of rivers, affecting habitat quality and the dynamics of the biota (Agostinho, Pelicice, Gomes, 2008). Reduced water flow, increased water residence time, thermal stratification, increased sedimentation rates and decreased dissolved oxygen concentrations. These changes can affect water quality, biota in the environments adapted to natural conditions (Pimenta, Albertoni, Palma-Silva, 2012), additionally it effects on the soil, vegetation, landscape, atmosphere, and therefore the basin.

Such projects also come at the expense of an increase in pollution. Chemical, thermal and physical changes on the effluents can seriously contaminate a reservoir and the rivers downstream. In the same way, as reservoirs trap river sediment coming from the basin, they also trap most of the nutrients carried by the rivers. Also, the human-induced soil erosion reduces soil productivity; compromises freshwater ecosystem services, and drives geomorphic and ecological change in rivers, their floodplain and therefore dam watershed. (Syvitski, 2018).

To predict these complex geometries, and behaviors, emerge Hydrologic /hydrodynamics/water quality models are commonly applied for management, planning and pollution control.

Due to the above-mentioned problems, it is necessary to use hydrodynamic, hydrological

and water quality models, and these methods are proposed in this research work. Specifically, two research questions are addressed in this work, the first one related to the relationship between hydro-meteorological and water quality variables in tropical reservoirs, and then the effect of air-water thermal exchange in the water column and the thermal dynamics of tropical reservoirs are analyzed.

Understanding the relationship between climate and thermal dynamics will allow to identify major environmental aspects affecting reservoir water quality. And understand the principal processes that affect multi spatial temporal scales problems fate and transport coupling.

Air-water exchange in thermodynamics is important because this work uses mathematical models to describe the complex exchange between air and water thermodynamics in tropical reservoirs, using computer simulations as an environmental software application. Tropical temperature and radiation conditions play an important role in reservoir ecological processes for sustainable water resource management and, in particular, decision support systems for climate change assessment. Ecological impacts can be understood and action plans can be more comprehensive.

This study provides a better understanding of the use of these full three-dimensional and statistical tools, as there is not much practice at these scales (space-time) on the subject of tropical thermodynamics. It allows to improve the understanding of the mathematical equations used so far. It allows the analysis of air-water transport phenomena from a integrated perspective.

In this research, it is evidenced that there is a constant state of stratification in the water column, and this especial feature must be taken into account in the models of tropical reservoirs.

i. State of knowledge

With regard to water quality models, a number of components or state variables have been gradually incorporated into the models over the past seven decades following the evolution of water quality problems (Rode Michael, 2010). Generally, water quality models are classified according to their complexity, application domain (catchment, receiving water body, or integrated models), and type of water quality variables predicted (e.g., nutrients, sediments, dissolved oxygen) (Borah et al., 2006).

On the other hand, hydrologic models (Pechlivanidis et al.,2011), have evolved the developments in data collection and processing, concepts and theories, integration with allied sciences, computational and analysis tools, and model interpretation. It is argued that with the aid of new information gathering and computational tools, hydrology will witness greater integration with both technical and non- technical areas and increasing applications of information technology tools (Singh, 2018).

The problem is that many of the deficiencies in the traditional approach (the hydrodynamic,

water quality and other components are decoupled in most of the cases), and the individual models cannot simulate all elements) relate to the modeling studies are not being fully integrated, and with each different model domain being calibrated independently (Boye, Falconer, Akande, 2015). So, there is a need for a combination of models. A combination model can include two or three individual models that simulate different elements. For the reservoir, it takes four models: a hydrodynamic model, a sediment model, hydrological model, and a water quality model, to provide a suitable result.

On the other hand, water quality studies cannot be based solely on large-scale process models. Instead, it would be valuable to combine scales and methods to a hybrid approach when studying the water quality-environment relationship across spatial scales and temporal periods. Mixed methods can produce reliable results on this relationship and the mechanisms of the underlying processes at different scales. This approach will provide more accurate and rapid knowledge about complex environmental phenomena without requiring large data sets (Varanka, 2016).

As noted by (Mooij et al., 2010), there is a clear need to find ways to integrate models that focus on spatial dynamics, hydrodynamics, water quality and hydrology, and lower trophic levels with models that focus on the whole view. Furthermore, those models should include an innate ability to increase and decrease the complexity of each process parameterization.

Thus, an imperative challenge in integrated modeling is to undertake studies to address the critical problems in spatio temporal-scale water quality modeling to accommodate the substantial spatial variability that frequently dominates the tropical hydrosystems behavior (Refsgaard, van der Sluijs, Hojberg, Vanrolleghem, 2007).

With the advent of the more powerful computer and complex algorithms, water quality models are becoming ever more complex, by taking into consideration landscape topography as well as intrinsic processes such as transport of reactive substances. So, the continuous demand to include as much knowledge as possible in state-of-the-art in-reservoir water quality modeling, taking in account hydrological, hydrodynamics and sediments models inevitably result in considerably more complex model structures (Rode Michael, 2010), this is our case. All of this is aimed at representing more accurately the hydrodynamics, hydroclimatic conditions, of tropical reservoirs and their implications for water quality.

ii. Objective of this thesis

Developing a framework for numerical simulation of water quality in tropical water systems

Specific objectives

1. To establish a relationship between water quality and hydrometeorological variables in tropical reservoirs

2. To Analyze different hypotheses for modelling air-water exchange and temperature evolution in a tropical reservoir

3. To develop a zero-dimensional integrated ecological model set to predict water quality in a river coupling Periphyton Biomass, Phosphate, Organic phosphorus, Nitrate, Ammonium, Organic nitrogen, Organic load, and Dissolved oxygen, by means of a set of resulting ordinary differential equations, as an adaptation of the WAQTEL numerical module adapted for the specific case of a tropical river.
4. To develop a methodology to develop integrated modelling tools (IMT) for analyzing socio-ecological systems.

iii. Approach

The above objectives required different approaches to be exhaustively examined. This research aims to define a well-accepted multi-spatiotemporal coupled approach to improve the water quality modeling approach for making better decision on a territory. In this regard, this study looks forward to appropriate model strategies.

The representation of these complex phenomena demands the development and use of better tools in numerical modeling. Therefore, it is necessary to implement another type of tools and the integration of other models, so better decisions can be taken on the different problems presented by the reservoirs, such as eutrophication (Roldán Pérez Ramírez Restrepo, 2008) sediment management among others (García, 2008, Morris and Fan, 1997, Vischer and Hager, 1998).

This research pretends to fill the gaps in water quality and provide an integrated multi-spatiotemporal coupled approach, the case of study will be applied to La Miel reservoir (This reservoir has been previously studied, has information, has issues with water quality and sediments) address to cover the mentioned deficiencies, and Cauca river.

In Colombia, the use of these type of tools will allow introducing towards the development of proposals for better environmental management of the water resource, both in the productive sector and in that of environmental authorities.

Finally, the need to have control measures and management strategies, covered by the official water quality standards, has forced to revise many of the criteria traditionally used in the evaluation of water quality and the uses that may be given to a reservoir. An important part of this strategy is the implementation of linking models that study the dispersion of pollutants and that also consider the change processes as appropriately as possible (Wainwright Mulligan, 2004, Caviness et al., 2006, Denzer et al., 2011). The results obtained will be contrasted with Colombian regulations (ANLA, CARS, IDEAM) and with international regulations (EPA, among others), with a view to establishing a criterion for the water quality reservoirs evaluation.

iv. Outline

All previously summarized steps are documented in detail in the following chapters 1 through 4. These chapters represent individual manuscripts, which have been published or submitted to international, peer-reviewed journals. The following overview out-lines each

chapter, as well as its implications for the overall aims.

Chapter 1
This chapter presents the theoretical background and the equations that serve as the basis for modeling the exercises in the thesis.

Chapter 2
This chapter aims to establish a relationship between water quality and hydrometeorological variables in tropical reservoirs to better estimate dissolved oxygen.

Chapter 3

This chapter presents an analysis of air-water exchange in a Colombian tropical reservoir. A coupled thermal-3D hydrodynamic model using TELEMAC-3D and WAQTEL is implemented to evaluate the dynamics of thermal processes in the reservoir. A sensitivity analysis is carried out on various modeling parameters, such as turbulence models, temperature diffusion coefficients, and heat exchange at the free surface based on observations.

Chapter 4
This chapter presents a zero-dimensional ecological model set is developed to predict water quality in a river. The proposed model couple Periphyton Biomass, Phosphate, Organic phosphorus, Nitrate, Ammonium, Organic nitrogen, Organic load, and Dissolved oxygen, by means of a set of resulting ordinary differential equations which are solved using Runge-Kutta scheme.)

Chapter 5
This chapter aims to develop integrated modelling tools (IMT) for analyzing socio-ecological systems is proposed. It is composed of three modules: the first one allows the simulation of the physical dynamics of the system, the second module uses the previous outputs as a basis for developing an aquatic ecosystem component, and the third module uses the physical and ecological results as a basis for a dynamical system-based model for ecosystem services and livelihoods.

Material and methods

The research was carried out in four phases:

Phase 1 (understanding)

At this stage, it focusses in more detail on the main processes that influence multi spatial temporal scales problems fate and transport coupling in tropical dynamics,
The activities carried out are:

- A review of the basic information available, and review of the state-of-the-art of models and its link with water quality modeling.
- Select relevant state variables and delineate system boundary for each component and process.
- Define a scaling term for each component, for each process and process prioritization.
- Construct a conceptual model where the principal processes are defined as well as its characteristics scales (space and time).

Phase 2 (Selection)

In this phase, the methodology is about how is the computational, mathematical, and more with respect to the available information required to feed the models and coupling. The activities carried out are:

- Initial selection of model features and water quality problems, related to the watershed.
- Select existing relevant models for each phenomenon.
- The determination of criteria for hydrodynamic, hydrological, chemical and biological model validation to be coupled.
- Review coupling models and methodologies
- Design and develop the methodology of coupling models and scales, from the conceptual model in previous activities.
- Have the mathematical equations organized, according to the models and the scales selected to perform the final coupling.

Phase 3 (Implementation of the integrated water quality model)

The objective was assembly model case. The activities carried out are:

- Assembly of the coupling tool and the real model cases.
- Analysis data for the case of study
- Implementation of the integrated water quality model

Phase 4

The aim was verification of the model. The activities carried out are:

- Determine the calibration and validation method.
- Define “validation criteria” of an integrated model.
- Calibrate/ Validation, and runs of the model, the creation of scenarios.
- Analyze model outputs, according to performance and verification criteria.

A general outline of this study is as follows:
The data analysis will be addressed in chapter 2, and the numerical area will be addressed in chapter 3, 4 and 5.

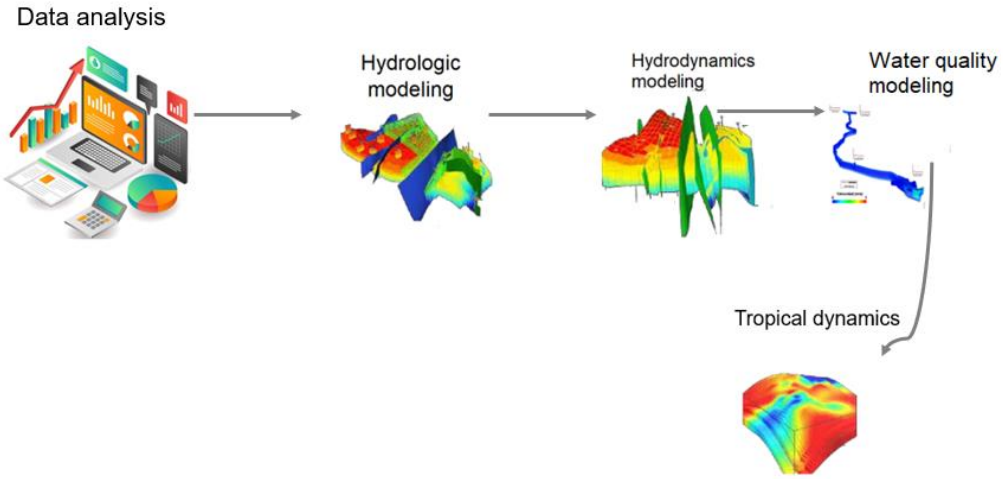

Figure 1 PhD overview

Chapter 1

1. Theoretical background

1.1 Mathematical Equations

This chapter presents the theoretical background for the thesis. The research proposed here is based on three fundamental laws of physics, with their mathematical equations such as the Navier stokes equation, shallow water equations, the transport equation and the energy equation, as well as approximations that were used to find the numerical solutions for each case raised.

These laws are based on the modeling based on physics which allows estimating the dynamics of the quantity of water in the reservoir by means of the conservation equation, the momentum equation helps to predict the movement of water in the reservoir, and the transport equation solves the transport of pollutants and the energy equation for the thermal dynamics and in this research, we are looking for the relationships between them.

Hence, these equations are the basis for the modeling of the exercises presented in the thesis, which are widely known for more detail can be found in Anderson, 1995, the purpose of presenting them is due to their importance, which will be detailed in Chapter 2.

Models based on first fundamental principles: conservation of mass, conservation of momentum, conservation of energy and constitutive relations.

The **Navier-Stokes equations** are themselves derived from the equations for conservation of mass and linear momentum. As shown below.

Conservation of the fluid mass:

Consider mass balance over a control volume Ω. Then

$$\underbrace{\frac{d}{dt}\int_{\Omega}\rho dV}_{\text{Time rate of change of total mass in } \Omega} = \underbrace{-\int_{\partial\Omega}\rho\vec{U}\cdot\vec{n}dS}_{\text{Net mass flux across boundary of } \Omega}$$

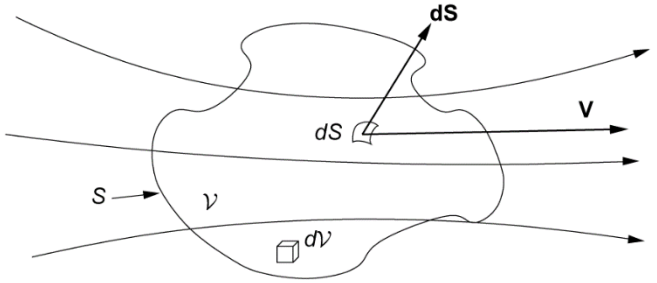

Figure 2 Finite control volume fixed in space (Anderson Jr., et al., 2009)

Where

ρ is the fluid density (kg/m3),

$\vec{U} = \begin{pmatrix} u \\ v \\ w \end{pmatrix}$ is the fluid velocity (m/s), and whose components are: (u, v, w) and

$\vec{n}$ is the outward unit normal vector on $\partial\Omega$.

Applying Gauss's Theorem gives

$$\frac{d}{dt}\int_{\Omega} \rho dV = -\int_{\Omega} \nabla \cdot (\rho \vec{U}) dV = 0$$

Assuming that ρ is smooth, we can apply the Leibniz integral rule:

$$\int_{\Omega} \left[\frac{\partial \rho}{\partial t} + \nabla \cdot (\rho \vec{U}) \right] dV = 0$$

Since Ω is arbitrary,

$$\frac{\partial \rho}{\partial t} + \nabla \cdot (\rho \vec{U}) = 0$$

Continuity equation (in conservation form)

Conservation of Linear Momentum:

Next, consider linear momentum balance over a control volume Ω. Then

$$\underbrace{\frac{d}{dt}\int_{\Omega} \rho \vec{U} dV}_{\text{Time rate of change of total momentum in } \Omega} = \underbrace{-\int_{\partial\Omega} (\rho \vec{U}) \vec{U} \cdot \vec{n} dS}_{\text{Net momentum flux across boundary of } \Omega} + \underbrace{\int_{\Omega} \rho \vec{b} dV}_{\text{Body forces acting on } \Omega} + \underbrace{\int T n dS}_{\text{External contact forces acting on } \partial\Omega} =$$

where

$\vec{b}$ is the body force density per unit mass acting on the fluid (N/kg),

and

T is the Cauchy stress tensor (N/m^2).

Applying Gauss's Theorem again (and rearranging) gives

$$\frac{d}{dt}\int_{\Omega} \rho \vec{U} dV + \int_{\Omega} \nabla \cdot (\rho \vec{U} \vec{U}) dV - \int_{\Omega} \rho \vec{b} dV - \int_{\Omega} \nabla \cdot T dV = 0$$

Assuming $\rho \vec{U}$ is smooth, we apply the Leibniz integral rule again:

$$\int_{\Omega} \left[\frac{\partial}{\partial t}(\rho \vec{U}) + \nabla \cdot (\rho \vec{U} \vec{U}) - \rho \vec{b} - \nabla \cdot T \right] dV = 0$$

Since Ω is arbitrary,

$$\frac{\partial}{\partial t}(\rho \vec{U}) + \nabla \cdot (\rho \vec{U} \vec{U}) - \rho \vec{b} - \nabla \cdot T = 0 \quad (2.2)$$

Combining the differential forms of the equations for conservation of mass and linear momentum, we have:

$$\frac{\partial \rho}{\partial t} + \nabla \cdot (\rho \vec{U}) = 0$$

$$\frac{\partial}{\partial t}(\rho \vec{U}) + \nabla \cdot (\rho \vec{U}\vec{U}) = \rho \vec{b} - \nabla \cdot T$$

To obtain the Navier-Stokes equations from these, we need to make some assumptions about our fluid (reservoir water), about the density ρ, and about the body forces $\vec{b}$ and stress tensor T. It is incompressible. This means that ρ does not depend on p. It does not necessarily mean that ρ is constant! In water surface modeling, depends on the temperature of the reservoir water.

Temperature is assumed to be constant throughout our domain, so we can just take ρ as a constant. So, we can simplify the equations:

$$\nabla \cdot \vec{U} = 0,$$

$$\frac{\partial}{\partial t}(\rho \vec{U}) + \nabla \cdot (\rho \vec{U}\vec{U}) = \rho \vec{b} - \nabla \cdot T$$

Surface water is a Newtonian fluid. This affects the form of T.

We know that gravity is a body force, so

$$\rho \vec{b} = \rho \vec{g} + \rho \vec{b}_{others}$$

where

$\vec{g}$ is the acceleration due to gravity (m/s²), and

b_{others} others are other body forces (e.g. the Coriolis force in rotating reference frames) (N/kg). We will neglect for now.

For a Newtonian fluid,

$$T = -pI + \vec{\vec{T}}$$

where p is the pressure (Pa) and $\vec{\vec{T}}$ is a matrix of stress terms.

So our final form of the Navier-Stokes equations in 3D are:

$$\nabla \cdot \vec{U} = 0,$$

$$\frac{\partial}{\partial t} \rho \vec{U} + \nabla \cdot (\rho \vec{U}\vec{U}) = -\nabla p + \rho \vec{g} + \nabla \cdot \vec{\vec{T}}$$

Navier-Stokes equation

The Navier-Stokes equations, are equations which can be used to determine the velocity vector field that applies to a fluid, given some initial conditions. They arise from the application of Newton's second law in combination with fluid stress (due to viscosity) and a pressure term.

1.1.2 Shallow water equations

The shallow water equations are derived from the Navier-Stokes equations, the general characteristic of shallow water flows is that the vertical dimension is much smaller than the typical horizontal scale. In this case, we can average over the depth to get rid of the vertical dimension.

The shallow-water equations describe a thin layer of fluid of constant density in hydrostatic balance, bounded from below by the bottom topography and from above by a free surface. They exhibit a rich variety of features because they have infinitely many conservation laws. Consider a typical water column, see Figure 2.

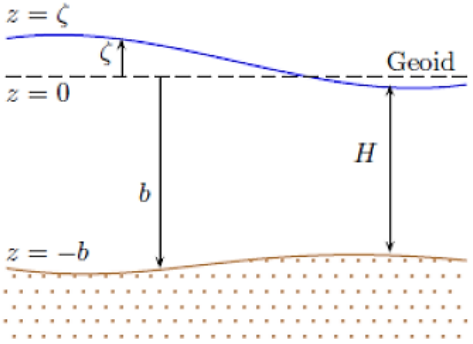

Figure 3 Water column

$\zeta = \zeta(t, x, y)$ is the elevation (m) of the free surface relative to the geoid.

$b = b(x, y)$ is the bathymetry (m), measured positive downward from the geoid.

$H = H(t, x, y)$ is the total depth (m) of the water column. Note that $H = \zeta + b$.

Figure 4 Bathymetry of the La Miel. Image courtesy Google Earth

We have the following boundary conditions:

1. At the bottom (z = -b)

   No slip: $u = v = 0$

   No normal flow: $u\dfrac{\partial b}{\partial x} + v\dfrac{\partial b}{\partial y} + w = 0$

   Bottom shear stress: $\tau_{bx} = \tau_{xx}\dfrac{\partial b}{\partial x} + \tau_{xy}\dfrac{\partial b}{\partial y} + \tau_{xz}$

   where τ_{bx} is specified bottom friction (similarly for y direction)

2. At the free surface $(z = \zeta)$

No relative normal flow: $\frac{\partial \zeta}{\partial t} + u\frac{\partial \zeta}{\partial x} + v\frac{\partial \zeta}{\partial y} - w = 0$

$p = 0$

Surface shear stress: $\tau_{sx} = \tau_{xx}\frac{\partial \zeta}{\partial x} + \tau_{xy}\frac{\partial \psi}{\partial y} + \tau_{xz}$

Before we integrate over depth, we can examine the momentum equation for vertical velocity. By a scaling argument, all of the terms except the pressure derivative and the gravity term are small. Then the z-momentum equation collapses to $\frac{\partial p}{\partial z} = \rho g$

implying that $p = \rho g(\zeta - z)$

This is the hydrostatic pressure distribution. Then

$$\frac{\partial p}{\partial x} = \rho g \frac{\partial \zeta}{\partial x}$$

with a similar form for $\frac{\partial p}{\partial y}$

We now integrate the continuity equation $\nabla \cdot \vec{U} = 0$ from $z = -b$ to $z = \zeta$. Since both b and ζ depend on t, x and y, we apply the Leibniz integral rule:

$$0 = \int_{-b}^{\zeta} \nabla \cdot \vec{U} dz$$

Finally, defining depth-average velocities as

$$\bar{u} = \frac{1}{H}\int_{-b}^{\zeta} u dz,\ \bar{v} = \frac{1}{H}\int_{-b}^{\zeta} v dz,\ \bar{w} = \frac{1}{H}\int_{-b}^{\zeta} w dz$$

We can use our BCs to get rid of the boundary terms. So the depth-averaged continuity equation is:

$$\frac{\partial H}{\partial t} + \frac{\partial}{\partial x}(H\bar{u}) + \frac{\partial}{\partial y}(H\bar{v}) + \frac{\partial}{\partial z}(H\bar{w}) = 0$$

If we integrate the left-hand side of the x-momentum equation over depth and considering the differential advection terms account for the fact that the average of the product of two functions is not the product of the averages.

We get a similar result for the left-hand side of the Y-momentum equation, integrating over depth, combining the depth-integrated continuity equation with the H and z of the depth-integrated x, y- and z-momentum equations, the 3D (nonlinear) shallow water equation in conservative form are:

$$\frac{\partial H}{\partial t} + \frac{\partial}{\partial x}(H\bar{u}) + \frac{\partial}{\partial y}(H\bar{v}) + \frac{\partial}{\partial z}(H\bar{w}) = 0$$

$$\frac{\partial}{\partial t}(H\bar{u}) + \frac{\partial}{\partial x}(H\bar{u}^2) + \frac{\partial}{\partial y}(H\bar{u}\bar{v}) + \frac{\partial}{\partial z}(H\bar{u}\bar{w}) = -gH\frac{\partial \zeta}{\partial x} + \frac{1}{\rho}\left[\tau_{sx} - \tau_{bx} + F_x\right]$$

$$\frac{\partial}{\partial t}(H\bar{v})+\frac{\partial}{\partial x}(H\bar{v}\bar{u})+\frac{\partial}{\partial y}(H\bar{v}^2)+\frac{\partial}{\partial z}(H\bar{v}\bar{w})=-gH\frac{\partial\zeta}{\partial y}+\frac{1}{\rho}\left[\tau_{sy}-\tau_{by}+F_y\right]$$

$$\frac{\partial}{\partial t}(Hw)+\frac{\partial}{\partial x}(Hwu)+\frac{\partial}{\partial y}(Hwv)+\frac{\partial}{\partial y}(Hw^2)=-gH\frac{\partial\zeta}{\partial z}+\frac{1}{\rho}\left[\tau_{sz}-\tau_{bz}+F_z\right]$$

3D Shallow Water Equation

The surface stress, bottom friction, and F_x, F_y and F_z must still be determined on a case-by-case basis.

1.1.3 Transport equations

The transport equation describes how a scalar quantity is transported in a space. Usually, it is applied to the transport of a scalar field (e.g., chemical concentration, material properties or temperature) inside an incompressible flow. From the mathematical point of view, the transport equation is also called the convection-diffusion equation, which is a first order PDE (partial differential equation). The convection-diffusion equation is the basis for the most common transportation models.

$$\underbrace{\frac{\partial(\rho C_i)}{\partial t}}_{temporal\_variation,T}+\underbrace{\nabla\cdot\left(\rho\vec{U}C_i\right)}_{convection,A}-\underbrace{\nabla\cdot J_i}_{diffusion,D}+\underbrace{R_i}_{Reactions,R}+\underbrace{S_i}_{sources/sinks,S}=0$$

Transport equation

Where C_i is the scalar field to be analyzed of species i,

R_i is the net rate of production of species i by chemical reactions; and

S_i are sources or sinks from the dispersed phase plus any other sources.

The convection term is the quantity of the transported field which moves across the boundaries because of the flow; thus, it is proportional to the velocity and can be written as convection=CU, where c is the transported scalar quantity and u is the velocity of the means which transports this quantity.

The diffusion term is the transportation of the scalar quantity according to its gradient, so diffusion=D∇C, where D is the diffusivity.

The pure source term (S) represents the creation/destruction rate of the field inside the volume. The reaction term (R) describes the creation/destruction of the transported quantity as a reaction to this quantity itself; it is, therefore, proportional to the transported field, it is a function of the transported scalar field. S and R is quite uncommon for engineering applications, so it is often neglected.

Transport Equation can thus be re-written in its fully developed form as:

$$\frac{\partial C}{\partial t}+\nabla\cdot(D\nabla C)+\nabla(\vec{U}C)=S+R$$

And heat Transfer.

$$\frac{\partial\rho c_p T}{\partial t}+\nabla\cdot(-k\nabla T)+\nabla(\vec{U}T)=Q+\varepsilon\sigma S(T_{hot}-T_{cold})$$

ρ is the material density

c_p cp is the heat capacity

T is the temperature

k is the thermal conductivity

Q is the volumetric heat flux

ε is the emissivity

σ is the Stefan-Boltzmann constant

A is the boundary surface in which heat is exchanged by radiation.

1.2 A review of different models

1.2.1 Overview of water quality models

Water quality models can be used to simulate and predict the fate and transport of water quality constituents or contaminants. Models simulate concentrations of nutrients, and other constituents in the water body based on analytical or numerical solutions equations describing physical, chemical and biological processes of importance. Ordinary and partial differential equations are used to describe the dynamics of phenomena occurring in the surface waters associated with the spread of various pollutants.

Water quality models can be classified as:

a) Physical models (laboratory)
b) Mathematical models, including:

-Analytical models - based on exact solutions of the equations of mathematical physics,
-Numerical models - using approximate solutions.

There are many varieties of environmental water quality modeling. These models vary both in complexity and in terms of the processes modeled to represent the state of a catchment, river, and reservoir based on hydrodynamic, chemical, and biological processes. These inputs are the framework of the software and understanding them is vital to applying the software accurately. The 3-D models solve the Navier-Stokes equations and do not simplify in the vertical direction. The quasi-three-dimensional (3qD) classification simplifies the Navier-Stokes equations in the vertical direction and assumes a hydrostatic vertical distribution. More processes modeled, the bigger the challenge in building a computational model. (See Table 1).

Table 1: Classification criteria for Water Quality Models

Condition	Classification
Time dependence	Steady or Unsteady
Spatial dependence	One dimension (1-D), Two dimensions (2-D), Three dimensions (3-D) or quasi three dimensions (q-3D)
Flow conditions	Laminar flow or turbulent flow
Initial phases of reactants	Single-phase, two-phase, or multiple phase
Sites of reactions	Homogeneous, Heterogeneous.
Rate of reactions	Chemical

Condition	Classification
	equilibrium (infinite rate) or finite
Degree of compressibility of flow	Incompressible flow or compressible flow

(Hernandez M, 2014)

The models shown in Table 1 represent the present "state of the art" in water quality modeling. These models have been used to assess the performance of ecological systems in rivers, reservoir, and wetlands. The selection of a model depends on the particular physical processes in the system under study.
Nevertheless, other types of water quality models are shown below.

Stochastic Models

Water quality problems and associated modeling studies are inevitably affected by the underlying uncertainties that affect the systems. Measuring hydrological and water quality variables are difficult, with at best 5% errors on flow measurement, and sampling and laboratory analytical techniques can introduce errors ranging from 5% to 20% (Whitehead, 2016).
One approach to resolve this problem is to make use of MC analysis. MC analysis is a technique in which multiple simulations are performed using a random selection of process parameters on input variables to generate multiple simulated outputs (Whitehead, 2016).
The second area of stochastic model techniques is that of generalized sensitivity analysis (GSA) as developed by Spear and Hornberger (Spear & Hornberger, 1980). The GSA technique is based on the utilization of a simulation model together with a classification algorithm.

Whole Catchment Models of Water Quality

There are relatively few models of whole catchments that incorporate the soil and groundwater components as well as river channel dynamics. This is somewhat surprising given that many problems are caused by nonpoint source or diffuse pollution. Where such models do exist, they are often driven by overly complex hydrological models (Whitehead, 2016).
For example, INCA, the model can simulate up to six different land uses: forest, arable, urban, surface vegetation (grazed or fertilized), and moorland. (Whitehead, 2016).

Academic water quality approach

There are some academic water quality models, where other types of phenomena are studied more thoroughly as:
A three-dimensional incompressible unsteady-flow model that is coupled with a water quality model via the Reynolds Average Navier-Stokes (RANS) equations called BioChemFOAM developed using the computational fluid dynamic software OpenFOAM (Hernandez M, 2014).

Three-dimensional water quality modeling with TELEMAC-3D, where the ordinary differential equations remain to be solved following the solution of the non-reactive transport equations using operator-splitting techniques solved using a fourth-order Runge- Kutta method.

Empirical models, also called data-oriented models (Afshar et al.,2012) or data-driven models (Elshorbagy and Ormsbee, 2006) are derived from the available data sets. They mainly consist of statistical relationships (called transfer functions) between predictor variables and response variables of interest (Vinçon-Leite & Casenave, 2019).

Statistical models of the 1970s and 1980s have evolved significantly over the last decade towards "data-driven" models. Such models need large data sets that were not available in the past, but that lake monitoring systems are now able to collect. Artificial neural networks (ANNs) are now commonly used to study lake eutrophication (Vinçon-Leite & Casenave, 2019).

Other data-driven models using machine learning techniques such as tree-based models (Fornarelli et al., 2013; Jung et al., 2010; Peretyatko et al., 2012), support vector machines (Diaz Muniz et al., 2015; Garcia- Nieto et al., 2018; Xu et al., 2015a, 2015b) or random forests (Hallstan et al., 2012) are also proposed. For short-term (day to weeks) forecast, such data-driven models give good results, but for the simulation of long-term prospective scenarios, they hardly can be used as it is necessary to include knowledge about the driving processes (Vinçon-Leite & Casenave, 2019).

Mechanistic models, also called process-oriented models (Arhonditsis and Brett, 2004), process-based models (Fornarelli et al., 2013) or theoretical models (Vanhuet, 1992), are based on the a priori knowledge of the driving processes of the ecosystem. Most of them consist of a set of differential or difference equations which describe in detail the biogeochemical processes and whose solution is obtained by numerical methods. In the 1980s, mechanistic models generally computed the steady-state concentration of variables, leading to nonlinear static relationships between variables of interest (e.g., Imboden, 1974; Schnoor and O'Connor, 1980; Vollenweider, 1975). These models are called "input-output" models (Vollenweider, 1975) or black-box models (Teruggi and Vendegna, 1986) and are sometimes considered as empirical models whereas their structure is directly deduced from dynamic equations of biogeochemical processes.

From box models to 3D models, to reproduce accurately the ecosystem dynamics, mechanistic models are frequently coupled with a hydrodynamic model that can be quite simple, simulating only the water temperature and the regime of temperature stratification and mixing or more complex, simulating also the current velocities and patterns. The spatial dimension of the coupled models varies from zero (box models): in that case "the water body of a lake or of each box within a lake is represented as a completely mixed stirred tank reactor" (Nyholm, 1978), to three: the spatial heterogeneity of the ecosystem is taken into account in all three dimensions. If a box model alone cannot account for the lake spatial heterogeneity, this can be obtained using a set of interconnected box models (Muraoka and Fukushima,1986; Nyholm, 1978).

A Fortran-based Framework for Aquatic Biogeochemical Models (FABM - Bruggeman and Bolding, 2014; Trolle et al., 2011a, 2011b) enables to easily couple hydrodynamic models with ecological models, whereas the project "Framework for Interoperable Freshwater Models" (FIFM) has investigated flexible computer-based frameworks for integrating freshwater models (Elliott et al.,2014).

A three-dimensional water quality model of nitrogen, "A coastal three-dimensional water quality model of nitrogen in Jiaozhou Bay linking field experiments with modeling", 3DWQMN where the dynamic parameters were updated according to field experiments (Dongliang, Keqiang, Shengkang, & Guohong, 2016).

It is estimated that currently there are at least several thousand surface water quality models derived from public or commercial basic modules and then adapted to the modeled stream or water reservoir.

1.2.2 Overview hydrological

Hydrological model is a simplification of a real-world system, used mainly for the prediction of hydrological processes and based on variables such as rainfall, drainage area (topography), soil properties, vegetation cover, and runoff models and can be defined as a set of equations that enables the estimation of runoff as a function of various parameters used for describing watershed characteristics (Honek, Caletka, & Šulc Michalková, 2018).

The traditional classification of hydrological models is based on hydrological model parameters and the models' sorting system following the established classifications (in accordance with stochasticity, space and time discretization) Bízek et al. (2011).

It is important to highlight Pechlivanidis et al. (2011) added the need of a "model set-up" and the quantification of uncertainty in the model's predictions and highlighted the recent developments in hydrological modeling. In this context, the land use changes in all scales are a frequently discussed topic and very often, the hydrological models pervade the group of erosion models in this subject matter. That's why some of the hydrological models can be also classified as erosion models, e.g., the SWAT model.

Stochastic models and deterministic models

Stochastic models calculate the probable occurrence of a given value at a particular point. The hydrologic process is defined along with a discussion of the tendency, periodicity, and stochasticity in the hydrologic series (Yevjevich 1987, Beven 2001 and Unucka 2014). In contrast, deterministic models are models in which outcomes are precisely determined through known relationships among states and events, without random variation. Deterministic models are more often used in hydrological research than stochastic models, and these models are divided into groups – conceptual, physical and empirical (Beven 2001, Bízek et al. 2011 and Unucka, 2014).

Space and time discretization

According to space-time discretization, the models are divided into distributed and semi-distributed models (Bízek et al. 2011 and Unucka 2014). In lumped models, a catchment is a single entity (or a small number of entities, such as reservoirs), and such models can simulate state variables and fluxes into and out of the catchment as a whole. Distributed models divide the original catchment into many entities (small representative parts) and the state variables and fluxes among the entities are defined across the catchment. Semi-distributed models are a combination of lumped and distributed models, dividing a catchment into

hydrotops (small elementary catchments with some homogenous parameters, e.g., soil type, vegetation cover, etc.) (Honek, Caletka, & Šulc Michalková, 2018).

A brief summary of the findings and developments in hydroclimatic models is presented below (Singh, 2018) as follow:

- Watershed geomorphology
- Hydraulic geometry
- Surface runoff
- Reservoir and channel flow routing
- Interception and depression storage
- Evaporation
- Infiltration and soil water flow
- Subsurface flow
- Groundwater
- Erosion and sediment yield
- Sediment transport
- Pollutant transport
- Reservoir operation
- Flood frequency analysis
- Drought analysis
- Watershed models
- Data observation and tools
- Geographical information systems
- Integration of concepts and processes

1.2.3 Overview of integrated water quality models

Different processes need to be modeled, and many of the processes interact with each other, so integration of the models is needed. There is also growing consensus that real-world problems are complex and interrelated, and to solve them an integrated approach is a must (Parker et al. 2002, Candela et al. 2012, Bulatewicz et al. 2013). However, easy and feasible integration of different models is hindered because models are founded on different concepts and have different spatial and temporal scales (Kumar Shrestha, Tolessa Leta, & Bauwens, 2017).

In this proposal, we review the current state of integrated water quality model.

Which kind of models has been integrated?

The following models integrate two or more areas (hydrology, water quality, sediment).

There are models that have certain modules coupled, the most common were hydrological models with some water quality module at the basin scale in a river, for example, SWAT, HSPF.

Sediment transport model coupled with a hydrological model (HSPF, INCA, SWAT).

Hydrological model coupled with hydraulic models (Sanz-RamoS, Amengual, Bladé, Romero, & Roux, 2018).

1-D hydrodynamic and water quality model of the river network, (Zhang, et al., 2009), in this case, model the groundwater is not considered as the water source.

Coupled hydrological, hydraulics (rivers) and water quality, (Zhang, et al., 2012), SWAT, HRUS, and QUAL2E (Shrestha, Leta, & Bauwens, 2017).
A few studies have attempted to link watershed models with reservoir models. For example, Wang et al. (2005) integrated AnnAGNPS and BATHTUB to simulate the response of the Cheney Reservoir, Kansas, to different land use and management scenarios.
Coupled hydrodynamics reservoir (SELFE, water quality (WASP), and Carbon and Nutrients Diagenesis (CANDI), (Li, Yang, Li, Mu, & Jin, 2018).
In some cases, is urban drainage water models with water quality, (Bach, Wolfgang, Mikkelsen, McCarthy, & Deletic, 2014).
Coupled components—hydrological (SWAT), hydraulic (SWMM) and stream water temperature (Leta, Griensven, Shrestha, & Bauwens, 2014).
Model integration platform across disciplines (Knapen, et al., 2013).
Other studies involving integrated watershed-reservoir modeling were reported in the literature (Cabecinha et al., 2009; Li et al., 2010; Mankin et al., 2003; Narasimhan et al., 2010; Reed- Andersen et al., 2000; White et al., 2010b).

There are two traditional kinds of approaches that study on integrated modeling feature:

(1) Use of existing integrated modeling software packages, (Brito, Ramos, Gonçalves, Morais, & Neves, 2018).
(2) Combination of different existing models into one larger integrated assessment tool, (Zhang, et al., 2009), (Shrestha, Leta, & Bauwens, 2017), (Zhang, et al., 2012).

1.3 TELEMAC as an integrating tool

The TELEMAC-3D code solves such three-dimensional equations as the free surface flow equations (with or without the hydrostatic pressure assumption) and the transport-diffusion equations of intrinsic quantities (temperature, salinity, concentration). Its main results, at each point in the resolution mesh, are the velocity in all three directions and the concentrations of transported quantities. Water depth is the major result as regards the surface mesh. The TELEMAC-3D's prominent applications can be found in free surface flow, in both seas and rivers; the software can take the following processes into account:

- Influence of temperature and/or salinity on density,
- Bottom friction,
- Influence of the Coriolis force,
- Influence of weather elements: air pressure and wind, Consideration of the thermal exchanges with the atmosphere,
- Sources and sinks for fluid moment within the flow domain, Simple or complex turbulence models (K-Epsilon) taking the effects of the Archimedean force (buoyancy) into account,
- Dry areas in the computational domain: tidal flats,
- Current drift and diffusion of a tracer, with generation or disappearance terms.

The code is applicable to many fields. The main ones are related to the marine environment through the investigations of currents being induced either by tides or density gradients, with or without the influence of such an external force as the wind or the air pressure. It can

be applied either to large extent areas (on a sea scale) or to smaller domains (coasts and estuaries) for the impact of sewer effluents, the study of thermal plumes or even sedimentary transport. As regards the continental waters, the study of thermal plumes in rivers, the hydrodynamic behaviour or natural or man-made lakes can be mentioned as well.

Position of the telemac-3d code within the telemac modelling system

The TELEMAC-3D code is part of a processing chain, namely the TELEMAC system. That package provides with all the required modules for constructing a model and for conducting simulations of hydrodynamic flow, contaminant and sediment transport.

The TELEMAC system comprises the following modules:

- The TELEMAC-2D software designed to perform the hydrodynamic simulation in two horizontal space dimensions. In addition, TELEMAC-2D can simulate the transport of dissolved tracers,
- The TELEMAC-3D software itself, designed to carry out the hydrodynamic simulations of flows in three space dimensions. Besides, TELEMAC-3D can simulate the transport of tracers. The SEDI-3D library contains of the relevant subroutines for the simulation of noncohesive sediment transport. The implementation of the TELEMAC-3D software is the subject matter of this document,
- The SUBIEF-2D software designed to carry out the simulation, in two horizontal space dimensions of the transport of suspended sediments and the transport of dissolved substances without any gravity effect. SUBIEF-2D particularly makes it possible to handle the water quality-related issues.
- The SUBIEF-3D software designed to make the three-dimensional simulation of the transport of dissolved substances without any gravity effect. SUBIEF-3D is also provided for handling the water quality-related issues.
- The SISYPHE software designed to carry out the simulation the transport of sediment through bed load traction and suspension.
- The ARTEMIS software designed to simulate the changes in the features of wave agitation either in a coastal water body or a harbour,
- The TOMAWAC software designed to simulate, through a spectral method, the sea state in permanent or transitory conditions,
- The ESTEL-2D software designed to simulate the underground flows in two vertical space dimensions,
- The ESTEL-3D software designed to simulate the underground flows in three dimensions,
- The POSTEL-3D software designed to prepare the 2D cross sections in the 3D result file, for a processing by the RUBENS graphics software,

As a complement to the TELEMAC chain, the FUDAA-PREPRO software (as developed from the FUDAA platform by the CETMEF's Recherche, Informatique et Modélisation Department) covers all the preprocessing tasks involved by the achievement of a digital hydraulic study.

Software environment

When he uses a simulation module from the TELEMAC system, the user may have to program specific functions which are not provided in the code's standard release. In particular, that is made through a number of so-called « user » subroutines the sources of which are supplied within the distribution. The procedure to be carried out in that case comprises the steps of:

- Recovering the standard version of the user subroutine(s) as supplied in the distribution and copying it into the current directory.
- Amending the subroutine(s) according to the model to be constructed.
- Concatenating the whole set of subroutines into a single Fortran file which will be compiled during the TELEMAC-3D launching process.

During that programming stage, the user can gain access to the various variables of the software through the Fortran 90 structures.

All the data structures are gathered within Fortran files, which are known as modules. For TELEMAC-3D, the file name is DECLARATION_TELEMAC3D. To gain access to the TELEMAC-3D data, just insert the command USE DECLARATIONS_TELEMAC3D into the beginning of the subroutine.
Adding the command USE BIEF may also be necessary in order to reach the structure in the BIEF library.

Nearly all the arrays which are used by TELEMAC-3D are declared in the form of a structure. The access to the water depth array will then be take place in the form H%R, %R meaning it is the "real number-typed field" component in the structure. In case of a integer-typed component, the %R is replaced by a %I. In order to avoid having to handle too many %R and %I, however, a number of aliases are defined, such as, for instance, the NPOIN3D, NELEM3D et NPTFR2D variables. For further details, the user can refer to the programming guide in (TELEMAC-3D, 2020).

Setting up the water-atmosphere exchanges

THE WIND

TELEMAC-3D makes it possible to carry out a flow simulation taking into account the influence of the wind blowing at the surface of the water body. The logicaL keyword WIND first enables to determine whether that influence is taken into account or not. The wind influence coefficient will then be yielded by the keyword COEFFICIENT OF WIND INFLUENCE. Lastly, the wind velocities along X axis and Y axis will be yielded by the keywords WIND VELOCITY ALONG X and WIND VELOCITY ALONG Y.

The whole formulation of the consideration of wind effects, through the keyword COEFFICIENT OF WIND INFLUENCE (refer to the Principle Note for the definition of that coefficient), on the surface flowsis fully stated in the BORD3D subroutine. Two options are available:

- the coefficient is that being set in the steering file,
- the coefficient depends on the wind intensity (an example is set forth in the BORD3D subroutine).

If the wind velocity is space- or time-variable, the user should act at the METEO subroutine.

THE TEMPERATURE

TELEMAC-3D makes it possible to take into account the heat exchanges between water and atmosphere through a direct programming in the BORD3D subroutine. An exemplary exchange with aconstant temperature atmosphere and a constant salinity sea is given as standard.

THE PRESSURE

The influence of air pressure is taken into account from the moment when the keyword AIR PRESSURE isset to YES (the default value is NO). The value of that pressure is directly set in the METEO subroutine. By default, the latter initializes a pressure of 105 pascals (1 atmosphere) over the whole domain.

OTHER PHYSICAL PARAMETERS

Upon the modelling of wide areas, the influence of the Coriolis force of inertia has to be talen into account, what is done by activating the logical keyword CORIOLIS (which is set to NO by default). In such a case, the value of the Coriolis coefficient (refer to the Principle Note) is yielded by the keywordCORIOLIS COEFFICENT. The latter should be computed according to latitude λ through the formula:

$2\omega \sin(\lambda)$ where ω is the Earth's rotational velocity of 7.27×10^{-5} rad/s and λ is the average latitudeof the model.

TELEMAC-3D additionally offers the opportunity to set the gravity acceleration (keyword GRAVITY ACCELERATION which, by default, is set to 9.81m/s2.

DIGITAL SETUP OF THE COMPUTATION

The digital setup is comparatively common to a hydrodynamic computation alone or with a tracer. Thus, in the following sections of this chapter, the digital parameters as applied to the solution of a tracer equation are integrated into the hydrodynamic parameters.

1.4 Temperature and thermal stratification

One of the most important physical variables in surface waters is temperature, which is crucial in hydrodynamic and water quality studies due to factors such as (Ji 2008):

Temperature gradients condition the hydrodynamic behaviour of the system.
The solubility of dissolved oxygen is determined by water temperature. The higher the temperature, the lower the DO concentration.
Many biochemical and physiological processes are governed by temperature: Increasing temperature can increase the metabolic and reproductive rates of organisms.

Thermal stratification is one of the typical characteristics of reservoirs, which is caused by the formation of horizontal layers of different temperature (and therefore different density). Such stratification affects the transport processes in the reservoir and conditions the spatial and temporal distribution of dissolved and suspended substances in the water.

One of the key factors in the formation of the thermal structure is the surface heat flux which is composed of solar radiation, incident and emitted longwave radiation, sensible heat flux and latent heat flux. Often, this energy flow results in an increase in the temperature of the surface layer of the reservoir and thus a decrease in its density. In contrast, the deeper layers remain cooler because they are less exposed to these heat sources as the penetration of shortwave radiation is limited and diffusive heat transport is too slow. There are other much more effective mechanisms for heat transport at depth, such as convective mixing due to surface cooling (e.g. at night) and the kinetic energy provided by the wind through the shear stress it exerts on the surface. This results in the formation of a totally or partially mixed surface layer called epilimnion, which constantly exchanges energy and mass (e.g. gases) with the atmosphere. If the reservoir is deep enough, a lower layer, isolated from atmospheric exchange, called hypolimnion, can be found. These two zones are separated by the metalimnion which is a layer with a strong temperature gradient. The thermocline is the plane in the metalimnion where the largest temperature gradient is observed.

In temperate zones, during the cold seasons (autumn and winter), systems tend to completely mix the water column, because the decrease in solar radiation allows the cooling of the surface layers, which activates convective mixing processes that can uniformize the entire water column. solar radiation allows the cooling of the surface layers, which activates convective mixing processes that can make the entire water column uniform. In contrast, in the tropics, the absence of seasons means that the difference between annual maximum and minimum irradiance is small. In addition, the total daily irradiance is very constant throughout the year, as there are no large variations in the number of daily daylight hours. This implies that there are not such marked variations in surface heat fluxes, so the seasonal pattern of stratification and mixing typical of temperate zones is not so clear for the tropics (Lewis 1987).
Another substantial difference that has been found is the smaller difference between bottom and surface temperature in tropical reservoirs compared to that found in temperate climates, hence the stability of the water column is lower and the thickness of the epilimnion has a

greater short-term variability caused by particular events such as strong winds or periods of low solar radiation incidence (Lewis 1987).

Transport and Mixing Processes

In addition to surface heat flow, there are various physical processes within the reservoir that can alter or even induce thermal stratification, which in turn are conditioned by thermal stratification. These include large-scale processes such as internal waves, density currents produced by rivers and selective abstraction by water abstraction structures. A brief description of these is given below.

Internal Waves

The effect of the wind on the water surface not only induces mixing in the surface layer, but its prolonged action in time induces currents in the wind direction, which tilts the metallimnion. If the wind stops, the system will try to return to its equilibrium state, thus generating an oscillation. Once the motion is initiated, non-linear processes give rise to higher frequency waves that trigger mixing processes on different spatial and temporal scales. Depending on the characteristics and oscillation modes of the internal waves, they generate different circulation patterns throughout the reservoir and are an important mechanism in the redistribution of suspended and dissolved substances, especially vertically. One of the pioneering works on this type of phenomena was developed by Mortimer, (1952) and a good review can be found in Csanady, (1975) and Imberger, (1998).

Density currents

The inflow of a tributary into the reservoir can occur as a surface flow, as a bottom flow or as an intrusive flow (**Figure 5**). The establishment of one of these three types of density flows depends basically on the relationship between the density of the influent and the density of the water body.

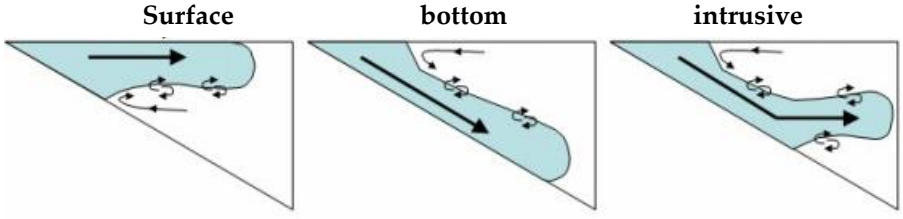

Figure 5 Dynamics of tributaries. Adapted from Vidal, (2007)

When a river enters the reservoir, its momentum displaces the impounded water forward. Once the baroclinic pressure gradient at the contact surface between the reservoir and the tributary offsets the initial momentum of the current, buoyancy will begin to dominate and, in the event that the tributary is less dense than the surface water in the reservoir, it will "float" forming a surface current. The point at which the tributary separates from the bottom is known as the point of separation. This type of flow has very clear implications in terms of its impact on water quality, because the nutrients supplied by the river will be immediately available for primary production at the surface.

If the tributary is denser than the surface water in the reservoir, it will submerge to travel along the bottom of the reservoir. The location of the submergence point is determined by a balance between the inertia of the current, the frictional forces and the pressure gradient

generated at the contact interface between the reservoir and tributary water (Ford & Johnson 1983). Once the density current is established and begins to travel along the bottom of the reservoir, the turbulence generated at the stream boundary causes some of the water in the medium to enter the stream and dilute it. This process, known as entrainment, was suggested by Ellison & Turner, (1959).

If the density of the bottom current equals the density of the surrounding water, it will acquire neutral buoyancy, so it will detach from the bottom and move horizontally through a layer of similar density. Such currents are called intrusive currents.

Both at the point of submergence and in the course of the river as a density current, mixing processes occur that modify the density of the current. For this reason, the depth of intrusion is less than that which would be estimated assuming that there is no mixing, i.e. identifying the depth in the reservoir at which the temperature is equal to that of the river (Rueda et al. 2007).

Baines, (2008) from laboratory experiments in stratified media, proposes to divide density currents into two types: plumes and gravity currents. Plumes correspond to vertical flows (like an inverted chimney) or flows with steep slopes, in which the behaviour of the current is largely governed by entrainment. Gravity flows, on the other hand, occur mainly on gentle slopes and in these, buoyancy is balanced by bottom friction. The exchange of mass with the medium in gravity streams is predominantly outward, a process known as detrainment (analogous to entrainment) and although there is also a flow from the medium into the gravity stream, it is much smaller than the flow from the stream into the medium.

When the density of the influent depends on its temperature, daily and seasonal variations in the behaviour of the density current can be observed. The seasonal dynamics of the influent have been reported by Carmack, (1979); Carmack et al, (1986); Armengol et al., (1999); among others. Pickrill & Irwin, (1982) showed the importance of considering the daily cycle in addition to the seasonal cycle and Román-Botero et al., (2010), through numerical simulation of La Fe reservoir (Colombia), show the influence of the daily cycle of tributary temperature on the dynamics of the thermal structure of the reservoir.

Selective abstraction

In stratified reservoirs, water abstraction generates flows in a layer that is vertically limited by density variations, called the selective abstraction zone (Imberger 1980). This process also influences stratification by modifying the temperature profile.

Different models have been proposed to predict the selective extraction layer: Pao & Kao, (1974) show that horizontally propagating shear waves appear with the opening of the catchment and are responsible for generating the flow in a layer of thickness d (Anohinet al., 2006). Different models for calculating the thickness of the extraction zone can be found in Martin & McCutcheon, (1999).

1.5 A Stratification in the tropics

For at least one authority on tropical limnology, the fundamental stratification behavior of tropical lakes and reservoirs is clear. Lewis (2000) states that "Tropical lakes are fundamentally warm monomictic with only the shallowest failing to stratify at least

seasonally, and that periods of destratification are typically predictable events coinciding with cool, rainy and/or windy seasons. Yet, there exists confusion in the literature. For example, the World Commission on Large Dams' technical report states that stratification in low-latitude reservoirs is "uncommon" (Mccartney et al., 2001). The authors provide no source supporting this statement, but the conclusion likely stems from the 70-year-old landmark lake classification system (Hutchinson and Löffler, 1956), which, based on very limited field data from equatorial regions, gives the impression that tropical lakes are predominately either oligomictic (mixing irregularly) or polymictic (mixing many times per year). The idea that low-latitude water bodies are fundamentally unpredictable or aseasonal, as well as Hutchinson and Löffler (1956) approach of classifying lakes without morphometric information critical to un- derstanding lake stability (Boehrer and Schultze, 2008), has been criticized repeatedly over subsequent decades as additional tropical lake studies have been published (Lewis, 1983, 2000, 1973, 1996). And yet, the original misleading classification diagram continues to be faithfully reproduced in contemporary limnology textbooks (Bengtsson and Herschy, 2012; Wetzel, 2001). Since much of the water quality challenges associated with damming develop from the thermal and/or chemical stratification of reservoirs, we take a critical look at the issue of whether tropical reservoirs are likely to stratify predictably for long and short periods.

1.6 Water Quality and Dissolved Oxygen

Water quality is a concept that involves the physical, chemical and biological characteristics of water in relation to the needs of the different organisms that are part of the aquatic ecosystem or to certain uses by man. There are a large number of parameters that are used to assess water quality, including: temperature, conductivity, DO concentration, pH, turbidity, BOD, colour, presence of pathogens and toxic substances, etc. Each of these parameters is important in relation to the specific use of the resource or the needs of the biotic community that uses it.

Dissolved oxygen (DO) is one of the most important variables in aquatic ecosystems and perhaps the variable that provides the most information about the general state of the resource (Ji 2008). Maintaining a certain minimum concentration of dissolved oxygen in the water is vital for the maintenance of fish and other aquatic organisms, and low concentrations of dissolved oxygen favour the production of harmful substances such as methane and hydrogen sulphide with harmful consequences for the balance of the ecosystem.

There are various physical, chemical and biological processes that affect the DO concentration in a reservoir. Typically, the sources of DO are atmospheric reaeration, input from rivers and photosynthesis by phytoplankton and macrophytes. On the other hand, it is consumed by respiration of aquatic organisms and by decomposition of organic matter (Williams 2007).

Chapter 2

2 On the Spatial-Temporal Behavior, and on the Relationship Between Water Quality and Hydrometeorological Information to Predict Dissolved Oxygen in Tropical Reservoirs. Case Study: La Miel, Hydropower Dam

*The results of this chapter were published in the Journal of Air, Soil and Water Research on January 25, 2023.

Abstract: Hydropower is currently one of the leading renewable energy sources in developing countries. Despite the benefits that it can provide, it also triggers significant environmental impacts, such as changes in the reservoirs' water quality. In quantifying those changes, dissolved oxygen (DO) is used as one of the water quality indicators and is the most used variable to quantify water quality and analyze water pollution. This paper aims to establish a relationship between water quality and hydrometeorological variables in tropical reservoirs to better estimate dissolved oxygen. Univariate and multivariate techniques were used to analyze temporal and spatial changes in watersheds to better select vital variables for the forecast model, such as Vector Autoregression (VAR). The results show that, for all monitoring stations, the water quality variables associated with the DO process are COD, BOD, and PO_4. Likewise, precipitation and flow discharge were the hydrometeorological parameters that had the most significant impact on DO. Also, the principal component analysis (PCA) allowed us to identify that the strength of the relationships between water quality and hydrometeorology changes depending on the location of the monitoring site. Finally, the implementation of a VAR model showed good performance metrics for dissolved oxygen predictions based on all analyses.

Keywords: Tropical reservoir, water quality, hydrometeorology, hydroinformatics, hydrological time series

2.1 Introduction

Hydropower is a significant source of renewable electricity, with a share of 16%–17% of the total world electricity generation (Killingtveit, 2019), and currently it is the main renewable energy source in most countries in Asia (Vaidya et al., 2021); Li, (Li et al., 2018), Europe (Alsaleh & Abdul-Rahim, 2021a); (Alsaleh & Abdul-Rahim, 2021b), Africa (Woldeab et al., 2018) (Gyimah et al., 2021), and South America (de Oliveira et al., 2021); (Semensatto et al., 2021). Furthermore, future hydropower development is primarily concentrated in developing countries and emerging economies of Southeast Asia, South America, and Africa, also with the Balkans, Anatolia, and the Caucasus being additional centers of future dam construction (Zarfl et al., 2015).

Despite the benefits that hydropower can provide, such as water supply to communities, flood control, and greenhouse gases reduction (Silva & Castillo, 2021), these structures can also trigger substantial environmental impacts like the disruption of aquatic ecosystems, reduction of riparian biodiversity, modification of stream morphology, or water quality degradation, among others (Zarfl et al., 2019); (Barbarossa et al., 2020). In the case of water quality inside the reservoir, this factor is affected principally by meteorological, hydrological, and geological factors, as well as land use (Marcé et al., 2010); (Dalu & Wasserman, 2018); (Vega et al., 2018); (Jerves-Cobo et al., 2020).

In the case of effects on reservoir water quality caused by meteorological and hydrological factors, these are described mainly based on geographic location. This is particularly the case for high and low-latitude systems also called temperate systems, where the four seasons have an impact on the system (Hwang et al., 2016); (Weirich et al., 2019). Most of the studies carried out focus mainly on the assessment of water quality and its relationship with meteorological, and anthropic variables in eutrophic reservoirs (Scott Winton et al., 2019). About the foregoing, it has been learned that nutrients and organic matter are responsible for most of the variation in reservoir water quality related to anthropogenic activities that directly impact the reservoir, followed by suspended solids related to both anthropogenic and natural processes, but not directly with dissolved oxygen (Mamun et al., 2021). In the same way, water quality parameters exhibited a seasonal fluctuation, with predominantly higher concentrations during the dry season than the wet season (Woldeab et al., 2018). Additionally, most of the best-documented examples of impacts —which stem from oligotrophication and water quality behavior, under this trophic state— come from temperate catchments with important and carefully monitored fisheries (Scott Winton et al., 2019). In temperate systems, seasonal patterns, hydrology, and watershed morphology are the main regulatory factor for the nutrient concentration in reservoirs (Mamun et al., 2018); (Nadarajah et al., 2019). Similarly, water quality variables, except total nitrogen, show vast seasonal differences as a result of high seasonality in water temperature and water flow (Varol, 2020b). However, all those conclusions cannot be directly applied to tropical case studies where the hydrological regime is different (Scott Winton et al., 2019). Nevertheless, based on the studies mentioned above, it is necessary to go deeper into studies that directly relate water quality to hydrological and meteorological factors in hydropower systems in tropical latitudes (Calamita, 2020).

Regarding tropical systems, water quality analysis has been applied, and the hydrological cycle was shown to affect reservoir water quality (Lobato et al., 2015) directly. However, the application of multivariate statistical analysis in tropical reservoirs is limited and concentrated in eutrophic systems impacted by intense anthropic activities (Ling et al., 2017), (Marques et al., 2019).

Statistical analysis and prediction play an essential role in processing surface water quality time series, with tools such as outliers detection, normality tests, and trend detection, among others, granting an excellent first approach (Fu & Gan Wang, 2012). To perform an integrated statistical analysis of water quality is necessary to consider hydrological, meteorological, and anthropic activities. Multivariate statistical analysis, such as principal component analysis and correlation analysis, facilitates integrated water quality data analysis since it allows the identification of factors that influence water quality (P. Chen et al., 2015); (Varol, 2020a). These methods exhibit a practical approach to assessing and forecasting the water quality of reservoirs and can be used as a tool for water quality management (Varol, 2020b).

Analyzing water quality is possible through dissolved oxygen (DO) because is used as one of the water quality indicators and is the most used variable to quantify water quality and analyze water pollution. Since it plays a substantial role in aquatic environment characterization and shows the equilibrium between the processes that produce or consume oxygen in that environment, predicting its concentration could be advantageous for the environmental custodians. Accurate predictions of DO concentrations can help better manage tropical ecosystems. Low DO concentrations can lead to the mortality of aquatic organisms and the release of nutrients from the sediments, among others (Vilas et al., 2018), which is why we should consider.

Concerning dissolved oxygen forecasting, previous studies have explored the prediction. Some of the statistical methods are multiple linear regression models, artificial neural networks, classification tree, principal component/factor analysis, discriminant analysis, and Normal hidden Markov models. They are used independently or jointly to predict the temporal evolution of water, and the results are of outstanding quality but do not take into account spatial and hydrological factors, (Liu et al., 2021). Regression models are most widely used for modeling the stochastic behavior of DO concentrations and artificial intelligence (Yaseen et al., 2018). Even so, regression models and neural networks require more data preprocessing, complex relationships cannot be modeled without transforming the input, and non-linear relationships cannot be captured, being very sensitive to different scales of variables. They usually require larger amounts of data for model training and require a lot of computing resources. Finally, knowing the rules or reasons why the artificial network returns those results is not usually easy and needs other analyses.

This study's main objective is to establish relations between water quality and hydrometeorological variables to predict and estimate the dissolved oxygen concentration in a tropical reservoir. The results obtained using vector autoregression (VAR) using different methods focus on key parameters and are predictively valid.
In this same sense, it is analyzed that changes in the dissolved oxygen are given by water

temperature, and the intensity of biological processes such as photosynthesis, respiration, and decomposition of organic matter (Rajwa-Kuligiewicz et al., 2015), due to changing hydrometeorological conditions(Rajwa et al., 2014), in the case of the reservoir it has been identified that DO have changes due seasonal and vertical dynamics (Lliev & Hadjinikolova, 2013), air temperature and nutrients (Dordoni et al., 2022) and physical process the atmosphere (Liqoarobby et al., 2021). Following this, we hypothesized that in tropical reservoirs the dissolved oxygen dynamics depend on the air temperature, Sunshine duration, flow discharge, and precipitation, and internal chemical process as water temperature and decomposition of organic matter and Chemical oxygen demand. Identifying the key variables will allow for a more accurate prediction of dissolved oxygen.

2.2 Study Area Description and Data Source

2.2.1 Study Area

"La Miel I" is a gravity dam located between 5°15' N ~ 5°35' N and 74°53' W ~ 75°15' on the riverbed of "La Miel" river in Caldas Department, Colombia, as is shown in Figure 4. Between 1997 and 2002, the dam was built for the primary purpose of hydroelectric power generation. It is 188 meters high, giving it a storage capacity of 571 million m3 and a surface area of 12.2 km2, with an installed generation capacity of 396 MW in three turbine units. Its commercial operation began in December 2002. In 2010, the Guarinó diversion dam on the Guarinó River was opened, and the Manso diversion dam began operating in 2013. Both divert water into the Amaní Reservoir through a tunnel.

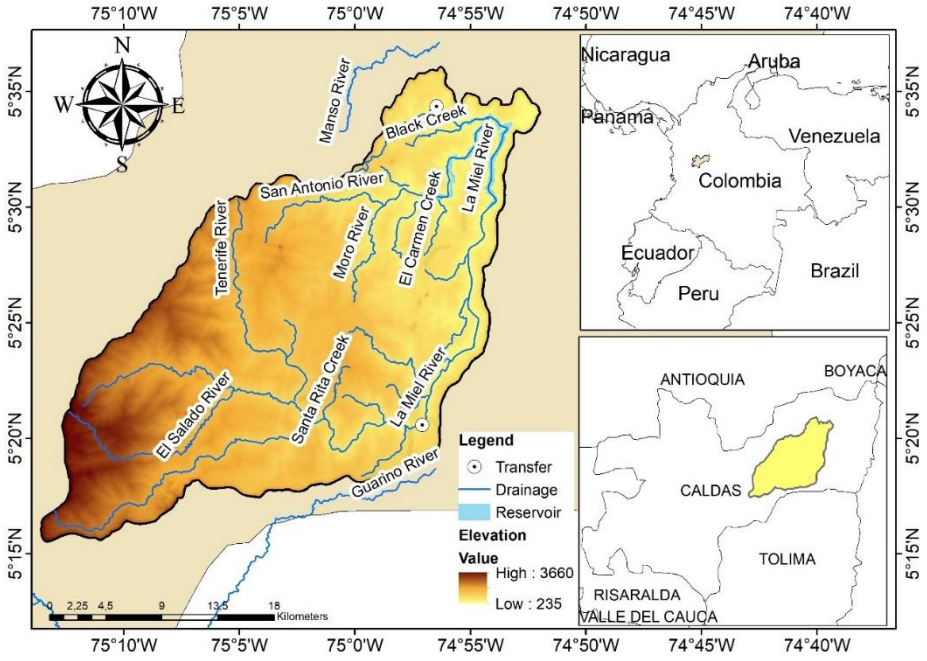

Figure 6 Location Area Study of" La Miel" Hydropower Dam and its Basin

In terms of hydrology, the watershed has a bimodal regime, composed of two wet and dry seasons. The average annual precipitation in the reservoir catchment is about 4428 mm, with

the heaviest rainfall occurring approximately in November with little precipitation between June and August. The dry season occurs from June to August, and the wet season —which is broken by dry periods— spans from May to November. Furthermore, the highest monthly evaporation rates occur in the dry season, with 165 mm/day rates, while the lowest evaporation rates occur in the wet season with an average of 46 mm/day. La Miel river basin experiences rainfall and a humid atmosphere throughout the year.

2.2.2 Hydro-Meteorological and Water Quality Data

Monthly data of water quality parameters, such as Temperature (T °C), pH, total suspended solids (TSS, mg/L), dissolved oxygen (DO, mg/L), and conductivity (μS/cm) were measured in situ, at the reservoir. In addition, other monthly data were taken to perform laboratory analysis to measure concentrations of chemical oxygen demand (COD mg/L), biochemical oxygen demand (BOD mg/L), ammonia (NH4 mg/L), nitrite (NO2 mg/L), nitrate (NO3 mg/L), total Kjeldahl nitrogen (TKN mg/L), phosphate (PO4 mg/L), Total phosphorus (TP mg/L). Inside the reservoir, there are five monitoring stations. These are distributed in two tributaries and the dam. The monitoring stations E4 and E6 are located in the Moro River. The monitoring stations E3 and E5 are in the La Miel river. Finally, the E7 monitoring station is at the dam, as shown in Figure 5. Measurements and samples were taken every three months from January 2002 to December 2015. Each monitoring station has measurements at various depths, in this case only data taken at the water surface will be used.

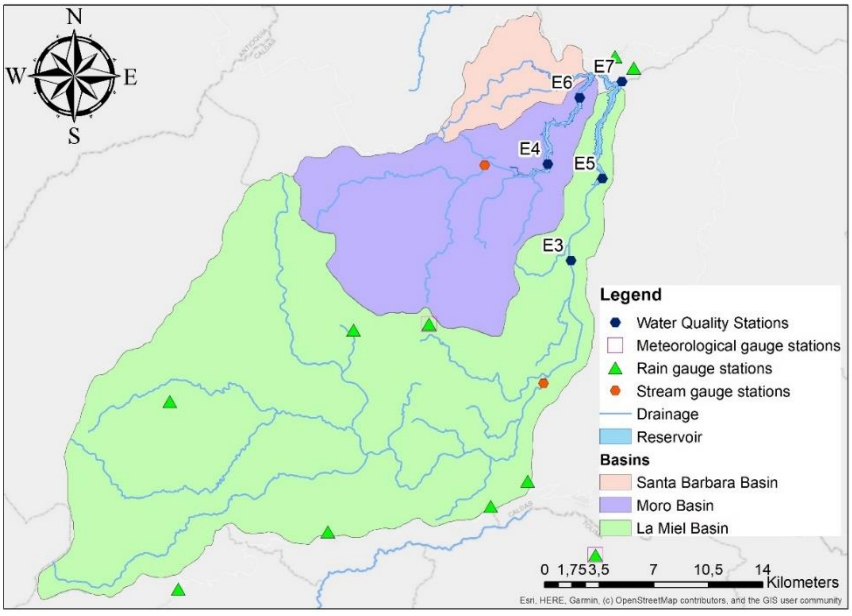

Figure 7 Location of Water Quality Monitoring and Hydrometeorological Gauging Stations

For the same period, seven hydrological parameters (discharge, precipitation, solar brightness, evaporation, relative humidity, cloudiness, and air temperature) were collected, covering all basin areas. These data were obtained from hydrological and meteorological gauging stations. Specifically, nine monitoring sites were used for measuring precipitation, four sites for discharge, and two sites for the other hydro-meteorological parameters. In addition, hydro-meteorological data were obtained from the DHIME website of the Institute

of Hydrology, Meteorology, and Environmental Studies (IDEAM, acronym in Spanish).

2.3 Methods

2.3.1 Data Treatment and analysis

Firstly, visual inspections such as scatterplots and boxplots were performed to test for outliers in water quality and hydro-meteorological time series, then anomalous values from the time series were identified and removed. Based on the hydrology described in the study area section, the time series were divided into the dry and rainy seasons for analysis, considering tropical seasonality.
Descriptive statistics were calculated with mean, maximum, minimum, and standard deviation values to identify the order of magnitude of water quality time series in each season. The dispersion of the data sets in each monitoring station assesses preliminary spatial and seasonal variation.

2.3.2 Univariate Statistical Analysis

The Kolmogorov-Smirnov one-sample test assessed the normality of the time series and the Shapiro-Wilk test with a significance level of 0.05, was applied to each parameter at each monitoring station. These tests determine whether parametric or nonparametric tests are more reliable for the following analyses. Afterward, a Pettitt and Mann-Kendall nonparametric test was performed to assess the homogeneity of the time series and the existence of a monotonic trend. In the case of Pettit's test, it identifies points where stepwise shifts (breaks) occur when inhomogeneity is extracted.
In addition, Kruskal-Wallis H tests were performed for each water quality parameter between the tail and mid sites and between the tail and dam sites.
Correspondingly, Levene and Mann-Whitney tests were applied to each parameter, assessing homoscedasticity and stationarity of time series between dry and wet seasons. A detrend of time series was applied for both, knowing that these analyses are affected by trends.

2.3.3 Multivariate Statistical Analysis with Missing Values

Correlation analysis was performed to measure the strength of the association between parameters from each monitoring site and between water quality parameters, hydro-meteorological parameters, and mixtures of water quality and hydro-meteorological parameters. The analysis was evaluated using the Pearson, Kendall, and Spearman correlation coefficients. The Pearson correlation coefficient is often used for jointly customarily distributed data (data that follows a bivariate normal distribution). For the latter case, the time series is normalized for better test results. For non-normally distributed continuous data, ordinal data, or data with correlated outliers, Spearman's rank correlation and Kendall's rank correlation can be used as measures of monotonic correlation (Schober, Boer, & Schwarte, 2018).

2.3.4 Data Imputation

Once univariate and correlation function analysis has been performed on all-time series, imputation techniques are applied to the time series to fill in the gaps.

Due to the fact that the next analyses require continuously sampled data, it is necessary to obtain the estimates of the missing values. The data produced by this method is used to define the most important variables, then to build possible modeling scenarios, and the analysis is performed using PCA.

In the first approximation, linear, quadratic, and cubic padding is applied. In the case of a large number of consecutive out-of-stocks, use the average value calculated before filling in the data.

Since these are univariate techniques, they do not obtain process variance. Hence, Multiple Imputation of Chain Equations (MICE) is applied as a multivariate technique, as this technique uses the time series of other variables to obtain their variances to complete the series of missing data. Therefore, the relationships and correlations discovered in the previous stages are considered and time series are selected to fill in the gaps.

In this study, the linear regression model of the MICE technique was changed by machine learning models, specifically Bayesian Ridge, Decision Tree Regressor, Extra Tree Regressor, and K-Nearest Neighbors. In addition, all search engines were evaluated, and the method that best preserved the variance of the existing data was selected.

To define the imputation technique that best fits the time series gaps to carry out the following statistical tests, a normality test was performed to compare the results before and after imputation, and it was found that all filling techniques maintained the results after imputation. Therefore, another validation for evaluating padding adjustments is to compare the mean and standard deviation of the time series before and after applying the imputation technique.

2.3.5 Principal Component Analysis (PCA)

This method is used to define the most representative climate and quality variables and to define modeling scenarios that allow the prediction of dissolved oxygen using the variables identified as significant for each site in the previous analyses. PAC helps you interpret your data, in this case, simplifying the complexities of high-dimensional data while preserving trends and patterns. Considering that there were at first 21 variables, it was necessary to determine, which of these were the variables that dominated the dynamics of the dissolved oxygen interaction. For this, multivariate analysis is required to analyze the arrangement in which several interrelated quantitative dependent variables describe the observations.

Its goal is to extract the vital information from the arrangement, to represent it as a set of new orthogonal variables called principal components, and to display the pattern of

similarity of the observations, and the variables as points (Abdi & Williams, 2010). To ensure that each variable contributed the same proportion to the analysis, the time series were normalized. After that, PCA analysis was applied.

The first two components are extracted and analyzed to complete and define the scenarios for the prediction, considering that they are the components that contribute the most to the variability of the system. Since they explain more than 70% of the variability of the data.

2.3.6 Forecasting Model Vector Autoregression (VAR)

In the previous phases are identified the main climatic and water quality processes that determine the OD behavior, then these processes are linked through univariate and multivariate analyses until reaching the definition of the main Spatio-temporal processes of water quality and climatology.

Dissolved oxygen is predicted using vector autoregression (VAR), which generalizes univariate autoregressive models and allows the modeling of multivariate time series systems. Each variable is modeled through a linear equation, including its lagged values, the lagged values of the other variables, and an error term.

To forecast dissolved oxygen in the E3 and E7 stations, the VAR model is used in two scenarios. The first scenario consists of variables associated with the first component found in the PCA analysis, and the second scenario consists of variables associated with the first two components produced by the PCA analysis.

The selected time series were divided into training and testing sequences; this separation was done using the last two years (of the time series) for testing and the rest for training. The stationarity test was again applied to the training series to evaluate whether all the time series were stationary. If any series is non-stationary, according to the test, then the time series is differential in this case. The Akaike Information Criterion (AIC) is used to determine the order of the model (Hurvich & Tsai, 1991) and the predictability of the developed model is evaluated and validated using statistical indicators such as root mean squared errors (RMSE) and mean absolute errors (MAE). All statistical analyses and methods were performed using Python 3.8.

2.4 Results and Discussion

2.4.1 Data analysis a general Overview of the Reservoir Water Quality

The mean and standard deviation of the Time series for the dam (E7) was plotted in **Figure 8**. These visualization techniques show that outliers are negligible. The order of magnitude corresponds to the expected value for such a system, considering the case of the water quality series.

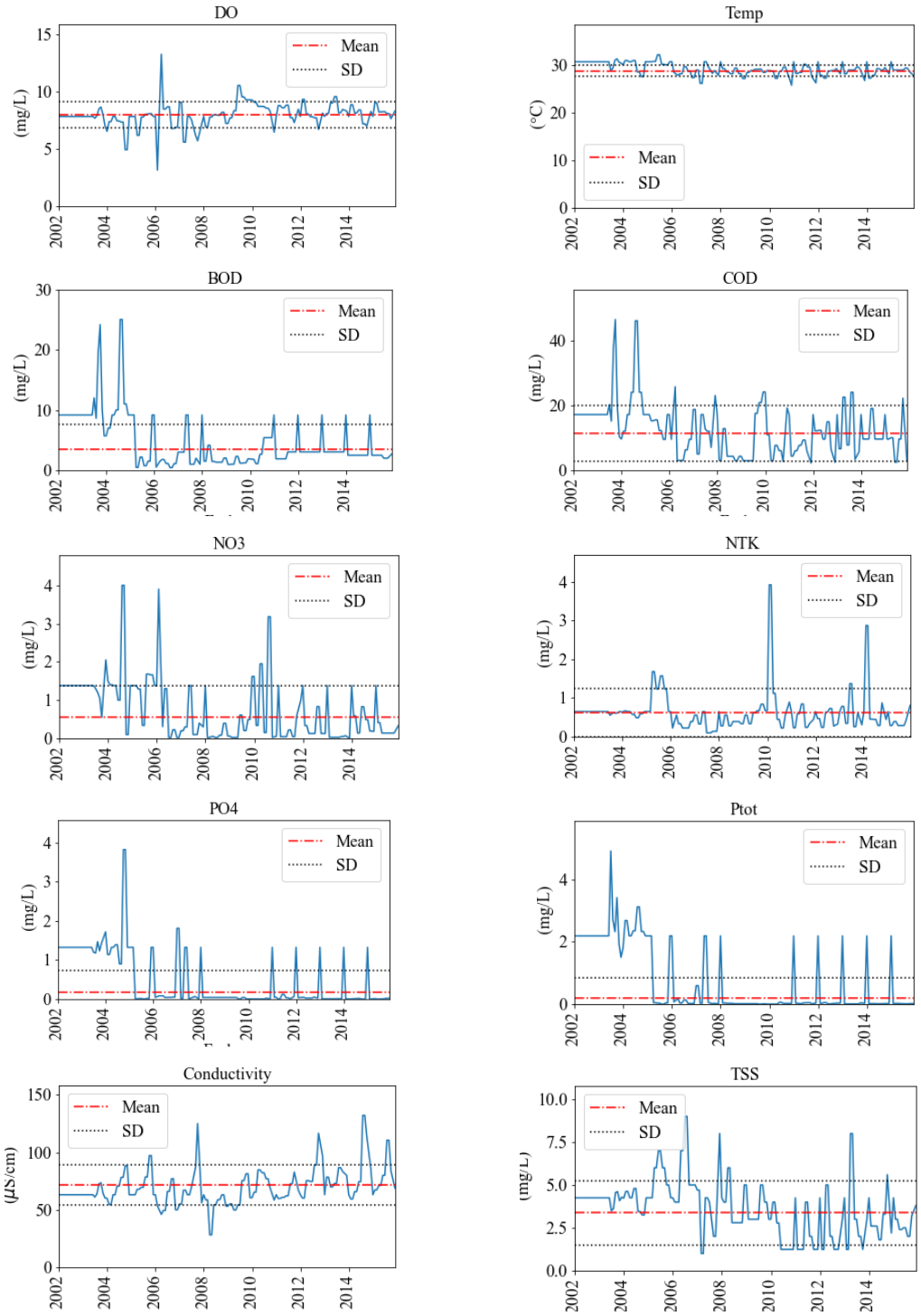

Figure 8 Mean and Standard Deviation of Water Quality Time Series at the Dam E7

In the case of water temperature, for both seasons, the lowest temperature was 23.4 °C. However, the highest temperature varied depending on the season, finding that the highest temperature was 32.8 °C for the dry season, and in the wet season, the highest temperature was 31.6 °C. It is also worth mentioning that the standard deviation does not exceed 1.2 °C. From these findings, it can be inferred that water temperature depends on water retention.

And solar radiation plays a decisive role in surface water conditions and is related to dissolved oxygen.

The dissolved oxygen levels measured at the water surface changed depending on the season for the maximum and the minimum values. For the dry season, the extreme values were 3.16 mg/l and 12.55 mg/l. For the wet season, the extreme values were 4.7 mg/l and 13.3 mg/l. The latter can be because the organic matter load is low, and turbulence is present during the rainy season. These findings are consistent with the low chemical oxygen demand (COD) observed, however there were not significant differences between seasons (p value= 0.16). For chemical Oxygen Demand (COD) revealed values between 1.0 and 11.8 mg/l for the dry season, and between 1.9 and 14.8 mg/l for the wet season.
For Biochemical Oxygen Demand (BOD) values were low, the measurements for the dry season and between 0.4 and 4.2 mg/l for the wet season, 0.6 and 8.9 mg/l, show higher loads for the rainy season, possibly due to sediment transport. All this, considering that COD and BOD are indicators of organic pollution of water bodies, in this case, low (Rangel-Peraza et al., 2009).

The study area has a low impact on anthropic activities. One possible reason that explains the observed loads can be the geological formation of the area. Finally, according to (Chapman, 2021), the observed COD concentrations in uncontaminated surface water are typically below 20 mg/l. Similar values for BOD are less than 2 mg/l for uncontaminated water. Based on these criteria, it implies that the water of "La Miel" hydropower has a low content of biodegradable organic matter and, in general, high dissolved oxygen levels.
The same behavior is observed for nitrogenous and phosphorous compounds for TKN. Measurements in the dry season are higher than in the rainy season. Average values between 0.26 and 0.28 mg/l and between 0.57 and 0.78 mg/l are observed for the dry season. The average values for the wet season are between 0.18 and 0.22 mg/l and between 0.52 and 0.57 mg/l. NO_3, PO_4, and TP describe similar behaviors. All mentioned nutrient values may be associated with good water quality and low nutrient content, in the reservoir, due to low TSS levels below 8.9 mg/L on average. Thus, it can be concluded that it is an oligotrophic reservoir.

These results showed that the year's season has a clear impact on water quality and DO throughout the reservoir. The latter indicates that the amount of rain or solar brightness that the system receives is vital to the reservoir's water quality and plays a vital role in dissolved oxygen behavior. On the other hand, the water quality variables that seem to have the greatest impact on dissolved oxygen are BOD, COD, and water temperature. In a smaller proportion, the nutrient is the most influential phosphate.

2.4.2 Temporal Variation of Water Quality Data and Hydrometeorology

The normality test results showed that none of the water quality time series described a normal distribution, which is why subsequent analyses were performed using nonparametric tests.

Four of the five monitoring stations showed changes points in water temperature. However, none of these changes coincided with the stations. In the case of nitrogenous and phosphorous compounds, all their chemical forms showed change points, but they did not coincide between compounds. On the other hand, dissolved oxygen and BOD showed change points in all stations and coincided with four of the five stations. From the latter, it can be inferred that changes in the processes, that affect them, affect the entire system.

On the contrary, COD showed change points in 3 out of 5 stations, but these changes did not coincide when the changes occurred. In addition, conductivity values showed that the change point at all sites and the date the change occurred were consistent with other water quality parameters, which, as expected, were previously influenced by other variables throughout the system. Finally, concerning water quality parameters, it is worth noting that the TKN did not show mean changes at any site. Therefore, this parameter was not affected by the processes that occurred in the reservoir throughout the years of measurement. In summary, the variables have a point of change and are related to changes in dissolved oxygen: water temperature, nutrients, BOD, and, a lesser extent, TSS.

Changes in hydro-meteorological variables, precipitation, flow, cloud cover, and evaporation occurred around the first half of 2005 and overlapped with the changes indicated by the water temperature at the dam site. Again, air temperature and relative humidity describe a change point, they are related to changes in dissolved oxygen.

Monitoring point E4 for water temperature showed an upward trend, and other monitoring points showed a downward trend.
Regarding nutrients, phosphorus compounds in all monitoring stations showed a downward trend, and nitrite in the study area also showed a downward trend. On the other hand, one station showed an increasing trend for nitrates(E3), and the rest of the monitoring site results showed a decreasing trend. On the contrary, ammonia showed a tendency in four stations (E4, E5, E6, and E7), describing an incremental tendency. All this allows us to infer that, although the amount of nutrients is low, the form of nitrogen available in water increasing is ammoniacal nitrogen, which, since it is not converted into nitrite to continue the nitrogen cycle, becomes a substance that generates pollution in the aquatic system.

COD and BOD showed decreasing trend effects in four stations (E4, E5, E6, and E7) and increasing trends in E3. However, dissolved oxygen showed an upward trend at all sampling stations. These results allowed us to presume that the surface water of the reservoir is evolving towards good aeration conditions. Conductivity shows similar behavior, as both parameters described dissolved solids. Conductivity shows an increasing trend in four sampling stations (E4, E5, E6, and E7). The latter behavior possibly occurs because this station is at the tail of the reservoir (E3), so as they belong to different basins, the quality characteristics come from different conditions.
In contrast, TSS showed a trend in four (E3, E5, E6, and E7) of the five sampling points, and this trend was decreasing, so this fact allowed us to see more clearly that the increase in free ions, that cause the increase in conductivity, is mainly related to the basin geology and not to inputs from suspended solids.

In brief, the trend analysis revealed that, in all monitoring stations, there is a decreasing trend for the parameters related to the nutrients of the system. Likewise, the fact that dissolved oxygen shows an increasing trend for all monitoring stations allows us to infer that the evolution of the study system tends to remain as a simple oligotrophic system. The water quality variables showed the greatest change over time, climate variables will not change significantly.

In addition, it is worth mentioning that there is no trend in evaporation, air temperature, flow, and precipitation. The sun's brightness and relative humidity showed a downward trend. These variables correlate in time with some slight changes in dissolved oxygen.

To determine the significance of seasonality on water quality and dissolved oxygen time series. Seasonality plays a significant role in the water quality state within reservoirs (Rangel-Peraza et al., 2009). The results of the Mann-Whitney U test denote that described seasonality, with intense periods every three months for water temperature ammonia and SST, Total Nitrogen, Phosphorus, BOD, and PO_4, six months for dissolved oxygen DO and COD, and twelve months for conductivity. The Levene test results contrast with the findings made before, where pH, TSS, NO_3, and TP were significantly different among seasons.

For all hydroclimate variables, the cycles show 6-month and 1-year cycles, which vary between dry and rainy seasons. This shows its main relationship with nutrients and TSS.

At this point, it was possible to establish to temporally the processes affecting dissolved oxygen fluctuations. Considering BOD, COD, water temperature, air temperature, solar brightness, relative humidity, and precipitation are key parameters of DO.

2.4.3 Spatial variation of water quality e hydrometeorological data

The results of the Kruskal-Wallis H-test, spatial analysis considering the arms of the reservoir. Significant differences were measured in DO, conductivity, NO_3, TSS, and water temperature for the principal arm between stations E3 and E5. Likewise, significant differences were measured on the other arm of the reservoir between stations E4 and E6 for DO, TP, and Water Temperature. At last, tail monitoring points were assessed at the dam site. It was come to know that: between stations E3 and E7, significant differences in conductivity, NO_3, pH, TSS, and WT were observed. On the other hand, between stations E4 and E7, significant differences in ammonia, DO, TP, and water temperature were noted. These findings confirm that Water Temperature is significantly different among all monitoring stations. Furthermore, conductivity, NO_3, and TSS are significantly different through the "La Miel river" arm and dam site, as DO and TP are significantly different through the "Moro river" arm.

The results of the Kruskal-Wallis H-test, hydroclimatological spatial analysis considering the arms of the reservoir. Significant differences were not founded in the flow discharge, precipitation, solar brightness, humidity, and air temperature for the principal arm between stations E3 and E5. Moreover, no significant differences were measured on the other arm of

the reservoir between stations E4 and E6 for all hydroclimatic variables. Tail monitoring points were assessed at the dam site. Between stations E3 and E7, significant differences in precipitation. And between E4 and E7 flow discharge is significantly different.

Using this technique, it was determined that the arm (E3) and the dam (E7) were the sites that better represented changes in water quality and DO. This implies that spatially important processes occur at E3 y E8.

2.4.4 Correlation of water quality and hydrometeorological seasonal data

In previous analyses, attempts were made to interpret the time series results and analyze spatial-temporal behavior that was important to predicting dissolved oxygen. A correlation analysis was performed to determine the direct relationship between water quality and hydro-meteorological data. Relationships which not demonstrated in the previous steps were done using this statistical technique, and for this analysis, the series was split between dry or wet seasons.

To gain an initial understanding of the complete monthly dataset relationships, Pearson, Kendall, and Spearman's methods were applied. Considering that the Spearman test is an appropriate tool for this type of assessment, as it targets non-normal data, allowing us to identify variables with better associations between them. The wet and dry season correlation matrices for all monitoring sites were produced.

For the analysis of the results, the correlations discovered between absolute values of 0.0 and 0.39 were considered weak or negligible. In contrast, the correlation between absolute values 0.4 and 1 is considered moderate or intense so the latter will be the correlation considered in the following analysis (Schober, Boer, & Schwarte, 2018).

The study revealed that whether it is the dry season or rainy season, the variables with the highest correlation coefficient are water quality variables among themselves. So then, there is a specific relationship between hydro-meteorological variables and water quality variables. In addition, the correlation in the dry season is more significant than that in the rainy season.

Moving on to a more specific analysis of the relationship between water quality and hydrometeorological variables, it was found that the most recurrent relationship in the sampling sites was between precipitation and conductivity for the dry and wet seasons, lacking only at the E3 site. This relationship is also noticed by (Ricardo et al., 2016)), and (Zhang et al., 2018), described as a possible consequence of runoff and soil type around the reservoir. Precipitation is also associated with nitrogen and phosphorus compounds, especially during the dry season, as studied by (Branco et al., 2019), showing that lower precipitation leads to increased nutrient concentrations due to lower dilution. In the same way, precipitation and air temperature were correlated with the water temperature at sites E6 and E7 behavior. These can be explained because these sites have the lowest surface water movement and the largest surface area in contact with the atmosphere. Lastly, another striking correlation was the one between solar brightness and PO_4 found for the dry season of stations E3 and E5, a link that was also found in (Li et al., 2019); (Yang et al., 2020)

highlighting the impact of solar radiation on phosphorus concentration in continental water systems.

The results described in the previous analyses showed correlations between water quality variables and hydro-meteorological variables. It asserts at this point and with these statistical methods and taking into consideration seasonal variations that the hydro-meteorological variables to be considered for accurate predictions of dissolved oxygen data are precipitation, flow discharge, relative humidity, air temperature, and solar brightness. And water quality parameters: water temperature, BOD, COD, and PO_4.

2.4.5 Data imputation, filling the water quality series with missing data

The results of the comparison of the different gap-filling methods at the five stations are presented in **Table 2**. These results are shown, where the best is near zero.

Table 2: Delta Mean and Delta Standard Deviation of Imputation Techniques for Each Station

Method	Mean Delta					Standard Deviation Delta				
	E3	E4	E5	E6	E7	E3	E4	E5	E6	E7
Linear	0.9	0.11	0.3	0.4	0.2	1.24	1.64	1.1	1.46	1.28
Bayesian	0.1	0.18	0.25	0.04	0.14	1.34	1.66	0.89	1.48	1.18
KNN	0.56	0.5	0.5	0.26	0.45	1.16	1.45	0.95	1.37	1.13
Extra Tree	0.22	0.24	0.16	0.33	0.97	0.98	1.42	1.03	1.41	0.99
DTree	0.8	0.29	0.21	0.5	0.7	0.59	0.46	0.33	0.26	0.33

Comparing the means between the initial series and the filled series, 0.06 for linear regression, 0.14 for Bayesian regression, 0.38 for Extra Tree regression, 0.45 for K-Nearest Neighbors, and 0.5 for Decision Tree regression. Shows better results for linear regression and Bayesian.

Comparing the standard deviation values between the initial series and the filled series, it is 1.34 for linear regression, 1.31 for Bayesian regression, 1.17 for Extra Tree regression, 1.21 for K-Nearest Neighbors, and 0.3 for Decision Tree regression. Shows better results for Decision Trees and Extra Trees.

Evaluation of the results of imputation techniques showed that MICE techniques estimated by machine learning methods achieved better results than mean, linear interpolation, or linear regression methods. And the estimator A Decision Tree regression was found to be a better estimator for the imputation process for missing data on water quality according to the metrics.

2.4.6 Principal Component Analysis (PCA) of water quality e hydrometeorological data

The results of applying the PCA in all water quality sampling stations revealed that it is possible to explain more than 70% of the accumulated variance of the data with only six principal components, which allowed for reducing the dimensionality from 9 selected in the previous steps to 6 dimensions.

In addition, it was learned that the more significant variance at each monitoring point of the time series is due to the first principal component, which changed as a function of the location of the station in the reservoir, showing that for E3 (First tributary La Miel river), which is the most upstream monitoring point of the reservoir, the first principal component was composed of hydro-meteorological variables like precipitation, flow, and air temperature, for points E4 (First tributary Moro river) and E5 (second tributary La Miel river) The first component is a mixture of climate and water quality variables, such as precipitation, air temperature, PO_4, and water temperature.
On the other hand, for points E6 (Second tributary Moro River) and E7 (dam), the first principal component consists of water quality variables such as PO_4, NO_3, BOD, COD, and water temperature, as shown for stations E3 and E7 in Figure 7 Where, which displays the differences.

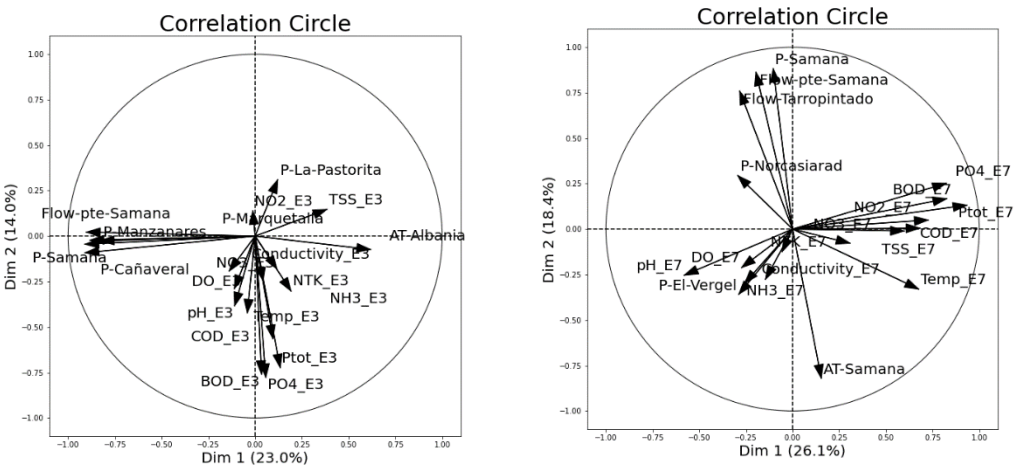

Figure 9 PCA Circle Plot for Stations E3 And E7

These results allow us to infer that the main drivers of the processes change depending on the location within the dam, being the upstream reservoir processes driven by meteorological variables, and as the location of the processes approaches the dam point, water quality variables take center stage as the main drivers of the processes in the reservoir.

The results also show that, for all monitoring stations, the water quality variables associated with the first or second principal component, depending on the location of the monitoring point in the reservoir, are PO_4, BOD COD and NO_3. Likewise, precipitation and currents at the Samaná sampling were the hydro-meteorological parameters that had the most significant impact on the first or second principal component, depending on the location of the monitoring points in the reservoir. Another important aspect highlighted from the PCA results is the TSS itself, as a single principal component. Therefore, it can be concluded that

the variance associated with SST is not related to any other climatic or water quality variables. Finally, it is observed (Figure 7) that the decrease in dissolved oxygen depends on the parameters of the first component for E3 and E7.

2.4.7 Dissolved Oxygen Prediction Model Based on Vector Autoregressive (VAR) technique

To perform VAR analysis to forecast dissolved oxygen in monitoring sites, E3 and E7, the PCA results were used as input to create the predictive model case, knowing that, at this point, all previous analyses allowed us to understand which variables were the main drivers of the reservoir process in Spatio-temporal context.

Two cases were implemented for the two monitoring sites, applying the variables from the first component of the PCA analysis and, in the other case, applying the variables from the first and second components. For site E3, Precipitation and Flow for Case 1 were selected, and for Case 2, the variables mentioned and BOD, COD, and PO_4 were selected. A site E7, the water temperature, BOD, COD, and PO_4 was selected for case 1, and for case 2, the variables mentioned as well as precipitation and air temperature were selected. Finally, after selecting the time series, splitting them into training and test data, leaving 5 years as test data and the rest as training data, the optimal model order was selected using the Akaike Information Criterion (AIC) by equating the maximum lag order to 14, to select the right order of the VAR model, we iteratively fit increasing orders of VAR model and pick the order that gives a model with least AIC, as is shown in **Table 3**.

Table 3: Performance Indicators of Var Predictive Model for Each Case

	Case 1	Case 2	Case 1	Case 2
0	17.06	20.58	5.104	13.29
1	16.79	20.65	5.274	13.35
2	16.23	18.94	4.438	12.09
3	16.3	19.22	4.53	12.29
4	16.0	18.57	4.348	11.9
5	15.98	18.71	4.553	12.24
6	15.82	18.52	4.402	12.03
7	15.76	18.44	4.583	12.06
8	15.6	18.12	4.489	11.79
9	15.63	18.27	4.403	11.19
10	15.48*	18.01	4.411	10.49
11	15.56	18.15	4.3	10.17
12	15.67	18.05	3.806*	8.494*
13	15.63	17.79*	4.009	9.088
14	15.67	17.9	3.936	9.432

Table 4 shows the performance metrics for the two cases at each site. It is shown that for station E3, and its case 1, an RMSE of 1.03 was found. For case 2, an RMSE of 2.04 was obtained, which is why it is considered that both models had a good performance in predicting dissolved oxygen. However, it could be inferred that for this station, a model based only on hydro-meteorological variables obtains a better approximation than a model where, in addition to the hydro-meteorological variables, water quality variables are included. Additionally, monitoring site E7, **Table 4** shows that for case 1, an RMSE of 0.84 was found, and for case 2, an RMSE of 2.09 was obtained.

Table 4: Performance Indicators of Var Predictive Model for Each Case

Case 1 Station E3		Case 2 Station E3		Case 1 Station E7		Case 2 Station E7	
Forecast Accuracy	DO	Forecast Accuracy	DO	Forecast Accuracy	DO	Forecast Accuracy	DO
MAPE	0.10	MAPE	0.21	MAPE	0.08	MAPE	0.21
ME	0.11	ME	0.52	ME	0.51	ME	0.32
MAE	0.79	MAE	1.66	MAE	0.68	MAE	1.69
MPE	0.03	MPE	0.04	MPE	0.06	MPE	0.03
RMSE	1.03	RMSE	2.04	RMSE	0.84	RMSE	2.09

As a result, although the metric results show that the model produces a good approximation, in this monitoring site, there is a significant difference between the performance metrics, indicating that Case 1 provides better prediction results than Case 2.

The behavior described by the performance metrics is also reflected in the graphs as presented in **Figure *10***, where for the monitoring site E3, the two cases present a similar forecast between them with minor differences. In case 2, the model better reproduces the variability of the system because it has more input variables but fails to improve the forecast compared to the results of case 1. Conversely, for monitoring site E7, it is observed that case 1 presents a better fit than case 2, showing for case 2 that the forecast values are above the expected mean values. Even though it well reproduces the variability of the series, in case 1, the variability also approaches the expected variability and, at the same time, yields values that are within what is expected.

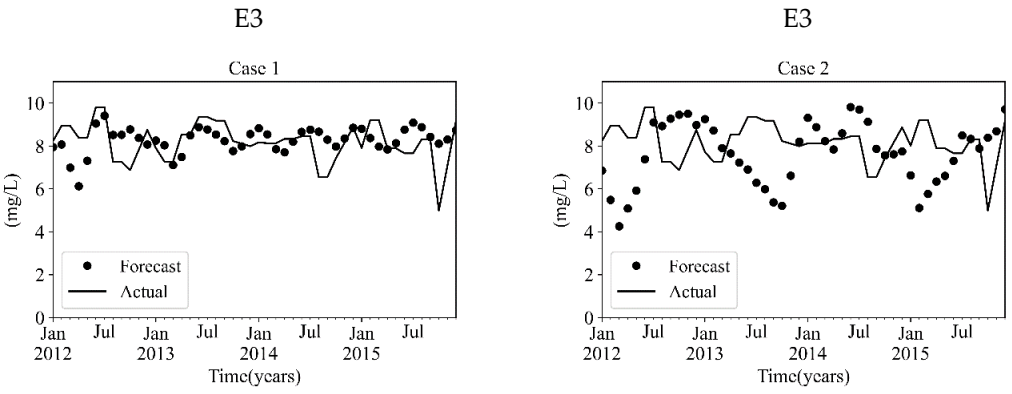

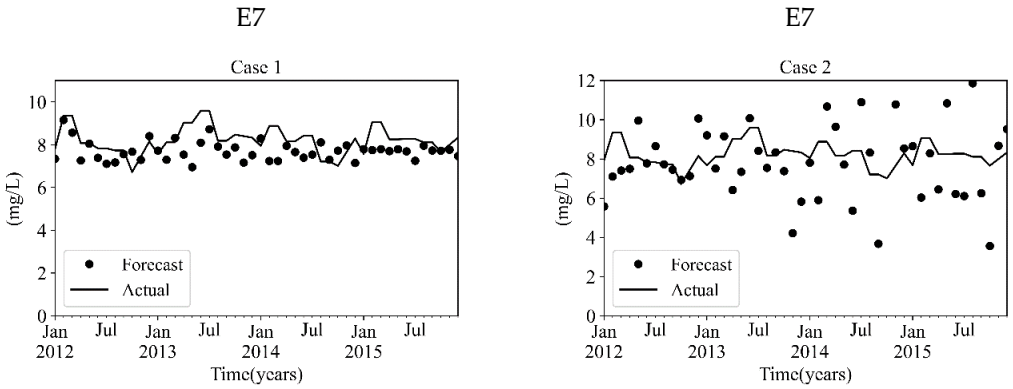

Figure 10 Case 1 and Case 2 Var Models for Stations E3 And E7

The model evaluation demonstrated that DO can be predicted as a function of precipitation and flow discharge in the E3 station and terms of air temperature, water temperature BOD, COD, and PO_4 in the E7 station.

2.5 Discussion

This study used various statistical tests to analyze water quality and hydroclimatological aspects and to forecast dissolved oxygen on a monthly basis. Since the selection of an appropriate set of input variables from all possible input variables during The VAR model development is important for obtaining a high-quality model. Many of the described methods for input variable selection are based on heuristics, expert knowledge, statistical analysis, or a combination of these. However, although there is a well-justified need to consider input variable selection carefully, there is currently no consensus on how to accomplish this task (Ranković et al., 2012). For this reason, it is imperative to correctly predict using multivariate statistical techniques and to assess spatiotemporal water quality and hydroclimate variables to select them appropriately.

In this study, exploratory data analysis was used to aid what variables should be used. Doing so, allowed a better understanding of the underlying process occurring in the basin that affects reservoir water quality and DO.

The input variables analyzed in this paper were: Temperature, pH, total suspended solids, dissolved oxygen, conductivity, chemical oxygen demand, biochemical oxygen demand, ammonia, nitrite, nitrate, total Kjeldahl nitrogen, phosphate, Total phosphorus, as well discharge, precipitation, solar brightness, evaporation, relative humidity, cloudiness, and air temperature. The number of total variables was 20 for 5 water quality stations in the reservoir. Throughout the process, variables were refined, and concluding that only 6 were the most appropriate for the prediction of dissolved oxygen and that a monthly period in two (E3 and E7) of the 5 stations in the reservoir could well represent the spatial and temporal dynamics of dissolved oxygen in the tropical reservoir. It was concluded that DO can be predicted as a function of precipitation, flow, air temperature, water temperature, BOD, COD, and PO_4.

Furthermore, as mentioned in (K. Chen et al., 2020) and (Yaseen et al., 2018), while the selection of variable key parameters for prediction is essential, there is clearly a need for reservoir zoning in addition to this. The latter allows refinements to improve the

performance of metrics and forecasts, as shown in case 2, where the performance did not improve. Identifying two dissolved oxygen dynamics related to the location of the reservoir stations, one in the tail E3 and the other in the reservoir vessel E7.

Other studies have found that water temperature, photosynthesis, respiration, and BOD ((Rajwa-Kuligiewicz et al., 2015),(Rajwa et al., 2014) seasonal variation, (Lliev & Hadjinikolova, 2013) air temperature and nutrition (Dordoni et al., 2022), are variables that affect dissolved oxygen.

Referring to the original hypothesis, it was found that variables such as water temperature, organic matter decomposition, and COD were indeed important succeeded by phosphates to changes in dissolved oxygen concentrations. And that these are the correct inputs for the prediction of dissolved oxygen in a tropical reservoir. However, nitrogen compounds, conductivity, pH, and suspended solids did not show much correlation in this investigation.

It was previously known that different climatic conditions and temperatures were the basis for determining DO dynamics, and this study also involved precipitation and flow discharge as fundamental variables for predicting DO.

Although climatic variables and chemical interactions should indeed be considered together for the prediction of dissolved oxygen, they should also be explored for future work, other variables such as water levels, wind speed and direction, relationships with geologic conditions, soils, and biological processes, since in this study due to the scarcity of information in these areas it was not possible to carry them out. Likewise, consider changes at finer scales than monthly, for example, consider the dynamics of oxygen at an hourly resolution.

Compared to current models, the power of VAR is a systematic yet flexible approach to capturing complex real-world behavior and exhibits better predictive performance as well as the ability to capture the interwoven dynamics of time-series data (Aptech, 2021) (González, 2019). For the VAR model, splitting the series into two groups, was sufficient to obtain high prediction rates.

In this study, it was evident that the VAR statistical tool has great potential, although its use is incipient in water quality analysis in reservoirs. For this reason, more research on this topic should be done. The results of this study can be compared with the results reported in the literature.

Future works will be important not only to the link between parameters but taking into consideration other statistical methods and do a comparison between knowing the Spatio-temporal processes that affect dissolved oxygen behavior in tropical reservoirs.

After all, accurate prediction of dissolved oxygen may provide a cost-effective solution to prevent water quality crises in a tropical reservoir. The models and methods presented here can be applied to dissolved oxygen prediction in other tropical ecosystems such as lakes and rivers.

2.6 Conclusion

This study applied a methodology that allows a determination of the behavior of hydro-meteorological and water quality variables in tropical reservoirs and establishes the relationship between water quality parameters and hydrometeorology to predict dissolved oxygen. Statistical tests and analysis showed a statistically significant influence of hydro-

meteorological variables like precipitation, flow discharge, relative humidity, solar brightness, and air temperature over water quality parameters, especially with nutrients, and dissolved oxygen. These analyses also showed that, as the relationship between water quality and hydro-meteorological variables varied from site to site, therefore the behavior of water quality parameters is influenced by the area within the reservoir.

When applied to water quality data analysis and prediction, nonparametric procedures have several advantages over parametric procedures. Some of these advantages are: 1) prior transformations are not required, even when approximate normality could be achieved, 2) normality for water-quality data is not required, 3) comparisons are made between central values such as the median rather than the mean; and finally, 4) data below the detection limit can be incorporated without fabrication of values or bias. So, the information contained in less-than-values is accurately used, not misrepresenting the state of that information. Furthermore, its ability to handle missing values, outliers, and its capacity to update, makes it ideal for prediction.

Descriptive statistical analyses are performed by separating the time series according to the climatic seasons showing significant differences between the dry and wet seasons. Similarly, the correlation analysis results of each season show that the reservoir is affected by seasons, and the influence of meteorological variables in the dry season is more evident than that in the rainy season. Therefore, this funding increases the metrics for DO predictions.

Only the variables that are part of the first principal component are recommended for DO forecasting. The combination of more components creates noise that reduces the quality of forecasting.

Due to the spatial and temporal heterogeneity of water quality in a tropical reservoir, water quality monitoring should be designed to capture the temporal dynamics close to dams' inlets to predict dam water quality. This finding suggests that designing and maintaining effective reservoir water quality monitoring is key to sustainable management and prediction.

It is essential to begin analyzing and modeling the environmental impacts of large dams more holistically to better inform stakeholders and decision-makers on the balance between exploiting hydropower potential and maintaining critical natural resources.

Chapter 3

3 Analysis of different hypotheses for modelling air-water exchange and temperature evolution in a tropical reservoir

*The results of this chapter have been accepted and will be published in the Journal of Water & Climate Change, 2024.

Abstract: This study presents an analysis of air-water exchange in a Colombian tropical reservoir. A coupled thermal-three-dimensional (3D) hydrodynamic model using TELEMAC-3D and WAQTEL is implemented to evaluate the dynamics of thermal processes in the reservoir. A sensitivity analysis is carried out on various modeling parameters, such as turbulence models, temperature diffusion coefficients, and heat exchange at the free surface based on observations. In particular, three different approaches have been tested to study the impact of air-water exchanges at the free surface: a constant water temperature, constant meteorological forcing and time-varying meteorological forcing. All the simulations correctly represent the constant heating at the free surface for the first meters. However, no simulation has been able to correctly reproduce the amplitude of temperature oscillations in the surface layers: only the simulations with time-varying meteorological forcing show temperature oscillations, but their amplitude is greatly overestimated. Eventually, the analysis shows that the most crucial parameter for a correct representation of the observed temperature behavior are the heat exchange coefficient and the wind. The different approaches tested all have limitations, but they can reproduce reservoir temperature trends at different depths with a maximum standard deviation ranging from 3°C to 8°C.

Keywords: 3D numerical model; thermal processes; heat exchange; tropical reservoir; water quality

3.1 Introduction

The construction, operation, and removal of large reservoirs is a fundamental environmental issue because of the benefits they generate and the environmental impact they have. Hydroelectricity production accounts for 16% of total energy production (Killingtveit, 2019), but in the American continent, it is the largest source of energy production. In addition, they have essential functions such as supplying water to cities, irrigation, and energy. While these dams have brought some benefits, they have also brought severe and irreversible changes to the natural hydrology of the river, affecting soil, vegetation, biodiversity, landscape, atmosphere, and, in turn, watersheds (Agostinho et al., 2008), reducing water flow, increasing water residence time, thermal stratification, increasing sedimentation rates and decreasing dissolved oxygen concentrations, among others (Pimenta et al., 2012).

The impact on reservoir water quality is a significant concern in ecological management. Life quality is highly constrained by water quality, which is affected by the quality of reservoirs built for hydroelectric projects and water supply. Building dams is particularly important for many Latin-American countries, where most of the electric supply comes from hydropower and many reservoirs. Thermal stratification caused by solar heating plays a significant role in determining water quality in the reservoir. In tropical countries, lakes and impoundments will stratify during the year as a result of increasing temperature differences between the warm upper (epilimnion) and cold lower (hypolimnion) layers of water (Halini Baharim et al., 2011). Air Temperatures can vary by up to 10°C from day to day, with water temperatures ranging from 20 to 32°C.

Temperature studies in reservoirs have ranged from field measurements to computer tools, such as modeling. In the case of tropical reservoirs, from a data analysis and statistical point of view, research focuses on 1) describing and characterizing thermal distribution by field observations, such as the characterization of the stratification pattern and affectation of these thermal regimes in response to climate variables; 2) reservoir biochemistry and aquatic biology and the relations between them.

In Labaj et al. (2018), a data logger recorded temperature profiles hourly and measured every 2 m at a point at a maximum depth of 30 m in four lakes in Ecuador. They observed that thermal stratification was significantly positively correlated with air temperature and negatively correlated with wind speed across all lakes, and the most critical finding was that the high-resolution data showed that stratification did not break down overnight. In Lewis (1996), a theoretical comparison of the characteristics of several tropical and temperate lakes was carried out. The main finding of this study was that the comparison of tropical and temperate lakes has excellent potential to demonstrate lake function in general and is typified by non-seasonal substantial variations superimposed on seasonal cycles in most cases. Elçi (2008) studies the effects of thermal stratification and mixing on reservoir water quality at one point in the reservoir over 14 days using a water-quality meter. Multivariate analysis was carried out on a data matrix of seven variables. Their results showed that air temperature, lagged wind speed, and humidity influence variations in water-quality parameters. In Rangel et al. (2009), temperatures are measured with a portable digital meter, in two main climatological seasons: cool-dry season and warm-rainy season, at a central reservoir point, at the surface, 1.5 m, 2.5 m, and 4m. The main finding of this study was that the thermal pattern strongly influenced the vertical distribution of the

phytoplankton community. Pajares et al. (2017a) observed that temperature and oxygen stratification shaped the distribution of picoplankton. In Huszar et al. (2006), the data set includes 192 aquatic systems sampled on seasonal bases for at least one year using average values. They found significant differences in nutrient-chlorophyll ratios and thermal profiles between tropical and temperate climates. C. A. Amorim et al. (2020) monitor ten reservoirs in Brazil to study cyanobacterial blooms. They demonstrated that omnivorous crustaceans and total dissolved phosphorus mainly influenced cyanobacterial biomass. Solar radiation, air temperature, mixing zone and salinity also significantly explain biomass behavior. These studies highlight the importance of thermal stratification as one of the main factors affecting variation within the water column of tropical lakes. However, in evaluating the thermal structure of the reservoir through data analysis, it is difficult to measure and verify the quality of the data, and it is difficult to propose an analysis and management scenario.

From a numerical point of view, 1D (one-dimensional) lake models have been built (Samal et al., 2009; Katsev et al., 2010) to assess ecosystem health, giving daily information at one-point, and at a depth interval of 0.5 m for three years daily. They observed that the changes in the stratification regime in these waterbodies affect the water quality and the ecosystem's health, primarily based on temperature and dissolved oxygen parameters. In Crowe et al. (2008), one monitoring station is used to examine the chemical composition of the water and estimate transport time scales in reservoirs; the main finding was that seasonal temperature variability affects biogeochemical cycling in lakes. Rueda et al. (2006), using 15 temperature and light profiles taken in the reservoir throughout one year, show that the temporal variations of mean residence times occur not only at seasonal time scales but also at shorter scales. Several 2D (two-dimensional) models have been built to characterize thermal stratification and assess water quality. In Rangel-Peraza et al. (2012) and Lindenschmidt et al. (2019), with monthly measurements, showed the influence of climate-change on water quality reservoirs. Mesquita et al. (2020), Basso et al. (2021), Azadi et al. (2019) modeled and analyzed different scenarios that could cause eutrophication processes using monthly measurements. Ziaie et al. (2019) and Chuo et al. (2019) found significant differences in nutrient entrance and the relationship with algae blooms with monthly measurements. However, most works have analyzed the water quality and thermal dynamics without considering 3D (three-dimensional) processes.

1D and 2D models have the advantage that they are much faster than 3D ones when performing numerical calculations; they allow long-term simulations and are easier to calibrate and validate as they depend on fewer parameters. For example, the 1D model revealed daily air and water temperature relationships but failed when the advective term was significant. It also fails to quantify the potential effects of climate change on water temperature in a shallow reservoir (Gooseff et al., 2005). Note that this approach cannot predict stratification dynamics. A 2D model is essential for studying stratification dynamics subject to horizontal advection. Even though 1D and 2D models can consider short and long-wave radiation in the thermal model, heat flux by evaporation/condensation, and the convection process at the free surface, they cannot capture the processes of heat exchanges with both the bottom and atmosphere, while the 3D does. Besides, the turbulence models have been demonstrated to be important in maintaining the thermoclines and are fully developed only for 3D models (Goudsmit et al., 2002).

In the case of 3D models, phenomena at multiple scales and couplings can be modeled. Other 3D flows, including gravity current, significantly affect the water quality and temperature (Kopmann & Markofsky, 2000). In complex geometries with highly three-dimensional flows, the more traditional depth or width-averaged models cannot accurately capture mechanisms affecting temperature transport and mixing (Politano et al., 2008a). Overall, 3D modeling tools are critical to understanding the interaction between all aquatic ecosystem components. 3D modeling enables a better assessment of the high complexity of the reservoir and its natural cycles.

Regarding 3D modeling, there are several studies for shallow reservoirs, such as: study of the influence of cold fronts on the heat fluxes and thermal structure in a tropical reservoir (Curtarelli, 2013), study of the circulation patterns in a shallow tropical reservoir (Yang et al., 2019), study of saline intrusion (Laval et al., 2005). However, while numerous studies have been conducted to characterize thermal stratification in temperate lakes and oceans, there have been fewer numerical studies of temperature dynamics in tropical reservoirs (Politano et al., 2008a).

3D modeling has proven to be a valuable tool to advance the understanding of the physical processes of fluid dynamics and water quality, thermal processes such as the effects of wind and temperature induced flow (Matta et al., 2017), the effect of the wind and tidal forcing (Moloney et al., 2016), thermal discharge released to coastal areas (Gaeta et al., 2015, 2020a), coupling with complex water quality process (Piccioni et al., 2021). It has also been used to assess environmental impacts from cooling and heating power plant production (Ligier & Okumura, 2019), to analyze flood and ebb events and analyze indicators of the contamination degree (da Silva et al., 2021), to evaluate E coli development scenarios (Bedri et al., 2013), to study the dynamics of geomorphological features (Lisboa & Fernandes, 2015), or the heating impact of a reservoir on downstream water temperature (Jiang et al., 2018; Plec et al., 2021). However, all these simulations have been performed without heat exchange with the atmosphere and not for tropical reservoirs.

Other 3D models use a simplified heat exchange model (Scanlon et al., 2020) to assess the climate change scenario's impact over a small tropical lake (Duarte et al., 2021), to evaluate the impact in coastal areas, simulate flooding and hydrodynamic patterns in wetlands (Costi et al., 2019), and to study thermosaline circulation in an estuary (Vouk et al., 2019). However, as explained by Politano et al. (2008b), these studies are not performed on tropical reservoirs, and other 3D models have been developed to use the entire Atmosphere-Water Exchange considering hydrometeorological conditions (Angelotti et al., 2021) but without complex geometry.

Some recent studies assessed the effects of the advection schemes and turbulence and other important numerical parameters with salinity as a tracer on 3D models (Justin-Brochet et al., 2021 ; Smolders et al., 2015 ; Chen, 2020), to evaluate the non-hydrostatic 3D model in rivers (Politano et al., 2008b), optimize numerical parameters in 3D models for the calibration in small lakes (Merkel, 2019), or coastal areas (Cooper & Spearman, 2017 ; Gaeta et al., 2020b), but they were not used to analyze those conditions in a stratified deep tropical large reservoir with spatiotemporal data of high frequency for calibration.

Complex reservoirs such as deep tropical lakes, with elongated heterogeneous basins, with the influence of several rivers or advective flows (Marín-Ramírez et al., 2020), are vertically complex systems, making difficult both the building and the implementation of a model

that correctly represents the thermal structure.

This is important because this work uses mathematical models to describe the complex exchange between air and water thermodynamics in tropical reservoirs, through computer simulation as an application of environmental software. Tropical temperature and radiation conditions play an important role in reservoir ecological processes for sustainable management of water resources and, in particular, decision support systems for climate change assessment. Ecological impacts can be known and action plans can be more comprehensive.

This study allows for a better understanding of the use of these full 3D tools, as there is not much practice at these scales (spacetime) in the topic of tropical thermodynamics. This allows the improvement in the understanding of the mathematical equations that has been used until now. It allows the analysis of air-water transport phenomena from a holistic perspective.

In this sense, the present work emerges as a response to integrating a robust water quality model that studies the effect of hydroclimatological variables such as air temperature, wind, and internal mixing process on the thermal dynamics of a tropical reservoir in Colombia, using highly resolved simulations of hydrodynamic, thermal, and energy processes. The importance of these processes has been demonstrated by data analysis from the observations of La Miel reservoir (Alzate-Gómez et al., 2023).

Based on the context discussed here, the study analyzes thermal dynamics over the vertical water column in a tropical reservoir. The objective is to analyze different modeling hypotheses for temperature and air-water exchange and evaluate the model performances on short periods according to the observations. Section 3.2 outlines the characteristics of the study site. Then, section 3.1 presents the available data. Section 3.2 describes the governing equations, and Section 3.3 details the model that has been implemented along with the performance criteria. Finally, Section 3.4 describes the results, and a discussion of the main findings is given in section 3.5.

3.2 Description of the study area

The study comprises the Amaní Reservoir, formed by the La Miel, Moro, and La Negra rivers, a hydroelectric power plant in Caldas, Colombia. La Miel river basin is in the Central Mountain range of the Colombian Andes, specifically in the Caldas department. The river reaches being studied have a length of 62 km and an upstream catchment area of 712 km2. In this area, La Miel has a variety of tributaries, including Tenerife, Salado, Manso, Moro, Pensilvania, and Samaná, among others, see as shown Figure 9.

"La Miel I" dam is a gravity dam located on the riverbed (see Figure 9) and was built between 1997 and 2002 for hydroelectric power generation. The tropical reservoir Amani (5.25° lat, -75° lon) is upstream of the dam. The dam is 188 meters high, giving it a storage capacity of 571 million m3 and a surface area of 12.2 km2 with a generation installed capacity of 396 MW in three turbine units. Its commercial operation began in December 2002. In 2010 the Guarino diversion dam on the Guarino River was opened, and the Manso diversion dam on the Manso River began operations in 2013. Both divert water into the" la Miel I" Reservoir through a tunnel.

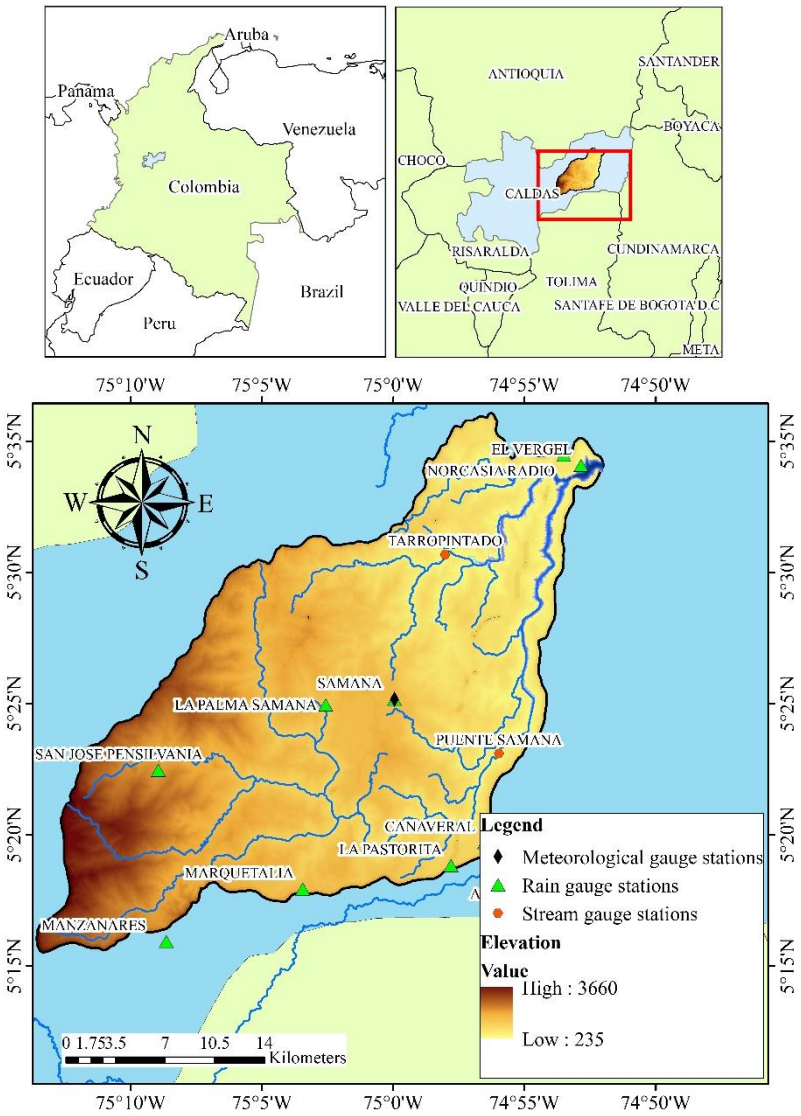

Figure 11 Study Area location and gauging stations (Accessed through ASF DAAC July 15th, 2015).

The reservoir is located in a deep canyon and comprises two main branches: the La Miel River, 20 km long, and the Moro River, 13 km long. The maximum width is 400 m near the dam. A tiny branch is also formed by the creek Santa Bárbara, a tributary of the Moro River, the location of which is shown by the stream point in Figure 11. Amaní reservoir presents permanent thermal stratification, although its thermal structure shows seasonal variations (rainy and dry periods), with daily changes.

Analyzing the data from the meteorological measuring stations described in section 3.1 Field Data and the Monitoring System, the average temperature is 25.3°C, the maximum temperature is 33°C, and the minimum is 18°C. The highest monthly evaporation rates occur in the dry season, with 188 mm/day, while the lowest evaporation rates occur in the wet season, with an average of 56 mm/day. Relative humidity varied between 40% and 100%, with a mean value of 80%.

The annual cycle of rainfall in the area presents a bimodal behavior, with maximum flows in November-December and March-April and recession in July-August and January-February, with the recession in July-August being considerably more substantial. The

lowest precipitation values occurred in July at 122 mm and the highest in October and November with values of 416 mm. The average flows of the La Miel and Moro rivers at the Puente Samaná and Tarro Pintado (see Figure 9 stream points) gauging stations are close to 50 m3/s and 20 m3/s, respectively (estimates made with data from 2003 to 2016).

3.3 Materials and methods

In this work, high-frequency field data were used, 3D simulations were performed, and the former was compared with the latter. The data needed for the implementation of the model are analyzed, the mathematical equations and their implications for the modeling are analyzed, and the model configuration is adjusted accordingly as a basis for the understanding of the thermal dynamics. The hydrodynamic model is calibrated according to the observed data and the error is quantified using metrics. Then, the model responses to different thermal forcing are analyzed and the results are compared with the observed data.

The materials and methods used for this purpose and the specifications for each stage are explained in Sections 3.1, 3.2 and 3.3.

3.3.1 Field Data and the Monitoring System

The monitoring system comprises water quality measurements at five stations, of which only the E7 station next to the dam will be used, in addition to thermistor chains and CTD (Conductivity Temperature Depth) instruments. For the same period, five hydrological parameters (flow rate, precipitation, evaporation, wind, and air temperature) covering all areas of the basin have been collected; specifically, seven monitoring stations have been used to measure precipitation, two stations for flow rate and two stations for the other hydrometeorological parameters (gauging stations, Figure 11).

In station E7 as shown Figure 10, water depth with ADCP (Acoustic Doppler Current Profiler) instrument and temperature measurements were made at five different depths: two in the epilimnion (subsurface and center), one in the middle zone, and two in the hypolimnion (center and three meters from the bottom). In addition, a thermistor (Figure 10) was installed near the dam (E7) to have a continuous temperature record from April to September 2016. In addition, four thermistors were placed in this reservoir at 1.5 m, 4.5 m, 15 m, and 40 m depth and allow to measure the typical behavior of the temperature profile. The thermistor located at 1.5 m records the temperature of the superficial mixed layer (epilimnion), the one at 4.5 m is located approximately in the thermocline, and the one at 15 m records the temperature of the hypolimnion above the intake structure in the layer that presents the most significant temperature variations and the 40m to capture the temperature at the bottom. All thermistors were programmed to collect data every 15 minutes. These measurements were taken between May 2016 and September 2016.

Additionally, three field campaigns were carried out to collect temperature on about 36 profiles (CTD points Figure 10) in the reservoir and tributaries. The campaigns were carried out on the following dates: 1) 6th and 7th July, 2015 (Monthly monitoring), 2) 16th and 17th

August, 2015, and 3) 22nd September, 2015. Vertical measurement profiles were taken at different reservoir points using a master CTD RBR profiler with temperature, turbidity, conductivity, and chlorophyll sensors. This equipment allows data to be taken with a frequency of 6 Hz along the vertical profile line. The obtained profile shows a resolution of about 5 cm.

Hydrological parameters were collected hourly for 183 days from 20th May, 2016, to 30th September, 2016 (El Vergel gauging station, Figure 11). Hydrometeorological data were obtained from the DHIME website (http://dhime.ideam.gov.co/atencionciudadano/) of the Institute of Hydrology, Meteorology and Environmental Studies (IDEAM, acronym in Spanish). The meteorological information used for the model was provided from the gauging station closest to the dam.

Some missing data as flow discharge from the other tributaries, Santa Barbara, San Luis, and Fraguas, and water temperature for all the tributaries, were calculated from the SWAT (Soil and Water Assessment Tool (Gassman et al., 2007)) model (see Figure 12 stream points). SWAT is a semi-distributed and physically based model for daily simulation of daily discharge, sediments, nutrients, and water quality parameters. The most critical processes simulated by the model are surface runoff, infiltration, lateral flow, base flow, evapotranspiration, and groundwater recharge (Tessema et al., 2021). The model was calibrated using daily discharges from the Puente Samaná and Tarro Pintado gauging stations from 1985 to 1990 and validated from 1990 to 1997.

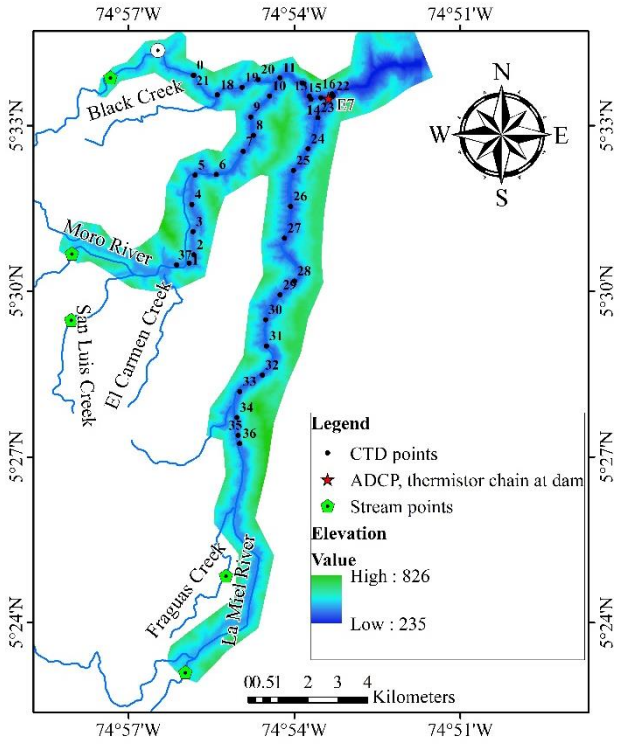

Figure 12 Data temperature and inlet measurement's location (Dataset: Bathymetry 2015, ISAGEN)

3.3.2 Topographic and bathymetric information

For the hydrodynamic model, topographic and bathymetric information was used, condensed in a digital terrain model (DTM) built with bathymetries of the river collected between 2015 and 2016, with a resolution of 5m x 5m (Figure 10).

3.3.3 Meteorological and hydrological forcing

Figures 11 to 15 show the temporal evolution of some field data collected during two months, August and September 2016, at the El Vergel measuring station shown in Figure 9, for two months in August and September 2016.

The hourly air temperature data from the El Vergel meteorological station near the dam were analyzed (Figure 11), and the monthly variations were minor. Figure 11 shows a cycle evolution, where the lowest temperatures are marked in the early morning (4 am) and the highest in the afternoon (3 pm). During the study period, the minimum temperature was 19.6°C, the average temperature was 26°C, and the maximum temperature was 35.1°C.

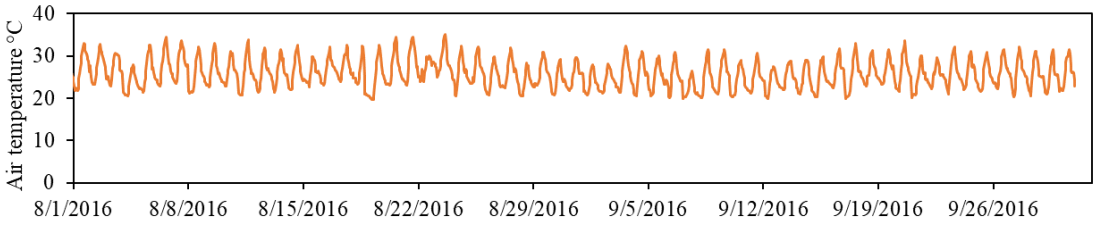

Figure 13 Air Temperature at Gauging station El Vergel, used as input on the thermic model

In Figure 12, the wind speed data is presented. During the study period, the minimum wind was 0.05m/s, the average wind was 0.73 m/s, and the maximum was 3.0m/s. The canyon topography of the area reservoir may explain the low wind speed values.

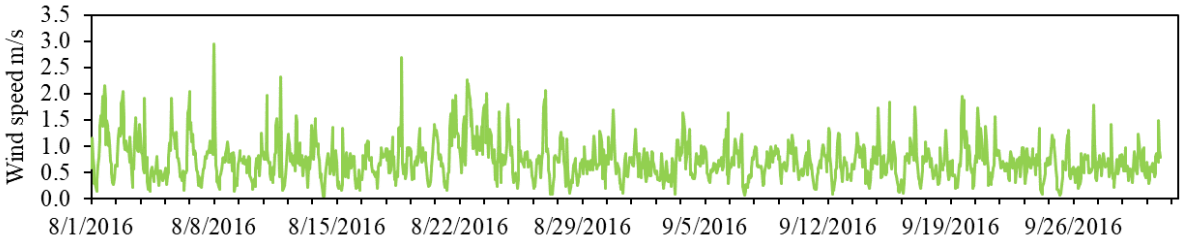

Figure 14 Wind speed at Gauging station El Vergel used as input on the thermic model.

The reservoir operated at a low water level in August, and the water level varied by 7m, reaching 406.5m on 27th August. The water level remained like this for two weeks, then rose again until it reached 417 m by the end of September (Figure 13).

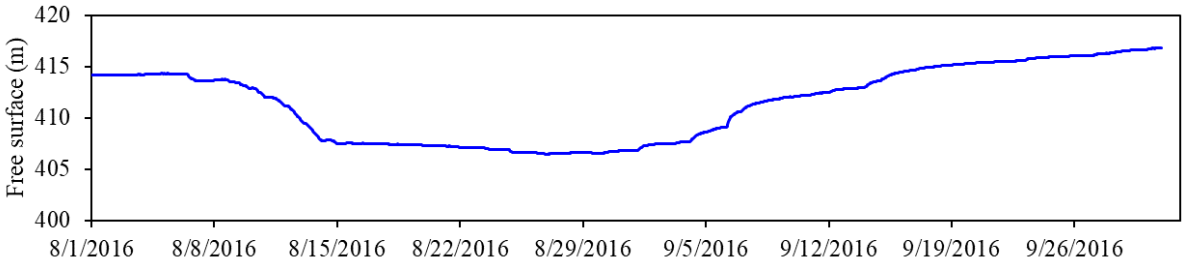

Figure 15 Water level at the dam used as observation for calibration of the hydrodynamic model

The inflow remained roughly constant during August, at 25 m3/s into Miel, except at the beginning of September, where the peak flow was as high as 65 m3/s in La Miel's arm. The reservoir presents indeed more inflow from the La Miel arm, as seen in Figure 14.

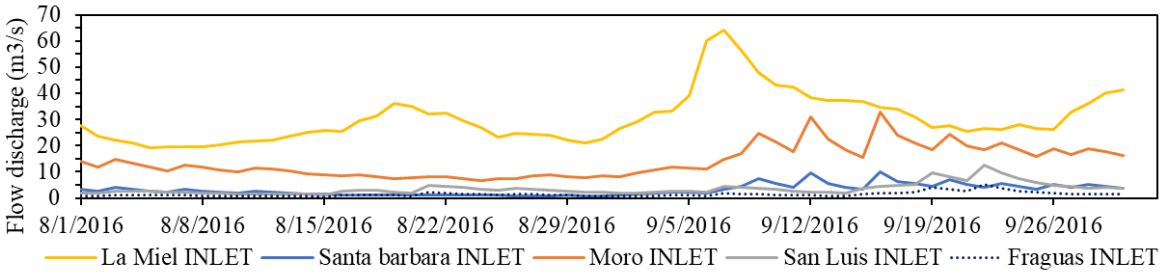

Figure 16 Inlet flow or boundary condition on the hydrodynamic model correspond to stream points in Fig 2

Figure 15 shows the water temperature for each tributary of the Amaní reservoir. For the La Miel river, the average temperature is 23°C. The creek Fraguas contributes to the river La Miel and presents an average temperature of 24°C. The Moro River has an average temperature of 25.5°C. San Luis, a tributary of the Moro, presents an average temperature of 24°C. Santa Barbara Creek presents an average temperature of 23.8°C.

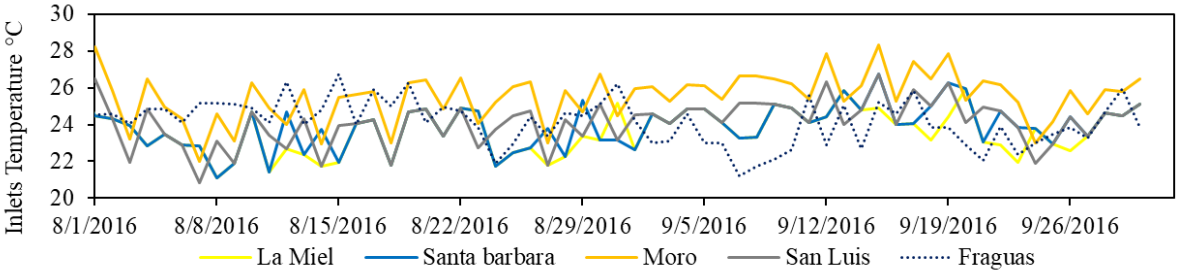

Figure 17 Water temperatures at the tributaries or boundary conditions used as input on the thermic model.

3.3.4 High-frequency temperature measurements at the dam

Figure 16 presents the high-frequency measurement of the vertical temperature profile at

the dam location from 1st August to 22nd September, 2015. Again, there is a permanent stratification in the reservoir: slightly significant differences are observed on the hourly and daily scale and non-very significant on the monthly time scale.

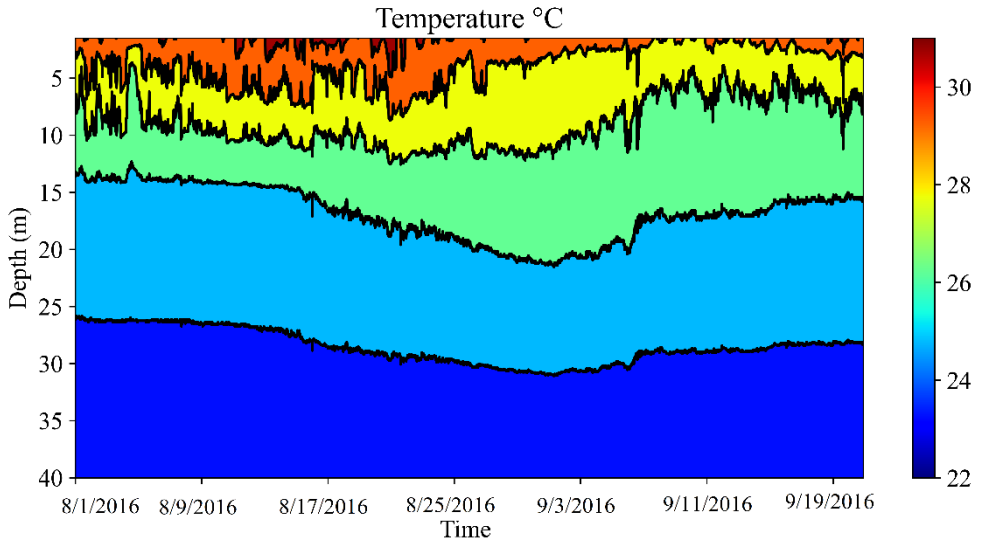

Figure 18 Evolution of the vertical distribution of the temperature using four sensors on a rope at the dam

The water temperature distribution in the analysis process presents no mixing phenomenon, and there are at least six layers in August-September. The layers that present the most significant variation are in the first meters up to 10 meters.

The temperature distribution of the first four layers varies greatly, while the temperature distribution of the two deepest layers does not change much. Also, the high-resolution data suggest that stratification does not break down overnight.

The vertical structure of water temperature is stable in different periods of each month, and the surface temperature is relatively high throughout the year, with a mean value of 29.6°C and a maximum of 31.8°C at the free surface. At depths between 25 m and 15 m, the temperature in the reservoir appears moderated by the temperature entering the tributaries. The temperature in the deep layers is between 22°C and 23°C. The analysis in the next section indicates that the external heat flux, which is determined by meteorological and inflow conditions, is insufficient for altering the nearly stratified state of the reservoir.

Clearly, there is a permanent stratification in the reservoir: hourly and daily fluctuations of the isotherms 28, 29 and 30°C in the epilimnion (of about 1 to 3 meters) are observed. On the monthly time scale, we also observe an overall increase of the temperature of about 2°C in the dam followed by a decrease of similar intensity, as the isotherms plunge by about 5m and get back to their initial location.

One of the critical factors in the formation of the thermal structure is the surface heat flux, which is composed of solar radiation, incident and emitted long-wave radiation, sensible heat flux, and latent heat flux. Often, this energy flow results in an increase in the temperature of the surface layer of the reservoir and, thus, a decrease in its density. In contrast, the deeper layers remain cooler because they are less exposed to these heat sources as shortwave radiation penetration is limited, and diffusive heat transport is too slow, as seen in the measurements (Figure 16). In the tropics, the absence of seasons means that the

difference between maximum and minimum annual radiation is slight. In addition, the total daily radiation is remarkably constant throughout the year since there are no significant variations in the number of daylight hours per day. This lack of variation in the daily radiation received means that surface heat fluxes do not vary so dramatically, and therefore, monthly patterns of stratification and mixing are not very pronounced in the present case.
From August to September, some variations in the reservoir temperature appear due to changes in the inflow and outflow of water, especially the difference in the operation level of the reservoir and meteorological conditions. Hence, the water temperature stratification pattern slightly differs from August to September as shown figure 18.

3.4 Governing Equations

In order to achieve the objectives outlined, it is necessary to have a 3D model of coupled hydrodynamics and temperature, which must be validated to ensure that what is simulated is representative compared to observed behavior.
For the hydrodynamic component, the code solves three-dimensional hydrodynamics equations with a coupled energy equation regarding temperature. The equations presented were obtained with the following assumptions (Hervouet, 2007):
- Three-dimensional equations of incompressible flow with a free surface changing in time (Eq. 1 and 2),
- Negligible variation of density in the conservation of mass equation (incompressible fluid),
- Hydrostatic pressure (Eq. 3),
- the Boussinesq approximation (Eq. 6) for the momentum (the density variations are only considered in the buoyant forces).
Due to these assumptions, the three-dimensional equations (mass and momentum) being solved are (Eq. 1 and 2):

$$\nabla \cdot \boldsymbol{U} = 0 \tag{1}$$

$$\frac{\partial \boldsymbol{U}}{\partial t} + \boldsymbol{U} \cdot \nabla \boldsymbol{U} = -\frac{1}{\rho_0} \nabla p + \frac{1}{\rho_0} \nabla \cdot (\mu_{eddy}(\nabla \boldsymbol{U} + {}^{t}\nabla \boldsymbol{U})) + \boldsymbol{g} + \boldsymbol{F} \tag{2}$$

The hydrostatic pressure assumption is (Eq. 3):

$$\frac{\partial p}{\partial z} = -\rho g \tag{3}$$

Where the density can be decomposed as in Eq. 4:

$$\rho = \rho_0 + \Delta\rho \tag{4}$$

Giving the following expression of Eq. 5 for the hydrostatic pressure:

$$\frac{\partial p}{\partial z} = -\rho_0 g \left(1 + \frac{\Delta\rho}{\rho_0}\right) \quad (5)$$

Finally, when the Boussinesq approximation is considered, the pressure expression will be as in Eq. 6 (TELEMAC-3D, 2020):

$$p = p_{atm} + \rho_0 g\,(Z_s - z) + \rho_0 g \int_z^{Z_s} \frac{\Delta\rho}{\rho_0}\, dz' \quad (6)$$

With:

- **U** (m/s) three-dimensional components of velocity,
- t (s) time,
- ρ (kg/m3) density,
- ρ_0 (kg/m3) reference density,
- **g** (m/s2) acceleration due to gravity,
- p (Pa) pressure,
- **F** (m/s2) represents the external forces,
- h (m) water depth,
- ZS (m) free surface elevation,
- p_{atm} (Pa) atmospheric pressure,
- μ_{eddy} (m2/s) eddy viscosity,
- x, y (m) horizontal space components,
- z (m) vertical space component.

To solve temperature, coupled with hydrodynamics, this study uses the evolution of the water mass temperature is derived through the evolution equation of internal energy. TELEMAC3D can be directly coupled (two-way coupling) with the WAQTEL module on the same computational mesh to reproduce the thermal dynamics. The thermic model WAQTEL (version 8.2) computes the water mass temperature through the evolution of internal energy (Eq. 7) with E = internal energy (J), λ = thermal conductivity (W.m-1. °C-1), with T = water temperature (°C), and Ssurf (W/m2) the surface sources, which are the exchange fluxes through the free surface (WAQTEL, 2021). The internal energy is formulated as a function of temperature T, considering that the internal energy E is expressed as formulated in Eq. 8. As thermal diffusivity is the thermal conductivity divided by density and specific heat capacity at constant pressure, the resulting equation is, therefore, presented in Eq. (9):

$$\frac{\partial E}{\partial t} + \boldsymbol{U} \cdot \boldsymbol{\nabla E} - \nabla \cdot (\lambda \boldsymbol{\nabla} T) = \frac{S_{surf}}{h} \quad (7)$$

$$E = \rho C_p T \quad (8)$$

$$\frac{\partial T}{\partial t} + \boldsymbol{U} \cdot \boldsymbol{\nabla T} - \nabla \cdot (\alpha \boldsymbol{\nabla} T) = \frac{S_{surf}}{\rho C_p h} \quad (9)$$

Where Cp is water-specific heat (J/kg°C) and ϱ (kg.m-3) is the water density, α is the thermic diffusivity coefficient (m2/s). The coefficient of turbulent diffusion (or dispersion) k_T is added to the diffusivity coefficient, which can generally be neglected as the value is low, which lead to Eq. 10:

$$\frac{\partial T}{\partial t} + \boldsymbol{U} \cdot \boldsymbol{\nabla T} - \nabla \cdot (k_T \boldsymbol{\nabla} T) = \frac{S_{surf}}{\rho C_p h} \tag{10}$$

The linearized formula of the balance of heat exchange fluxes at the free surface is used to represent the interchange between water and atmosphere, where the thermal power liberated into the atmosphere per surface unit, denoted as Φ, is assumed to be proportional to the difference in temperature (T - Tair) where Tair is the air temperature. So, Φ = A (T - Tair), where A is the exchange coefficient in W/m2/°C. The heat flux leaving the water domain is (Eq. 11):

$$\boldsymbol{\Phi} = -\rho C_p k_T \nabla T \cdot \boldsymbol{n} = \rho C_p k_T \frac{\partial T}{\partial z} \tag{11}$$

With n the average vector pointing outward the free surface and k_T the molecular heat diffusion coefficient in water in m2/s. Then, equating the two formulations of Eq. 11 leads to the boundary condition at the free surface (Eq. 12):

$$k_T \frac{\partial T}{\partial z} = -\frac{A}{\rho C_p}(T - T_{air}) \tag{12}$$

Note that A includes radiation, air convection in contact with water, and latent heat from evaporation. It is here modeled as in Hervouet (2007) (Eq. 13).

$$A = (4.48 + 0.49\mathrm{T}) + 2021.5b(1 + V_{wind})(1.12 + 0.18T + 0.00158T^2) \tag{13}$$

The parameter b depends on the location site and will be calibrated in this work, V_{wind} is the wind velocity (in m/s), and T is the water temperature at the free surface in °C.

3.5 Model setup

3.5.1 Mesh

The unstructured mesh comprises 4.779.814 nodes and 8.909.098 triangular elements with a minimum size of 0.7 m in a 2778.4 km2 area, created with the software Blue Kenue. The mesh is made of prisms representing the spatial variations in the surface area. The model mesh is developed as a series of planes between the bed and the free surface. Twenty-three planes are used to describe the water column. These layers have a percentage distribution of 10m at the bottom to 0.5m near the free surface. It is a classical sigma transformation that follows the shape of the terrain (TELEMAC3D, 2020).

A mesh independence test was performed, varying the size until the changes in the results were small enough not to compromise the accuracy of the simulations. The test was performed on several geometries with longitudinal variations ranging from 50 to 500m, 20 to 400 m, 10 to 300 m, 2 to 200 m, 0.7 to 160 m, 0.5 to 140 m, and 0.1 to 35 m. Figure 17 shows the geometry from 0.7 to 160 m was finally chosen as the best compromise.

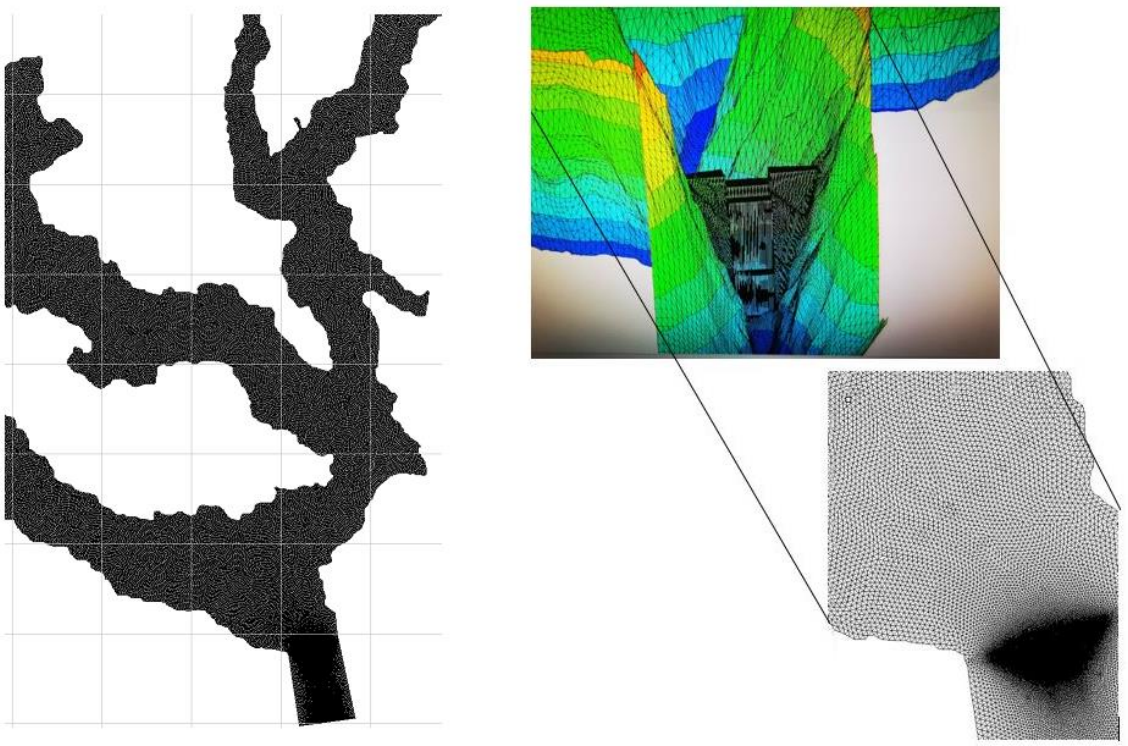

Figure 19 Mesh used in the model. Left: general structure of the mesh in the reservoir Right: detail of the geometry and mesh at the dam location

3.5.2 Initial and boundary conditions

Considering that the study focuses on the sub-daily temperature variations and that the hydrodynamics do not change significatively, it is assumed that the hydrodynamic model conditions are stationary. In contrast, the conditions for the thermic model are transient.

A constant water level of 410 m above the sea level measured on 6th July, 2015, is used as the initial condition for the hydrodynamic model. A warm-up time is needed to obtain a velocity field until the velocity components are developed within the computational domain.

The hydrodynamics boundary conditions are as follows. First, this research imposes the flow rate at the upstream part of all the rivers using the collected field data (Q1=9.91 m3/s, Q2=4.96 m3/s, Q3= 6.97 m3/s, Q4=6.91 m3/s, Q5=2.87 m3/s), and the turbine water or intake was added as a source, with a constant value of -32 m3/s at a depth of 380 m above the sea level. Then, the lateral boundaries were set as closed walls with slip conditions. Their location is shown in Figure 18.

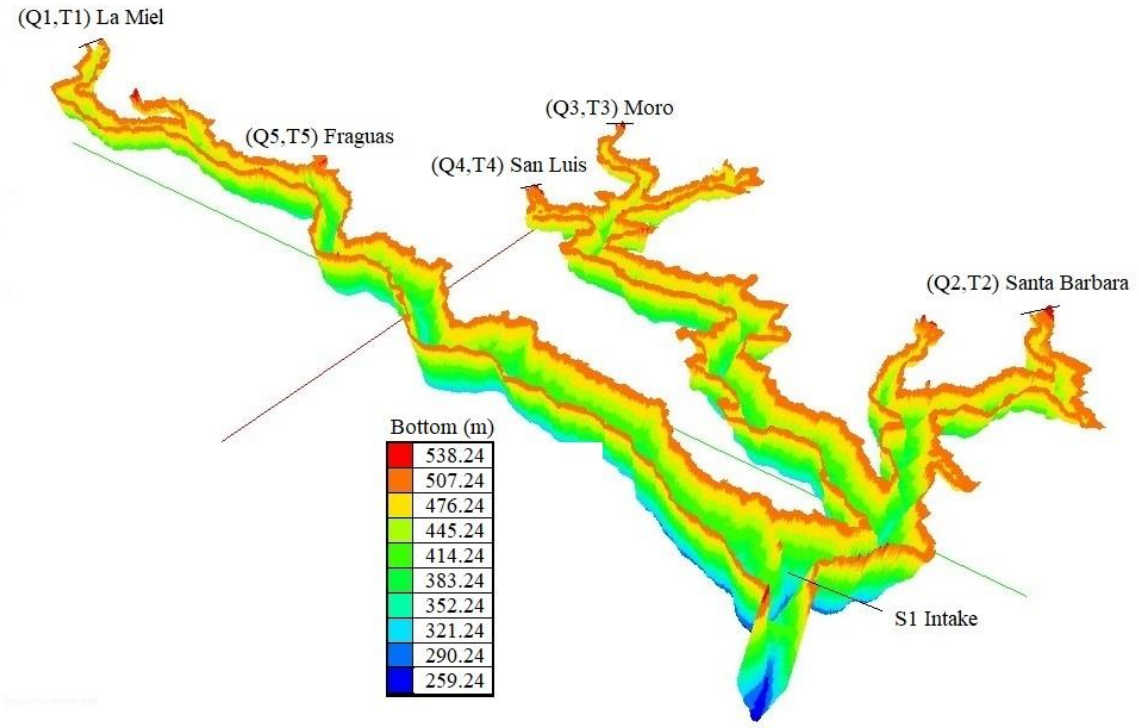

Figure 20 Numerical setup and boundary conditions used. 3D view of the bathymetry

For the thermic model, the initial condition is as shown in the Figure 19 of the whole computational domain was constructed from the field measurements of the CTD of 6th July 2015 at station E7.

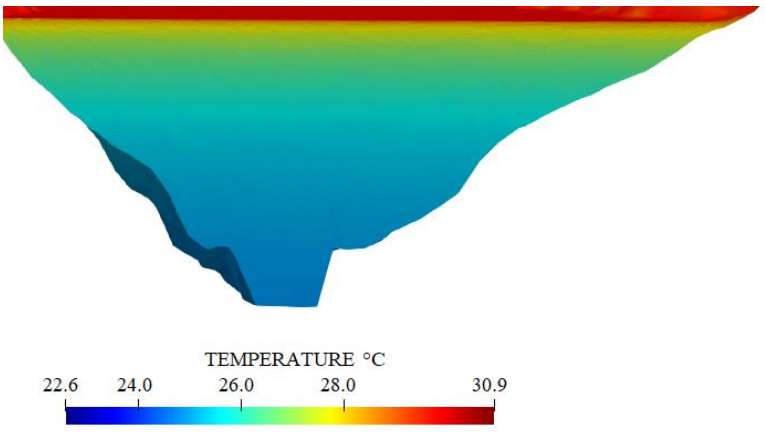

Figure 21 Thermic initial condition near the dam at station E7

As boundary conditions this research imposes a constant temperature at the inflows (of T1= 22.9 °C, T2= 22.6°C, T3= 24°C, T4= 23.4°C and T5 = 23°C) (see Figure 19). The boundary condition imposed on the free surface was Dirichlet for one case study and Newman for the other (Eq. 12), using air temperature, wind direction, and velocity based on data collected from the local and nearby weather stations. These approaches are developed in detail in

section 4.2.

The modules employed were TELEMAC-3D-WAQTEL version v8p2 (TELEMAC-3D, 2020). The simulations were conducted for each case investigated through parallel computing on the supercomputer OLYMPE from the CALMIP computing center for public research in Toulouse.

3.5.3 Numerical and physical parameters

The numerical parameters were defined by trial-and-error, where the model was run several times and yielded the following results. The set of selected numerical and physical parameters is summarized in Table 4.

Table 5: Parameters used in the calibration of the hydrodynamic model.

PARAMETERS	VALUE
Scheme for advection of temperature	EXPLICIT SCHEME + MURD N SCHEME
Linear solvers	
Solver	GMRES
Krylov subspace	4
Turbulence	
Vertical turbulence model	CONSTANT VISCOSITY
Horizontal turbulence model	CONSTANT VISCOSITY
The coefficient for horizontal diffusion of velocities (m^2/s)	0.001
The coefficient for vertical diffusion of velocities (m^2/s)	0.001
Law of bottom friction	STRICKLER LAW
The friction coefficient for the bottom	30

To solve all processes, including hydrodynamics and thermals, the GMRES solver was chosen based on mass conservation and computational cost.

To simulate all the physical processes, this study uses a constant viscosity model for the turbulence model (Hervouet, 2007; Hinkelmann, 2005). The turbulent viscosity value was fixed at 10-3 m2/s in all directions, as a results of previous simulations using Smagorisky as a turbulence model. Several simulations were run for a time step ranging from 0.1 to 5 seconds. The time step was set to 1 second since it provided the best compromise between stability and performance.

The Multidimensional Upwind Residual Distribution (MURD) method was applied for the advection of three-dimensional variables under TELEMAC3D, and the boundary conditions were applied following the method of characteristics. The advection of tracers was solved using the distributive MURD N method. Section 5 discusses the parameter choice.

3.5.4 Model validation

The model's calibration and validation were done by comparing the modeled results with the field measures, especially the variation of the water level and the temperature profile at several points and in time with high-frequency data at the dam (station E7). This comparison is the first indication that the model represents a hydrodynamic and thermal stratification. Traditionally, estimated standard errors have been used to measure the efficiency of model calibration. The most common indices to analyze time-dependent variables are the mean absolute error—MAE (Eq. 15), Nash–Sutcliffe index (Eq. 16), and root mean square error—RMSE (Eq. 17) and Relative Error (Eq. 18).

$$MAE = \frac{1}{n}\sum_{i=1}^{n}\left|\widehat{X}_\iota - X_i^o\right| \tag{14}$$

$$E_f = 1 - \frac{\sum_{i=1}^{n}\left(\widehat{X}_\iota - X_i^o\right)^2}{\sum_{i=1}^{n}(X_i^o - \overline{X^o})^2} \tag{15}$$

$$RMSE = \sqrt{\frac{1}{n}\sum_{i=1}^{n}\left(\widehat{X}_\iota - X_i^o\right)^2} \tag{16}$$

$$Re = \sum_{i=1}^{n}\frac{\left|\widehat{X}_\iota - X_i^o\right|}{X_i^o} \times 100 \tag{17}$$

In the equations, n is the sample size, $\widehat{X}_\iota$ is the predicted value of the output (water level or temperature) at time or location i, Xoi is the corresponding measured value, and $\overline{X^o}$ is the mean of the measured values.

The MAE and RMSE have been used as standard statistical metrics to measure model performance in meteorology, air quality, and climate research studies. The difference is that the MAE gives equal weight to all errors. At the same time, the RMSE penalizes the variance, giving more weight to errors with larger absolute values than to errors with smaller absolute values. As a result, when both metrics are calculated, the RMSE is never lower than the MAE (Chai & Draxler, 2014).

Another critical aspect of the error metrics used for model evaluations is their capability to discriminate among model results. In this case, the advantage of the Nash–Sutcliffe index is that it can be applied to a variety of model types. This efficiency index ranges from -∞ to + 1, 1 being the best. As well as RMSE and MAE, the Nash–Sutcliffe is a helpful index; however, it can be sensitive to several factors, including sample size, outliers, magnitude bias, and time-offset bias. So, using a combination of those indexes to assess the model is better. These statistics are commonly used to evaluate the model's goodness that fits the observed data (L. F. Amorim et al., 2021a; Lindim et al., 2011).

3.5.5 Analysis of water atmosphere exchange approaches

Considering that the model is very sensitive to the temperature forcing given by the

atmosphere-water exchange, it is necessary to analyze the thermodynamic behavior of the exchange process concerning the different forcings. Based on this, the following approaches are defined for the temperature boundary condition at the free surface:

A. A constant water temperature Twater, of 29.8°C, at the free surface (Dirichlet) without exchange with the atmosphere, considering the stability of the thermal stratification according to field measurements. The A approach was simulated until a steady state was reached. This approach served as initial conditions and reference for comparison with the other approaches.

B. Exchange with the atmosphere at the free-surface boundary condition (Eq. 12) with meteorological forcing (air temperature Tair and wind velocity Vwind) constant in time. A value of 32°C is imposed for Tair based on the maximum value measured for the day of the analysis. Vwind = 0.6 m/s refers to the mean value over the period.

C. Exchange with the atmosphere at the free-surface boundary condition (Eq. 12) with meteorological forcing changing over time. This last approach uses observed hourly data of Tair and Vwind over the period.

The proposed approaches simulate the temperature profile in the reservoir under different forcings and parameters that best represent tropical conditions. They will be compared with the field thermistor data covering the period from 11th August to 19th August, 2016. The same boundary conditions concerning the flow, source or intake, and tributaries temperature were set up for the three approaches; they have been detailed in section 3.3.2 Initial and boundary conditions. These approaches were chosen for the sake of simplicity (number of parameters), data availability, and computation time.

3.6 Results

3.6.1 Hydrodynamics

In this section, this study compared observation and simulation of the water level and velocities within the computational domain. The chosen period for the calibration was from 1st August until 1st September, 2016. For this period, observed data is available daily. The measurement water level at point 16 is used for calibration purposes. The results of the TELEMAC-3D model calibration exercise are presented in Figure 20, where comparisons of the water level simulations with observations are presented within each seven days' interval.

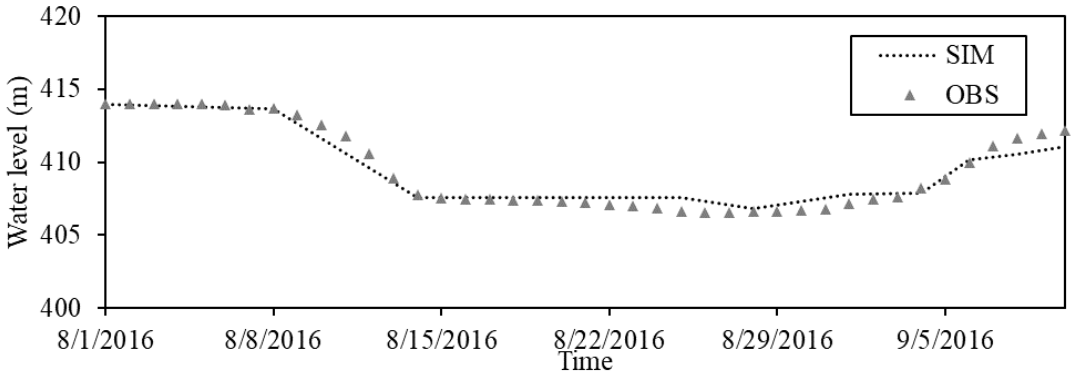

Figure 22 Time evolution of the water level at point 16 corresponding to the dam location (Fig. 10)

The statistical calibration indices found for the simulations show good performance with Ef = 0.95, MAE = 2.46 m and RMSE = 3.22 m.

In order to analyze the spatial performance of the model, a correlation graph between the simulated water depth and the measured water depth was produced at 37 points inside the reservoir, as shown in Figure 21.

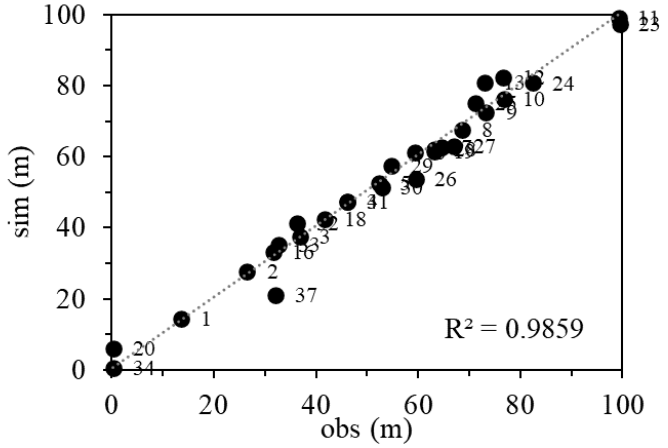

Figure 23 Water height (in meters) at all the points displayed in Fig. 2 for August 17th 2016 with CTD.

According to Figure 21, the hydrodynamic model is adequately configured since the observed water depths correspond to the simulated values in TELEMAC 3D, with an R2 close to 1.

3.6.2 Velocities results

As expected, the order of magnitude of scalar velocity is lower inside the reservoir, and the velocity is highest at the inlets as shown in the Figure 22. The order of magnitude of the velocities ranges from 0.1 m/s to 0.9 m/s, with the highest velocities occurring at the inlets. It is the lowest near the dam and ranges from 0.001 m/s to 0.01 m/s. In the same way, it can be observed in Figure 23 that the velocity decreases in the vertical direction, with the highest velocity in the upper layers.

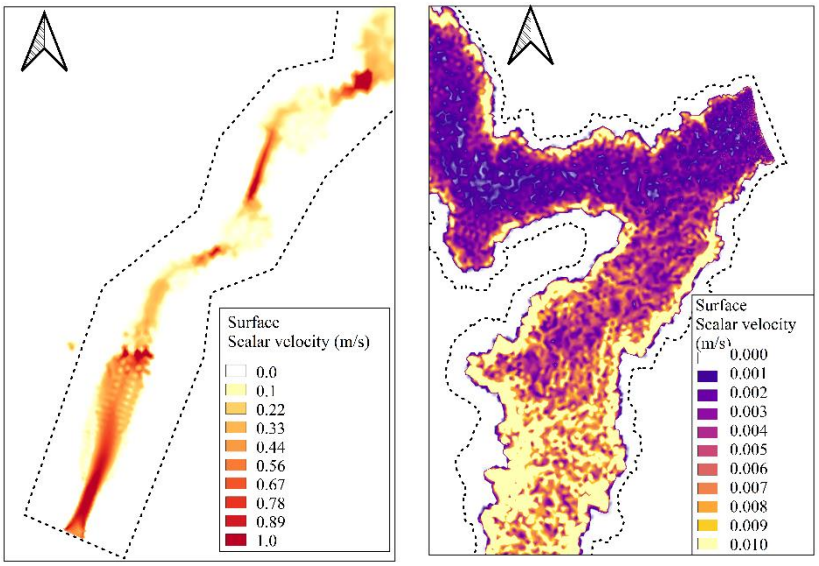

Figure 24 Free surface scalar velocity at La Miel river entrance (left) and at the dam (right)

Low velocities in the lower layers may indicate that there is little potential for convective transport near the bottom of the reservoir, making convection less likely to occur than in the upper layers. Therefore, convection can exist in the upper layers, but in the other layers, the process is probably reduced to diffusive transport.

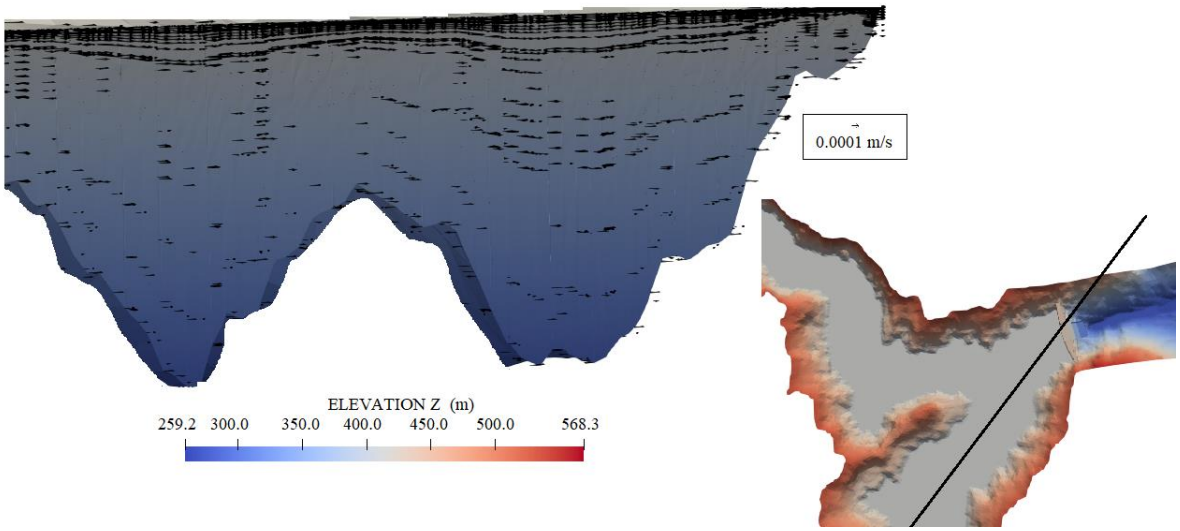

Figure 25 Velocity field (left) along one cross-section at the dam (right) for the hydrodynamic calibration model.

3.6.3 Thermic model

The results of the temperature model for the three approaches mentioned in section (3.5.5), which differ in the way they treat the water-atmosphere exchange, will be presented

section 3.6.2 Considering the model's sensitivity to the parameters of this exchange, it is necessary to perform a detailed analysis of the impact of the physical parameters of the different models.

3.6.4 Sensitivity analysis

Sensitivity analysis of the thermic diffusivity of water (k_T) and the coefficient of the atmosphere-water exchange model b is required according to the governing equations (Eq. 12 and 13) of the thermal model described in Section (3.4). Table 5 presents the values tested for these coefficients in each approach. For the local sensitivity analysis, the simulations were performed using the "one-at-the-time" approach (Simmons et al., 2015) by increasing each parameter by a given percentage while leaving all others constant and quantifying the change in model output. This method is applied at the highest computational cost.

Table 6: Simulations performed in this work. A, B, and C refer to the scenario type (see §3.3 for details).

Case name	**Approach**	b	κ_T (m²/s)	*Comment*
NO EXCH 1	(A)	N/A	1.0×10^{-6}	The Prandtl number $Pr = \nu/\kappa_T = 1$
NO EXCH 2	(A)	N/A	1.4×10^{-7}	$Pr = 7$
NO EXCH 3	(A)	N/A	0	$Pr = \infty$
CAL0	(B)	0.0025	1.0×10^{-6}	
CAL1	(B)	0.0035	1.0×10^{-6}	
CAL2	(B)	0.01	1.0×10^{-6}	
CAL3	(B)	0.1	1.0×10^{-6}	
CAL14	(B)	0.01	0	V_{wind} =0 m/s
CAL 1C	(C)	0.0035	1.0×10^{-6}	
CAL 2C	(C)	0.01	1.0×10^{-6}	
CAL 3C	(C)	0.1	1.0×10^{-6}	
CAL4	(C)	0.03	1.0×10^{-6}	
CAL5	(C)	0.05	1.0×10^{-6}	
CAL15	(C)	0.1	0	Taking as IC CAL3 last time step
CAL17	(C)	0.0025	1.0×10^{-6}	

3.6.5 Analysis and Metrics of simulated cases for the Exchange

A sensitivity analysis was performed on thermic drivers for air-water exchange included in the simulations to define which of them primarily influenced the models' performance as being sensitive to the variation of the simulated processes.

The analysis was carried out at the four depths of the dam, where depth 1 corresponds to the temperature at the free surface, depth 2 corresponds to the temperature at 4 m, depth 3 corresponds to the temperature at 15 m, and depth 4 corresponds to 40 m. These points were selected to represent the stratification; the field measurement data used to evaluate

the simulations were taken between 11th August to 19th August, 2016.
A spatial assessment compared to the temperature profiles measured by the CTD for 17th August was also performed.
To investigate model performance, relative error (RE), root mean square error (RMSE), and mean absolute error (MAE) and between measured and simulated temperature values were calculated.

Approach A: Constant water temperature at the free surface without exchange with the atmosphere

Approach A; the analysis was applied to the different drivers included in the simulation, as listed in Table 5, considering the thermal diffusivity (k_T) of water for three runs.

The influence of the simulated processes strongly depends on the investigated location's depth in Figure 24. In particular, points evaluated in Depth 2 present the highest errors in the case NO EXCH 1, ranging between 14.2% RE, 4.4°C for RMSE, and 4.1°C for MAE. When the thermic diffusivity of water was zero (NO EXCH 3), the simulations reported better results. Hence, heat transfer is favored to occur by fluid momentum rather than by fluid conduction. The results are discussed in detail in the next paragraph.

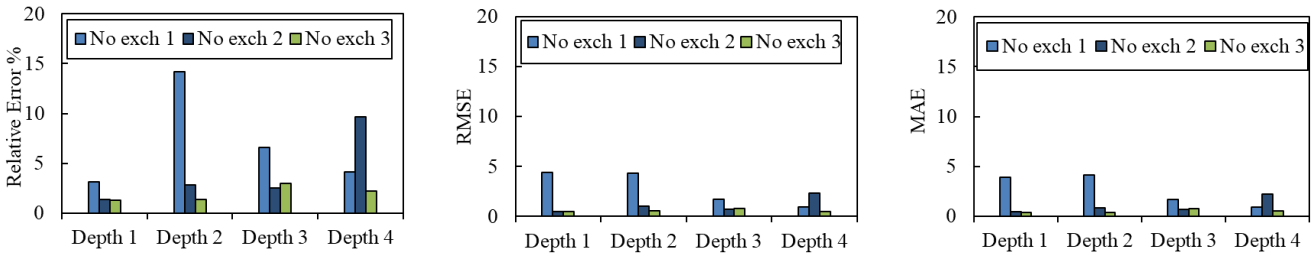

Figure 26 Metrics for approach A, at different depths in the dam

Observed and simulated water temperatures at the four depths during the analysis period are presented in Figure 25, showing the difference between the surface and bottom layers for measured and simulated water temperature.

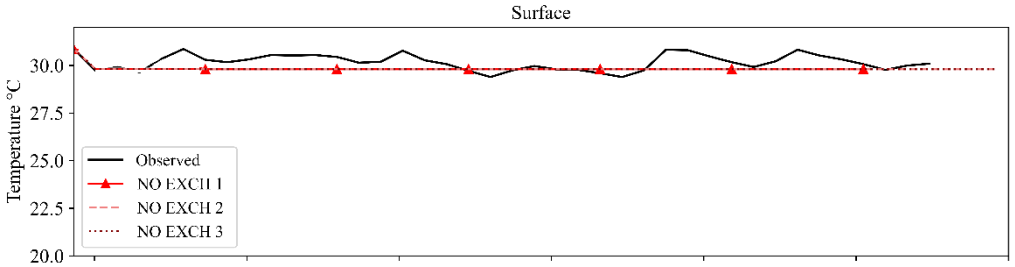

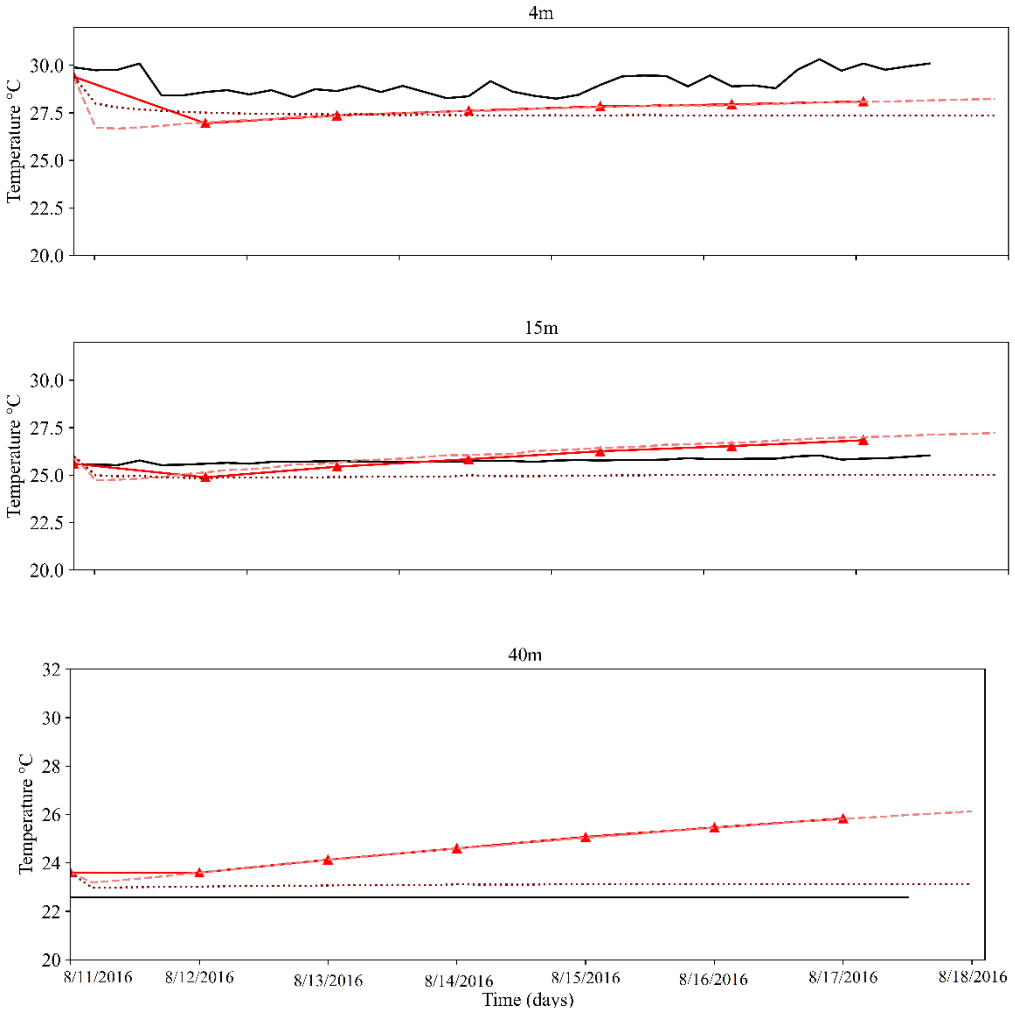

Figure 27 Time variation of the observed and simulated temperatures at the dam without exchange with the atmosphere

According to Figure 25, the model could represent the main observed patterns, the first layer being the constant water temperature boundary condition at the free surface: (i) the second layer shows a slight observed variation in temperature between 28.0°C and 31.41°C for the period at an hourly scale. At 4 m after a transition period, NO EXCH 1 and NO EXCH 2 exhibit almost the same results with an increase of temperature which is not observed, whereas NO EXCH 3 simulates a constant temperature; the same behavior appears in the simulated results at 15 m; (ii) the cooling at the reservoir bottom, shows an overestimate of 0.5°C for NO EXCH 3 and more than 2°C and increasing with time for the other cases. For the cases of NO EXCH 1 and NO EXCH 2, there is a tendency for the bottom temperature to increase, which is not representative of the current situation for reservoirs with little change over time; (iii) the duration of the stratification period that never breaks in all cases; (iv) using approach A, it was not possible to reproduce the temperature oscillations, only the mean values which is due to the constant water temperature boundary condition at the free surface.

Figure 26 shows the simulated and observed temperature profiles: vertical profiles at different points in the dam at a given time. It shows that the model can reasonably simulate

the vertical stratification characteristics of the water temperature of the Amani Reservoir, and case NO EXCH 3 is in good agreement with the observed water temperature structure of each analysis point. However, the model simulates only one thermocline, not the two that occur in the Amaní tropical reservoir. Results are very similar for cases NO EXCH 1 and 2 with an increase of temperature near the bottom: mixing phenomena are simulated, which do not represent measurement data (Figure 26 for points P20, P29, P10, and P16).

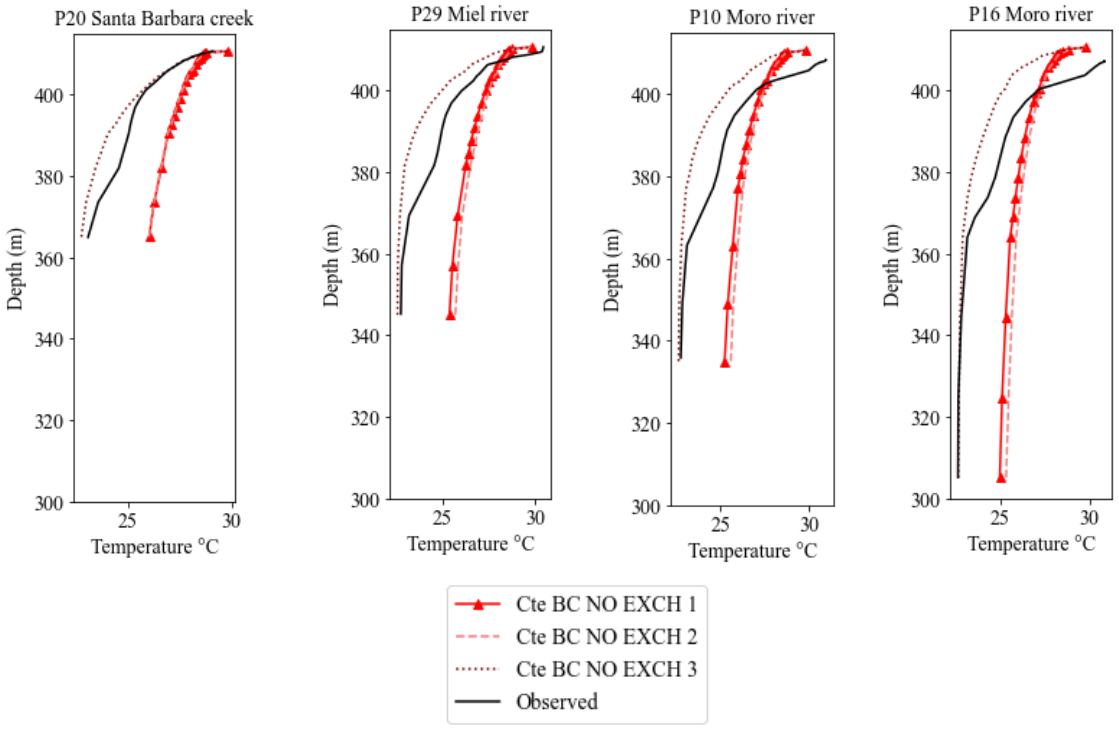

Figure 28 Comparison between the vertical temperature profiles measured from the field and the simulated ones (August 17th, 2016)

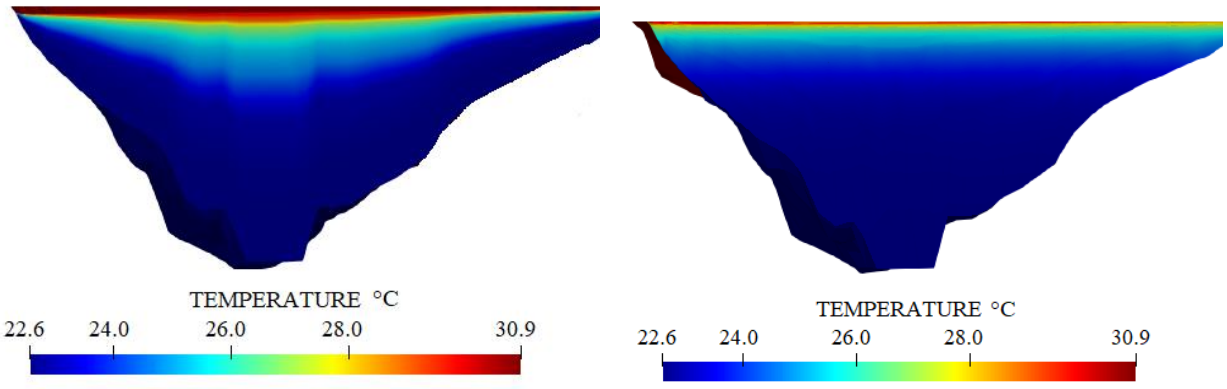

Figure 29 The temperature distribution in a vertical plane near the dam (August 17th, 2016). Left: field data. Right: simulation result (case NO EXCH 3).

The thermal structure along the reservoir near the dam is shown in Figure 27 for case NO EXCH 3. Generally, the water temperature was not homogeneous during the analysis period. With reported air temperature values of around 28°C during the analysis period, a

warmer layer of water developed at the surface, eventually developing into a strongly stratified thermocline at two depths in 5 m and 10 m, but as already mentioned it was not possible to reproduce the deeper thermocline at 10 m with approach A.

Unlike many natural lakes that experience overturning depending on weather conditions, no overturning was observed during the study at Amani Reservoir because it is a tropical lake, and the surface water temperature never drops below 16°C. During the study period, strong stratification was observed in the Amani reservoir, with a temperature difference between the surface and the bottom reaching 8°C according to both measurements and simulations. The water temperature difference between the surface and bottom was 4°C in NO EXCH 1 and NO EXCH 2 along the reservoir in all simulated times, while its maximum of 7°C was reached at NO EXCH 3.

The thermal structure of simulation NO EXCH 3 exhibit fewer layers of stratification than actually observed.

Approach B: Free-surface boundary-condition (Eq 12) with meteorological parameters constant in time

Approach B explores what happens to the temperature profile for different values of the exchange coefficient A (Eq. 13) with constant meteorological forcing.

The heat transfer coefficients or A value reported in (Williams, 1963) for reservoirs present a range between A∈[113, 378] W/m2/°C. It was not possible to find more recent values reported in the studies. As shown in Table 5, this study varied b (involved in eq. 13) in the range [0.001, 0.1]. The latter values correspond to a range of A∈ [15, 900] W/m2/°C.

Table 6 shows the different values of the evaluated exchange coefficient A; however, only the results of the five most representative cases will be shown here.

Table 7: Tested values of *A* exchange coefficient

b	*A* (W/m²/°C)
0.001	15
0.0025	30
0.0035	40
0.01	97
0.03	275
0.05	450
0.10	900

The influence of the simulated processes does not depend on the investigated location's depth but rather on the A value that shows a significant influence, with better results for higher values of A, as shown in the Figure 28. The cases with the best results are CAL2 and CAL3. The values of b are respectively 0.01 and 0.1, corresponding to A = 97 and 900 W/m2/°C respectively. The case of CAL14 with a wind speed value of zero exhibited the

highest error between 9.1% and 4.5% RE, RMSE between 2.4°C and 1.2°C, and MAE between 2.1°C and 1.2°C. Also, for these evaluated cases, the thermal diffusivity (k_T) does not show as significant an effect as in approach A. None of the cases presented a Relative error value of more than 10%. Furthermore, the RMSE and MAE values are below 5°C.

Generally, the model has the most difficulty reproducing the behavior of the second layer and the bottom (Depth 2 and 4). The best results according to the metrics are discussed in detail in the next paragraph.

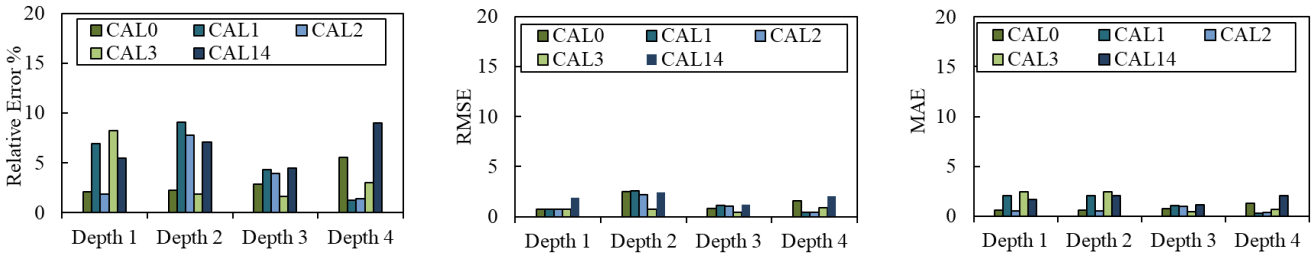

Figure 30 Metrics for approach B, at different depths in the dam

Observed and simulated water temperatures at the four depths during the analysis period are presented in Figure 29, showing the difference between the surface and bottom layers for measured and simulated water temperature.

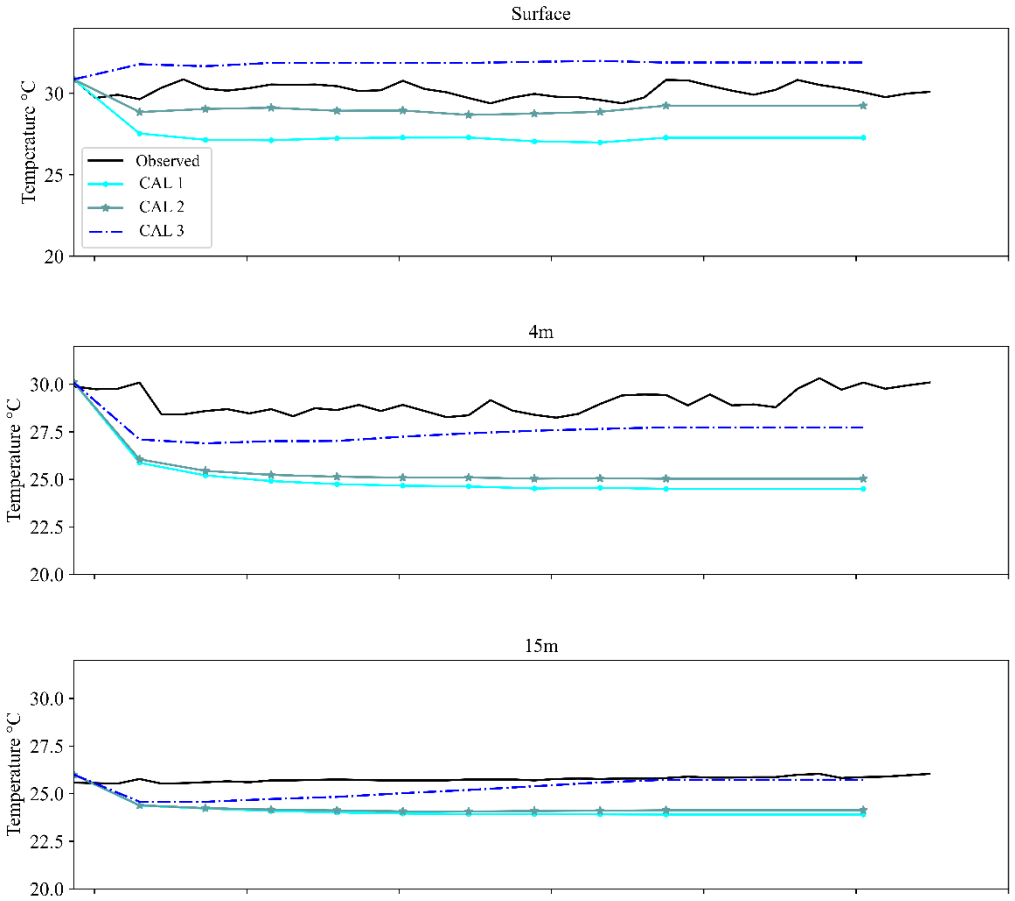

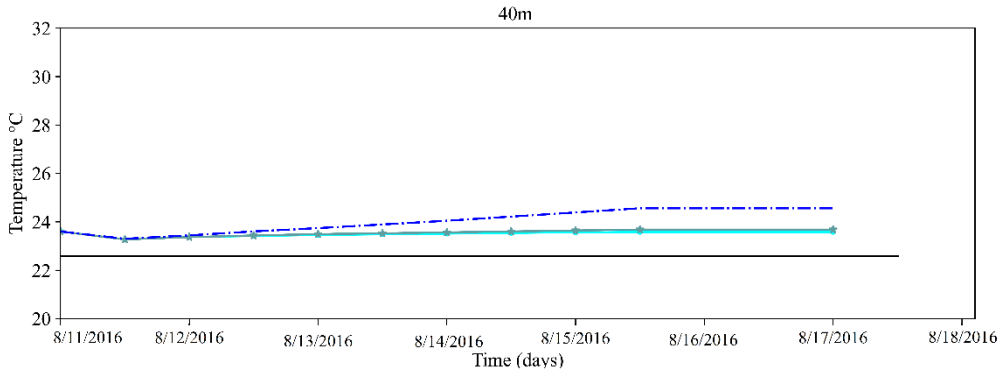

Figure 31 Time variation of the observed and simulated temperatures at the dam with constant meteorological parameters

According to Figure 29, the model could represent the main observed patterns: (i) the mean value at hourly time scale on the first layer of the surface, which shows a value of 32°C in CAL3, 28°C for CAL2 and 26°C for CAL1, for the period of analysis; (ii) Cooling at the bottom of the reservoir revealed a 0.3°C overestimation of CAL1 and CAL2, and 1°C and more for CAL3. For the case of CAL3, there is a light tendency for a depth of 15 m and the bottom temperature to increase; (iii) the duration of the stratification period that never breaks in all cases, and is best represented for CAL3, with the exception of the bottom layer; (iv) Again, using approach B, it was not possible to reproduce the temperature oscillations in the upper layers, only the mean values. This is probably due to the meteorological forcing, constant in time.

Temporally, water temperature changes depend on the A air-water exchange coefficient. When A is lower, there is less exchange, and the water temperature experiences a drop, while when the A coefficient is higher, the water temperature rises. The case CAL2 is the one that is closest to the values observed at the free surface with an average of 28°C; for the deeper layers, the A value that better represents the mean values is CAL 3.

Figure 30 shows the simulated and observed temperature profiles: vertical profiles at different points on the dam at a given time. It shows that the model can reasonably simulate the vertical stratification characteristics of the water temperature of the Amani Reservoir, and case CAL3 is in good agreement with the observed water temperature structure of each analysis point. However, for these study cases, there is no mixing phenomena as identified for approach A, suggesting that it is necessary to determine the value of A that facilitates heat exchange to represent the vertical distribution of tropical reservoirs correctly.

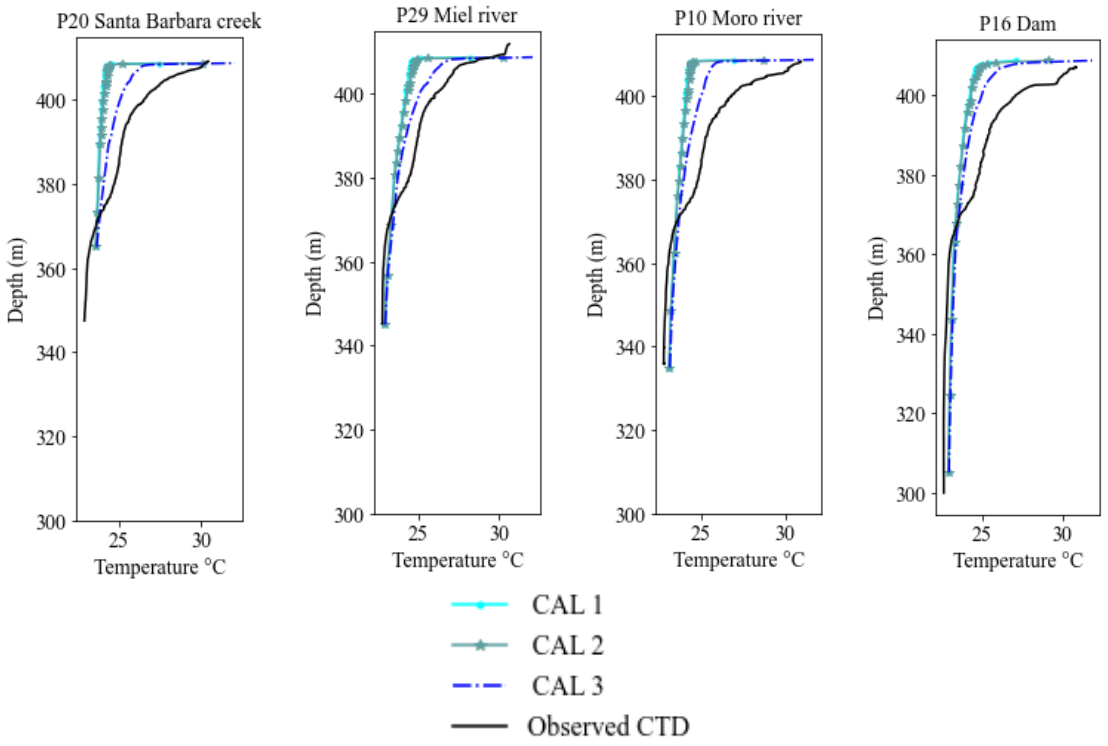

Figure 32 Comparison between the vertical temperature profiles measured from the field and the simulated (August 17th 2016).

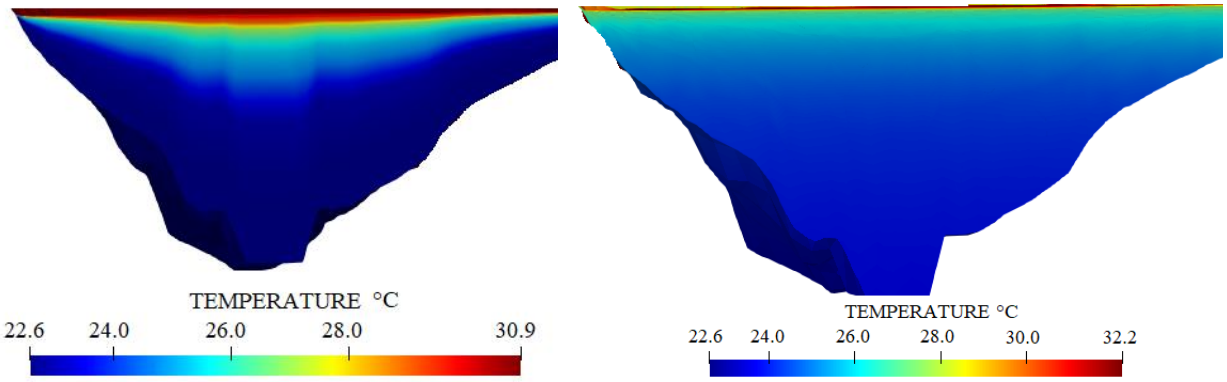

Figure 33 The temperature distribution in a vertical plane near the dam on August 17th, 2016. Left: field data. Right: simulation result (case CAL3).

The thermal structure along the reservoir near to dam is shown in Figure 31 for case CAL 3. As for approach A, it was not possible to reproduce the strongly stratified thermocline at depths of about 5 m and 10 m with any simulations of approach B.

Vertically, strong stratification was observed in the reservoir for those scenarios, with the surface-bottom temperature difference reaching 8°C in all the cases according to Figure 30. In agreement with other studies, stronger stratification has been reported in other deep reservoirs. Among them, the temperature difference between the surface and the bottom of the reservoir reaches 10°C (70 m deep), and the maximum temperature difference of the other reservoirs even reaches 14°C (200 m deep) (Plec et al., 2021). One main reason for these

gradients is the depth of the Amaní reservoir with 120 m. By preventing the penetration of solar radiation and wind-driven eddies, large bodies of water like the Amaní reservoir impede heat transfer and make it difficult to achieve a homogeneous temperature. These variables, included in the A coefficient, represent radiation, air convection in contact with water, and latent heat. Its correct determination improves the simulation results compared with Approach A from a temporal and vertical point of view.

Longitudinally, the simulations of the temperature at the free surface drops at the entrance of the tributaries, and as the tributaries flowed toward the reservoir all the way down the dam, the simulated water surface temperature increases by 3.5°C. Unfortunately, observed data do not provide any information on this phenomenon.

The latter means that the heat transport in the reservoir is mainly due to advective transport, as was hypothesized, and in the first layer, it is due to the exchange of air-water and the atmospheric variables, mainly the exchange between air and water. Water is a poor conductor of heat, so thermal diffusion is slow in a reservoir. Therefore, the flow transfers energy with very high specific heat.

Approach C: Free-surface boundary-condition (Eq (12) with meteorological parameters changing over time.

The analysis of Approach C explores what happens to the temperature profiles for different values of the exchange coefficient A when air temperature and wind change over time for a total of 7 runs.

The influence of the simulated processes does not depend on the investigated location's depth, but the A values as well as the oscillation of air temperature values show an influence of this location, with better results for lower values of A according Figure 32. The cases with the best results are Case CAL 1C with A = 40 W/m2/°C, followed by CAL2 C with A = 97 W/m2/°C. Case CAL 17 was used to evaluate whether to further reducing the value of A=15 W/m2/°C would improve the performance of the model, but it was not the case. In the case of CAL 15, since the initial conditions were taken from the last time step of CAL 3 and the diffusion coefficient was then set to zero, the results might have improved as the simulation time increased, but this did not happen, on the contrary.

CAL3C exhibited the highest errors with RE up to 16.3%, RMSE 5.0°C, and MAE 3.7°C. Furthermore, the A coefficient does not show as significant an effect as in Approach B for these evaluation cases.

All the simulations failed to reproduce the observed temperature at the free surface and the bottom (Depth 1 and 4). Those results are discussed in detail in the next paragraph.

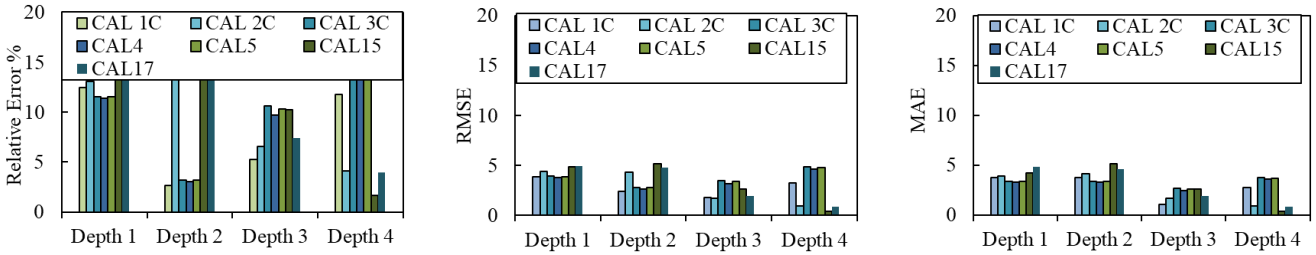

Figure 34 Metrics for approach C, at different depths in the dam

Observed and simulated water temperatures at the four depths during the analysis period are presented in Figure 33, showing the difference between the surface and bottom layers for measured and simulated water temperature.

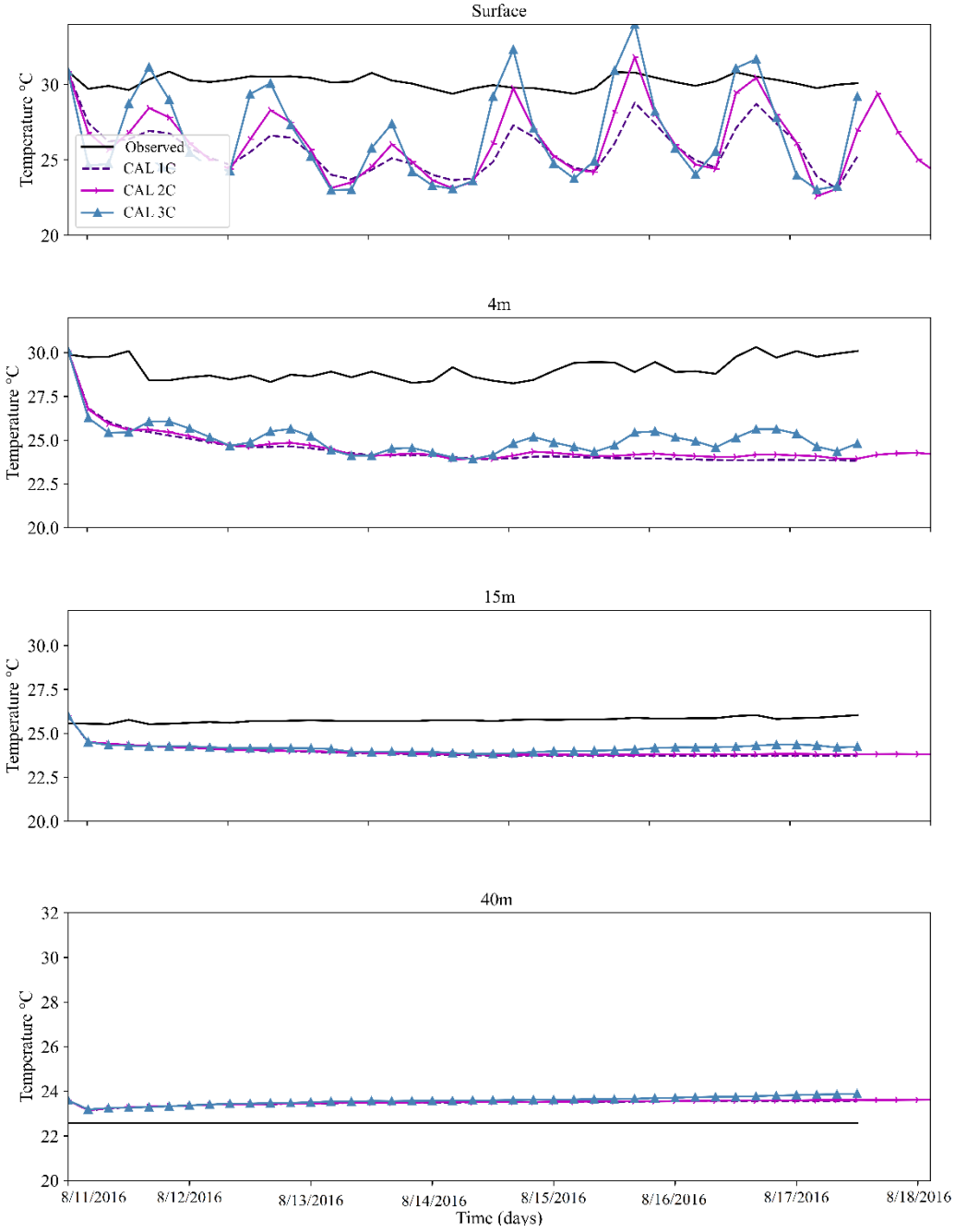

Figure 35 Time variation of the observed and simulated temperatures at the dam with exchange with the atmosphere, with meteorological parameters changing

The cases analyzed for Approach C reproduces the observed temperature oscillations at the free surface and the 4 m layer, but they differ in the standard deviation temperatures. Data measured at the free surface exhibited temperature oscillations of up to 1.5°C, compared to 2°C for the studied CAL1C case, 3.5°C for CAL2C, and 4.5°C for CAL3C.

Indeed, the amplitude of daily temperature variation decreases with A. Temporally, water temperature changes with air temperature. When the air temperature was lower than the water temperature, the water temperature experienced a drop, while when the air temperature was higher than the water temperature, the water temperature rose.

According to Figure 33, the model could represent the main observed patterns: (i) the value at hourly time scale on the first layer of the surface, with a daily heat loss of about 4°C for CAL1C, about 5°C for CAL2C, and about 8°C for CAL3C, for the period of analysis ; (ii) At 4m only CAL3C could reproduce water temperature oscillations but the average temperature is underestimated ; (iii) Cooling at the bottom of the reservoir revealed an overestimation of 0.4°C for CAL1C and CAL2C and 0.7°C for CAL3C.

Figure 34 shows the simulated and observed temperature profiles: vertical profiles at different points on the dam at a given time. It shows that the model can simulate a vertical stratification characteristic of the Amani Reservoir's water temperature but does not agree with the observed water temperature structure at each analysis point. For these study cases, the mixing phenomena identified for approach A were not found here. Vertically, the water column along the reservoir is always stratified regardless of its position and depth (Figure 34 for points P20, P29, P10, and P16).

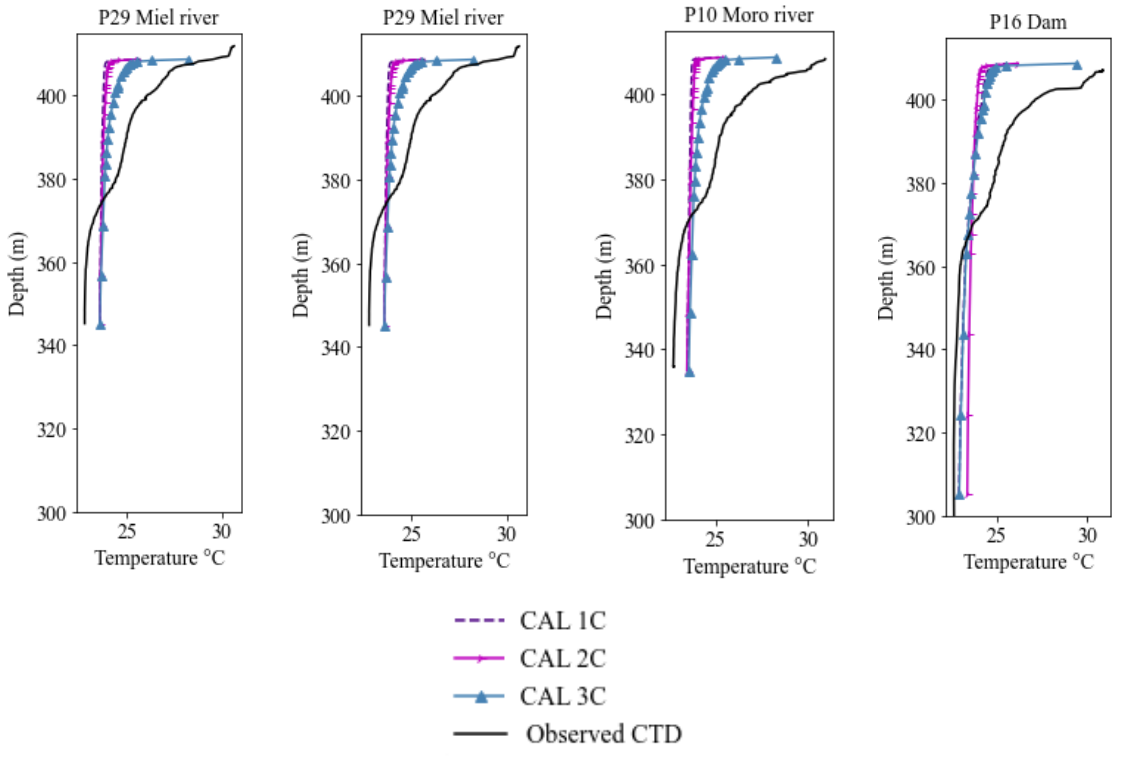

Figure 36 Comparison between the vertical temperature profiles measured from the field and the simulated (August 17th)

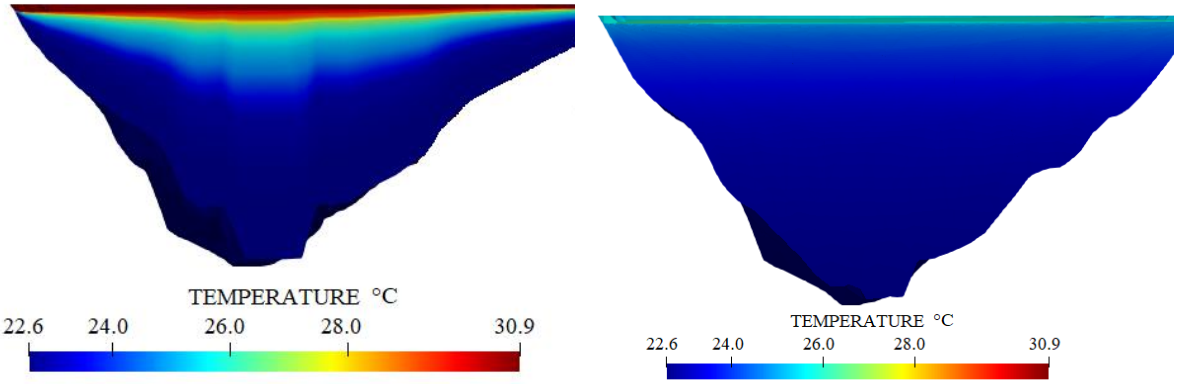

Figure 37 The temperature distribution in a vertical plane near the dam on August 17th, 2016. Left: field data. Right: simulation result (case CAL 1C).

The thermal structure along the reservoir near the dam is shown in Figure 35 for case CAL1C. All simulations showed a maximum drop in water temperature of 8 °C at the free surface, but this was not observed. However, the case of CAL1C came closest to the data.

For this approach during the period of study, only weak stratification was simulated in the thermal distribution, with the surface-bottom temperature difference reaching only 4°C. In comparison, much stronger stratifications were simulated and observed at approach B.

In the case of Approach C, the temperature oscillations at the free surface and at 4 m are simulated but the model still suffers from excessive heat losses, as the temperature of the layers below the air surface shows too significant daily decreases, which is not the case according to the observed data, as the air temperature shows oscillations of up to 14 °C. In contrast, the observed free surface temperature in the reservoir shows much smaller oscillations.

3.7 Discussion

This study aims to understand the spatiotemporal exchange of tropical thermodynamics with the atmosphere. There are simulation tools that allow us to dig deeper into issues and knowledge, and potentially address scenarios such as climate change. However, when these tools are applied to an area as large as this case study, it often becomes a computational problem rather than a physical problem.

First, the use of a supercomputer includes decisions such as the number of processors and the desired computational time. This research used the OLYMPE supercomputer of CALMIP, supercomputing center which is providing resources and services for the entire scientific community of the Université Fédérale de Toulouse Midi-Pyrénées (UFTMiP). OLYMPE has a SEQUANA Cluster (ATOS-BULL) 1,365 Pflop/s, 374 computational nodes (36 cores/node), Intel® Skylake 6140 Processor at 2.3 Ghz 18-cores.

For hydrodynamics simulations, 36 cores showed real-time performance with a ratio of actual computational time to simulated time of 0.8 to 1. However, the thermal equations solution required more cores to achieve similar performance when solved simultaneously with hydrodynamics.

Different configurations were tested using 36, 64, 120, 180, 288, and 324 cores. Using 324 processors makes simulations very fast, e.g., it took 16 to 18 hours to run eight days of thermic simulations; however, increasing numbers of cores exhibit diminishing returns, and this study believes that using 180 cores (which takes approximately 24 hours to run an 8-day simulation) provides the best balance between runtime and computing resources.

From the hydrodynamic perspective, several factors were analyzed, and it was found that specific parameters did not affect the thermal distribution, such as the use of hydrostatic pressure, horizontal turbulence models (Constant Viscosity, Smagorinsky, k-ω, and k-ε), coefficient for horizontal diffusion of velocities and the friction coefficient. While the number of vertical planes, Boussinesq approximation, the boundary conditions on the free surface, the vertical turbulence models (constant viscosity, mixing length, Smagorinsky, k-ω, and k-ε), and the value of the coefficient for vertical diffusion of velocities influenced the temperature distribution in the vertical direction. In several cases, the mixing-length turbulence model results in faster mixing in the vertical direction than the observed thermal profile data, while constant viscosity best represents the thermal distribution in the vertical direction.

Regarding the thermal dynamics, this research found that the structure of the solution was very sensitive to the choice of an advection scheme. Seven methods for linear advection treatment (1) Method of characteristics, 2) Streamline Upwind Petrov Galerkin (semi-implicit), 3) Explicit finite volumes, 4) Explicit scheme + MURD (Multidimensional Upwind Residual Distribution) N scheme, 5) Explicit scheme + MURD PSI (TELEMAC, 2020) (Positive Streamwise Invariant) scheme, 6) Explicit Leo Postma scheme for tidal flats, 7) Explicit scheme + MURD N scheme were used to analyze the behavior of the solution. Only the most relevant simulations were shown here for the sake of conciseness. Compared to other schemes, it was found that the MURD N scheme produces fewer numerical oscillations, less diffusion perpendicular to flow and thermodynamics, and is less computationally expensive. The scheme is also characterized by being conditional on a Courant number less than 1, satisfying the stability criterion.

The exchange process with the atmosphere is an essential and well-studied physical process. The tools used for its mathematical representation are still very limited, e.g., in the first layer of water temperature, the exchange between air and water also explains the behavior. The observations indicate that the external heat flux, which is determined by meteorological and inflow conditions, is insufficient to modify the nearly stratified state of the tropical reservoir. Many formulae in the studies can be used to compute this term (Eq. 10) but selecting an appropriate one is debatable. Generally, the net heat flux is calculated based on the water temperature and various meteorological data, primarily based on air temperature, air humidity, air pressure, measured shortwave solar radiation, and wind speed (although many others may be taken into account). An estimate of the net heat flux at the water–air

interface turns out to be a challenge, especially when it comes to 3D modeling.

The first problem concerns obtaining the necessary input data for the analyzed site. Intuitively, the nearest meteorological station is the best source for meteorological data. Unfortunately, in many cases, the nearest station does not provide all the necessary data or is still too far from the considered study zone. Another problem is the differences in data obtained from the neighboring stations. Even in conducive situations when the necessary meteorological data are available near the reservoir, there are still uncertainties related to the station's location, for which conditions such as shading or wind speed are often considerably different from those at the reservoir.

The problem is widely discussed in the work (Garner et al. 2014; Benyahya et al. 2010). Moreover, some measured quantities may vary along the reservoir (or even across the reservoir width). Finally, very different values of net heat flux may be obtained. Williams, G. P. (1963), for example, measured the heat fluxes for several reservoirs in different conditions. The results showed that the final sum of heat fluxes measured ranged between 113-378 W/m2/°C. In this case shows that A coefficient exchange value depends on the meteorological conditions, if they are constant over time or changing, and this research found the approximate values that can be used in tropical environment reservoirs.

Additionally, each term in Eq. (12) is sensitive to several factors, and the chosen computation method, i.e., different formulae, may lead to varying results since they often depend on not well-defined parameters, factors, or coefficients site-specific. Moreover, in the "competition" for the best formula, increasingly "more accurate" formulae take into account more and more factors and thus require more and more input data, which, again in practical applications, are rarely available or highly uncertain.

3.8 Conclusion

In this work, different modeling assumptions for tropical reservoir temperature and air-water exchange are analyzed based on observations. This study evaluated the performance of various hypothesis in resolving hydrodynamic, thermal, and energetic processes, including the effect of hydroclimatological forcings such as air temperature, wind, and the internal mixing process (turbulence), and different boundary conditions in the free surface. The following conclusions can be drawn:

Reservoir water temperature is affected by heat exchange between the water and the atmosphere. This exchange is evident in the upper layer (O (<10m)), and it is this dynamic in the first layer governs the distribution within the water body in areas where there is no advective flow from tributaries, which for the reservoir analyzed is on the order of 80%.

It was observed that the reservoir is permanently stratified and, unlike other reservoirs in the temperate zone, is not significantly affected by meteorological conditions outside the water body. This means that the thermal dynamics inside the reservoir remain very constant.

In this work, numerical methods are used as a tool to study exchange. This research finds that a good definition of the boundary conditions at the water-free surface is crucial for a correct representation of the thermodynamics inside the water body.

The hydrodynamic TELEMAC-3D model has been satisfactorily calibrated using one month of daily water level observations at one point in the reservoir. Sensitivity analyses highlighted the importance of vertical turbulence models and vertical diffusion coefficient for a correct representation of the observed behavior.

Overall, reservoir water temperature is strongly influenced by heat exchange between water and the atmosphere. Accurate modeling of such phenomena is thus necessary. Three different approaches have been tested to study the impact of air-water exchanges at the free surface: a constant water temperature without exchange with the atmosphere (approach A), meteorological forcing with atmospheric parameters constants in time (approach B), meteorological forcing with atmospheric parameters varying in time (approach C).

Not considering the exchange process at the free surface can produce a good performance in the first layers of the reservoir (approach A). However, it may lead to overestimating the measured temperature in the deepest layers due to non-observed mixing processes. Moreover, it does not allow to simulate daily temperature oscillations.

Approach B with constant values of air temperature and wind, is the one that best represents the thermal stratification in terms of thermal distribution in the reservoir; however, there are excessive heat losses, which do not occur in reality. To better control these losses, Mesquita et al. (2020) recommend explicitly simulating evaporation in the reservoir.

Although Approach C is the only approximation that shows hourly fluctuations in the temperature of the first layer of the reservoir, these fluctuations are larger than the observed ones. Simulation results show oscillations between 2°C and 4.5°C, whereas observed variations range between 1 and 2°C. This may be due to the fact that the reservoir is located in a relatively sheltered canyon, as mentioned by Plec et al. (2021).

The results show that the parameter that mainly influences the thermal exchange model, thus improving the numerical reproduction of the thermal stratification processes, is the exchange coefficient A. A represents processes such as radiation, air convection in contact with water, and latent heat. Its correct determination improves the simulation results. According to the results of this study, when taking into account the exchange process between the water and the atmosphere under different forcings of the meteorological variables, a range of variation of A◎ [100, 900] W/m2/°C is best when the air temperature remains constant over time and lower values of A◎ [30, 40] W/m2/°C are best when weather conditions vary over time.

Although some uncertainties are present in the current numerical study about the A exchange coefficient tested in the simulations, the results are in a satisfactory agreement to data, especially considering the complexity of the studied phenomenon, as well as the equally complex dynamics of the various processes' interactions involved in its numerical simulation. In particular, regarding the water temperature at different depths, the following convergence results are observed: approach A maximum deviation from data reaching 3°C, approach B maximum deviation from data reaching 4°C, and approach C maximum deviation from data reaching 8°C.

In conclusion, it can be stated that if site conditions and air-water temperature differences are known, A coefficient can be used as an approximate method of estimating the rate of exchange of natural water surfaces in a reservoir on an hourly basis during every period in the year.

Future works will require rethinking the exchange formulas for the tropical context

including evaporation, as the existing ones are not able to reproduce the variations in the water column of the reservoirs.

Chapter 4

4 A model to describe the effects of low flow on benthic algae and nutrients in the Cauca River (Colombia)

*The results of this chapter is in review in the Journal of Inland water, 2024.

Abstract: The rivers of the neotropical region of the Andes present a seasonality in the water flow that is intensified during extreme climatic events. Climate change projections suggest that droughts will be much more intense in the coming decades. With a total length of 965 km, the Cauca River is one of the most important ecosystems in Colombia. Hence, extreme climatic events strongly impact the organization of aquatic communities and environmental services. Benthic algae are good indicators of the impact of environmental and anthropogenic stressors. Because local and regional factors in these environments change at different time scales, the factors that make up algal communities may also change over time. However, the temporal dynamics of communities have rarely been assessed, and how they relate with nutrients for extreme drought. This study investigated the impact of two severe droughts with low flows on benthic algal communities in the Cauca River. A zero-dimensional mathematical model based on a set of ordinary partial differential equations was developed to analyze the substrate, space requirements, temperature, light, nutrient availability, organic load, and algal biomass changes. The results showed that the Cauca River is an ecosystem enriched with nutrients and with a high physical instability of the substrate, where algal biomass can be recovered in a few days after a low flow period. According to the analysis, diatoms and cyanobacteria have strategies to persist during periods of intense shallow water flow.

Keywords: water quality, benthic algal, nutrients, modelling, reservoir impacts.

4.1 Introduction

The Colombian rivers in the tropical region of the Andes present a seasonality in the flow that intensifies during extreme climatic events. Climate change projections suggest that droughts will be much more intense in the coming decades (Cerón et al., 2022).

The Cauca River is one of the most important ecosystems in Colombia, running through the country from south to north along 965 km. Therefore, extreme climatic events have a strong impact by affecting the organization of aquatic communities and environmental services. Some of the problems in the Cauca River basin have been progressively deteriorating, which has affected its quality (Sánchez Torres et al., 2022). Currently, the river shows a critical condition for 36 hydrographic subzones which form the Cauca River, 34 subzones have high pressure for demand and climatic variability; 28 have very high pressure on ecosystems; 26 subzones have high pressure due to contamination (IDEAM, 2019).

In year 2019, the river experienced one of these extreme low-flow conditions due to an anthropic incident, due to the closing of the gates of a dam located on the Cauca River in the municipality of Ituango. The gate closures during January and February 2019, caused a decrease in water flow in the Cauca River downstream of a dam. The event had several impacts on hydrodynamics, sedimentology and hydraulic behavior, aquatic biota, and water quality. From the point of view of the biotic communities, the response to this eventuality may vary according to the strategies and evolutionary traits developed by the organisms. For this type of event, organisms such as periphytic algae have developed interesting adaptation strategies (Sabater et al., 2016).

Benthic algae play a fundamental role in the food webs, and they are a good indicator of the effect of environmental and anthropic stressors on rivers (Lake, 2003). Some studies have demonstrated the role of periphyton in shallow streams, especially regarding (i) the nitrogen cycle, and (ii) the cycle of organic matter (Flipo et al., 2004). Other what water velocity and nutrient concentrations are among the most important factors influencing periphyton biomass in streams (Saravia et al., 1998a) and as well taking about the influence of the light environment on the interactions between these communities (Sánchez et al., 2017). Thus, since in these environments the local and regional factors change at different temporal scales, factors structuring algal communities might also differ over time. However, the temporal dynamics of communities have rarely been assessed and their relationship with nutrients for low flow, using modeling.

Periphyton modeling has historically been dominated by empirical approaches. Structured empirical modeling has a long history in limnology for predicting (periphytic) algal biomass concerning nutrients (Larned, 2010) (Saravia et al., 1998b). Regression models relating periphyton biomass to nutrient concentrations and other variables have been used for rivers in Missouri (Lohman et al., 1992), a river in Montana (Dodds et al., 1997), and rivers in New Zealand (Biggs Barry J. F. & Kilroy Cathy, 2000). Empirical models use aggregate data representing average conditions to reveal average system-level responses based on correlations. Mechanistic models use disaggregated data representing specific conditions to reveal system-level responses based on an understanding of the underlying processes. But this type of modeling rarely links elements such as hydrology, hydraulics, water quality, and biota.

The models mentioned above allow simulating the changes that occur over time due to the

series of flows that occurred for the contingency event; however, accurate modeling remains a challenge. Many traditional models have been developed to predict periphyton biomass under different conditions, but they are only useful under specific conditions and cannot accurately model the wide range of factors that co-control the periphyton biomass. Alternate systems, including artificial intelligence methods, have advantages in dealing with non-linear relationships in a complex system (Huang et al., 2021). Only a few water quality models simulate periphyton in streams with any accuracy because of the many factors affecting them, such as: 1) Periphyton mats include live algae and detritus, 2) Periphyton may be stimulated by nutrient enrichment, 3) Shading by riparian vegetation may severely limit available light, 4) High flows may cause sudden sloughing, 5) Snails and other animals may graze heavily on periphyton. However, there is currently no evidence of the impact of hydrology and hydraulics on periphyton, coupled hydrodynamic models, water quality, habitat changes, and changes in flow rates under low-flow conditions.

It is analyzed that the stability of the ecosystem is given by the resistance or the insensitivity to the disturbance, and the resilience or the resilience after the disturbance (Shade et al., 2012), in the case of the rivers it has been identified that they have low resistance, but high resilience, due to the duplication times of organisms (Stanley et al., 2010). When periods of low flow or drought are more extreme than those experienced on average, the biota may not have the necessary adaptations for adequate resistance or resilience (Rolls et al., 2012). In a river or in an area of the river that dries up, there are several shelters for microorganisms, such as perennial pools, leaf litter packets (Ylla et al., 2010a), and subsurface sediments, which can temporarily provide wet environments. This may be enough as long as the humidity remains, but the prevalence of microorganisms depends on the intensity and severity of the drought. Alternatives for some organisms are to go dormant until conditions are favorable again, or they can colonize the particular habitat from the outside (Sabater et al., 2016). Accordingly, and taking into account the short duration of the drought, we hypothesized that the recovery capacity of the periphyton is very high and that the negative effects of low flow are attenuated under conditions with a high nutrient concentration in the Cauca River basin.

In this same sense, the study aims to investigate the influence of extremely low flow conditions on environmental factors and the benthic algal community in the Cauca River. A coupled mathematical model was developed to analyze the substrate, space requirements, temperature, light, nutrient availability, organic load, and algal biomass changes, under two drought scenarios. Owing to the unexpectedness of the flow reduction, there are no algal biomass data during the two sudden flow reductions reported in 2019 and the subsequent recovery. Therefore, this model contributes to the assessment of the impacts of the disturbance. This leads to analyzing different modeling assumptions and evaluating model performance over short days based on observations. Section 2 outlines the characteristics of the study site. Then, next subsections present the data source, the governing equations and mathematical model, and details the model configurations that has been implemented along with the performance criteria. Finally, Section results describes the results, and a discussion of the main findings is given.

4.2 Materials and methods

4.2.1 Study case

The Cauca River is the second most important river in Colombia, after the Magdalena River and is the main tributary of it. It is located among the central and western mountain ranges along 1,350 km, covering seven departments from its source at 3,900 meters above sea level (masl) until it reaches the Brazo de Loba near the municipality of Pinillos in the department of Bolivar (see **Figure 38**). In 2012 began the construction of The Ituango Hydroelectric Project in the Cauca River. It is the largest hydroelectric project in the country, with a generation capacity of 2,400 MW. The project includes a 225 m high dam that stores up to 20×10^6 m3 and an underground plant with eight generation units. During construction, in 2019, several problems at the site caused a sudden reduction in water flow in two moments (EPM, 2020) leading to the closing of the sluices gates.

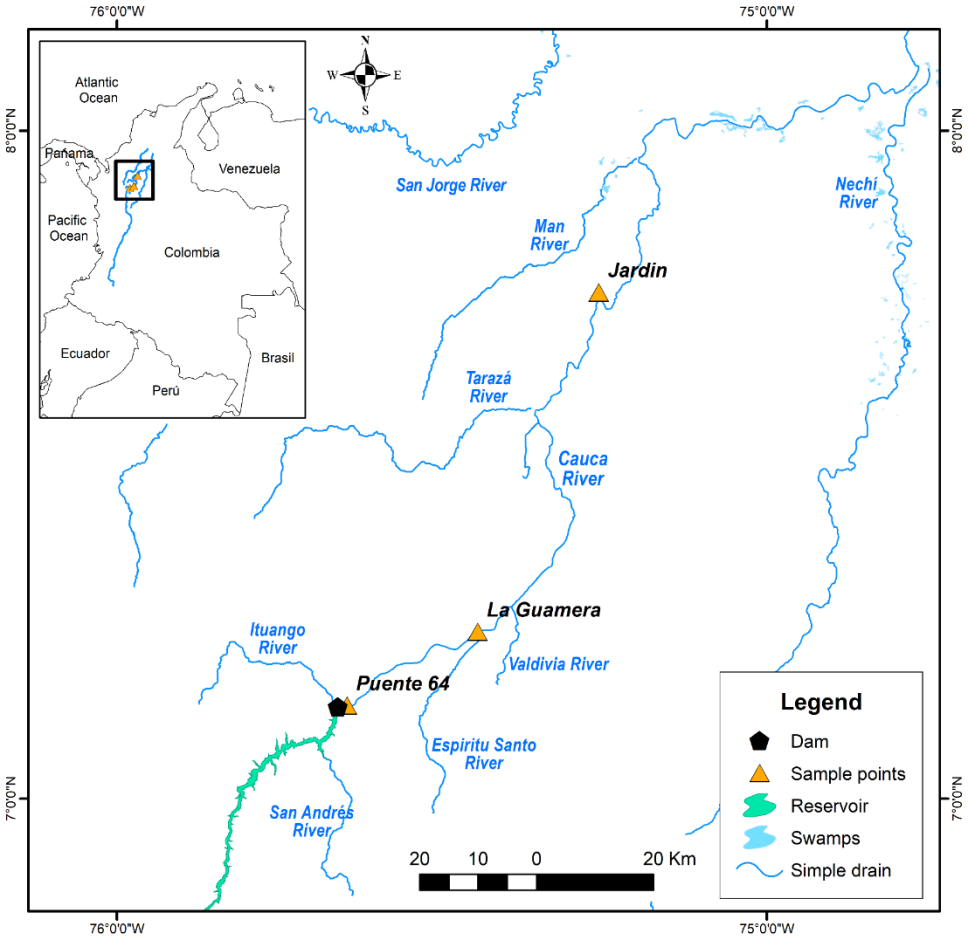

Figure 38 Study area in the Cauca River, Colombia

Gate closures during the 2019 emergency resulted in very low water levels and could be considered an ecological disturbance affecting the river (Resh et al., 1988). These occur at different spatial and temporal scales and are characterized by intensity, severity, frequency, predictability, and spatial extent along with the responses of organisms (Rolls et al., 2012b). These events can have cumulative effects in time and space, and configure disturbance regimes, that is, continuous transformation processes that move the system away from its

historical ranges of variability (Gaiser et al., 2020), (Lake, 2000). Identifying different types of disturbances is particularly useful for studying those disturbances that are of anthropogenic origin and often do not fit well into traditional definitions (Stanley et al., 2010).

4.2.2 Data source

Data on water quality parameters such as temperature (T °C), turbidity (Turb), and dissolved oxygen (DO, mg/L) were measured monthly on site. In addition, other monthly data were taken to perform laboratory analysis to measure concentrations of biochemical oxygen demand (BOD5 mg/L), ammonia (NH4+ mg/L), nitrate (NO3- mg/L total organic nitrogen (TON mg/L), phosphate (PO43- mg/L), and organic phosphorus (organic P mg/L). There are 33 monitoring stations on the river. Three sites were selected downstream of the dam: Puente 64, Guamera, and Jardin (see **Figure 38**) The first point is very close to the reservoir dam at 1.76 km, the second point is at 29.5 km and the third point is the farthest at 106.1 km. The measurements and samplings were carried out between the years 2012 and 2020.

For algae, monitoring was carried out using periphyton data from the stations Puente 64, La Guamera, and Jardin stations between 2013 and 2018. In the analysis, we considered activities carried out between January, February and March, which correspond to periods of low precipitation and low flows. See Table 8.

Table 8: Physicochemical characteristics of the Cauca River in the sample points studied.

Station	Puente 64			Guamera			Jardin		
	Mean	Min	Max	Mean	Min	Max	Mean	Min	Max
DBO_5 (mg/L)	5.1	2	12.7	<5			2.12		
PO_4^{3-}(mg/L)	0.32	0.08	1.69	0.29	0.1	0.63	0.21	0.06	0.54
P organic (mg/L)	0.11	0.02	0.73	0.26	0.04	0.87	0.44	0.04	1.15
NH_4^+ (mg/L)	1.21			<1			<1		
NO_3^- (mg/L)	1.87	0.33	3.89	0.26	0.04	0.87	2.3	0.67	3.82
TON (mg/L)	1.21			<1			<1		
OD (mg/L)	8.5	6.18	9.98	8.3	7.54	9.14	7.94	7.25	9.38
T (°C)	26			26.5			26.7		
Turbidity (NTU)	132.5	10	850	200			67		
Periphyton Biomass ($\mu gC/m^2$)	4.51	0.01	65.74	3.97	0.01	40.46	1.23	0.02	20.4

TON: Total organic nitrogen, DO: dissolved oxygen, T: water temperature, Min: minimum, Max: maximum

The calibration data used correspond to the year 2018 and contain 280 data from water quality campaigns, taking historical records into account.

The hydroclimatological information used in the simulations was obtained from the stations at the Presa, Valdivia, and Cuba hacienda sites for January, February, and July 2018 and 2019, which were selected for the modeling scenarios. Data come from the DHIME website of the Institute of Hydrology, Meteorology and the Environment (IDEAM, acronym in Spanish). Hydrodynamic parameters such as friction and water velocity were obtained from

calibration models of the study area performed in January and February 2016 and January and February 2019.

4.3 Proposed Mathematical model

A model set is developed to predict water quality in a river. The proposed model couple Periphyton Biomass, PO43-, organic P, NO3-, NH4+, TON, BOD, and DO, employing a set of ordinary differential equations which are solved numerically using the 4th-order Runge-Kutta method.

The model is composed of two modules (**Figure 39**). The hydrodynamic module is based on the computational tool TELEMAC 2D (TELEMAC, 2020) to obtain velocity, friction velocity, and water depth, simulations run for January and February 2016 and January and February 2019. The second module corresponds to the water quality model developed in this work.

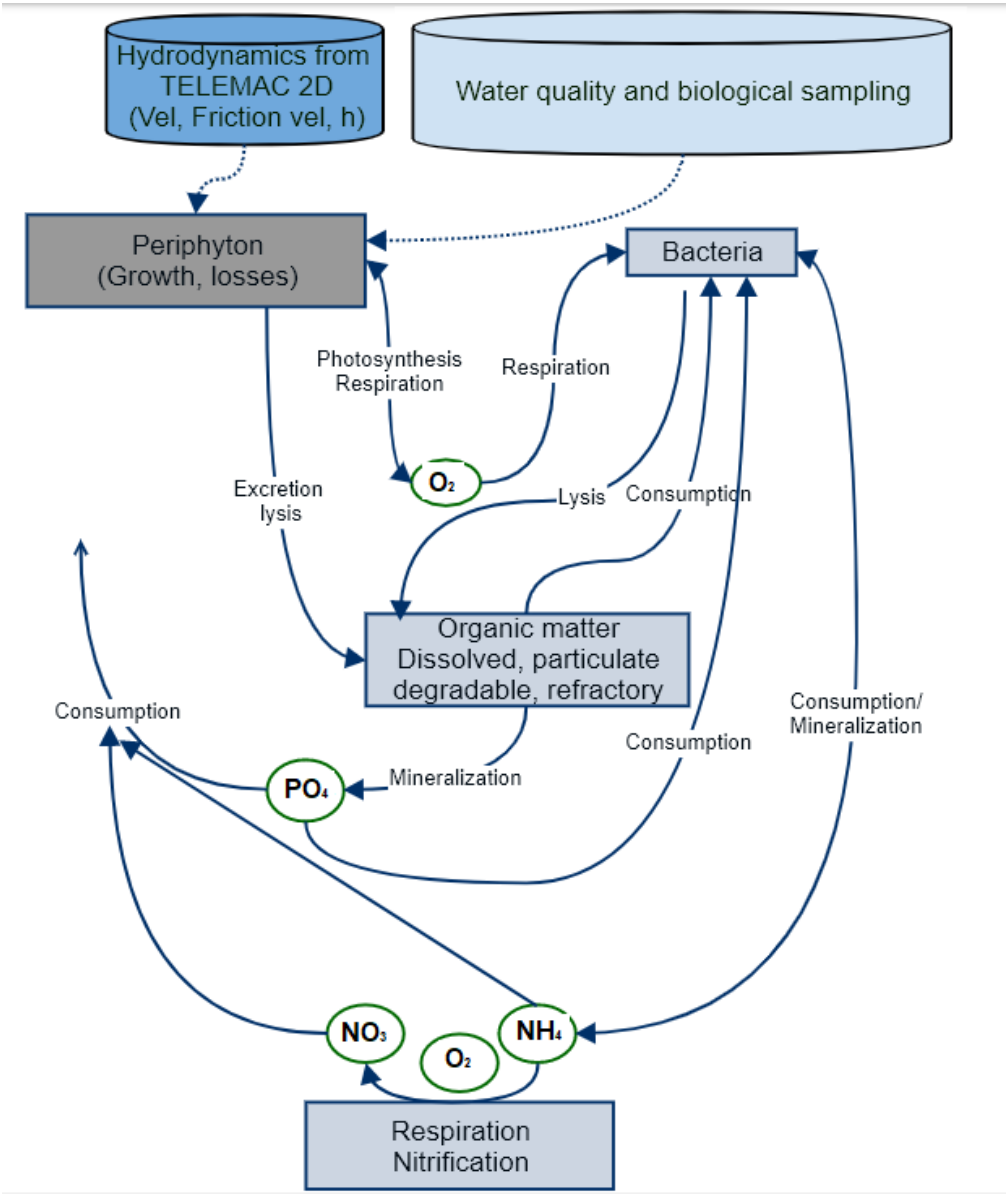

Figure 39 The conceptual model of the modeling approach used.

The water quality model is an adaptation of the WAQTEL numerical module (WAQTEL, 2021), where the primary producer was modified from phytoplankton to periphyton, and subsequently, the processes from periphyton described by the governing equations were adapted for the specific case of a tropical river.

4.3.1 Governing Equations

The periphyton is a component of aquatic communities, composed of microbiota attached to different substrates; It plays a fundamental role in the transfer of matter and energy through trophic networks and its study is important both from ecology, to understand ecosystems, and from an environmental point of view since the periphyton is a good indicator of processes and environmental conditions. The periphyton plays an important role in the processes of river ecosystems, especially at high and intermediate nutrient levels where the contribution of the periphyton to primary production can be similar to or exceed that of the phytoplankton. Given the above, here we study the influence of environmental and spatial factors over time in the periphyton community in the Cauca River system.

In equations 1, 2 and 3, the change in the biomass of the periphyton concerning time was quantified through the growth mechanisms (Gper) and the mechanisms of biomass loss (Ls), where Gper is a function of φTemperature, φI (light), φNutrients and φPeriphyton and the losses as a function of respiration (R), grazing (G), shedding (S) and mortality (Mper) (Kuczynski, 2019).

$$\frac{dPER}{dt} = GPer\ [PER] - Ls[PER] \tag{1}$$

Periphyton growth

$$GPer = \mu max\ \times \varphi Tper \times \varphi I \times \varphi N \times \varphi P \tag{2}$$

Periphyton losses

$$Ls = R + G + S + Mper \tag{3}$$

When the substrate, space requirements, temperature, light, and nutrient availability, hereinafter referred to as environmental forcing conditions are favorable, the rate of periphyton biomass production increases. When the resulting net growth rate or the difference between growth and removal rates is positive, biomass is gained (accumulated); when it is negative, biomass is lost. The modeling challenge lies in describing and quantifying the effects of each term in the Equation well enough to predict biomass with an acceptable level of precision. In this matter, for example, the extinction coefficient ke was calculated using the following expression (see Eqn. 4), which was an empirical relationship of the data from the measurements on the Cauca River. Correlations were established between turbidity data and coefficients reported in the literature.

$$ke = (0.62 * Turbidity)^{0.5} - 0.08 \tag{4}$$

On the other hand, normally the processes that are modeled in water quality correspond to DO, BOD5, nutrients, and primary production centered on phytoplankton. In the case of the study, the model is developed in MATLAB so that the entry of new processes and new functional relationships (equations) is possible, through a model where the primary

producer corresponds to the periphyton.

Coupling of periphyton with quality variables suspended in the water

The Periphyton equation (1) is coupled with the following equations to generate a set of ordinary differential equations. The equations related to primary production processes, organic matter decomposition and nutrient utilization by periphyton are shown below, as well as the system of equations coupled to the model for periphyton and their exchange with nutrients.

$$\frac{dPO_4}{dt} = fp(dtp.Ls - Gper)PER + Kp.g2.POR \quad (5)$$

$$\frac{dPOR}{dt} = fp(1 - dtp)Ls.PER + Kp.g2.POR - \frac{FOR}{H} \quad (6)$$

$$\frac{dNO_3}{dt} = -fn(1 - Rn)Gper.PER + KNit.g2.NH4 \quad (7)$$

$$\frac{dNOR}{dt} = fp(1 - dtn)Ls.PER + KN.g2.NOR - \frac{NOR}{H} \quad (8)$$

$$\frac{dNH_4}{dt} = -fn(dtn.Ls - Rn.Gper).PER + KN.g2.NOR - KNit.g2H4 \quad (9)$$

$$\frac{dBOD_5}{dt} = f.Mper.PER - kL.g3.BOD_5 - \frac{LOR}{H} \quad (10)$$

$$\frac{dDO_2}{dt} = (Gper - RP.g1)PER - n.KNit.g2.NH4 - kL.g3.DBO + k2.g4(Cs - O2).\frac{BEN}{H} \quad (11)$$

Where, fp is average of the portion of phosphorus in the cells of the periphyton (mg P/mg C /l) , dtp is portion of the phosphorus directly assimilated by the dead periphyton (%), kP is rate of transformation from POR to PO43- through bacterial mineralization (day-1), g2 is effect of temperature, g3 is effect of temperature on the degradation of the organic load, g4 is effect of temperature on natural re-aeration, FPOR is sedimentation rate of organic phosphorus (m/s), FNOR is organic nitrogen sedimentation rate (m/s) , kNit is Nitrification kinetics at 20 ° C (day-1), fn is average of the nitrogen portion in the cells of the periphyton (mg N/mg C /l), dtn is portion of nitrogen directly assimilated in dead periphyton (%), n is amount of oxygen consumed in nitrification (mgO2/mg NH4+), kN is NOR to NO3- transformation rate through autotrophic and heterotrophic bacterial mineralization (day-1), kL is organic matter degradation constant at 20 (day-1), FLOW is sedimentation velocity of the organic load (m /s), f is amount of oxygen produced in photosynthesis (mg O2/mg C/l), BEN is benthic demand (gO2/m2/d), k2 is reaeration coefficient, Cs is saturation oxygen (mg O2 /l) and T is Water temperature (°C). These constants were calibrated and adjusted according to field data from the sampling stations of the Cauca River, described in the section data source.

To carry out the coupling of the equations with the periphyton, conversions to carbon were carried out since the entire system of equations was coupled to the units of Chlorophyll (µg

Clh-a /l). The tracer reactions are to analysis in terms of dry carbon biomass. The conversion rates of O2 (mg O2 /mg C), nitrogen (mgN / mg C), and phosphorus are expressed in the equations by the constants f, fn and fp. These transformations are adjusted during the calibration process. Details of the model are shown in the supplementary material (S1).

4.4 Model configuration

In this work, field data are used, 0D simulations are performed and compared. Sensitivity analysis was performed using R software via GSA.UN (ref). Allowing focus on key variables and coefficients. In order to calibrate, the Ostrich tool (ref) was used to determine the parameters that best fit the time series.

The data required for model implementation are analyzed, the mathematical equations and their implications for modeling are discussed, and the model is adjusted accordingly as a basis for understanding periphyton dynamics.
The hydrodynamic model and periphyton are calibrated against observational data, and the errors are quantified using the NSE metric. The Nash–Sutcliffe model efficiency coefficient (NSE) is used as a performance metric (see Eqn.).

$$NSE = 1 - \frac{\sum^{n} (\widehat{Xi} - Xi)}{(Xi - \overline{Xi})} \tag{18}$$

In the above equation, n points to the sample size, e is the error, (Xi)ˆ is the predicted value of the criterion, Xi is the measured value of the criterion, and (Xi)¯ is the mean of the measured values.
Once the model was calibrated, we proceeded to run 2 scenarios, for which it is important to consider macro climatic phenomena (ENSO: El niño –oscilación sur) caused by the increase or decrease in the average surface temperature of the equatorial Pacific Ocean. Surface waters are relatively warmer (El Niño) or colder (La Niña) than normal in the central and eastern tropical Pacific, off the coasts of northern Peru, Ecuador, and southern Colombia. Due to their climatological importance. Next, analyze the model's response to different scenarios and compare the results with observational data. To evaluate the model of two drought scenarios for the Cauca River (showed in **Figure 40**), one event being a moderate drought and the other a complete loss of water flow over three days.

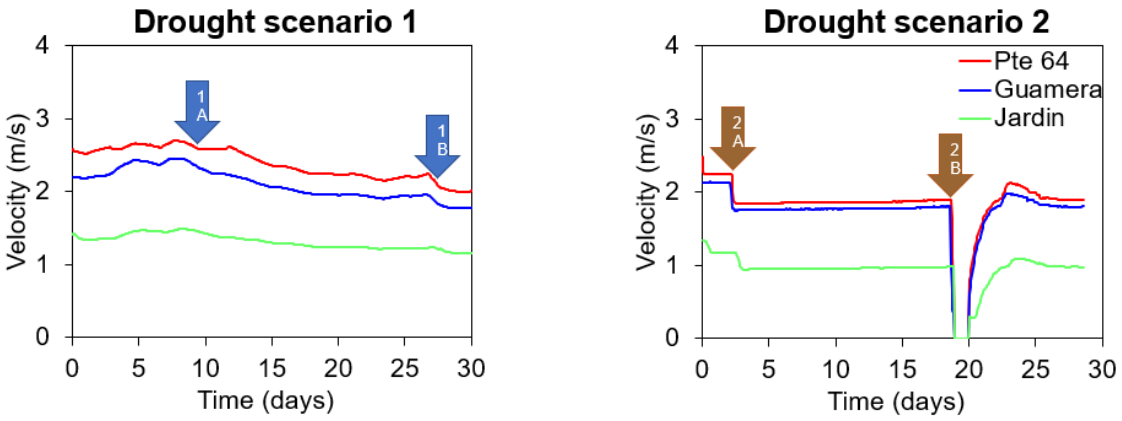

Figure 40: The scenario of low flow in Cauca River. Arrows indicate a significant reduction in the water flow during drought scenario 1 (blue) and scenario 2 (Brown).

Considering that the research focus is on sub-daily water quality changes and hydrodynamics, the hydrodynamic model conditions are assumed to be transient time series data in January and February 2019.

The information used as an initial condition in the periphyton model corresponds to the average water quality and periphyton concentrations presented in the months of January and February. In the case of 2019, the data measured for the months immediately prior to the modeling month were taken.

The hydrodynamic boundary conditions are as follows. First, this research imposes the flow rate at the upstream part of the rivers using the collected field data (medium value Q1=23.1 m3/s, Q2=19.6 m3/s, Q3= 20.2 m3/s, Q4=16.6 m3/s, S5= 49.4 m, Q6= 59.7 m3/s, Q7=9.9 m3/s, Q8= 18.7 m3/s, Q9= 5.0 m3/s. Q10= 15.1 m3/s and Q11= 1056.6 m3/s), and as a downstream boundary condition free surface with medium SL(5)= 49.4 m. Their location is Q1 in Espiritu Santo River, Q2 in Cauca River Valdivia, Q3 in Creek Corrales, Q4 Tamana Creek, S5 downstream boundary condition Cauca River, Q6 in Taraza river, Q7 in Puqui Creek, Q8 Pescado river, Q9 Guamera river, Q10 Sinitave river and Q11 Cauca River upstream boundary condition. For water quality models that include periphyton, the boundary conditions are the same and their concentrations correspond to historical data measurements.

Modeled scenarios take into account changes in hydrodynamic conditions and water quality concentrations. The first hydrodynamic scenario simulated here corresponds to the first flow reduction in a typical neutral or normal year between January 14 and February 20, this event occurred when there were two sudden traffic decreases, on January 24 (1A) and February 14 (1B),.The second scenario corresponds to the drought during the 2019 contingency between January 14 to February 20, in which two moments with a significant reduction in flow occurred on January 17 (2A) and February 5 (2B), respectively, reaching the minimum level in Valdivia on February 6, see in **Figure 40**.

In addition, the water quality forcing with nutrient simulations was performed to compare the model response as follow: 1. Low concentration of nutrients (historical data), 2. Mean concentration (historical data), 3. High concentrations of nutrients (historical data).

Simulations varying the values of velocity and nutrients were performed to contrast the model response against the expected results from the literature.

4.5 Results

4.5.1 Characterization of the periphytic communities in the Cauca River.

Historical basin monitoring data show that during the regular dry season, which is similar to the conditions presented for drought 1, the benthic algal communities are dominated by diatoms and cyanobacteria (**Figure 41**). These groups have strategies that allow them to persist in extreme periods with very low flow.

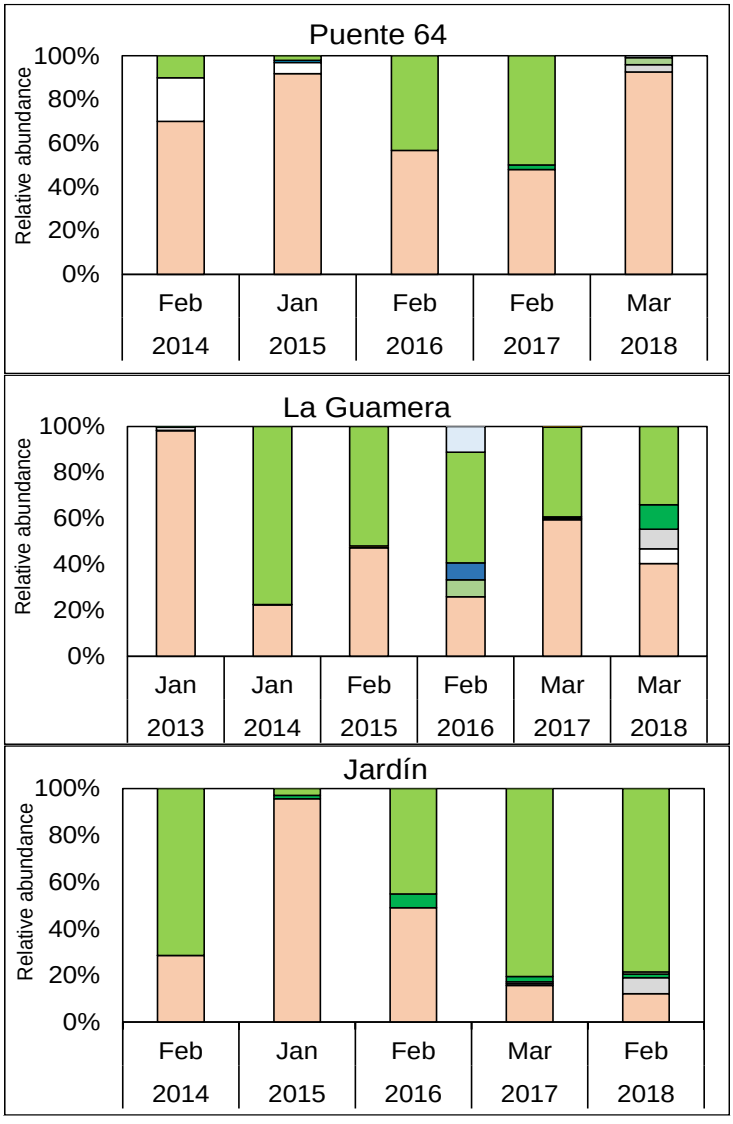

Figure 41: Composition of periphytic algae in the Cauca River between 2013 and 2018

The dominance of the Bacillariophyceae group in rivers during periods of low flow has been reported in other types of ecosystems such as the Mediterranean streams (Caramujo et al., 2008) the ecological strategy of these organisms favors their presence in ecosystems subjected to environmental stress due to their high recruitment rates and reproductive strategies quickly colonize the epilithic environment. Diatoms have different forms of resistance and

resilience to substrate emergence, so the response to desiccation depends on the history of disturbance and the response creates heterogeneity in the structure of the community (Cassler et al., 2008) (Ledger et al., 2013). The most obvious strategies for desiccation resistance are mobility to seek moisture in the hyporheic zone, high physiological plasticity, formation of mucilaginous tubes that prevent desiccation, obtaining energy through the heterotrophic pathway, among others (Sabater et al., 2016c). The latter strategy has been well documented in the genera Navicula and Nitzschia (Kamikawa et al., 2015), which were dominant during some campaigns corresponding to the lowest flow season in the Cauca River and its marshes. Also, adnate/prostrate and erect/stalked species are more resistant and resilient than the other life forms (SCHNECK & MELO, 2012). This includes a large proportion of the dominant forms in the periphytic diatoms of large rivers. Some diatoms migrate to deeper areas of the sediment to prevent desiccation (McKew et al., 2011).
The other dominant group during this seasonal cycle in the Cauca River and its floodplains were cyanobacteria, these organisms have a multilayer of peptidoglycans with a thickness of 20 to 40 nm that are part of their cell membrane, usually forming a physical barrier to desiccation (Hoiczyk & Hansel, 2000). Additionally, the excretion of polysaccharides by cyanobacteria facilitates water retention in the biofilm and makes rehydration possible during periods when water levels are low (Ylla et al., 2010b).

Cyanobacterial mats composed of algae of the genus such as *Nostoc* have been documented to dry completely after five hours of sun exposure, with re-wetting in 10 minutes to regain their photosynthetic capacity. However, its nitrogen-fixing activity takes approximately 24 hours to reactivate. Algae of the genus *Phormidium* are not as tolerant but can be recovered in 10 days. After three years of drying cyanobacterial mats, it was possible to find viable diasporas (Hawes et al., 1992). The species *Oscillatoria agardhii* and *Lyngbya martensiana* survived between 5 and 10 days of desiccation respectively (Agrawal & Singh, 2002), examples that illustrate the ability of these organisms to withstand extreme environmental conditions. Therefore, it is difficult to quantify instantaneous losses when their recovery rate is so high. However, the data suggest that the recovery capacity of the periphyton is very high, so the energy supply to the food web was little affected.

4.5.2 Sensibility and Calibrations

To calibrate the parameters, 30 cases were carried out, some parameters were adjusted, the metrics results are shown in **Table 9** and **Table 10** show the values chosen for each periphyton variable. For all the variables analyzed, the metrics presented a good fit.

Table 9: Summary table performance of periphyton model calibration coefficients with NSE index

Metric/site	Puente 64	Guamera	Jardin
Nash Metric Per	1.16	0.00	1.23
Nash Metric PO_4	1.95	1.67	0.54
Nash Metric POR	1.07	3.61	0.79
Nash Metric NO_3	0.0	0.00	1.07
Nash Metric NOR	0.0	0.00	0.00
Nash Metric NH_4	4.82	0.00	0.00

Nash Metric BOD	1.76	0.00	0.00
Nash Metric DO	0.83	7.52	1.06

Table 10: Values of the biological parameters of algal periphyton used in the model for each sample point.

Calibrated parameters	Symbol	Reference values*	Pte 64	Guamera	Jardin
The maximum growth rate	Umax	0-300	5.0	300.0	4.68
Rate of photosynthesis	Ps	0.3-9.0	1.0	0.5	1.0
Max rate of photosynthesis	Pmax	0-1500	150	1500	150
Carrying capacity	Kr	Max 0.5	0.05	0.01	0.05
Grazing	G	-	0.00001	0.00001	0.00001
Mortality	Mper	0.05	0.0005	0.00005	0.00005
Degree of sloughing	d1	-	0.02	0.0001	0.02

* from WASP 2006

In the case of nutrients, and nitrate in particular, it was identified as not good adjustment however, the concentration value was found to be within the range of values it has historically presented. The model is validated using expert criteria, general historical trends, and parameters.

The results show good performance of the calibration parameters according to metrics based on observational data. In the **Figure 42** results obtained comparing simulated vs. observed are presented. The figure shows the results for some quality variables, such as periphyton, O_2, PO_4^{3-} and NO_3^-.

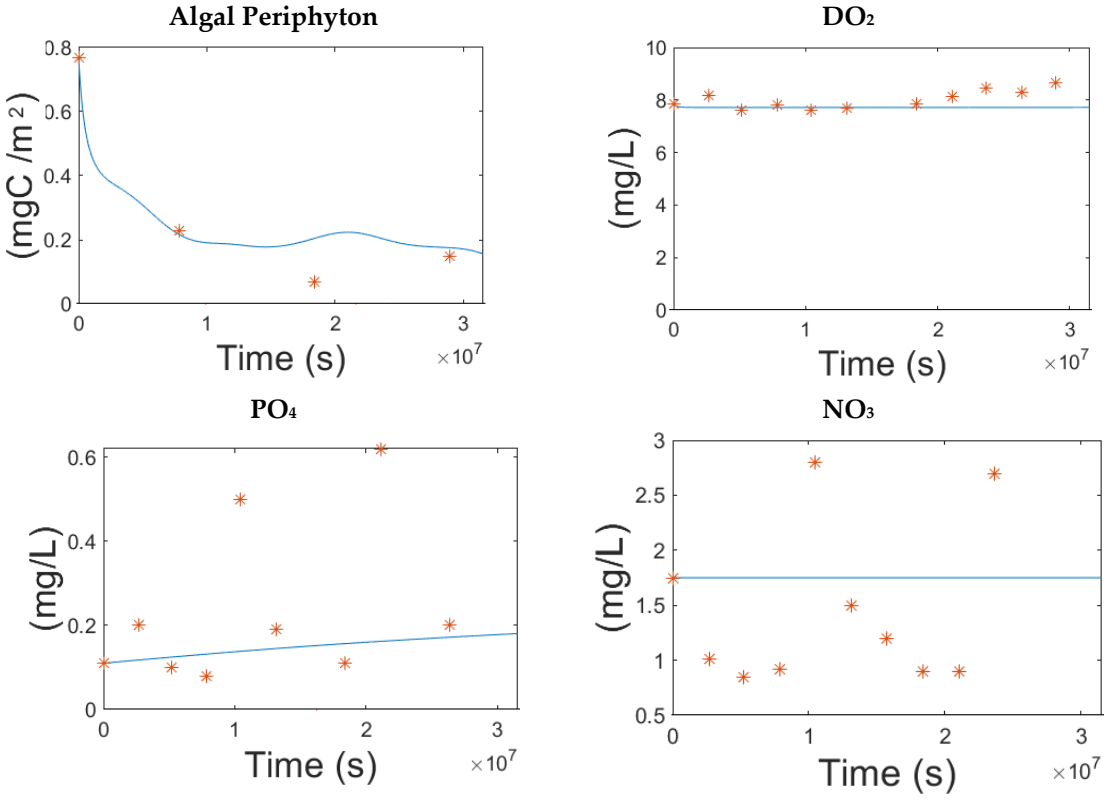

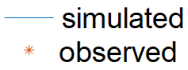

Figure 42: Comparison between the simulated and the observed values in the sample point Puente 64.

4.5.3 Nutrients and algal biomass response to the low flow scenarios

DO at the site, Pte 64 presented the lowest values for drought scenario 2 with low nutrients, this being the most critical scenario. This behavior was also seen in Guamera and Jardin. For the nutrient NO_3^- there was not much variation in the simulated scenarios at all analysis points. The fast algae response to the drought occurred in the mean and highest nutrient concentration models. For both drought scenarios, PO_4^{3-} was depleted in Guamera and Jardin. Organic matter showed complete degradation in Guamera and did not show significant changes in concentrations in simulated scenarios. (**Table 11**).

Table 11: Water quality parameters simulated for the drought scenarios

Station	Simulated values	PO_4^{3-}(mg/L)	NO_3 (mg/L)	DBO_5(mg/L)	OD (mg/L)	Periphyton Biomass (µgC/m²)	Nutrients condition
			Drought 1				
Puente 64	Min	0.08	0.33	1.12	3.06	0.39	**Low P and N**
	Max	0.09	1.69	2.00	7.87	4.51	
	Min	0.32	1.87	2.86	4.84	1.20	**Mean N and P**
	Max	0.32	3.23	5.10	8.50	4.51	
	Min	0.91	3.89	7.11	5.92	4.51	**High N and P**
	Max	1.69	5.25	12.70	9.98	50.26	
			Drought 2				
	Min	0.08	0.33	1.12	3.05	1.43	**Low P and N**
	Max	0.08	1.69	2.00	7.87	4.51	
	Min	0.31	1.87	2.86	4.83	2.37	**Mean N and P**
	Max	0.32	3.23	5.10	8.50	4.51	
	Min	1.42	3.89	7.11	5.91	4.51	**High N and P**
	Max	1.69	5.25	12.70	9.98	43.12	
			Drought 1				
Guamera	Min	0.04	2.64	0.00	5.43	0.03	**Low P and N**
	Max	0.06	3.73	0.00	7.95	3.97	
	Min	0.29	2.98	0.00	5.84	0.18	**Mean N and P**
	Max	0.31	4.07	0.00	8.30	3.97	
	Min	0.00	3.40	0.00	6.32	2.13	**High N and P**
	Max	0.63	4.49	0.00	9.14	6.62	
			Drought 2				
	Min	0.04	2.64	0.00	5.02	0.32	**Low P and N**
	Max	0.06	3.74	0.00	7.95	3.97	
	Min	0.29	2.98	0.00	5.52	0.32	**Mean N and P**
	Max	0.30	4.08	0.00	8.30	3.97	
	Min	0.00	3.40	0.00	6.10	1.37	**High N and P**
	Max	0.63	4.50	0.00	9.14	46.20	
			Drought 1				
Jardin	Min	0.06	0.67	0.21	7.15	0.14	**Low P and N**
	Max	0.06	1.88	2.12	7.91	1.23	
	Min	0.00	2.30	0.21	7.18	1.23	**Mean N and P**
	Max	0.21	3.51	2.12	7.94	19.14	
	Min	0.00	3.82	0.21	7.24	1.23	**High N and P**
	Max	0.54	5.03	2.12	9.38	31.44	

			Drought 2			
Min	0.06	0.67	0.58	5.21	0.50	**Low P and N**
Max	0.06	1.91	2.12	7.91	1.23	
Min	0.13	2.30	0.58	5.57	10.74	**Mean N and P**
Max	0.22	3.54	2.12	7.94	33.78	
Min	0.35	3.82	0.58	6.25	14.06	**High N and P**
Max	0.54	5.06	2.12	9.38	48.79	

According to the results found in the simulated cases, DO and PO_4^{3-} are the most sensitive variables in the drought scenario in terms of the behavior of periphyton algae. The compounds recovered their mean concentrations after a few days of low flow of velocity.

Periphyton concentrations peaked in all cases of the high trophic scenario, suggesting that the scenario may favor their growth. Concerning the drought scenarios, the peaks in Pte 64 presented higher concentrations for drought 1. In the other monitoring points, it was for drought 2.

Analyzing the behavior of periphyton, taking into account that the losses of its concentration are related to the detachment caused by velocities. The modeling shows the response of algal biomass to changes in velocity Figure 3, consisting of two phases. First, there is an increase in mean biomass with decreasing in velocity. This phase is characterized by the predominance of the positive effects of velocity and an enhancement of nutrient uptake and is more evident in high nutrients scenarios. When biomass reached a maximum, the second phase starts, and the negative effects of velocity begin to predominate, and biomass loses. The velocity for this time series was close to zero during drought period 2, showing in most cases a biomass pike. The different cases had almost the same qualitative response to changes in the velocity. They always showed the highest biomass when the lowest velocity was observed. The maximum biomass loss rate showed higher values for the high-velocity (2,5 m/s) sites but influence as well for high nutrient concentration. These responses are a consequence of the values of the uptake function parameters.

The influence of the velocity, nutrients, light, and temperature through the growth and biomass loss mechanisms was able to describe the fluctuations expected in biomass concentration (**Figure 43**). With water flow velocities close to zero during drought scenario 2, it indicates a biomass pike in most cases.

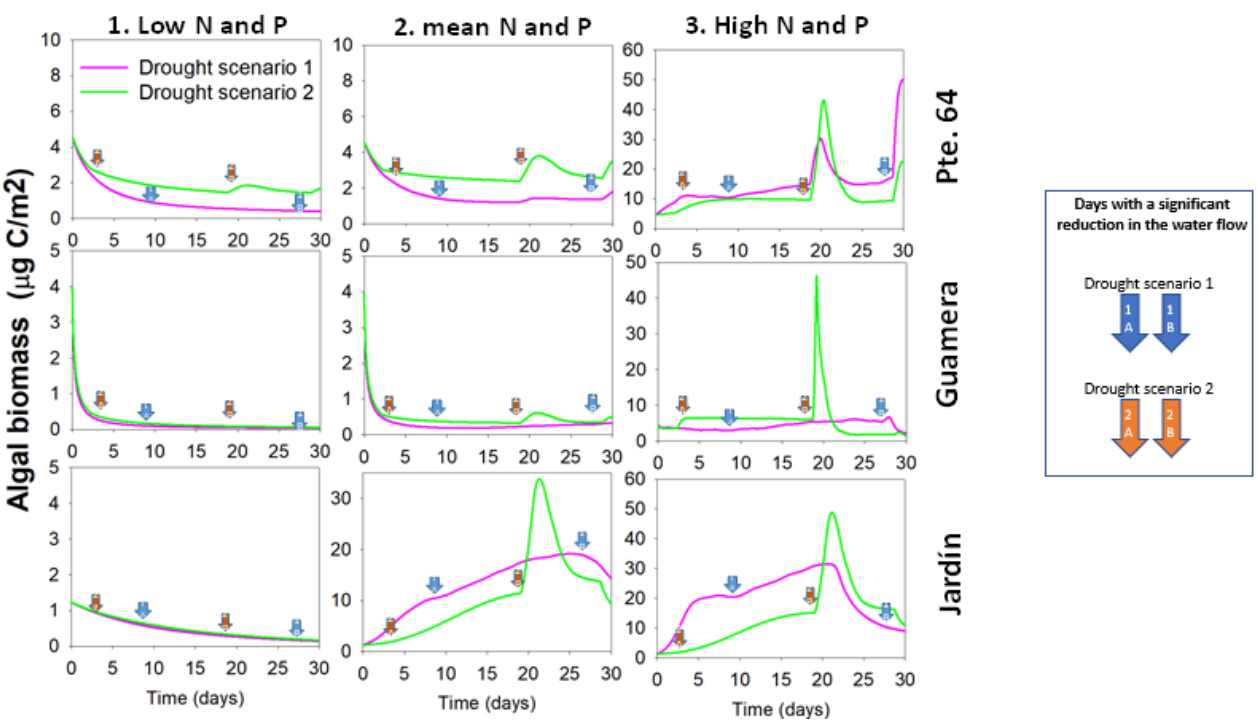

Figure 43 Temporal changes in the algal biomass (µg C/m2) for the drought scenarios.

The total biomass in a section of the river (**Figure 44**), presented a behavior very different from the values calculated per area. The results show that in a scenario with low nutrient concentration, the Guamera and Jardin stations do not show a significant reduction in algal biomass in the two drought scenarios and the reduction in biomass follows the seasonal trend caused by the loss of the flooded area. In the case of Puente 64, the first event had a greater impact. For cases with medium and high concentrations of nutrients, the behavior is different, with an increase in total algal biomass after the second drought. In the case of the Jardin station for medium and high concentrations and Puente 64 in conditions with a high concentration of nutrients, the algal biomass showed an increasing trend.

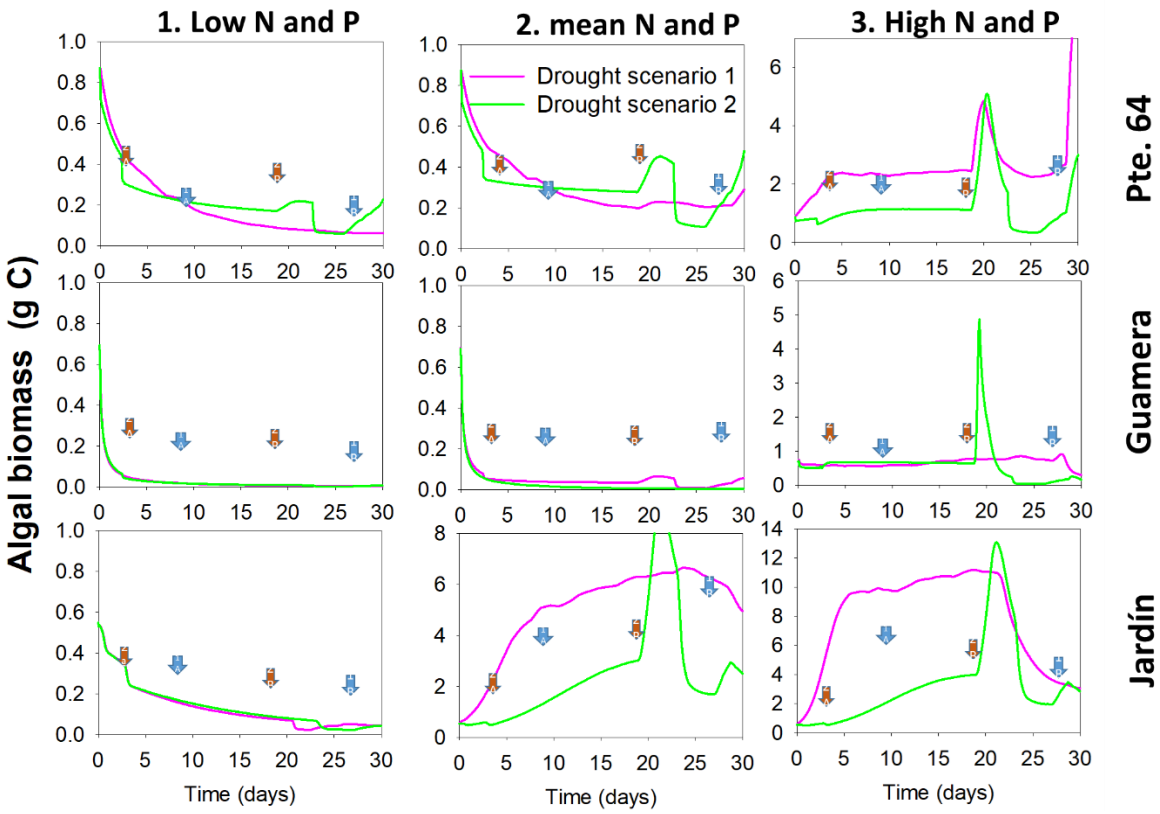

Figure 44: Total algal Biomass of a river width section of 400 m. for the drought scenarios.

After the river flow was reduced, a gradual increase in algae density was observed. During the closure of the floodgates in February, the model showed a reduction in algae density during the three days that the water flow was interrupted. This behavior was similar in the four stations analyzed. Subsequently, a rapid increase in algal density was observed, with a recovery of the average values in three days. The simulation results are consistent with the type of algae expected during the concept review and contingencies. This community has different low-flow response strategies and when they occur in such a short period, the rapid growth of the algal biofilm is stimulated after the flow of water returns. Flow pulse promoted periphyton growth, mainly when the bed is exposed to high-light conditions (Calvo et al., 2022). In addition, the conditions of the low flow can change macroinvertebrates and fish assemblages and finally promote a trophic cascade that increases periphyton biomass (Fournier & Magoulick, 2022). On the other hand, rivers in the medium and low basins have low canopy cover, which allowed primary producers to grow during fewer cloudy days (Hosen et al., 2019).

4.6 Discussion

Hydrological, hydraulic, and chemical conditions control periphyton biomass in riverine ecosystems. Findings in the model suggest that hydraulics are the main factor regulating the growth of periphyton algae, followed by high nutrient availability in the Cauca River. The model suggests that epiphytic biomass exhibits peaks in biological responses to reduced nutrient concentrations and fluxes (Maret et al., 2010; Resh et al., 1988). Based on the results

shown, this situation may imply the possibility of increased periphyton biomass in short-term low-flow reaches. These findings are consistent with those of previous studies in river systems that are located downstream of dams (Calvo et al., 2022).

One of the causes of the overgrowth of periphytons is the change in the downstream flow regime, which changes the hydrodynamic flow dynamics and promotes the overgrowth of periphytons downstream of dams. The findings indicate that those conditions are affecting the Cauca River ecosystem.

The performance of the model showed that it can predict periphyton biomass in the low-flow condition river downstream of the dam. Compared to other studies as (Graba et al., 2014; Huang et al., 2021; Kazama & Watanabe, 2018; Rutherford & Cuddy, 2005; Yahya et al., 2019). The model used in this study has some advantages for dealing with multiple factors controlling the temporal pattern and magnitude of periphyton in this stream. Using field data, the model can accurately reflect the actual process of periphyton growth and losses in the river and hence can be used directly verified model by applying it to independent data on the same stream, with good agreement between observed values and model predictions. In contrast, some statistical models cannot be easily applied to streams or rivers, in spatial and temporal variations and extreme conditions as described in this study. The model can be described as an integrated method.

As for the issue of the peripheral communities, the results showed that it is possible that a sudden decline in flow, such as the closure of the dam sluice gates of the Cauca River, did not cause a significant effect on the biomass of these organisms.

Despite the rapid changes in flow, the algae communities of the Cauca River have high resilience and a high capacity for recovery from sudden changes in water flow. The dominant communities in these ecosystems respond quickly to the reduction in water flow and can maintain the productivity of the river. The resilience mechanisms allow biomass recovery in less than a week after the disturbance. Our results suggest that the algae communities are adapted to sudden changes in water flow so that the impacts of the two low-flow events do not have long-term repercussions.

4.7 Conclusions

This research used short-term field data to develop a mechanistic model of periphyton biomass-nutrient interactions. The results show that was possible to calibrate the model with experimental data, and calculated nutrients, space requirements, and losses due to detachment and friction velocity. And this study demonstrates the necessity to model nutrients, hydrological factors, and friction velocities to estimate detachment to accurately simulate periphyton. The model showed the response to low flow in two phases due to the adaptation of algae.

The Cauca River is an ecosystem enriched with nutrients and with a high physical instability of the substrate, where algal biomass can be recovered in a few days after an extremely low flow.

Funding details

This Project was supported by the agreement N° CT – 2019 – 000585 Empresas Públicas de Medellín-EPM and Pontificia Universidad Javeriana.

Chapter 5

5 A methodology for the development of integrated modelling tools to simulate socio-ecological systems

*The results of this chapter is in review

Abstract: In this work, a methodology to develop integrated modelling tools (IMT) for analyzing socio-ecological systems is proposed. It is composed of three modules: the first one allows the simulation of the physical dynamics of the system, the second module uses the previous outputs as a basis for developing an aquatic ecosystem component, and the third module uses the physical and ecological results as a basis for a dynamical system-based model for ecosystem services and livelihoods. The IMT is applied to analyze the affectation of the Ituango Hydroelectric Project, over 400 km along the Cauca River in Colombia. Results allow dimensioning the level of affectation in terms of flooded areas, fish species habitat suitability, and quantification of ecosystem services, among others. Finally, a discussion about the need for this type of integrated tool to represent complex real systems and its potential for decision-making is presented.

Keywords: Integrated modelling tool, Socio-ecological systems, Environmental management, Aquatic ecosystems, Decision-making tools, Mega-engineering projects.

5.1 Introduction

Mega-engineering projects (MEP) generate great benefits for society (Wang et al., 2022). However, they represent significant challenges in terms of construction, operation, and risk management, which usually increment with the scale of the project (Juang et al., 2019). Environmental management is also one of the most important processes to consider before, during, and after the construction of MEP, due to the complexity of its dynamics which have different temporal and spatial scales (Ladau and Eloe-Fadrosh, 2019; Tibebe et al., 2019). Because of this, the relationship between communities and ecosystems, and their contributions to human well-being i.e., ecosystem services, tend to be compromised (Livesley et al., 2016). Given that, the construction and operation of MEP involve the quantification of various physical, chemical, biological, environmental, and social processes that need to be considered in an integral approach.

On one hand, different models and frameworks have been proposed to evaluate and integrate natural processes with anthropogenic factors. For example, Yin et al. (2015) proposed a novel approach to the evaluation of anthropogenic impacts on flood risks in coastal mega-cities. The work incorporated anthropogenic variables such as land subsidence, urbanization, and flood defense within a scenario-based framework where numerical modelling was undertaken to quantify the risks. Nevertheless, it remained to investigate the integration of the combined impact of natural processes such as sea-level rise and storm surge. Likewise, Bazilian et al. (2011) described some of the linkages at a high level of aggregation and via case studies, for addressing the nexus between the areas of energy, water, and food. Also, they presented the attributes of a modelling framework to address this nexus, to inform more effective national policies and regulations. Yet, the necessity of a holistic approach and the involvement of the knowledge of scientists who usually are experts in only one of the three fields presented a great challenge. Similarly, in Amjath-Babu et al. (2019) the authors aim to quantify the benefits of proposed water resource development projects in the transboundary basin in terms of hydroelectric power generation, crop production, and flood damage reduction. A hydro-economic model was constructed by soft coupling hydrological and crop growth simulation models to an economic optimization model. Still, quantifying the negative social and environmental impacts required a different methodological approach, typically based on non-market valuation methods considered in their study.

On the other hand, socio-ecological systems (SES) approaches have been proposed over the last decade as a framework to describe the state of a system including the anthropogenic influence, determining its interrelationships and interdependencies within it. For example, Schlüter et al. (2017) provided a framework to facilitate a broader inclusion of theories on human decision-making in formal natural resource management models, which may enable modelers to find and formalize relevant theories. Moreover, Hagenlocher et al. (2018) propose a modular indicator library-based approach for the assessment of multi-hazard risk of SES across and within coastal deltas globally. Furthermore, Kok et al. (2016) presented a method for the analysis of socio-ecological patterns of the vulnerability of people being at risk of losing

their livelihoods as a consequence of global environmental change.

In addition, one of the biggest challenges in integrating these processes is the high variation in the spatial and temporal scales among them in the environmental system (Binley et al., 2015; Liu et al., 2015). Although various studies assess some processes effectively, investigations on their integration have several limitations and are scarce when human interaction needs to be considered (e.g., Amjath-Babu et al., 2019; Shiru et al., 2020). In contrast, SES-based frameworks seem to clarify human-ecosystem interactions, however, few assessments seem to lead to tangible outcomes (Whitney et al., 2017). Therefore, several authors emphasize the necessity of integrated approaches and models for environmental management and ecosystem-based strategies (e.g., Leslie et al., 2015; Shiru et al., 2020; Whitney et al., 2017). Given that, research linking MEP, SES, and ecosystem services, has failed in the proposal of management practices that lead to decision-making tools.

According to the above, this paper presents a methodology to develop an integrated modelling tool (IMT) that quantifies the affectations in SES due to the presence of MEP, in order to improve environmental assessment. As a case study, the Ituango Hydroelectric Project (IHP) in Antioquia, Colombia, is considered to evaluate the methodology.

5.2 Methodology for the construction of the IMT

The methodological approach for constructing the IMT proposed in this study consists of four phases described below.

5.2.1. Case study

First, the case study that involves the SES needs to be studied and described in detail. The evaluation of the study area's environmental, ecological, hydrographic, and social conditions is the starting point to identify the characteristics that will delineate the SES. As well, it allows us to better understand specific problems or conditions that need to be considered due to the nature of the study.

5.2.2. Conceptual model

The conceptual model seeks to understand the SES in an integrated manner, defining its processes and dynamics, based on existing data to be used and the specific problem of consideration, according to the case study. Also, it defines the relationships between the SES processes, for which flowcharts explaining its interrelationships and interdependencies can be constructed (Schlüter et al., 2019), based on expert knowledge and literature review (e.g., Arif and MacNeil, 2022; Heinze and Dunkler, 2017). For its development, it is necessary to count on the participation of different disciplines and experts in engineering, natural, social, and economic sciences, among others.

5.2.3. Modules and components

Three groups of modules are proposed to describe the SES in the IMT, and each one of them is composed of components that will represent different processes and scales in detail. The first module is the forcing module, which will group the components that directly condition the environment, associated with the dynamics of water, sediments, and their interaction with biogeochemical cycles. The second module is the aquatic ecosystems module,

which is constituted of components regarding biological and chemical processes that change aquatic ecosystems. The third module is the ecosystem services and livelihoods module, which presents the dynamics of the ecosystem services such as fishing, livestock, and mining, based on changes in the considered environmental area. Subsequently, based on these changes, the financial, physical, human, and social capitals established for the study area are articulated. As an example, **Figure 45** presents a diagram with the three proposed modules (blue, green, and orange boxes), which in turn contain components that have relationships between them (represented by arrows). It is worth mentioning that each one of the modules can have an unlimited number of components; the conceptual model will define the exact number of components required for each IMT.

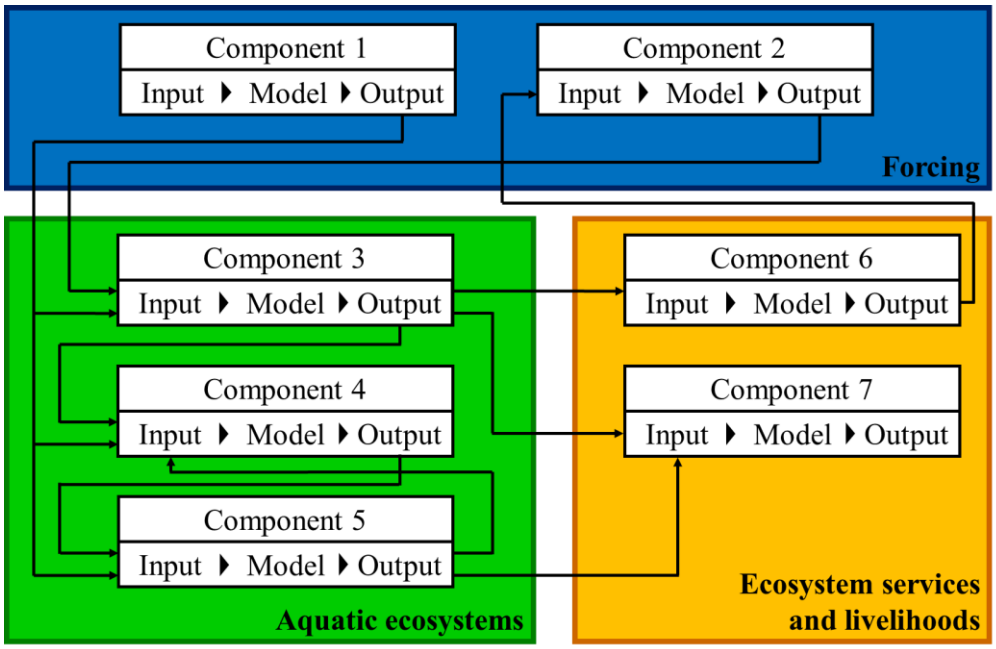

Figure 45: IMT scheme.

Given that, the definition of relevant variables to describe each component of the SES is a fundamental step to represent how the phenomenon or problem will be evaluated. For this, considering the expert knowledge and the existent data to be used is fundamental to making an optimal selection of regarding variables. Furthermore, usually not only the SES needs to be delineated, but specific environmental problems or situations as well, for which variables of study may be added responding to certain problems or clients' requests.

2.2.4. Determination of models, inputs, and outputs

Mathematical and computer experiments are designed for each component considering the information and the available tools, also based on expert knowledge and the literature consulted. Different types of models need to be considered, such as the first principles models (based on physics, biology, and chemistry) (Rajulapati et al., 2022), data-based models (which correspond mainly to statistical inferences) (Brahma et al., 2021), and knowledge-based models, according to the expert knowledge of the executing team and the possible uncertainty that may arise in the modelling exercises. However, various models can exist for similar purposes, for which the selection of the optimal model can be difficult. For this, a vast literature

review and the criteria and knowledge of expert scientists are crucial. Furthermore, the SES is described by various processes that interact between them, where a single model cannot delineate the entire dynamics. Then, various models need to be selected to describe all the pertinent variables and components of the IMT. Consequently, the inputs and outputs of these models are determined.

5.2.5. Functional relationships between components

The interaction between the SES processes requires the articulation of each model that separately studies a single phenomenon, for which functional relationships between components are needed. Once the relationships have been established by the conceptual model, the coupling of the components is performed through mathematical or analytical expressions that relate the outputs with the inputs of the models (as shown in Fig. 1). The expressions can be obtained from the literature review, expert knowledge, or from different existing tools for this purpose. Moreover, there are two types of functional relationships. i) One-way relationships, where the output of a model is used as the input for another model (e.g., functional relationship between Component 2 and 3 in Fig. 1). ii) Two-way relationships, where the output of a model A is used as the input for a model B, and the output of this model B is used again as the input for model A (as occurs between Component 4 and 5 in Fig. 1). This last is used to better describe two dependent processes that vary alongside in time.

5.2.6. Verification of the models

Once the modelling process has been completed, verification techniques for the results need to be performed. Nevertheless, as various model types can be considered, different verification techniques or strategies need to be selected. Initially, first principle models have widely documented modelling protocols based on the calibration and validation of computational tools, which are based on universal principles and laws of the natural sciences (e.g., Mardani et al., 2020). As well, statistical metrics to measure the model performance and the amount of error are well-known, and can be implemented for first principle, data-based, and knowledge-based models (e.g., Mengistu et al., 2019). This exercise is of great importance since it is the one that gives validity to the results of the IMT.

5.2.7. Design of the scenarios of analysis

The scenarios of analysis are specific situations that occur within the study area, that will respond in accordance with the study problem, the computational capacity of the proposed IMT, and/or regulation standards that need to be followed. Therefore, these scenarios are different for each case study. Given that, the use of the IMT for each one of the proposed scenarios will give different results, with which comparisons can be made. Then, scenarios that want to be analyzed need to be established to determine variations in the SES. Finally, the results need to be collected, analyzed, and presented, and given that SES-related projects usually involve various social actors (e.g., Iwanaga et al., 2021; Lippe et al., 2019) these results should also be presented in a way that non-scientists can understand to improve further decision-making processes.

5.3 Application of the methodology

In this section, an IMT has been proposed to bring a response to the affectations of the Ituango Hydroelectric Project (IHP) on the SES downstream of the dam, which will be described in detail in Section 3.1. This representation articulates aspects of the system's water dynamics, such as hydrology, hydrodynamics, sedimentology, and water quality, with ecological aspects, such as the suitability of habitat for the different fish species found in the study area, the movement of ichthyoplankton and the periphyton growth process. Additionally, both the hydric and the ecological aspects are articulated with the dynamics of the ecosystem services and the livelihoods of the communities of the study area.

5.3.1. Case study

Hidroituango Dam is a hydroelectric project constructed in the Cauca River basin in the North of the Department of Antioquia (west of Colombia). It is a 220 m high Earth-Core Rock-fill Dam with the following design parameters: a reservoir of 2700 Mm^3 with regular operation on 420 masl (meters above sea level); a spillway designed for a discharge capacity of 23,250 m^3/s under four radial gates; an intermediate discharge tunnel with a capacity up to 450 m^3/s; and three diversion tunnels. Fixed trash racks allow the flow of water to eight turbines assembly fixed in vertical axes in the powerhouse, which are connected with two surge tanks downstream and four discharge tunnels. The flowing water returns back to the Cauca River through the discharge tunnels (Suárez et al., 2022). In addition, due to the geomorphological configuration of the zone, this reservoir is relatively close to a large floodplain, so the impact that the construction can have on the ecosystem is great.

On April 28, 2018, two months prior to the starting of the scheduled fill of the reservoir, a collapse occurred in the diversion tunnel and the Cauca River was diverted through an auxiliary tunnel. This tunnel had been in operation for about seven months until a landfall blocked the tunnel access. This blocking resulted in the anticipated filling of the reservoir, exposing the dam and the spillway to the risk of overtopping. At that time, the level constructed of the dam was 385 masl (77% of the total height) (Suárez et al., 2022). Because of the adverse condition, since May 10, 2018, it was necessary to divert the water through four of the eight adduction tunnels of the intake structure, aiming to prevent the overflow in the dam and the spillway. As the powerhouse was not finished, the connection of penstocks and spiral cases of the turbines was not over, and the diversion led to the flooding of the machines' room. This situation forced the closure of two gates which, in consequence, the remaining flow passing through adduction tunnels peaked at roughly 725 m^3/s, resulting in induced rock instability around two wells, making a rock hollow. These adverse events led to the immediate closure of two gates against the free flow, which extremely reduced the discharge of the Cauca River. Furthermore, between the end of January and the beginning of February 2019, the closing of the last gates that allow the passage of water to the powerhouse was carried out, reducing the river flow to a historical minimum. Due to these contingencies, it was necessary to evaluate the effects in the area of influence of these sudden changes in water dynamics, and at the same time establish the possible effects that could be generated during the operation of the hydroelectric plant. Given that, the IMT proposed in this section seeks to study the affectations that the IHP can generate in the SES.

The study area starts from the dam site, along the main channel of the Cauca River, to its mouth in the Magdalena River, in the municipality of Pinillos (Department of Bolivar) (Fig. 2). Moreover, the floodplain of the Cauca River and its tributary rivers are considered. This area comprehends wetland lentic systems where biological and chemical dynamics occur, as well as impacts on the ecosystem services that this region provides, and on the livelihoods of the communities that inhabit it. Also, the neighboring municipalities (see **Figure 46**) are evaluated. It is worth mentioning that certain ecosystems within this study area will also be delineated.

Regarding the temporal domain, the affectations of the SES are analyzed from 1985 to 2070 considering the milestone of the starting of closure of the dam gates in 2018, which changed the sedimentological dynamics of the SES. In the same way, the milestone of the start of the operation of the project in 2022 is considered.

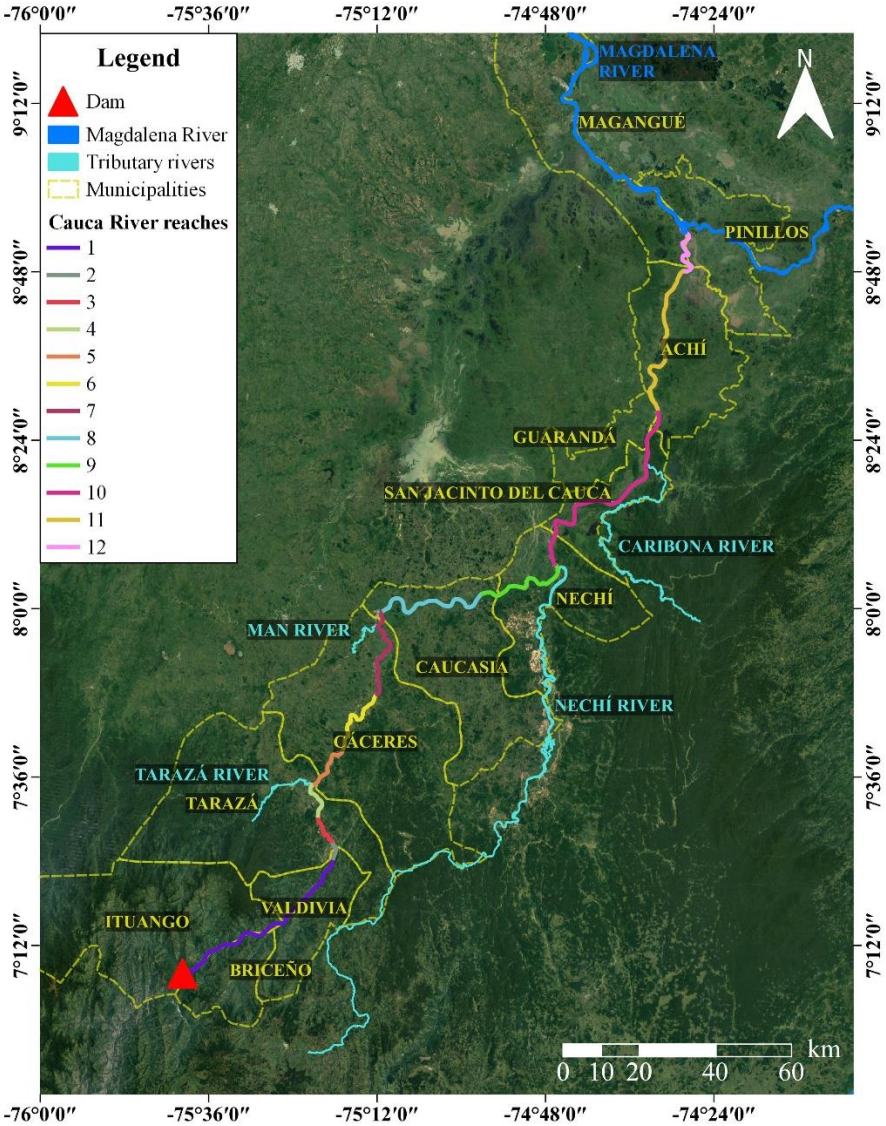

Figure 46: Study area. There is presented a division of the Cauca River into 12 reaches for analysis purposes, which is described in detail in Section 5.3.4.

5.3.2. Conceptual model

Given the case study, a social and ecological situation can be derived from the IHP context: how does this mega-engineering project affect the hydrosedimentological and ecological dynamics, and therefore, the livelihoods of the surrounding communities? To bring a solution to this question, first, the quantification of the affectation on the livelihoods of people needs to be delineated, which can be performed through a capital approach (e.g., Jha et al., 2021; Tessema and Simane, 2019). Then, the changes in these capitals can be estimated through the ecosystem services existing in the study area, such as livestock, fishery, and mining. However, this last is affected by the changes in the SES, which depend on the biological, chemical, and physical dynamics of the Cauca River within the study area. Given that, is crucial to understand and establish the relationships between the abiotic, the biotic, and the social system. For this case study, according to the experts' knowledge, the abiotic system can be evaluated through the hydrosedimentological dynamics of the Cauca River, its tributaries, and wetland complexes. In contrast, the biotic system comprehends the aquatic habitat, periphyton growth, and ichthyoplankton transport. Furthermore, there are factors that, at least in the short term, cannot be conditioned by human activities, which are hydrological dynamics and climate variability, for which the aforementioned processes are initially controlled by these.

According to the above, a conceptual model describing the SES associated with the study area, which we will call an amphibian territory, i.e., a combination of wet, dry, and transitional ecosystems, is developed and presented in **Figure 47**, which considers the processes and dynamics mentioned in the previous paragraph, designated as components.

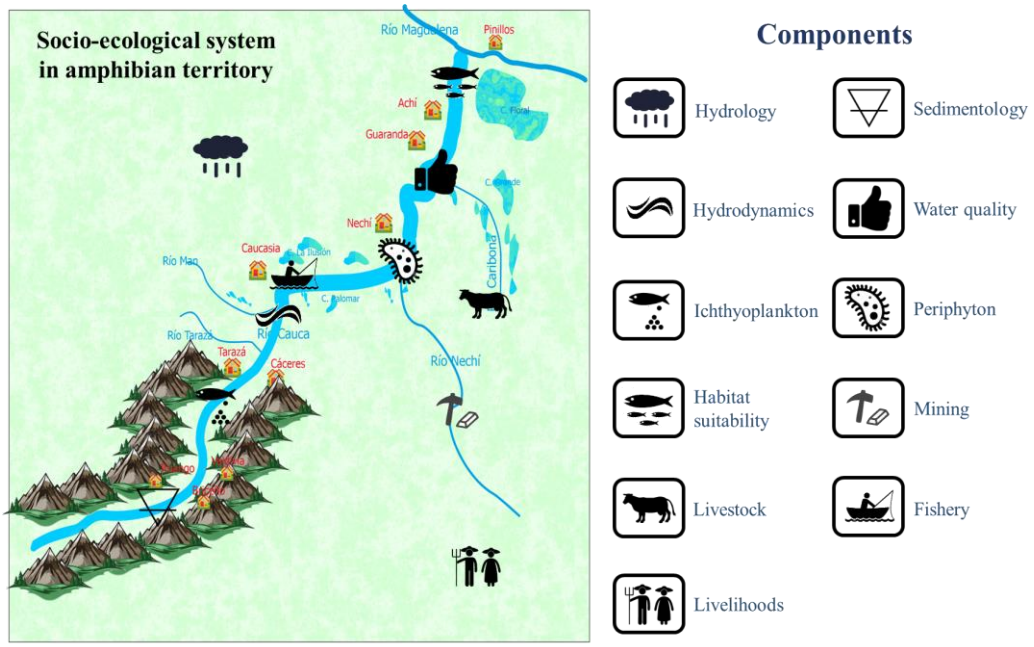

Figure 47: Conceptual model of the case study.

5.3.3. Modules and components

In this section, we describe the components proposed in the conceptual model, which will be arranged in each of the three methodology modules, as presented in Fig. 1. Then, the

forcing module is composed of four components: i) hydrology, ii) hydrodynamics, iii) sedimentology, and iv) water quality. For the aquatic ecosystems module, there are three components which are: v) habitat suitability, vi) periphyton, and vii) ichthyoplankton. Finally, the ecosystem services and livelihoods module seeks to quantify the affectations to the livestock, fishery, and mining and how this can be quantified in social, physical, human, and financial capital. **Figure 48** presents a scheme of the components and modules of the proposed IMT, along with its variables and the way they relate between components through functional relationships represented by the arrows, which will be discussed in Section 5.3.3. Therefore, in the following subsections, each component will be described along with its determined models, the description of the inputs that are required, and the outputs that are generated.

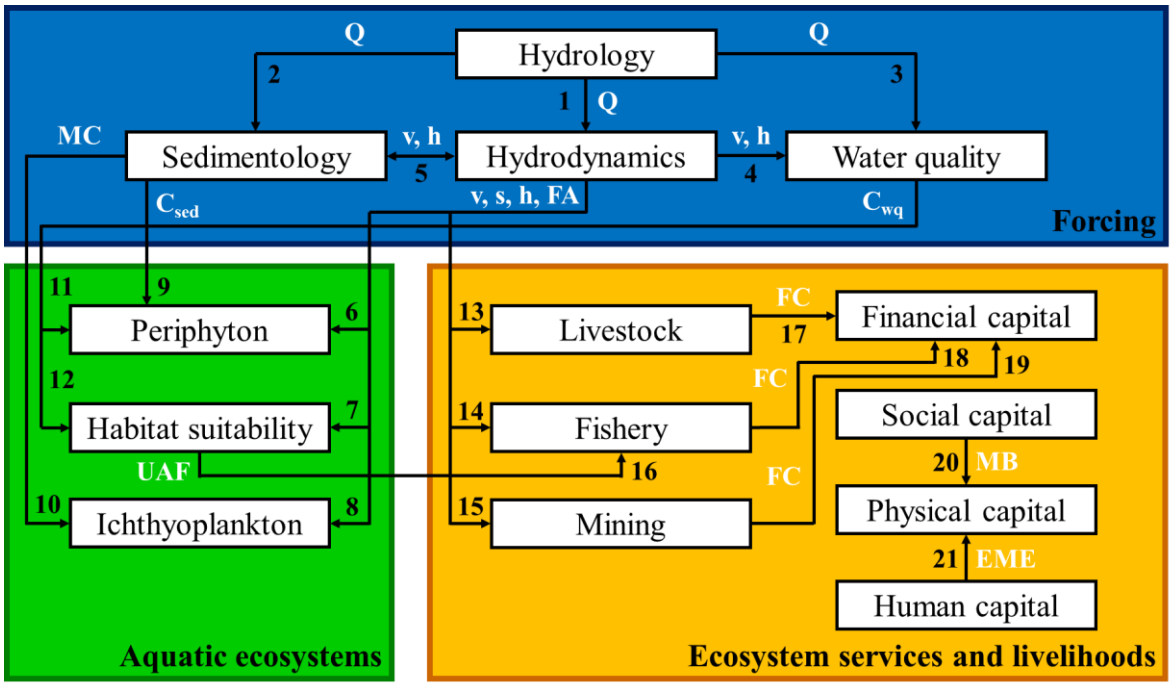

Figure 48: Modules and components of the IMT according to the case study and conceptual model. The letters in white represent the variables, being Q: water discharge, v: water flow velocity, h: water level, s: water shear velocity, FA: flood areas, MC: morphology change, C_{sed}: sediment concentration, C_{wq}: concentration of water quality substances, UAF: useful areas for fishing, FC: financial capital, MB: membership benefits, and EME: event management experience. The numbers in black from 1 to 21 represent the functional relationships, which are described in detail in Table 2.

5.3.4. Determination of models, inputs, and outputs

Table 12 presents a summary of the selected models, required inputs, and expected outputs of each one of the proposed components of the IMT.

5.3.5. Functional relationships between components

Table 13 describes the functional relationships between each one of the proposed components of the IMT.

Table 12. Models, inputs, and outputs for the components.

Component	Model	Inputs	Outputs
Hydrology	● TopModel (Beven, 1997). ● SWAT (Arnold et al., 1998).	● Precipitation and temperature from surface and satellite gauge stations. ● Digital elevation models (DEM) from satellite images. ● Vegetation cover and land soil maps, from IDEAM and Agustin Codazzi geographic institute.	● Liquid flow rate of watersheds. ● Suspended solids, soluble phosphorus, nitrates, dissolved oxygen (DO), and biological oxygen demand (BOD).
Hydrodynamics	● OpenTELEMAC (Galland et al., 1991).	● Liquid flow rates and water levels along the Cauca River and its tributaries. ● DEM with topographic and river bathymetric information. ● Satellite images to delineate the wetland's flood spots. ● Field measurements of the wetland's depth.	● River flow velocity and depth fields that evolve over time. ● Wet areas in wetlands and rivers. ● Potential points where there may be a disconnection between rivers and wetlands.
Sedimentology	● OpenTELEMAC – GAIA module.	● Sediment and granulometric curve information. ● Series of liquid flow rate and suspended sediment load. ● River flow velocity and depth fields.	● Changes in total suspended sediment concentration transported by river flow. ● Bed aggradation and degradation processes.
Water quality	● OpenTELEMAC – WAQTEL module.	● River flow velocity and depth fields. ● Field measurements of DO, BOD, nutrients, zooplankton, phytoplankton, and temperature.	● Concentration fields of zooplankton, phytoplankton, DO, BOD, phosphates, organic phosphorus, nitrates, ammoniacal nitrogen, and organic nitrogen.
Habitat suitability	● OpenTELEMAC.	● River flow velocity and depth fields. ● Curves of habitat generated by expert knowledge. ● Dissolved oxygen field.	● Habitat suitability maps. ● Weighted usable areas (WUA).

Periphyton	• OpenTELEMAC – Eutro module.	• Concentration fields of the water quality variables described above. • Field measurements of water quality variables. • River flow velocity and depth fields.	• Periphyton production.
Ichthyoplankton	• OpenTELEMAC.	• Information on areas and magnitude of spawning. • River flow velocity and depth fields.	• Positions, counting, and trajectory of particles (representing eggs) in time.
Livestock	• Dynamic systems. • Forrester diagrams.	• Inundation areas. • Reforestation rate. • Sales percentage. • Deforestation rate. • Price of cattle. • Rate of transition from pastures to crops. • Rate of conversion from crops to pastures. • Male and female fraction of the livestock population • Powering rate. • Dewatering time. • Percentage spent on inputs. • Natural mortality rate.	• Livestock income and expenses.
Fishery	• Dynamic systems. • Forrester diagrams.	• River flow velocity and depth fields. • WUA for the survival of the fish. • Individuals per hectare. • Average potential catch of fish. • Percentage of females and mature fishes. • Percentage of capture of the species. • Weight per individual. • Spawning per individual. • Percentage of self-consumption. • Survival percentage.	• Fishery income and expenses.

		• Price per pound. • Mortality rate. • Monthly costs of the execution of fishing. • Number of fishermen.	
Mining	• Dynamic systems. • Forrester diagrams.	• River depth field. • Gold productivity by area. • Price per gram of gold. • Sold gold. • Mining execution costs.	• Mining income and expenses.
Social capital	• Dynamic systems. • Forrester diagrams.	• Community connection rate. • Productive linkage rate. • Support group rate for events. • Community union before events. • Rate of positive perception of government aid. • Rate of non-linkage with organizations related to extreme events. • Family bonding rate.	• Flow of money of the relationship between the benefits obtained by belonging to a community and the benefits lost by disengagement from the community.
Human capital	• Dynamic systems. • Forrester diagrams.	• Number of homes. • Formal education level. • Age of the population. • Health status rate. • Event management experience. • Main activities developed in the sector. • Number of households that migrated due to drought. • Number of households that migrated due to the flood.	• Flow of money of the value acquired by a person or population due to the execution of a job.
Physical capital	• Dynamic systems. • Forrester diagrams.	• Type of housing. • Infrastructure oriented to event management. • Obtaining objects.	• Flow of money of the goods focused on production and that are used in the main economic activities of the region,

		• Agricultural and livestock infrastructure. • Permanence benefits community organization. • Benefit of belonging to a productive association. • Event management experience.	these being livestock, fishery, and mining.
Financial capital	• Dynamic systems. • Forrester diagrams.	• Colombia's minimum wage. • Amount of donations made. • Amount of income from wages. • Amount of income per remittance. • Costs for improvements. • Livestock income and expenses. • Fishery income and expenses. • Mining income and expenses.	• Flow of money generated and spent by the execution of the different economic activities of the study area.

Table 13. Description of functional relationships between components. The numbers in bold from 1 to 21 refer to Fig. 4.

Components	Description
1 Hydrology and Hydrodynamics	The hydrology component provides the hydrodynamic component with the flow series of the tributary basins of the reaches of the river that will be modeled, and the series of water levels at the downstream point on the river. These points are usually chosen strategically to coincide with the installed hydrological stations, in order to make comparisons.
2 Hydrology and Sedimentology	The hydrology component generates series of suspended sediment transport, simulated for the different tributary basins of the Cauca River.
3 Hydrology and Water quality	The hydrology component provides the water quality component with continuous series of different quality variables, simulated for different tributaries and on the Cauca River.
4 Hydrodynamics and Water quality	Once you have the velocity and depth fields, which are the result of the hydrodynamic model, the substances will respond to the velocity patterns and will be distributed in the domain. The above, according to the phenomena of diffusion and advection of substances dissolved in water.

Components	Description
5 Hydrodynamics and Sedimentology	Suspended sediments respond to diffusion and advection phenomena that depend on the velocity field. Additionally, morphodynamics interacts with the flow in a two-way relationship, i.e., the flow modifies the bed and in turn, this change in the bed modifies the flow, and this corresponds to the phenomenon of bottom sediment transport.
6 Hydrodynamics and Periphyton	The productivity and shedding of the periphyton, with optimal light and temperature, is controlled by geomorphology and hydraulics, which is analyzed with the depths and velocities of river flow.
7 Hydrodynamics and Habitat suitability	Hydrodynamics will define which areas of the river will be preferential for the species that live there. The above is done through the habitat suitability index by species, which mainly relates flow velocity, dept, and DO.
8 Hydrodynamics and Ichthyoplankton	Because the ichthyoplankton movement model is based on particle tracking, hydrodynamics will be the driving force for it, since a particle that is placed over the river will move according to the velocity fields that are calculated.
9 Sedimentology and Periphyton	The periphyton is directly related to the extinction coefficient, which requires turbidity that is established based on the suspended solids. Therefore, the sediment component delivers continuous series of suspended solids to the periphyton component to establish turbidity in the analysis scenarios.
10 Sedimentology and	The sediment component defines the resulting bathymetry based on the associated geomorphological change, which is a fundamental input used for the ichthyoplankton movement model.

Components	Description
Ichthyoplankton	
11 Water quality and Periphyton	Within the periphyton component it is necessary to establish its concentration and to define the losses and the growth factors. The latter depends on the quality of the water.
12 Water quality and Habitat suitability	The water quality component provides the habitat suitability model with the value of DO for stationary scenarios, a variable required to define the habitat suitability of the species.
13 Hydrodynamics and Livestock	Since the livestock model is based on the available grazing areas, hydrodynamics will affect these areas due to the movement of flood spots, that is, in high waters there will be less grazing area and in low waters more grazing area.
14 Hydrodynamics and Fishery	The river hydrodynamics directs processes related to the dynamics of biological populations and the structuring of food networks, for which flow velocity and depth are provided.
15 Hydrodynamics and Mining	The mining model corresponds to the relationship between the gold obtained in the study area regarding the levels reached by the river, which is obtained by the hydrodynamics model.
16 Habitat suitability and	The habitat suitability model establishes areas in which fish can comfortably inhabit. These defined areas for each selected species are the initial input for the fishery component. The above, since these areas can be multiplied by the density of fish of each species and in this way define the initial value of the fish population of each species.

Components	Description
Fishery	
17 Livestock and Financial capital	The ecosystem services component is responsible for defining all the income of each livestock, fishery, and mining activity, as well as other income such as remittances, wages, and government incentives. In addition, this component establishes the costs of each of the aforementioned commercial activities. All of the above corresponds to a fundamental input to define financial capital.
18 Fishery and Financial capital	
19 Mining and Financial capital	
20 Social capital and Physical capital	The social capital establishes a quantification of the benefits of belonging to a community or productive association. This is used as input for the quantification of the physical capital.
21 Human capital and Physical capital	The human capital establishes a quantification of the event management experience of a person. This is used as input for the quantification of the physical capital.

5.3.4. Design of scenarios and analysis of results

The SES dimensioning downstream of the IHP based on the IMT has the objective of evaluating its impact during the construction of the dam, the closing of the gates, and the operation. In order to know the changes to which the SES was subjected before the periods of construction and operation of the IHP, the IMT analyzes two scenarios that represent a condition with dam and without dam, henceforth called "dam scenario" and "no-dam scenario", respectively. This section presents the analysis of results in terms of the affectations to the abiotic and biotic systems, and the ecosystem services and livelihoods. Therefore, the abiotic affectations are changes in the rivers and wetlands systems referring to flood areas, velocities, depths, suspended sediment loads, and their morphology, the biotic affectations comprehend the changes in water quality and fish habitable areas, and the ecosystem services and livelihoods affections are presented as the increase or decrease of their capitals. In addition, considering that climate variability in time is a factor that controls the IMT proposed components, forcing factors are planned to evaluate the effects in the SES from 1985 to 2070 under two representative concentration pathway (RCP) atmospheric conditions. Given that, considering the milestones of the closing of the gates in 2018 and the start of the operation of the project in 2022, the scenarios combining the dam presence and the climate forcings are:

- Climate forcings of El Niño, La Niña, Neutral years, from 1985 to 2018.
- Optimistic climate forcing RCP 4.5, from 2022 to 2070.
- Pessimistic climate forcing RCP 8.5, from 2022 to 2070.

For analysis purposes, the Cauca River was divided into 12 reaches based on morphological considerations. These reaches are specified in **Table 14**. Therefore, the following sections of the text will present the most important result and its discussion regarding the study area reaches.

Table 14. Description of the reaches of study.

Reach	Description	Length (km)
Reach 1	Dam site – El Quince	53.550
Reach 2	El Quince – El Doce	5.195
Reach 3	El Doce – El Cinco	8.671
Reach 4	El Cinco – Pte. Antonio Roldán	10.903
Reach 5	Pte. Antonio Roldán – Pto. Bélgica	13.798
Reach 6	Pto. Bélgica – Piamonte	21.135
Reach 7	Piamonte – Caucasia	27.408
Reach 8	Caucasia – Margento	35.224
Reach 9	Margento – Nechí	27.701
Reach 10 - Cauca	Nechí – Guarandá (Cauca River)	62.622
Reach 10 - Caribona	Nechí – Guarandá (Caribona River)	-
Reach 11	Guarandá – Vida Tranquila	43.671
Reach 12	Vida Tranquila – Coyongal	19.457

5.3.4.1. Abiotic affectations

The abiotic components of the IMT showed that the dam scenario, on average, reduces flooding processes compared to the no-dam scenario. On average, the area affected in the canyoned reach of the river is 1.24% (decrease in the area), and in the reaches that are connected to wetland systems, the changes are on average 1.48% lower. Regarding the wetland systems, there is a greater percentage decrease in the reaches where the shallowest wetlands exist, for example: La Ilusión wetland has an average change of 1.62 ha, Los Copa of 1.08 ha, and Palomar of 3.08 ha.

In case of extreme events, the dam scenario generates greater flooding with high flows, and reduces the water surface area in case of minimum flows, accentuating extreme events (maximum and minimum), for the wetlands present in the study area. In the dam scenario for maximum events, the area increases on average by 37.78 ha for each of the wetlands, which represents 415.58 ha in the entire study area. Regarding the changes in areas under minimum flows, the water surface area of the wetlands decreases to 819.2 ha, and on average for each of the wetlands, there is a difference of 74.47 ha. In contrast, the changes in river velocities and depths are not significant, however, they can represent significant changes in the water surface of the wetlands.

Regarding the suspended sediment load in the main reaches of the Cauca River, it can be concluded that the impact generated by the dam is stronger in the canyoned reach, while downstream, a recovery of the channel can be highlighted in terms of transportation of suspended sediments. In the operating stages, the macroclimatic conditions of La Niña, El Niño, and the Neutral year tend to considerably reduce the suspended sediment load of the Cauca River in the connections with Los Copa and La Estrella wetlands. About the wetlands, its responses vary due to the local characteristics they present.

Comparing the scenarios with and without dam, the morphological changes generated on the Cauca River presented greater variation in the El Cinco – Nechí River reach, while in the Nechí – Coyongal reach no considerable bed aggradation and degradation processes were generated along the Thalweg. In the operating stages, the dam scenario conditions tend to slightly reduce the sedimentation of the Cauca River in the connections with its wetlands from Caucasia to Pinillos. For the no-dam scenario, it can be observed that important aggradation processes are estimated on the Cauca River in the areas where the main tributaries are located. The maximum point of degradation occurs with a depth of 13.85 m in the area upstream of the confluence with the Magdalena River and a sediment accumulation of 14.54 m further upstream of it. The same dynamic is reflected at the confluence with the Nechí River. Likewise, it can be observed that the no-dam scenario does not show considerable changes concerning the dam scenario for the area closest to the dam site.

For the area downstream of the IHP, a maximum increase in sedimentation is projected in the dam scenario for year 25 of operation around the El Cinco area, recording values of 6.17 m for a 10-year period. In the same way, for 25 and 50 years of operation, aggradation processes located in the El Cinco area are projected. For the no-dam scenario, an aggradation of 4.62 m

with some degradation peaks of 5.9 m in this same area is estimated. There are also degradation zones no greater than 3 m deep for 25 and 50 years. For the scenario with the operation of the IHP, the simulation results project a slight decrease in the bed aggradation processes on the Cauca River, presenting some sedimentation peaks that do not exceed 2 m, while the areas and intensity of the erosion processes are maintained.

Table 15 presents a summary of the most relevant results of the previously mentioned variables, for both optimistic and pessimistic forcing in the dam scenario.

5.3.4.2. Biotic affectations

For the biotic analysis, one of the main effects of the construction of the IHP was the modification in the physicochemical characteristics of the water. Particularly in the dam area, there was a decrease in temperature and an increase in DO, pH, and nitrates, as a result of the increase in turbulence and potential changes in the aquatic communities of the impounded water. However, these effects have a range of a few kilometers, due to the resilience capacity of the river, which recovers the values quickly. The river presents a decrease in total solids, turbidity, total coliforms, iron, and sulfates, as a result of the physical retention of suspended particles by part of the dam that serves as a barrier. This has the greatest impact along the river channel and its effects on the aquatic biota could be maintained in the long term.

The simulated water quality between 1985-2018 for the dam and no-dam scenarios did not present major differences, while the simulation between the years 2022-2070 in a pessimistic climate change forcing will have significant changes in water quality. Regarding the wetland systems, the modelling suggests a slight improvement in water quality. However, the dam generates a reduction in the concentration of suspended solids, which could affect the functioning of the ecosystem. Nitrogen concentrations also seem to suffer a slight increase.

The results of the periphyton biomass model show a difference in the response along the Cauca River influenced by climatic seasonality when, in dry months, greater radiation stimulates algal productivity. For neither of the two conditions evaluated, differences were observed in the simulations between El Niño and La Niña years. In the wetland systems, the composition of periphytic algae was represented by organisms that have a high capacity to resist environmental stress due to the heterogeneity of the environment. In terms of the habitats offered by the ecosystem due to the presence of macrophytes and the seasonal changes given by the connection and/or disconnection with the river, in the same way as in the river in 2017, a change occurred.

The analyses of the planktonic community in the wetlands are specific and do not allow inferences to be made regarding the possible impact due to the construction of the dam, but they do allow us to show that seasonality is the key factor in determining the composition of the community and the effects of human activities on surrounding areas. The phytoplankton models do not suggest an effect of the presence of the dam on water quality and the observed behaviors suggest that the complexity of each of the systems can influence the response observed in each ecosystem. The analysis of the macroinvertebrate community by year allowed us to observe that the most recurrent morphotypes remained relatively stable over time, making it difficult to identify any impact on this community. At a temporal level in the

wetlands, no distinctive pattern was observed between the organisms of the macroinvertebrate community.

The analysis of the suitability of the hydraulic habitat for the species Striped Catfish (P. magdaleniatum), Blanquillo (S. cuspicaudus), Bocachico (P. magdalenae), Moncholo (Hoplias malabaricus), and Viejito (C. magdalenae) in the dam scenario presented a more suitable habitat in high water conditions and La Niña years, this trend was the same for 39 species. El Viejito and Moncholo do not have an ideal habitat in the canyon area of the river and their distribution is more suited to the lower areas and wetlands. Simulations of changes in fish populations indicate that, in the current hydrological scenario, the presence of the dam would not have a negative impact on the number of individuals of Striped Catfish, Bocachico, and Blanquillo. The results of the models suggest that the pessimistic forcing of global change will not significantly affect the populations of the species of interest. The contribution of these results is aimed at expanding specific knowledge of the populations that require greater care and management at the time of decision-making.

The expected changes in the river's bathymetry by 2050 will have an impact on the entry of ichthyoplankton into the wetlands. The general trend is that the likelihood of more eggs entering the wetlands will increase. This raises the need for detailed monitoring of the bathymetry of the channels in the next 50 years, in order to guarantee conditions that favor the development of migrating fish populations during their reproductive phase. The models suggest that the reduction in river sedimentation favors a greater flow at the entrance to the wetlands, but other factors could affect the sedimentation of the channels, which is why annual monitoring of the bathymetry of the wetlands and their channels is necessary.

Table 15. Summary of the most relevant abiotic variables results for the dam scenario.

Reach	Optimistic forcing				Pessimistic forcing			
	Inundation area change (%)	**Maximum velocity change (m/s)**	**Maximum difference in depth (m)**	**Suspended sediment difference (%)**	**Inundation area change (%)**	**Maximum velocity change (m/s)**	**Maximum difference in depth (m)**	**Suspended sediment difference (%)**
Reach 1	0.560	0.086	7.156	93.550	0.350	0.247	4.622	-94.380
Reach 2	2.440	0.195	4.291	-91.990	1.410	0.195	3.501	-93.100
Reach 3	0.290	0.863	6.365	-92.240	0.190	0.239	4.199	-93.400
Reach 4	1.210	0.105	2.896	-76.390	0.670	0.111	2.185	-78.550
Reach 5	0.960	0.107	4.076	-82.120	0.420	0.139	2.679	-84.320
Reach 6	1.970	0.040	3.859	-81.320	0.630	0.116	2.779	-83.330
Reach 7	1.980	0.037	2.855	-77.860	0.730	0.083	2.302	-76.500
Reach 8	2.380	0.022	3.178	-62.830	0.710	0.095	3.454	-60.550
Reach 9	2.560	0.026	3.486	-62.530	0.420	0.114	3.607	-61.860
Reach 10 - Cauca	0.960	0.073	4.027	-33.430	0.830	0.056	4.001	-32.960
Reach 10 - Caribona	0.760	0.089	2.599	-7.130	0.590	0.100	2.474	-4.090
Reach 11	1.670	0.025	4.488	-34.190	1.240	0.010	4.122	-33.600

Reach	Optimistic forcing				Pessimistic forcing			
	Inundation area change (%)	**Maximum velocity change (m/s)**	**Maximum difference in depth (m)**	**Suspended sediment difference (%)**	**Inundation area change (%)**	**Maximum velocity change (m/s)**	**Maximum difference in depth (m)**	**Suspended sediment difference (%)**
Reach 12	0.520	0.066	6.994	-21.640	0.280	0.026	6.689	-18.640

5.3.4.3. Ecosystem services and livelihoods affectations

Due to the existing relationships between the variables of socio-ecosystem models, changes in biotic and abiotic variables can increase, decrease, or regulate the characteristics associated with these models. Therefore, the review of the variation of these behaviors compared to the results obtained, allows the simulation and the general monthly forecast determined from different expected conditions. To review the change in these behaviors, this section contemplates the analysis of both the relationships between the input variables and the respective results obtained from the social models executed for the study area, in each of the ecosystem services components.

5.3.4.3.1. Fishery component

The model related to fishing activity comprehends the analysis of the areas suitable for the survival of fish, the change in the fish population and its relationship with the study area, and the financial capital generated by fishermen of the study sector, considering three study species: Striped Catfish, Bocachico, and Blanquillo.

For the Striped Catfish, it is observed that the lowest financial capital is obtained at the beginning of the dry year (El Niño year), while, on average, it is observed that the financial capital due to Catfish fishing is greater for a Neutral year and lower for a wet type year (La Niña year). It is found an average financial capital of 842 million COP per month with a standard deviation of 182 million COP. Regarding Blanquillo fishing, throughout the three climate forcings, no appreciable variation in their behaviors is observed. Therefore, on average there is a financial capital of 17 million COP per month associated with Blanquillo fishing, with a standard deviation of 4.7 million COP, finding that the financial capital associated with this species is the lowest compared to the three different analyzed species. For the Bocachico fishing, in the different climate forcings, it shows that the financial capital associated with fishing of this species does not depend on the climatic behavior of the study area, since the forcings do not present significant differences between them. Likewise, the average financial capital associated with Bocachico fishing is observed to be 1,092 million COP, with a standard deviation of 496 million COP, being fishing of this species the one that represents the greatest proportion of the financial capital of economic activity.

Finally, because a large percentage of the financial capital corresponds to the Bocachico, the monthly behavior of these capitals is expected to be similar. Therefore, the behavior of the capital does not directly depend on the selected forcing, as seen in **Figure 49**, obtaining that in the wet period the financial capital is 1,999 million COP, in the neutral period it is 2,079 million COP, and 1,774 million COP in the dry period.

From the above it can be inferred that the fishing of the main species in the study area does not depend on the average climatological events, therefore, it would be expected that changes in the flow represent few variations of financial capital. However, it must be considered that the models do not show dependence on the values associated with the river sediment, and this being the variable most affected by the IHP, the expected changes could be greater than those shown here.

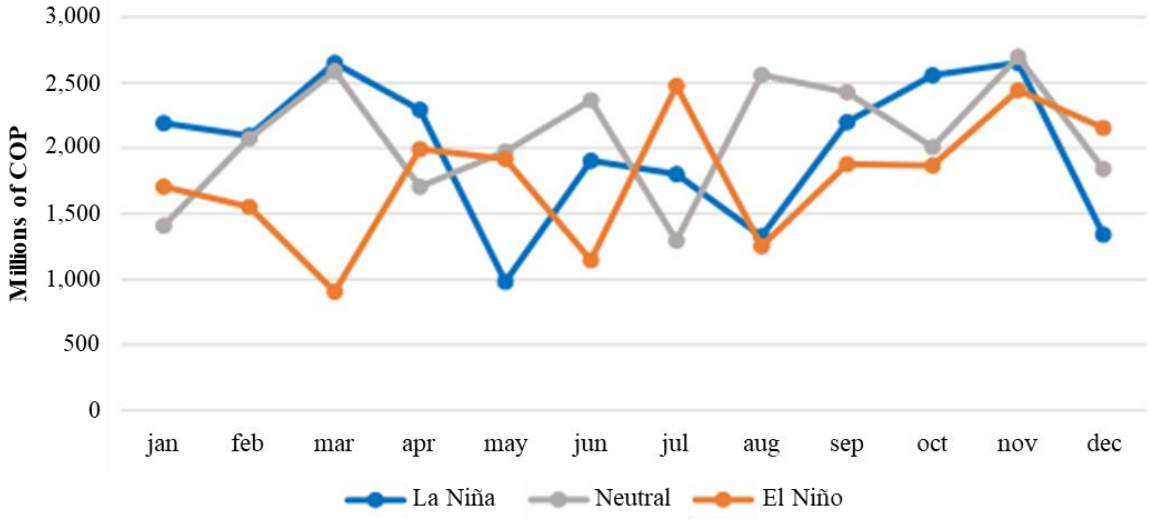

Figure 49: Financial capital for fishery component.

5.3.4.3.2. Livestock component

The livestock model includes the relationships between the changes in the areas dedicated to livestock and the capital generated due to the sale of cattle, having as the main drivers the floods generated by the river and the changes in land use.

Figure 50 shows the change in financial capital depending on the climate conditions of the study area, showing that the behavior for a dry period and a neutral period do not differ. However, for a wet period, a decrease in financial capital is observed, as a result of the inclusion of events caused by flooding in livestock (death of livestock due to flooding of pastures). Likewise, these differences are due to the rainy season in the study sector, since these occur between the third and fourth quarters of the year, times when livestock financial capital presents its greatest falls. It should be considered that, due to the low spatial resolution of the data from the study sector, which in some cases is only of a departmental extent, there is no adequate initial value of livestock individuals or livestock financial capital. The above is not a limitation for the objective of comparing results depending on the climatological characteristics of the sector.

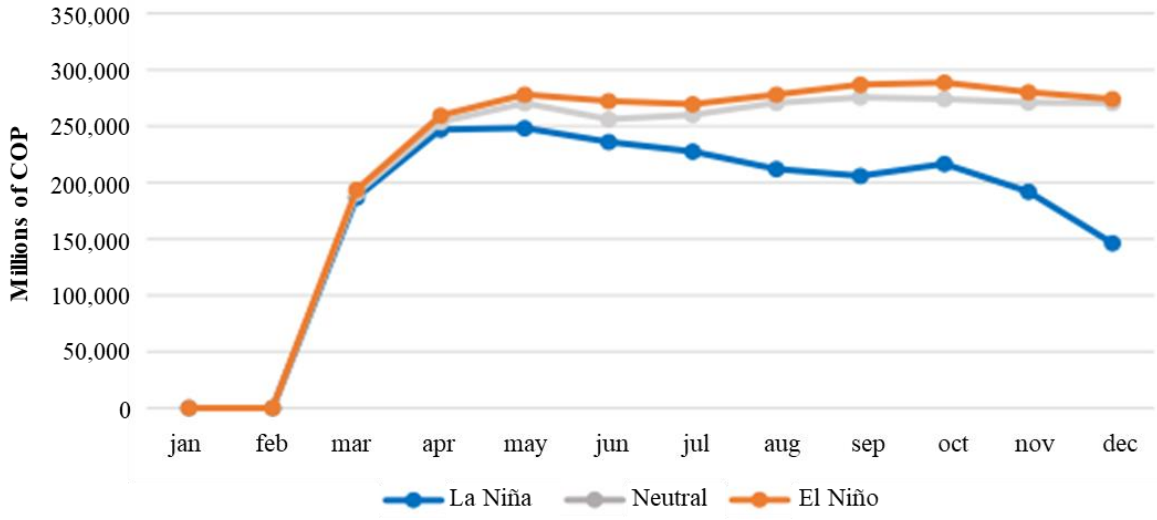

Figure 50: Financial capital for livestock component.

5.3.4.3.3. Mining component

The mining model corresponds to the relationship between the gold obtained in the

study area with the levels reached by the river along its channel. Because two of the large gold-producing regions near the study sector (on the banks of the Nechí River and in La Mojana) do not present direct interaction with the Cauca River in the study area, the information associated with this relationship was inferred from the behavior of the price of gold. **Figure 51** shows that the mining financial capital, generated from the production and sale of gold in the study sector, is not dependent on the climate or hydrological conditions of the area. On the contrary, given the high informality and illegality of the population in the execution of this economic activity, its extraction depends to a greater extent on the laws and projects proposed and executed in this study location.

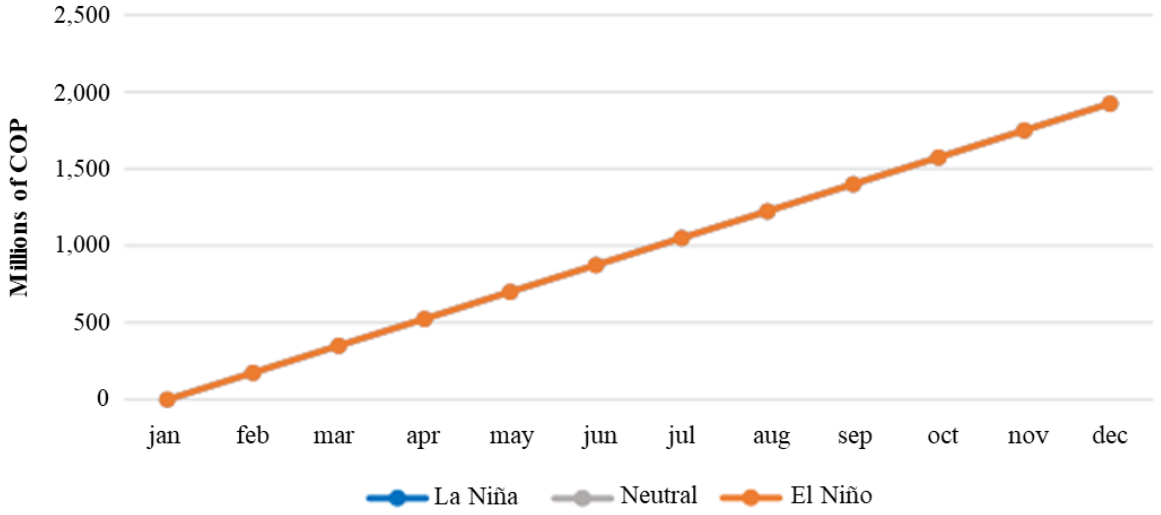

Figure 51: Financial capital for mining component.

5.3.4.4. Financial capital analysis in simulated scenarios

The first finding from the simulations made for typical years and future scenarios shows that there are different change processes that are associated with system disturbances that can be positively related to the financial capital of households, specifically with their agricultural and non-agricultural strategies. This demonstrates that livelihood conditions are extremely limited in the regional analyzed context, and that innovation in the behavior of the system represents a valuable opportunity over time. This agrees with the system's measurements in a typical year, where according to the simulated data, financial capital is lower than in El Niño and La Niña years. For collective improvements in capital and livelihoods, changes and disruptions must be introduced in the system to generate opportunities in livelihood strategies and purposes, an issue that is more critical in the final moments of the year (**Figure 52**). Although these results are important in terms of the integration process, they should be carefully reviewed as they assume high levels of aggregation and synthesis of variables of different types and levels.

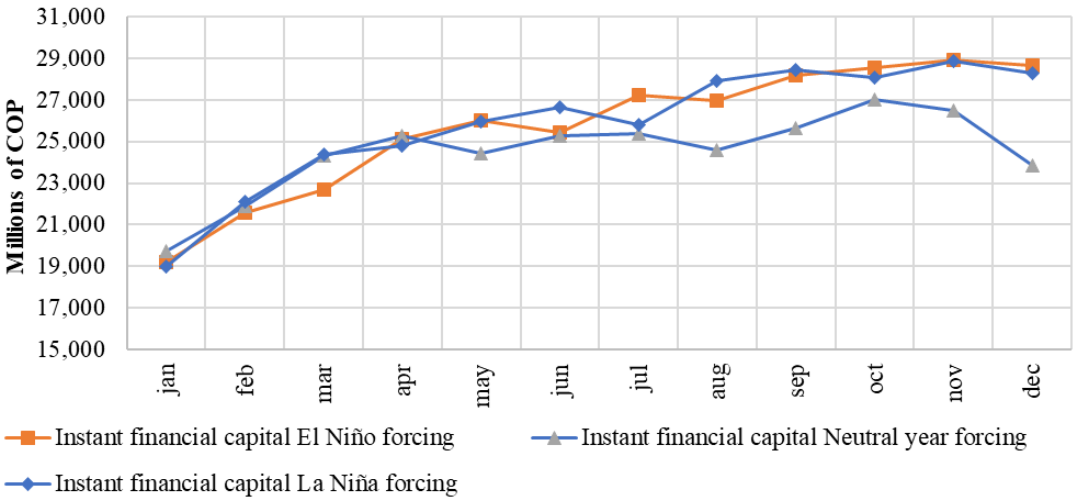

Figure 52: Financial capital for climate forcings.

When the monthly productive and extractive strategies were analyzed in the three ecosystem services throughout the different scenarios, it was always seen that the greater the participation of livestock in the financial capital, the greater the participation of livestock in a typical year of agriculture than in extreme years (El Niño and La Niña). This is interesting, as it supports the differences between more moderate and extreme climate change scenarios, where there is more stability and benefits for non-extractive activities. At the same time, these results demonstrate differences in the magnitudes of the strategies that make up livelihoods, where fishing and mining have less weight in the regional context than agriculture and livestock, which are more important in the local context (Fig. 9).

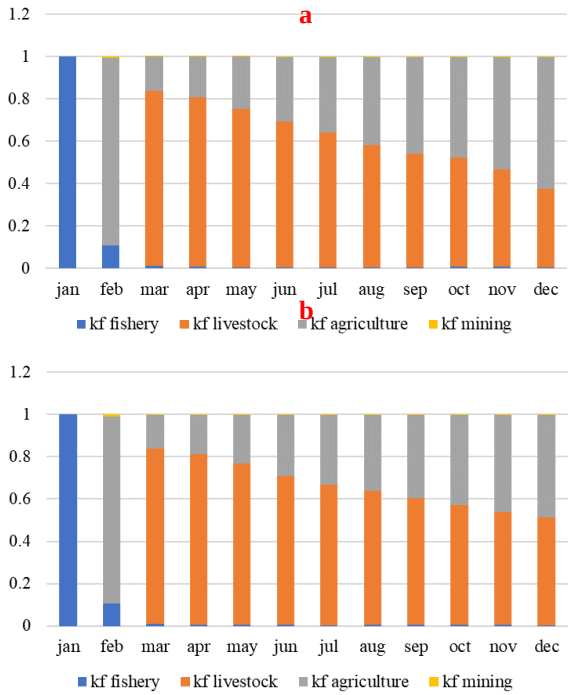

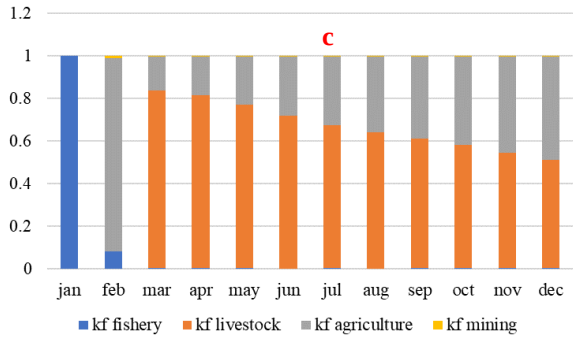

Figure 53: Distribution of contribution of productive strategies to the financial capital for a) La Niña, b) Neutral, and c) El Niño climate forcings.

Now, when we analyze the difference between the dam and no-dam scenarios in the values of financial capital, we notice differences between the behavior of the capital in climate change forcing; without the dam, the capital falls become more pronounced in the RCP 8.5 scenario (**Figure 53** and **Figure 54**). Although much more data and model sensitivity analysis are needed to draw robust conclusions, the observed results suggest that the dam plays a flow-stabilizing role in extreme scenarios, which, if managed appropriately, can play a key role in the social well-being at the local and regional levels.

The data from the analysis of RCP scenarios 4.5 and 8.5 with and without dam did not provide data that would allow accurate conclusions to be made about the behavior of social capital. However, they allowed us to build hypotheses related to the behavior of the capital and the level of impact that households may have as long as their extractive and productive strategies are compromised. In both cases, forcing RCP 8.5 reveals less strong effects on capital changes (softer oscillations). However, it would be necessary to evaluate the relationships that could be built with other variables of the model, to investigate the contribution of flood dynamics on productive areas and see if among these scenarios the greatest commitments occur within extractive strategies (fishing and mining).

A complementary analytical perspective that would be key to addressing the previously stated hypothesis would have to do with a separate analysis of the behavior of the capitals of extractive and productive activities over the 50-year horizon in the different scenarios. This would allow us to examine in more detail the relationship between changes in the river and financial capital flows in the regional context. An urgent task in this case would be to analyze the trends also by reaches.

a

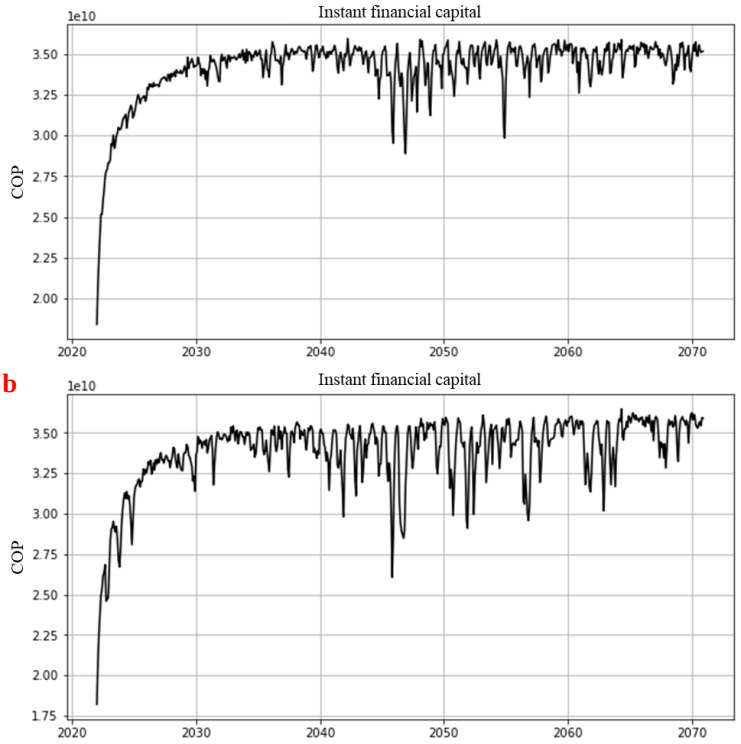

Figure 54: Financial capital for the dam scenario in a) pessimistic and b) optimistic forcings.

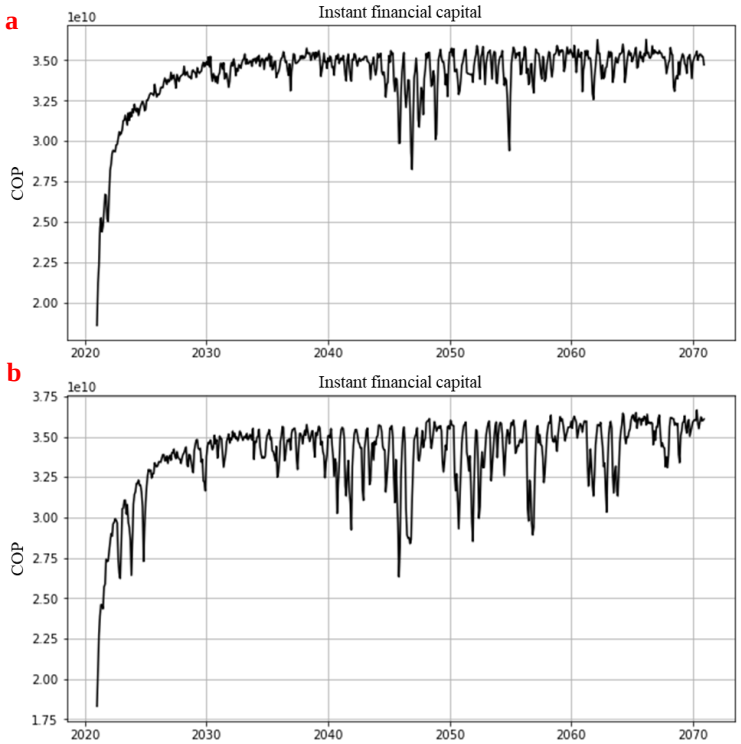

Figure 55: Instant financial capital for the no-dam scenario in a) pessimistic and b) optimistic forcings.

5.4 Discussion

From the proposed methodology and the modelling exercise regarding the case study, various aspects can be discussed. First, due to the difficulty of considering all the processes and dynamics of a SES in a proper way, various limitations arise. To run each model of the

proposed components, several data need to be collected. This required the necessity of making field campaigns, reviewing secondary information sources, and collecting information from experimentation, among others. Furthermore, the information on some variables is easier to collect. For example, large topographical information at a regional scale is widely found, but terrain data for the bathymetry of specific rivers is scarce (Bio et al., 2022; Liu and Song, 2022), for which field campaigns are usually required. Likewise, information on precipitation and river flow is highly measured by national institutions worldwide, but river sediment-related data is also scarce (Gwapedza et al., 2021). As well, biotic information is more difficult to find and also to measure (Hadjisolomou et al., 2021). Moreover, the information needed to quantify the ecosystem services and livelihoods responds to each specific case study and needs to be collected for each specific purpose. As well, the modelling proposal has a regional and aggregate focus that makes it difficult to see changes at the local level. This aspect must be considered to analyze the results, evaluate trends, and recognize biases in the information resulting from the simulations. Given the difference in resolutions between components, it is key to understand that, from this perspective, the results must be analyzed with caution and analytical strategies must be sought in accordance with these asymmetries in information.

Additionally, another limitation of the IMT is the integration of the modules and components. One main problem of this is the different time and spatial scales between processes. For example, the rate at which the water flow is mainly studied for soil degradation is in terms of minutes and hours, but the rate of changes in fish population or vegetation growth in a river is studied in terms of months. This creates a problem between the coupling of the models, where working on the same temporal scale can pose a problem of computational cost. In fact, in the case study presented in this paper, the ichthyoplankton component, which was performed through a particle tracking approach, was highly computationally demanding, for which the study of every forcing scenario of the proposed IMT could not be performed. Moreover, the abiotic components tend to describe better the phenomena with highly detailed mathematical models, whereas the biotic components still use models with high uncertainty in the definition of the phenomenon (Schuwirth et al., 2019).

On the other hand, there are also limitations in the arrangement of the modules and components and their functional relationships. For example, on the proposed IMT, there can exist a two-way relationship between the water quality of the river and its wetlands and the ecosystem service of livestock. The livestock activity can generate contamination flows to the near water bodies (Cesoniene et al., 2019), for which the output of this component can be a new input for the water quality module. Likewise, the human activities that involve the construction of hydraulic structures in the Cauca River will change its hydrodynamics and it will therefore generate a new output for all the modules that require its results as input. However, these two cases were not considered because of the complexity that two-way functional relationships generate in modelling formulation, verification, and computational resources. It is worth mentioning that, the coupling of components by these functional relationships involves their discussion between specialists from different fields, which could represent one of the biggest challenges presented in the IMT proposal. The diverse approaches, modelling techniques, and theoretical arguments of each scientist can generate difficulties when it comes to agreeing on a specific process to model.

Given that, the proposed IMT for the case study can be improved by the following

considerations: i) establishing better relationships between aquatic ecosystem components and the ecosystem services and livelihoods. There is only a functional relationship between habitat suitability and fishery components, while periphyton and ichthyoplankton components were used only as biological indicators. However, these last components can also determine the dynamics of fish population and therefore could be linked to the ecosystem services. ii) Formulating two-way relationships between components because, as mentioned in the previous paragraph, there are processes that are directly related between them for which their output (results) should be used as input even when the models have been executed. iii) Use standard methodologies for the verification of the models and the functional relationships between them, such as sensitivity analysis, and statistical metrics, among others, which can allow comparisons between components that use different variables and temporal and spatial scales. Nevertheless, it is worth mentioning that each model independently has a verification, calibration, and/or validation process, to perform an adequate modelling activity. iv) Approaches different to dynamic systems can be considered to estimate the affectations of the ecosystem services and livelihoods (e.g., Asmus et al., 2019; Borges et al., 2021; LaRota-Aguilera and Marull, 2023).

Finally, we recommend some future work to follow on the improvement of the proposal of IMT. Investigations should be performed for the extrapolation of the proposed methodology for its use in non-aquatic ecosystems, as well as its use in other latitudes outside tropical zones. Different modules could arise from this approach, modifying the initial proposal but maintaining the basis of the methods. Likewise, the results of livelihoods through capital theory could be replaced by studying diverse approaches that can possibly give an approximation of qualitative and quantitative social analysis. A strategy for appropriation, validation, and building trust in the model through workshops with officials and key actors in these projects (for example, construction of hypotheses, forcing of the model, and discussing implications, among others), could be developed. Furthermore, the IMT can be used to study a wide variety of analysis scenarios, not only the affectation to SES due to the presence of MEP. Research could be directed to the understanding of specific ecosystem dynamics involving its forcings and parallel socio-ecological processes, or even directed to the evaluation of the sensitivity of environmental variables (e.g., Martínez-Fernández et al., 2021), but applying an IMT.

5.5. Conclusions

In this study, a methodology to develop an IMT for analyzing SES is proposed. It is composed of four phases which are the analysis of the case study, the generation of a conceptual model, the proposal of modules and components, and the design of scenarios of analysis. To describe the SES, the methodology specifies the study of three modules: the first one allows the simulation of the physical dynamics of the system, the second module uses the previous outputs as a basis for developing an aquatic ecosystem component, and the third module uses the physical and ecological results as a basis for a dynamical system-based model for ecosystem services and livelihoods. Therefore, the methodology is applied and an IMT is generated to analyze the affectation of the IHP, over 400 km along the Cauca River in Colombia. Results allow dimensioning the level of affectation in terms of flooded areas, fish species habitat suitability, and quantification of ecosystem services, among others.

As presented in Section 1, there has been a necessity for tangible solutions in the study

of SES, that has not been yet satisfied. The methodology proposed in this paper brings a possible solution to assess this problem. The generation of an IMT can involve the most important aspects that compose an environment, where each component can be studied independently and linked between them. This summarizes the complexity and variability of a SES in a tool that can bring specific quantitative and qualitative results to help decision-making in environmental management. Furthermore, this tool can also be used in the estimation of the affections of the SES due to the construction or presence of MEP, from the present date to the impact it can cause in future years. This also clarifies the feasibility process of the project and brings prediction of specific environmental data that can be used to prevent the affectation to the ecosystem and the hydric resources of the area. Moreover, the social component of the system is not forgotten and the modelling of the environmental process is related to social dynamics that as well can be estimated for future years. Nevertheless, future work is still needed to nourish this methodology and expand its applicability in a wide variety of SES.

6 General discussion

The representation of complex phenomena requires the development and use of better modelling tools. Here, different approaches and methodologies for model integration were implemented, taking into account spatio-temporal variations and scales so that better decisions can be made on the different problems presented by tropical systems, such as climate-related water quality problems and more details on water-atmosphere exchanges and their implications for water systems.

With the results of this research is possible to have control measures and management strategies, covered by the official water quality standards, since this research has revised many of the criteria traditionally used in the analysis and prediction of water quality and the uses that may be given to a tropical water system (Wainwright Mulligan, 2004, Caviness et al., 2006, Denzer et al., 2011). Furthermore, the results can be compared with Colombian regulations (ANLA, CARS, IDEAM) and international regulations (EPA, etc.) to establish standards for the assessment of the water tropical hydrosystems evaluation.

In the case of Colombia, the use of such tools will contribute to the development of better proposals for the environmental management of water resources in the productive and environmental sectors.

This investigation allowed to better predictions of water quality, using the relationship between variables, and be able to Understand the principal processes that affect multi spatial temporal scales problems fate and transport coupling in tropical dynamics and later coupling other areas. Allowed to dig deeper into issues and knowledge, and potentially address scenarios such as climate change in tropical conditions. Also shows a range of values of the net heat flux at the water–air interface in tropical hydrosystems.

Regarding river systems and aquatic biota, on the other hand, this study highlights hydraulics as the main factor regulating the growth of algae, followed by high availability of nutrients finding characteristics time scales for phenomena such as drought in the tropics, and numerical and mathematical couplings that can be established to analyze the response of tropical systems to different hydraulic, water quality, and hydrometeorological forcings.

Finally, based on all the research results, a methodology for the development of integrated modeling tools (IMT) for the analysis of socio-ecological systems can be proposed. Which is composed of three modules: the first one allows the simulation of the physical dynamics of the system, the second module uses the previous outputs as a basis for developing an aquatic ecosystem component, and the third module uses the physical and ecological

results as a basis for a dynamical system-based model for ecosystem services and livelihoods.

7 Conclusion and outlook

A reference framework was developed for the simulation of water quality in tropical systems, this framework is composed of two phases, the first one relating the most important variables in the dynamics of water quality in tropical systems and the second one to the thermal dynamics of tropical reservoirs.

The chapter 2 applied a methodology that allows a determination of the behavior of hydro-meteorological and water quality variables in tropical reservoirs and establishes the relationship between water quality parameters and hydrometeorology to predict dissolved oxygen. The following conclusions can be drawn:

Statistical tests and analysis showed a statistically significant influence of hydro-meteorological variables like precipitation, flow discharge, relative humidity, solar brightness, and air temperature over water quality parameters, especially with nutrients, and dissolved oxygen. These analyses also showed that, as the relationship between water quality and hydro-meteorological variables varied from site to site, therefore the behavior of water quality parameters is influenced by the area within the reservoir.

Descriptive statistical analyses are performed by separating the time series according to the climatic seasons showing significant differences between the dry and wet seasons. Similarly, the correlation analysis results of each season show that the reservoir is affected by seasons, and the influence of meteorological variables in the dry season is more evident than that in the rainy season. Therefore, this funding increases the metrics for predictions.

Due to the spatial and temporal heterogeneity of water quality in a tropical reservoir, water quality monitoring should be designed to capture the temporal dynamics close to dams' inlets to predict dam water quality. This finding suggests that designing and maintaining effective reservoir water quality monitoring is key to sustainable management and prediction.

It is essential to begin analyzing and modeling the environmental impacts of large dams more holistically to better inform stakeholders and decision-makers on the balance between exploiting hydropower potential and maintaining critical natural resources.
The chapter 3, different modeling assumptions for tropical reservoir temperature and air-water exchange are analyzed based on observations. This study evaluated the performance of various hypothesis in resolving hydrodynamic, thermal, and energetic processes, including the effect of hydroclimatological forcings such as air temperature, wind, and the internal mixing process (turbulence), and different boundary conditions in the free surface. The following conclusions can be drawn:

Reservoir water temperature is affected by heat exchange between the water and the

atmosphere. This exchange is evident in the upper layer (O (<10m)), and it is this dynamic in the first layer governs the distribution within the water body in areas where there is no advective flow from tributaries, which for the reservoir analyzed is on the order of 80%.

In this work, numerical methods are used as a tool to study exchange. This research finds that a good definition of the boundary conditions at the water-free surface is crucial for a correct representation of the thermodynamics inside the water body.

The hydrodynamic TELEMAC-3D model has been satisfactorily calibrated using one month of daily water level observations at one point in the reservoir. Sensitivity analyses highlighted the importance of vertical turbulence models and vertical diffusion coefficient for a correct representation of the observed behavior.

Overall, reservoir water temperature is strongly influenced by heat exchange between water and the atmosphere. Accurate modeling of such phenomena is thus necessary. Three different approaches have been tested to study the impact of air-water exchanges at the free surface: a constant water temperature without exchange with the atmosphere (approach A), meteorological forcing with atmospheric parameters constants in time (approach B), meteorological forcing with atmospheric parameters varying in time (approach C).

Although some uncertainties are present in the current numerical study about the A exchange coefficient tested in the simulations, the results are in a satisfactory agreement to data, especially considering the complexity of the studied phenomenon, as well as the equally complex dynamics of the various processes' interactions involved in its numerical simulation. In particular, regarding the water temperature at different depths, the following convergence results are observed: approach A maximum deviation from data reaching 3°C, approach B maximum deviation from data reaching 4°C, and approach C maximum deviation from data reaching 8°C.

It can be stated that if site conditions and air-water temperature differences are known, A coefficient can be used as an approximate method of estimating the rate of exchange of natural water surfaces in a reservoir on an hourly basis during every period in the year.

As General Conclusions:

- Tropical reservoirs differ from temperate reservoirs in that they are permanently stratified.
- The dynamics of the tropical reservoir is related to both the hydrometeorology and the water quality itself and its dynamics depend on the location in the reservoir.
- The equations proposed so far must be adapted to tropical conditions.
- The use of hydrometeorological variables for water quality prediction improves the results in the case of the tropics.

- The factors affecting thermal dynamics in other reservoirs, e.g., wind, radiation, are slightly different for tropical reservoirs, with latent heat and evaporation being more significant in this case.

- The stratification in the area of the reservoir is very similar, from 2 meters it begins to stratify and is maintained.

- As the stratification is homogeneous in tropical reservoirs, not so many monitoring points are required to represent the dynamics.

- As for the measurement campaigns in tropical systems, more detailed measurements are required in the first 10 meters, fewer points at 40 meters, and then the temperature remains constant.

Future works

- Some future work will add some water quality findings and water column behavior that can be verified by modeling and taking into account turbulence and physical phenomena
- Future works will require rethinking the exchange formulas for the tropical context including evaporation, as the existing ones are not able to reproduce the variations in the water column of the reservoirs.
- Future works will require rethinking thermic modelling including evaporation, precipitation.
- Owing to the temperature variations at sub daily level, computational tools are required to simulate it, in the Telemac, it is necessary to use a multi-core process to implement the sinusoidal equation since the process is only implemented for a single core.
- Future works will require run cases with inputs sensitivity (hydrological, thermic)
- Future works will require run cases climatic change scenarios.
-

A. Supplementary material to Chapter 2

This appendix provides the supplementary material to Chapter 2.
The data series used in the statistical analysis is presented below.

Hydroclimatologycal analisys

Sunshine duration

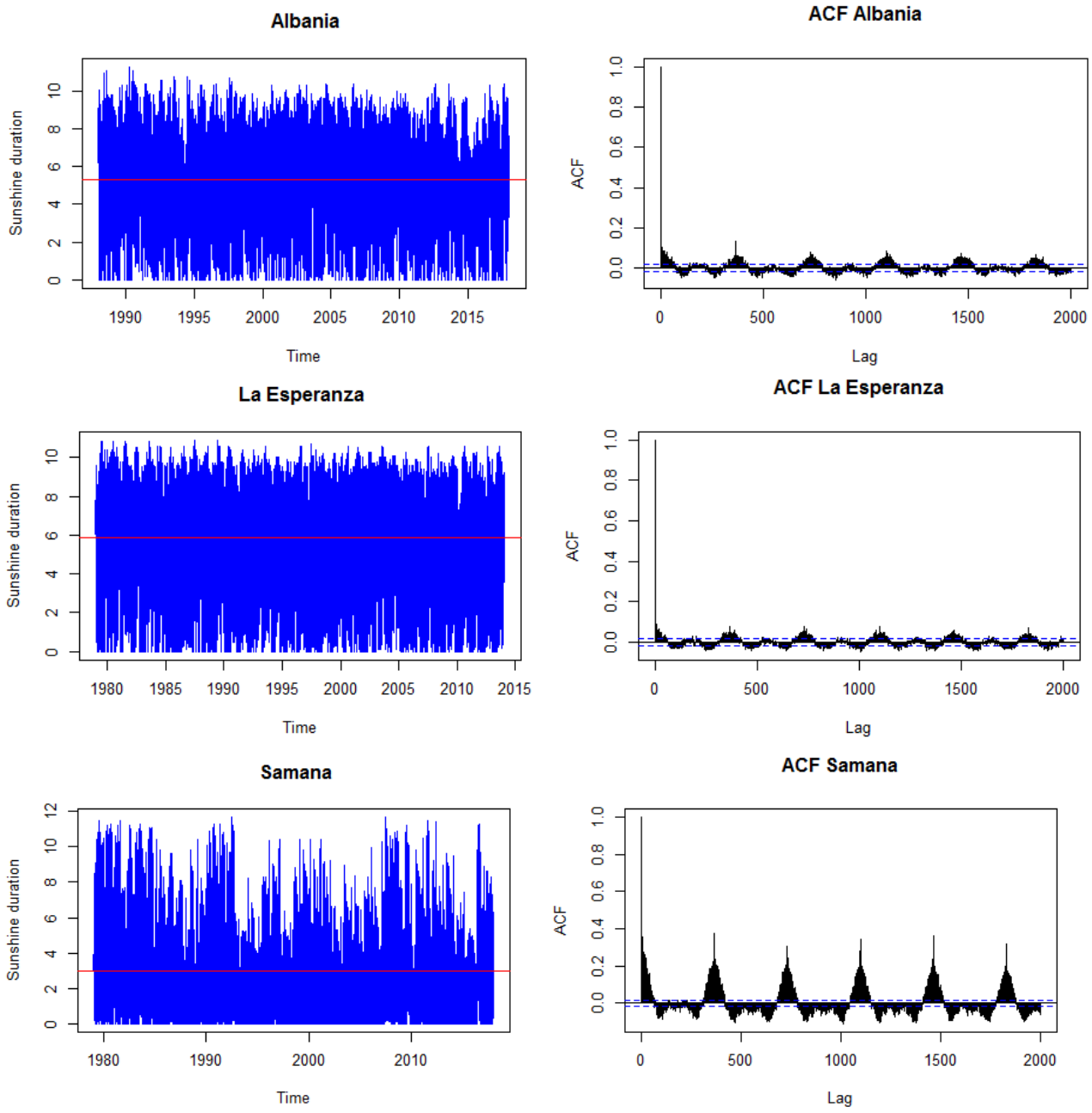

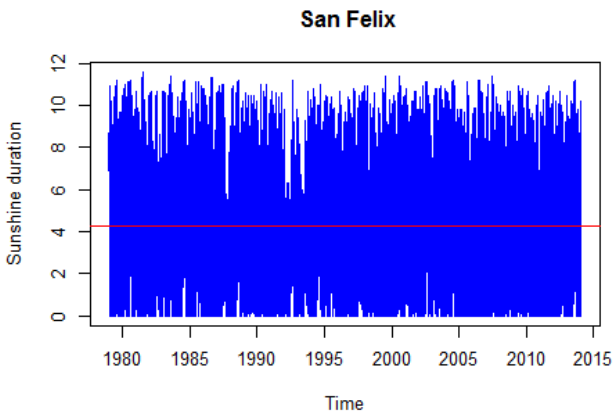

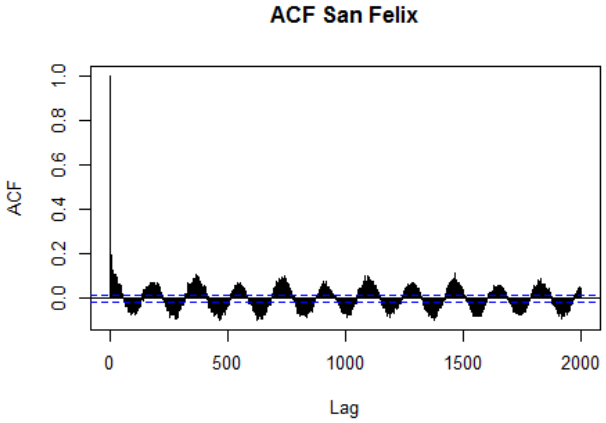

Evaporation

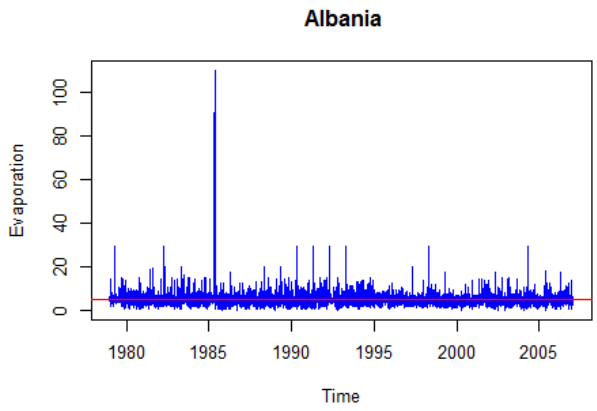

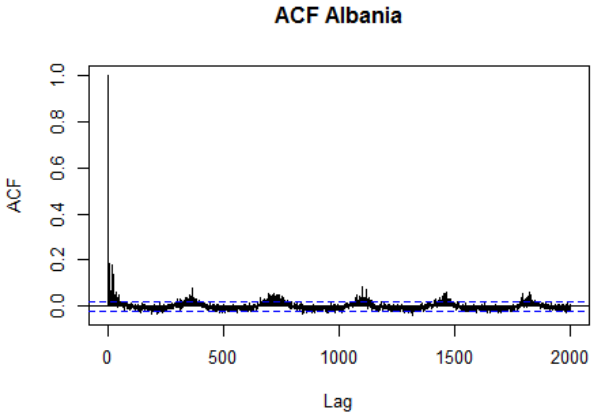

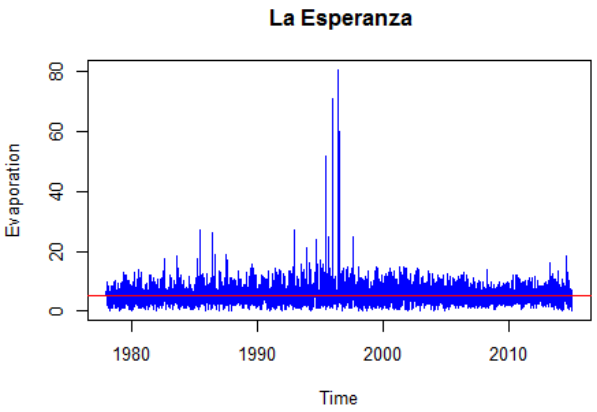

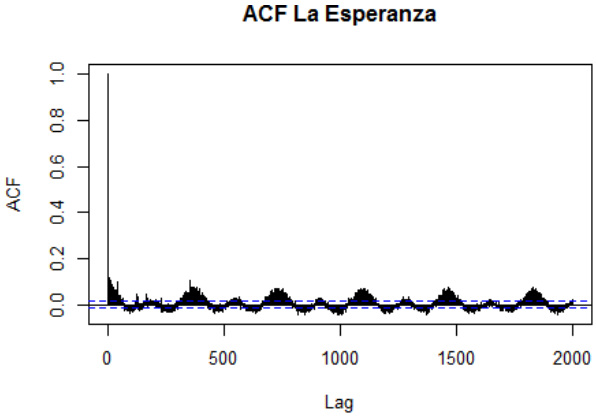

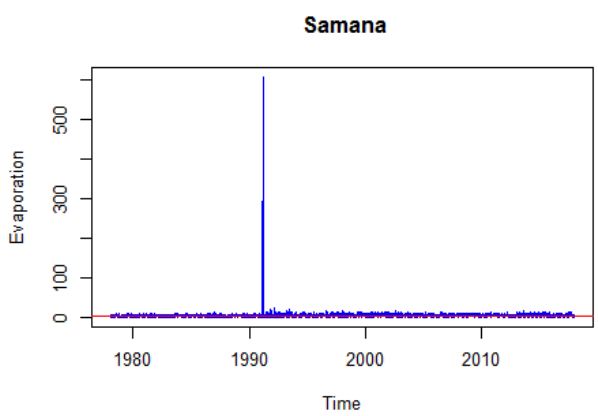

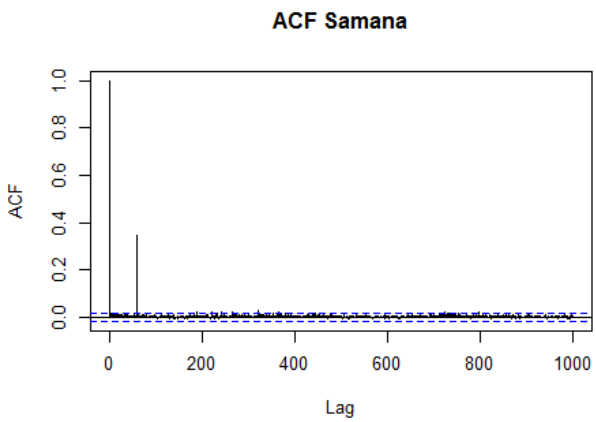

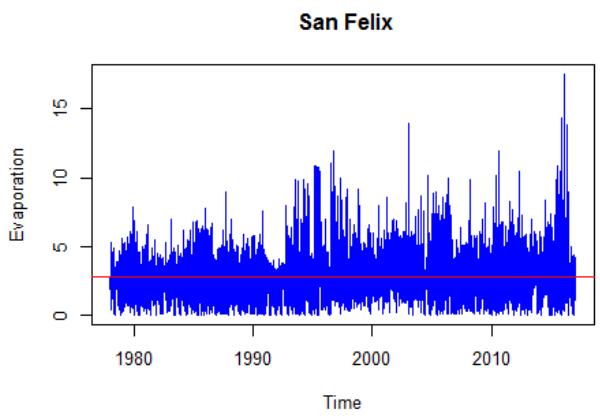

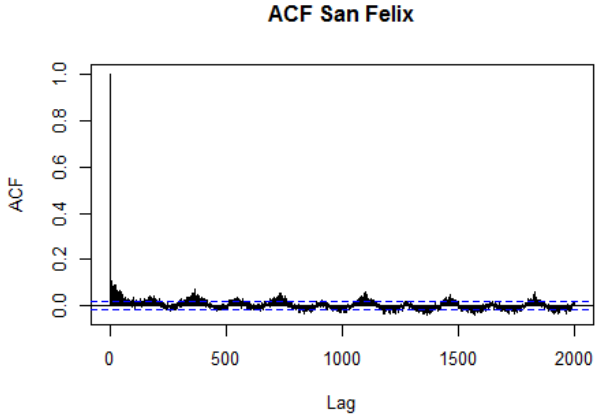

Relative humidity

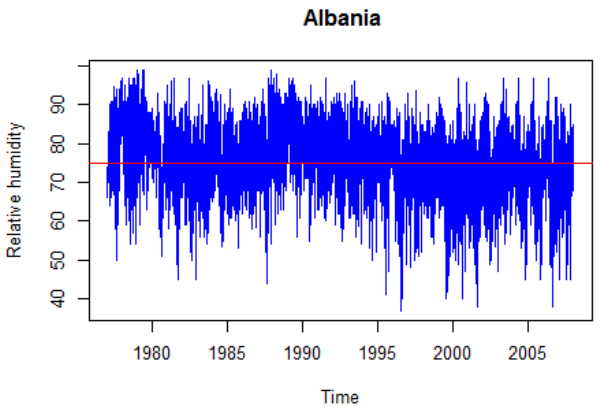

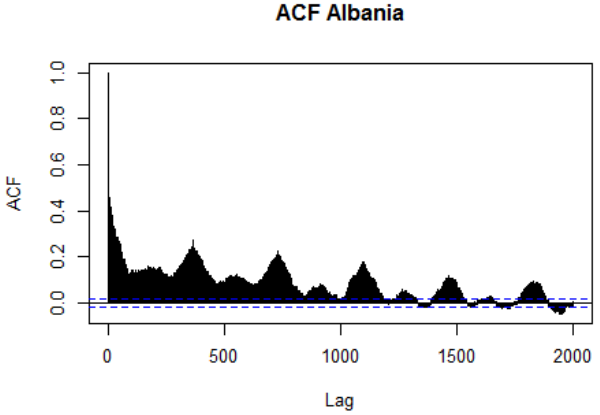

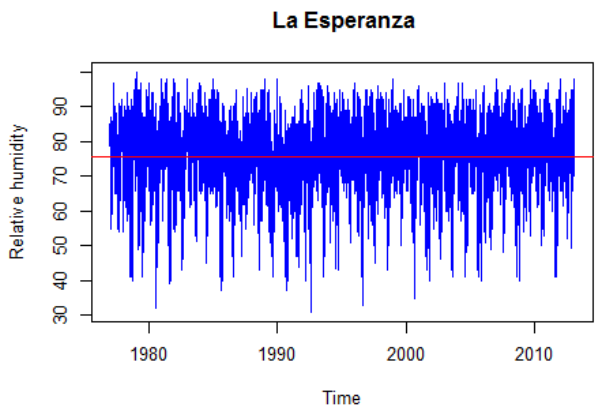

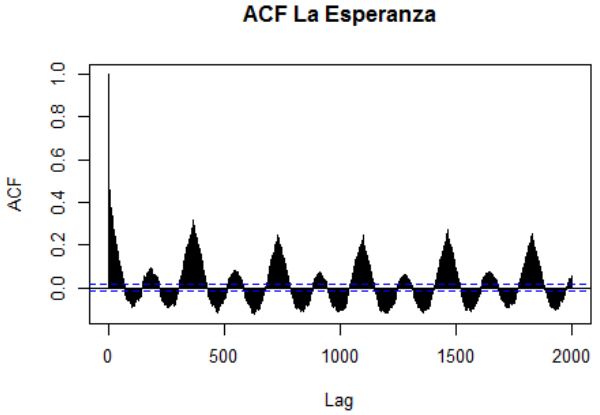

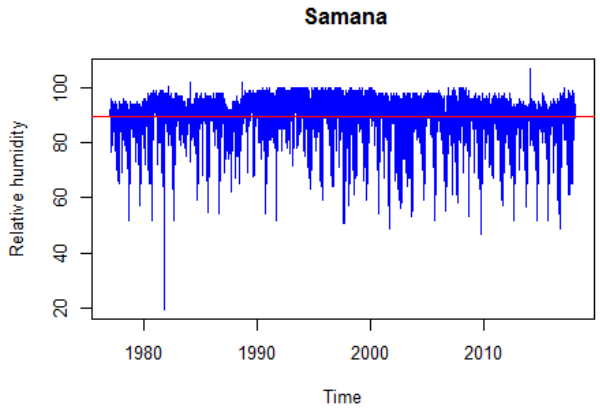

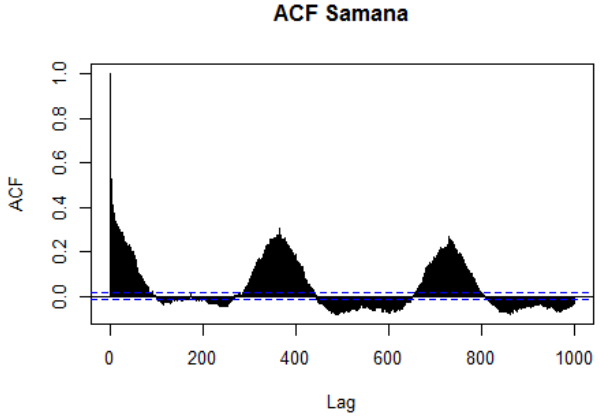

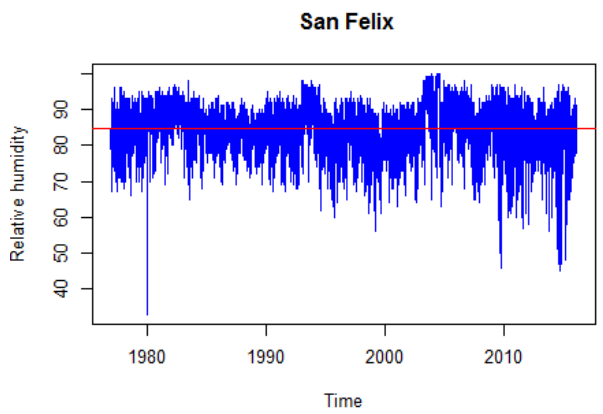

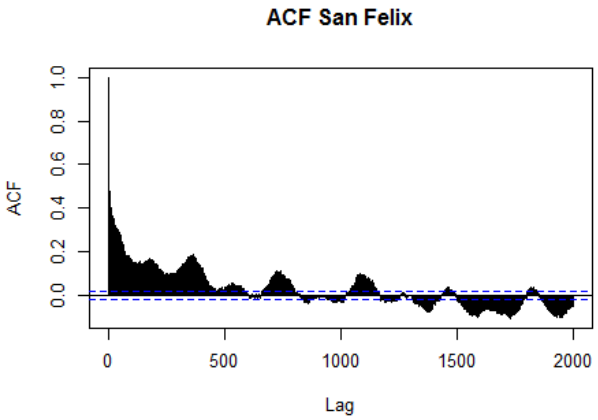

Air Temperature

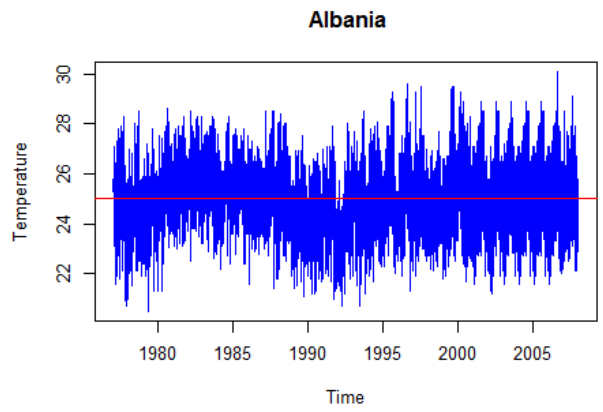

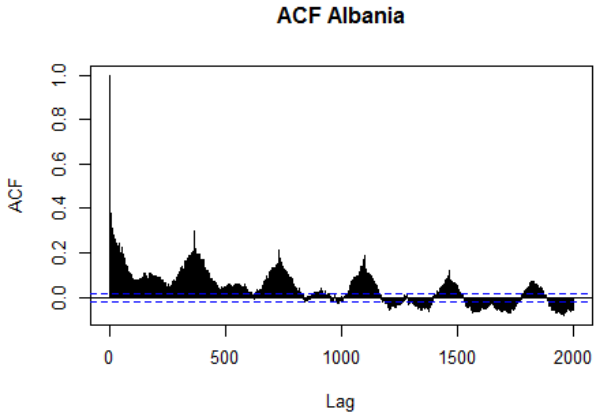

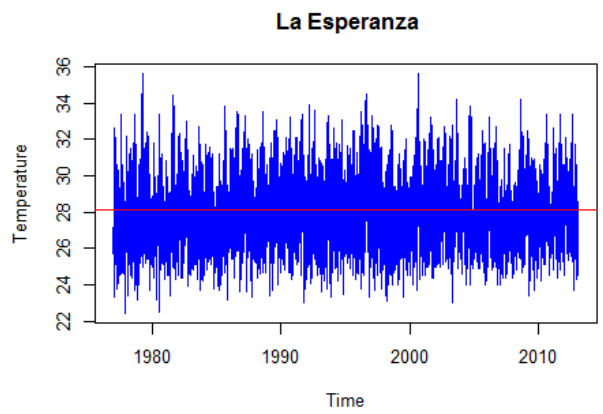

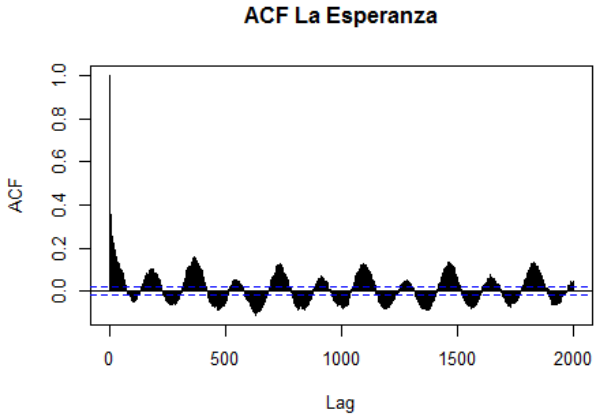

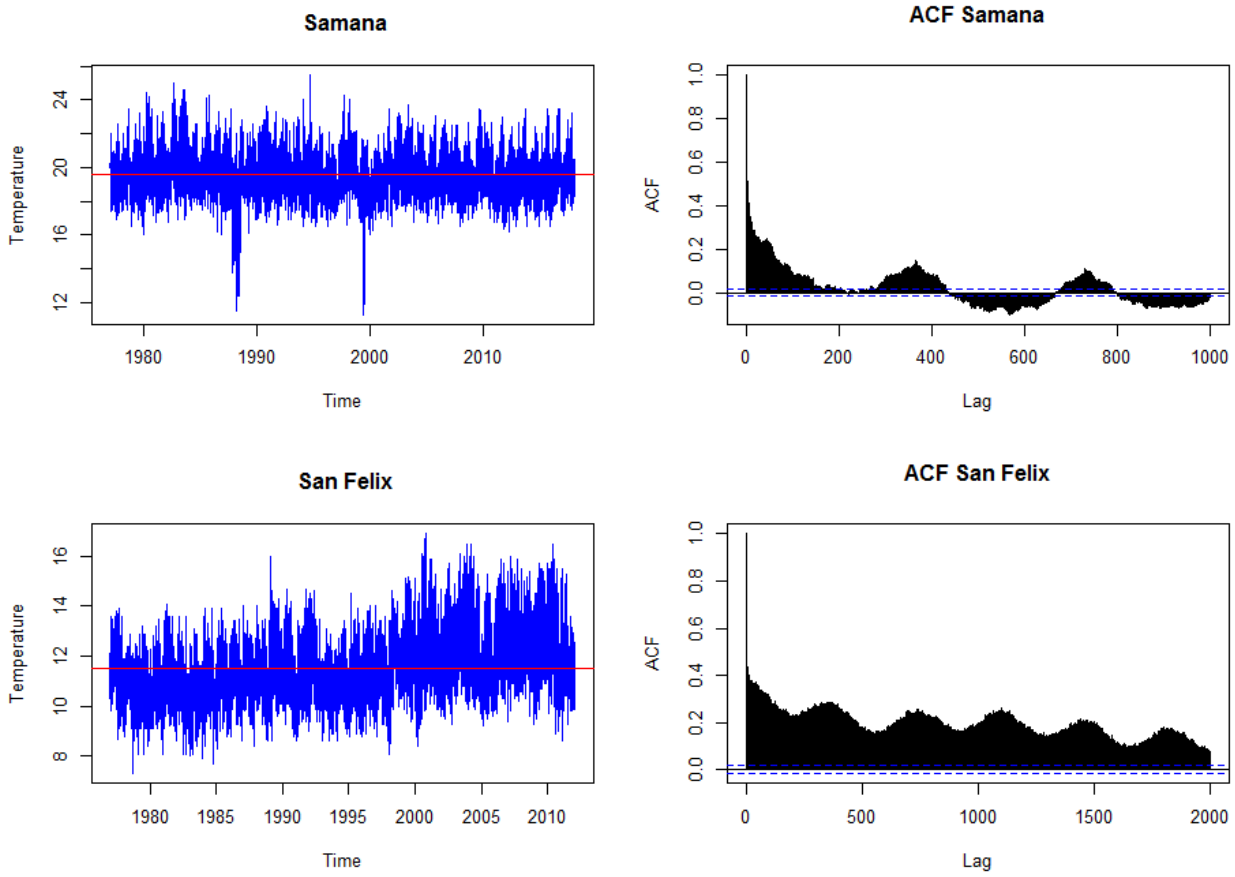

Daily discharge

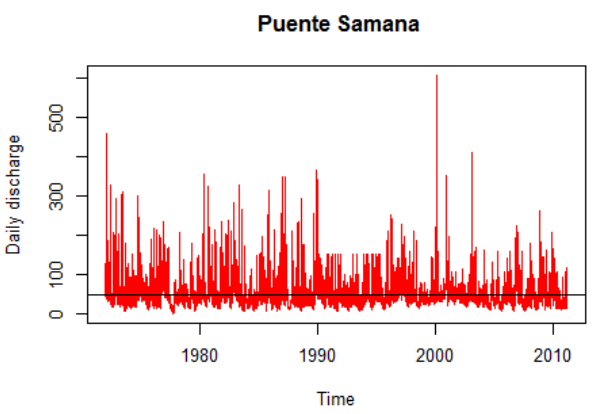
Puente Samana
Daily discharge
0
100
300
500
1980
1990
2000
2010
Time

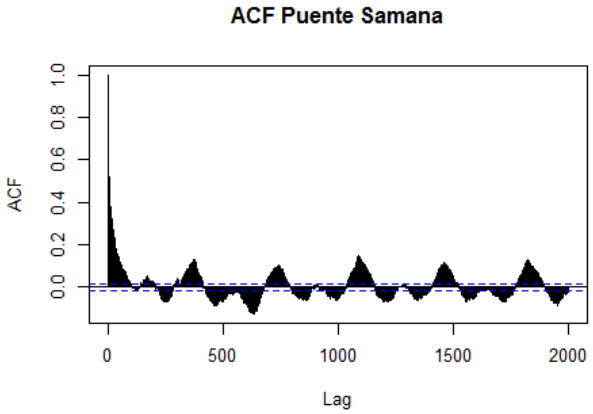
ACF Puente Samana
ACF
0.0
0.2
0.4
0.6
0.8
1.0
0
500
1000
1500
2000
Lag

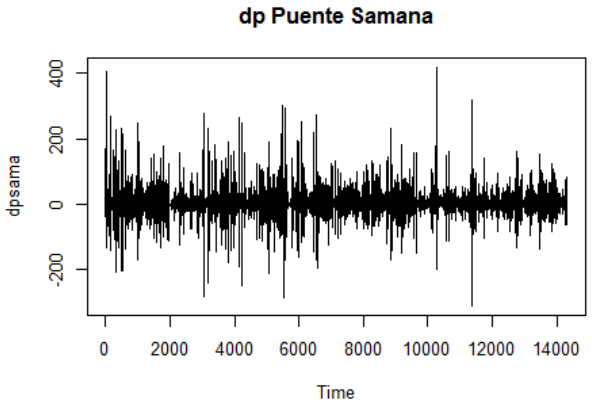
dp Puente Samana
dpsama
-200
0
200
400
0
2000
4000
6000
8000
10000
12000
14000
Time

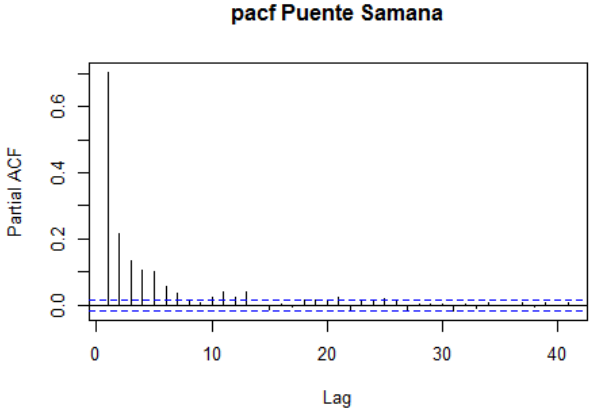
pacf Puente Samana
Partial ACF
0.0
0.2
0.4
0.6
0
10
20
30
40
Lag

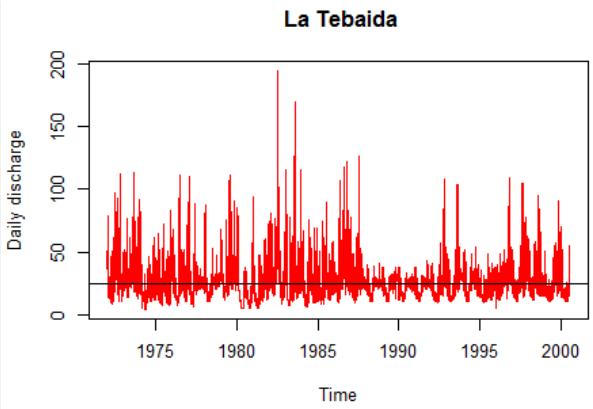
La Tebaida
Daily discharge
0
50
100
150
200
1975
1980
1985
1990
1995
2000
Time

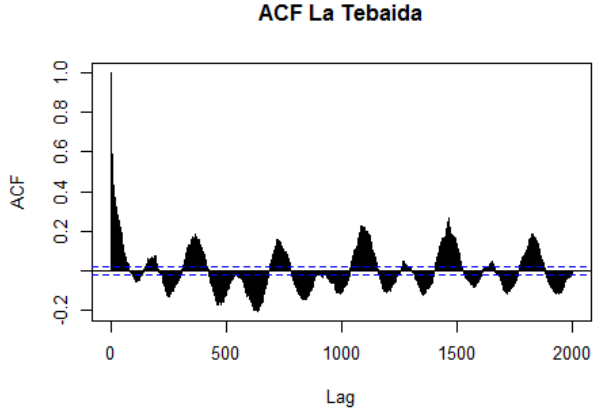
ACF La Tebaida
ACF
-0.2
0.2
0.4
0.6
0.8
1.0
0
500
1000
1500
2000
Lag

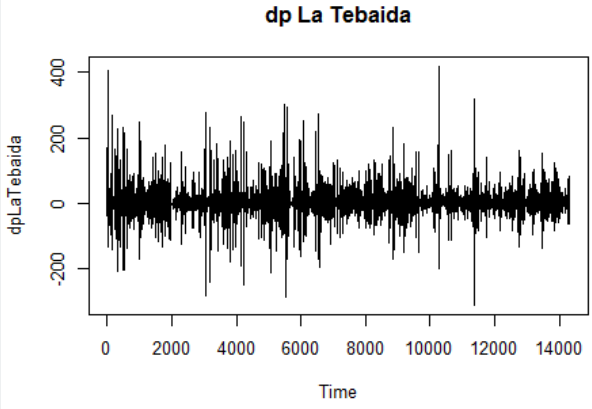
dp La Tebaida
dpLaTebaida
-200
0
200
400
0
2000
4000
6000
8000
10000
12000
14000
Time

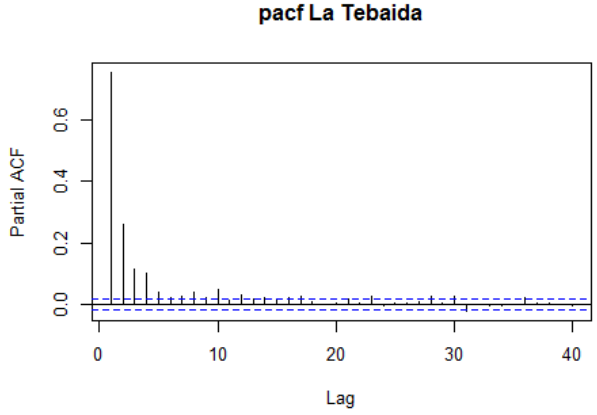
pacf La Tebaida
Partial ACF
0.0
0.2
0.4
0.6
0
10
20
30
40
Lag

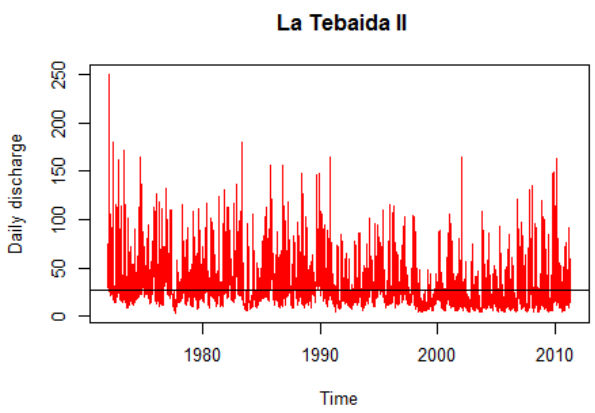
La Tebaida II
Daily discharge
0
50
100
150
200
250
1980
1990
2000
2010
Time

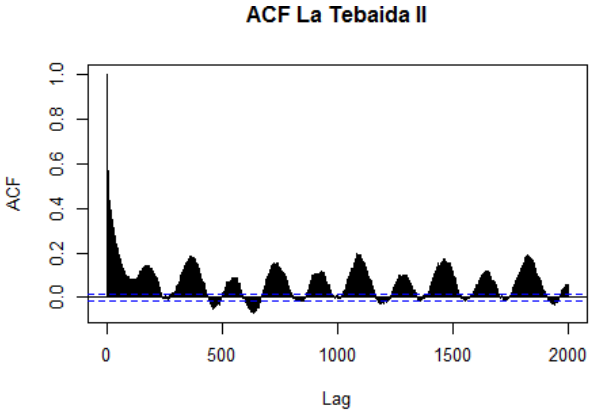
ACF La Tebaida II
ACF
0.0
0.2
0.4
0.6
0.8
1.0
0
500
1000
1500
2000
Lag

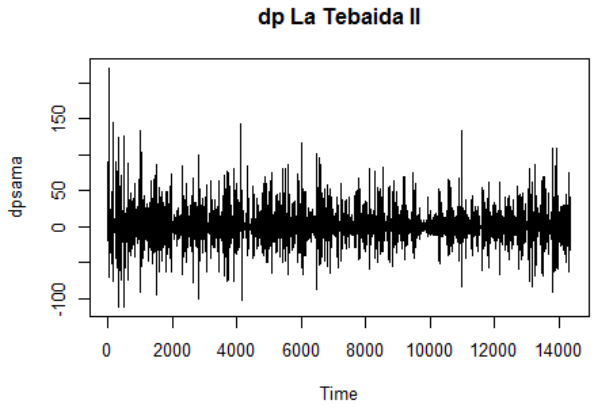
dp La Tebaida II
dpsama
-100
0
50
150
0
2000
4000
6000
8000
10000
12000
14000
Time

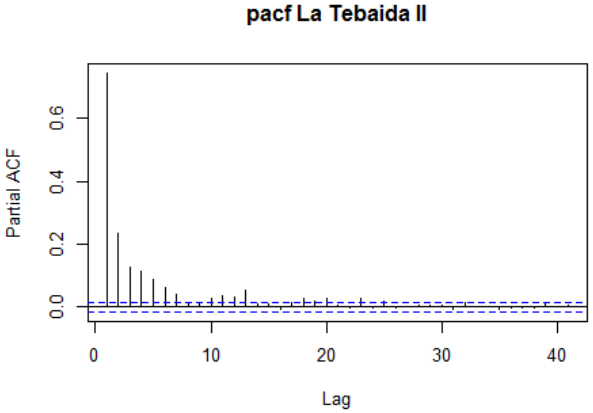
pacf La Tebaida II
Partial ACF
0.0
0.2
0.4
0.6
0
10
20
30
40
Lag

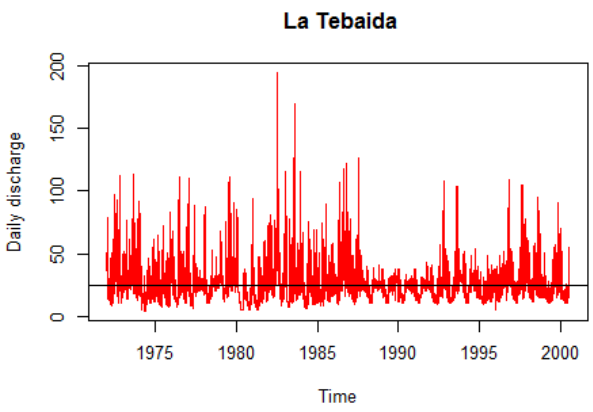
La Tebaida
Daily discharge
0
50
100
150
200
1975
1980
1985
1990
1995
2000
Time

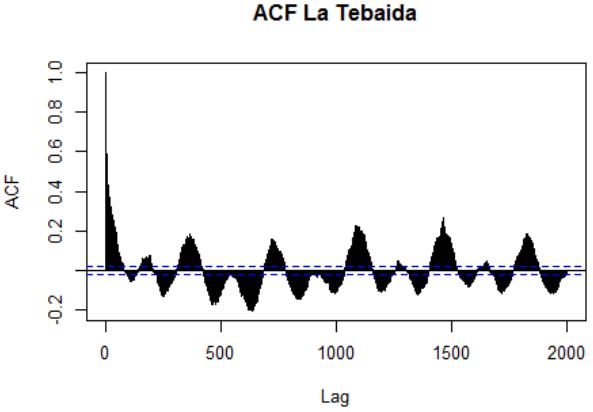
ACF La Tebaida
ACF
-0.2
0.2
0.4
0.6
0.8
1.0
0
500
1000
1500
2000
Lag

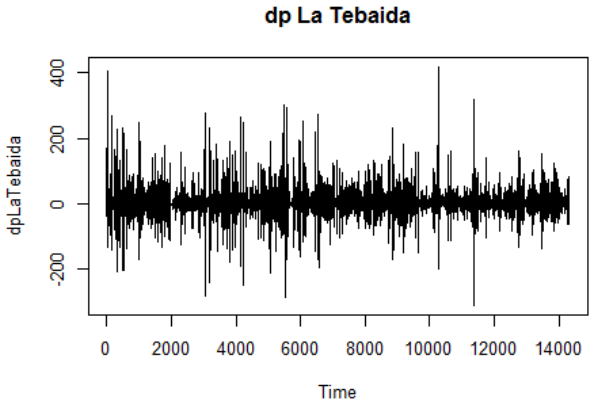
dp La Tebaida
dpLaTebaida
-200
0
200
400
0
2000
4000
6000
8000
10000
12000
14000
Time

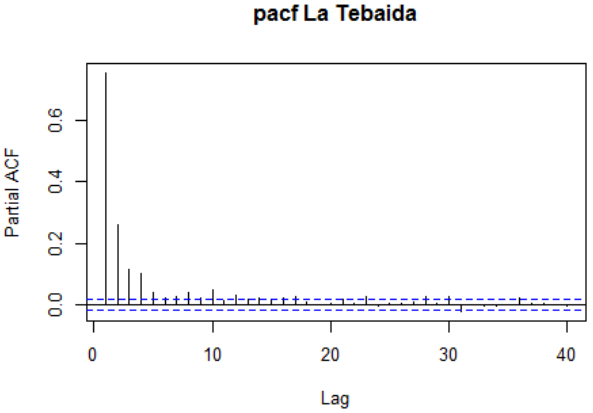
pacf La Tebaida
Partial ACF
0.0
0.2
0.4
0.6
0
10
20
30
40
Lag

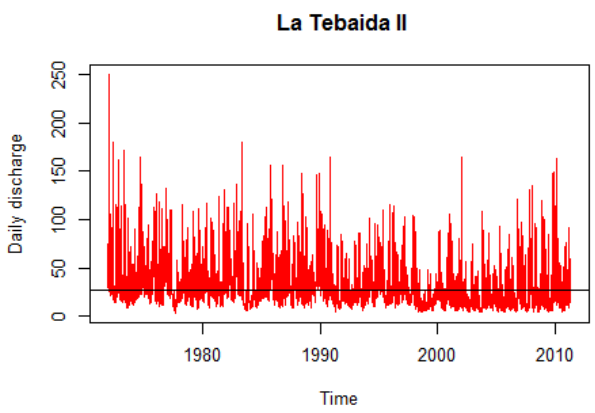
La Tebaida II
Daily discharge
0
50
100
150
200
250
1980
1990
2000
2010
Time

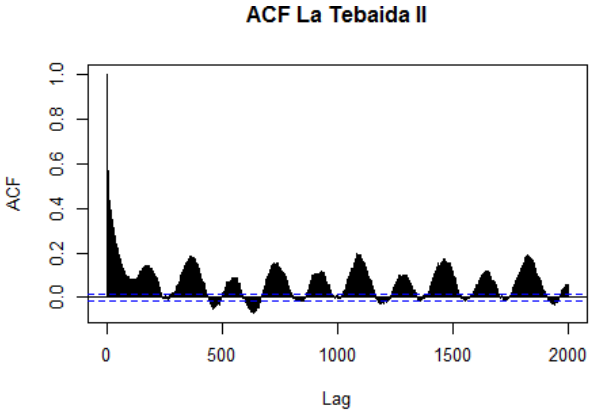
ACF La Tebaida II
ACF
0.0
0.2
0.4
0.6
0.8
1.0
0
500
1000
1500
2000
Lag

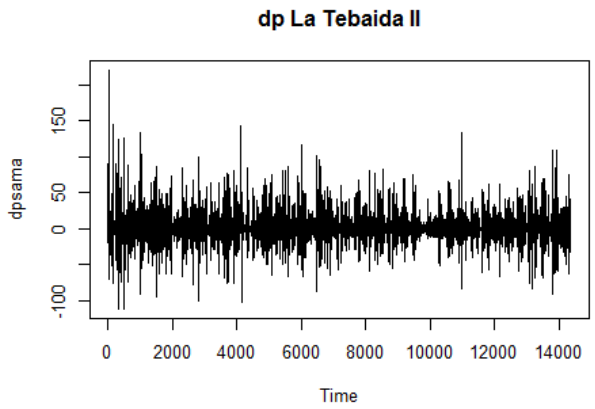
dp La Tebaida II
dpsama
-100
0
50
150
0
2000
4000
6000
8000
10000
12000
14000
Time

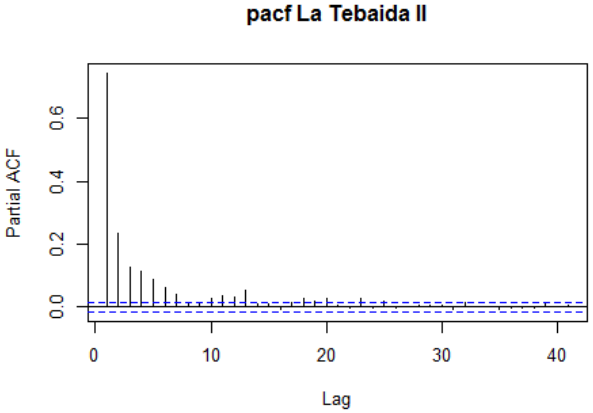
pacf La Tebaida II
Partial ACF
0.0
0.2
0.4
0.6
0
10
20
30
40
Lag

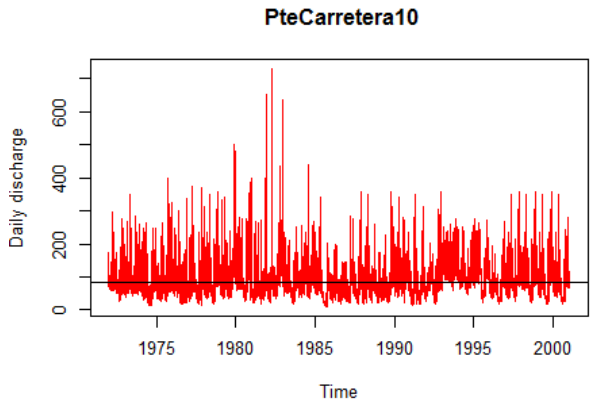
PteCarretera10
Daily discharge
0
200
400
600
1975
1980
1985
1990
1995
2000
Time

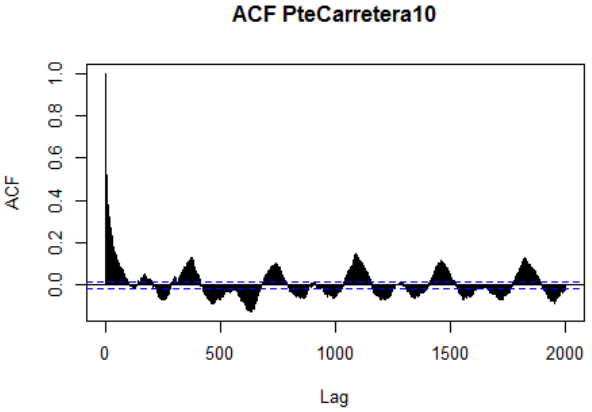
ACF PteCarretera10
ACF
0.0
0.2
0.4
0.6
0.8
1.0
0
500
1000
1500
2000
Lag

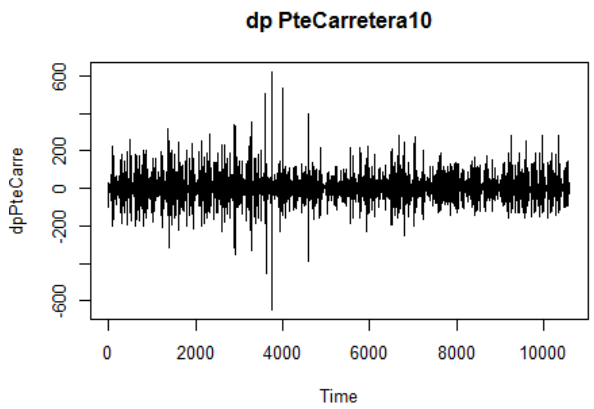
dp PteCarretera10
dpPteCarre
-600
-200
0
200
600
0
2000
4000
6000
8000
10000
Time

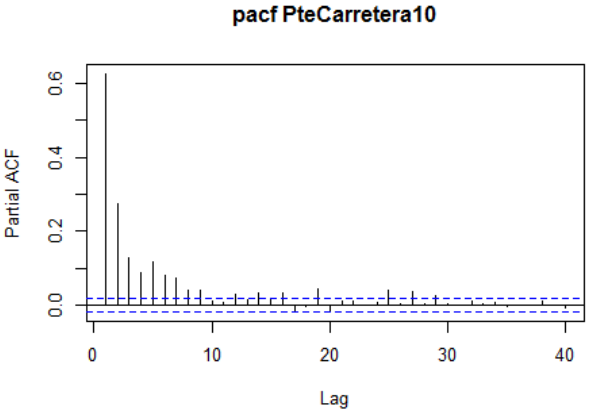
pacf PteCarretera10
Partial ACF
0.0
0.2
0.4
0.6
0
10
20
30
40
Lag

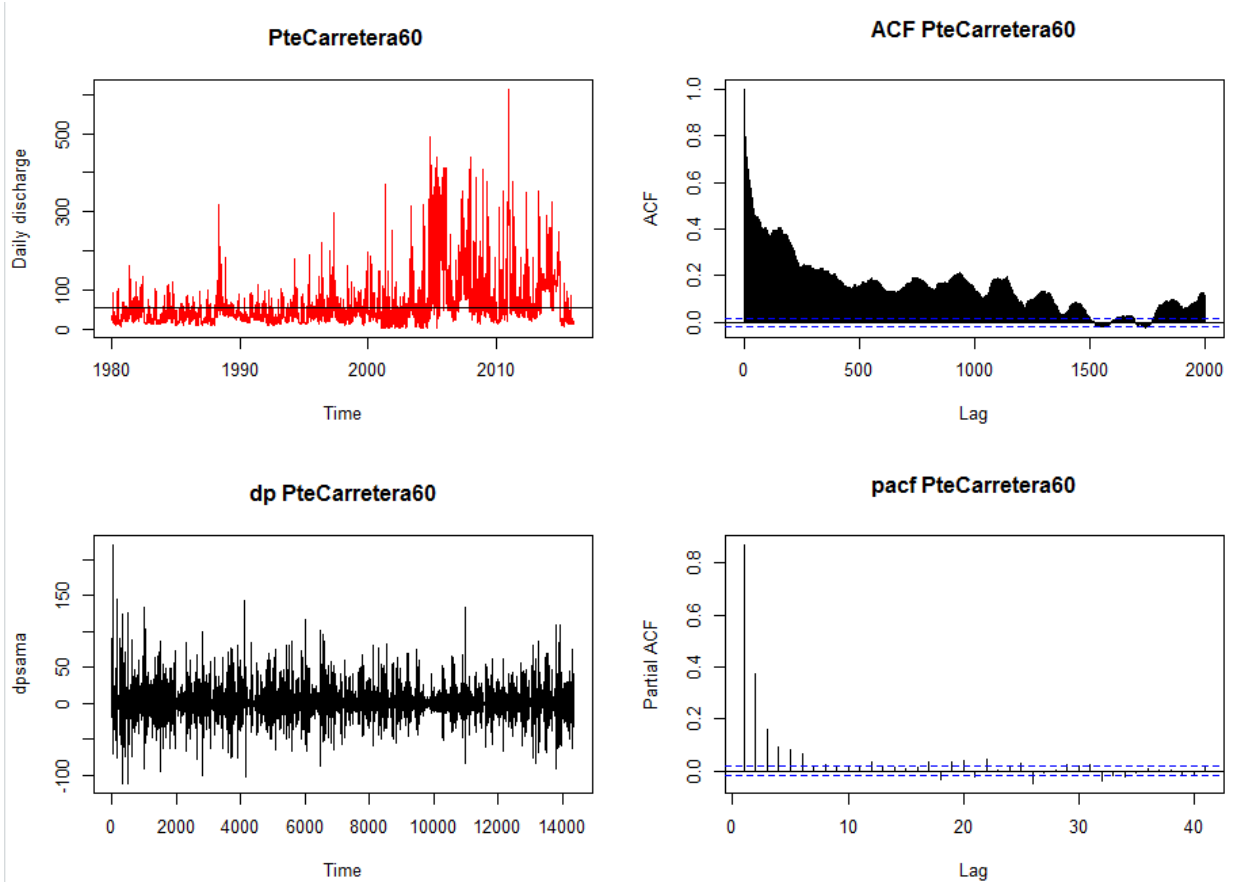
PteCarretera60
Daily discharge
0
100
300
500
1980
1990
2000
2010
Time

ACF PteCarretera60
ACF
0.0
0.2
0.4
0.6
0.8
1.0
0
500
1000
1500
2000
Lag

dp PteCarretera60
dpsama
-100
0
50
150
0
2000
4000
6000
8000
10000
12000
14000
Time

pacf PteCarretera60
Partial ACF
0.0
0.2
0.4
0.6
0.8
0
10
20
30
40
Lag

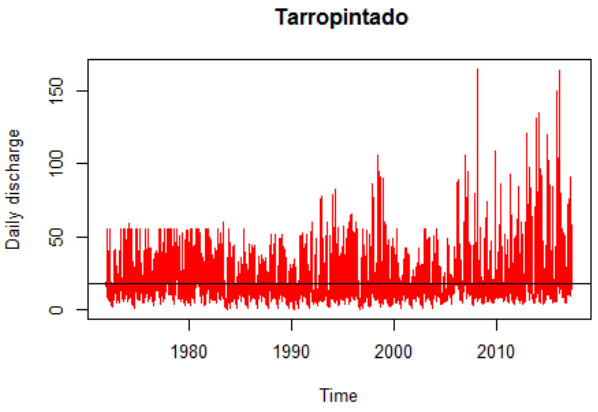
Tarropintado
Daily discharge
0
50
100
150
1980
1990
2000
2010
Time

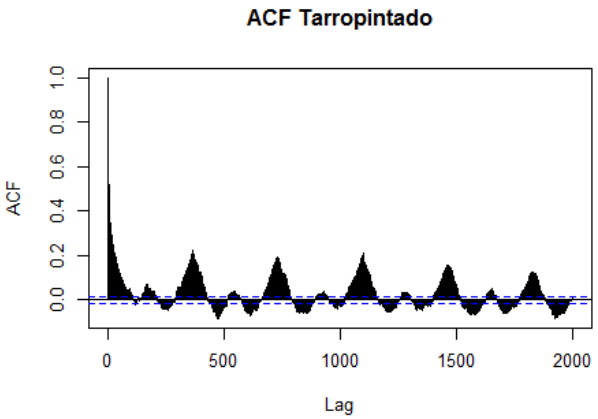
ACF Tarropintado
ACF
0.0
0.2
0.4
0.6
0.8
1.0
0
500
1000
1500
2000
Lag

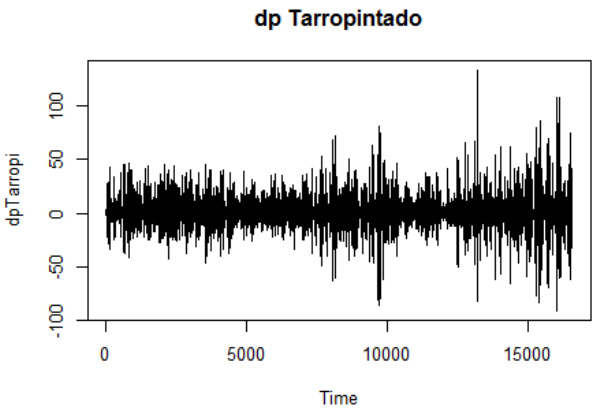
dp Tarropintado
dpTarropi
-100
-50
0
50
100
0
5000
10000
15000
Time

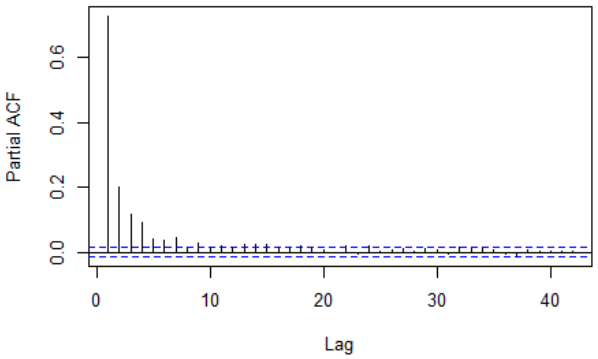
pacf Tarropintado
Partial ACF
0.0
0.2
0.4
0.6
0
10
20
30
40
Lag

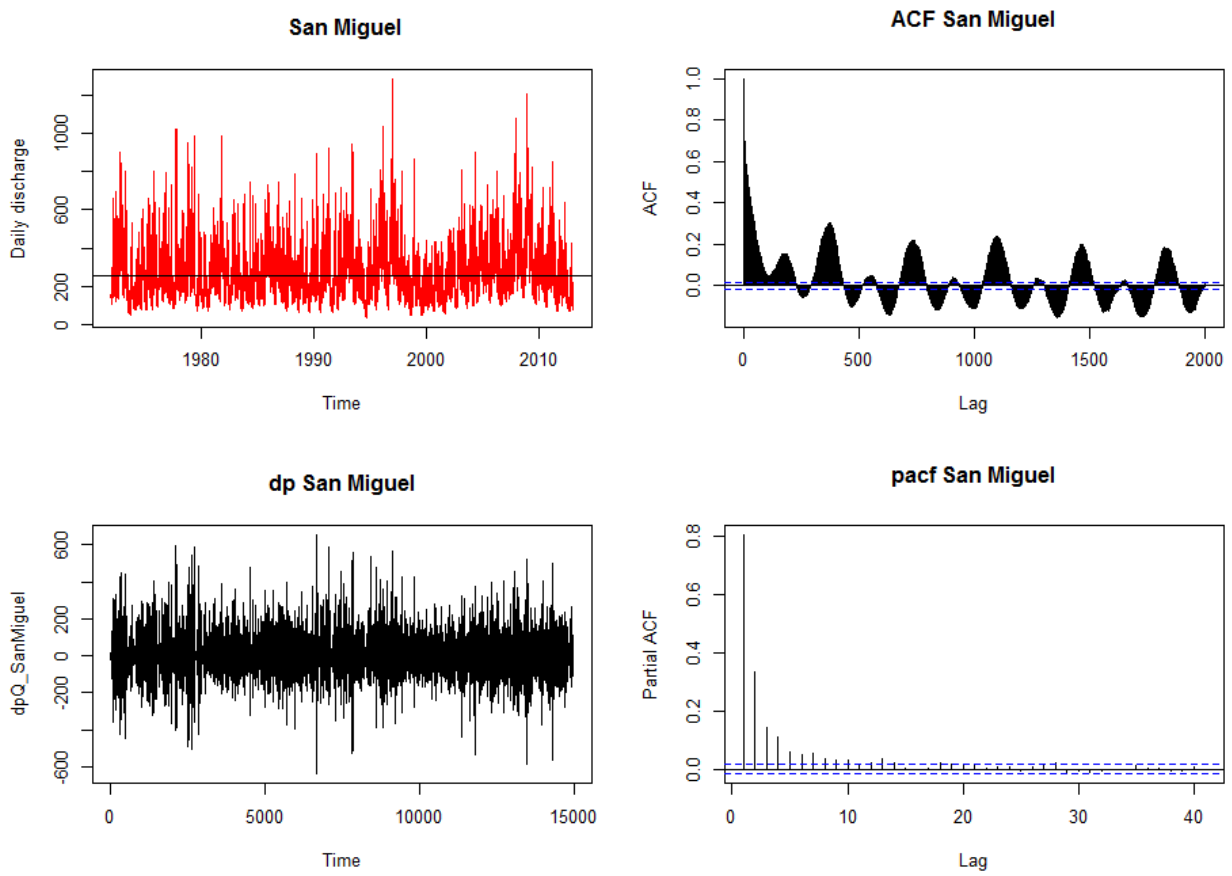

Precipitation

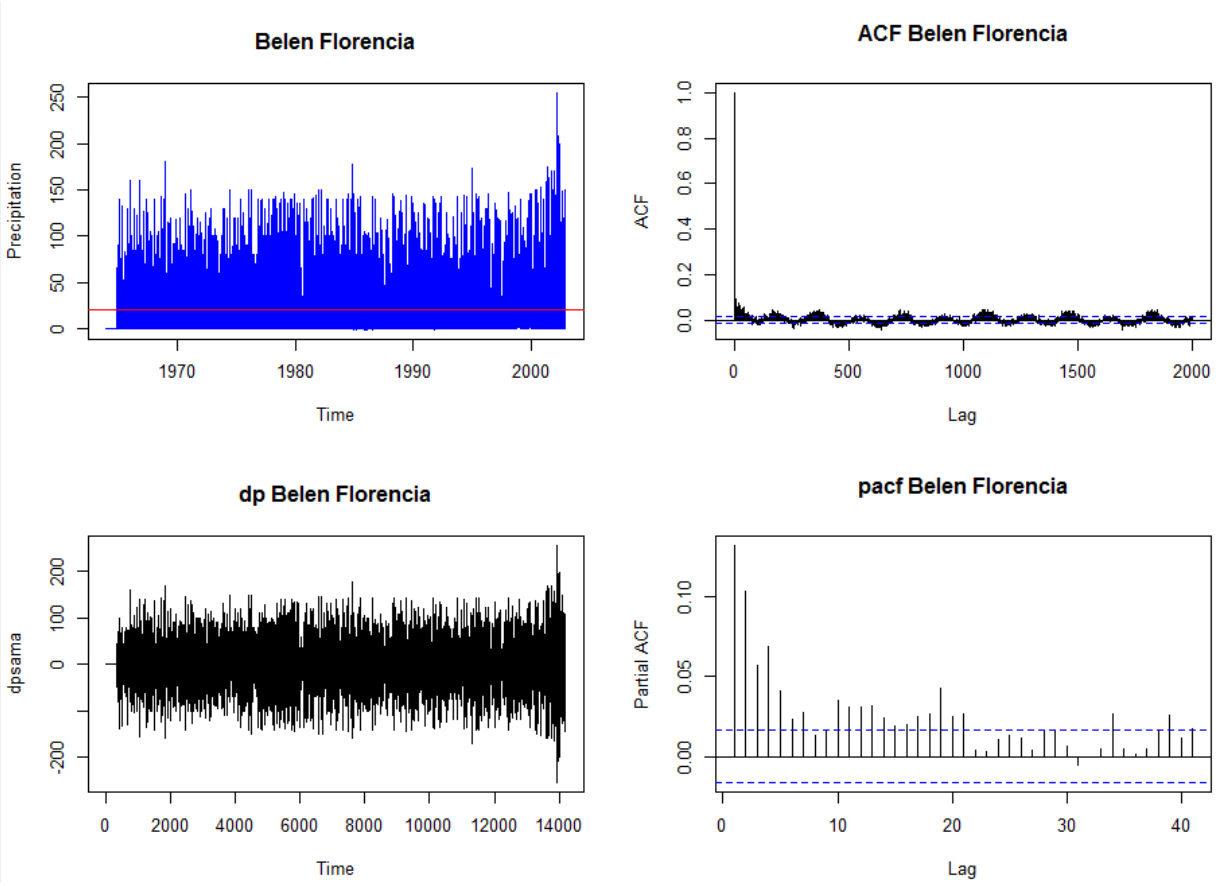
Belen Florencia
Precipitation
0
50
100
150
200
250
1970
1980
1990
2000
Time
ACF Belen Florencia
ACF
0.0
0.2
0.4
0.6
0.8
1.0
0
500
1000
1500
2000
Lag
dp Belen Florencia
dpsama
-200
0
100
200
0
2000
4000
6000
8000
10000
12000
14000
Time
pacf Belen Florencia
Partial ACF
0.00
0.05
0.10
0
10
20
30
40
Lag

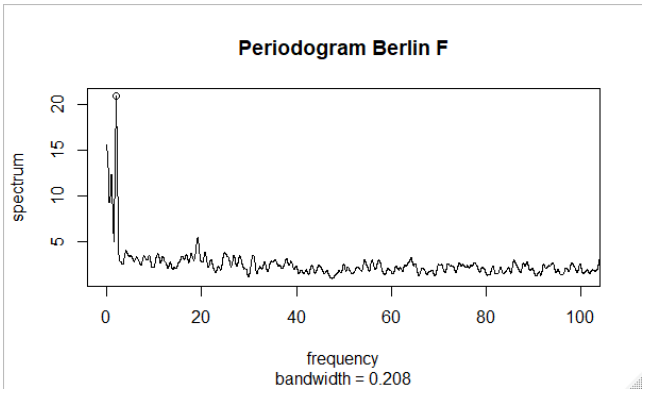
Periodogram Berlin F
spectrum
5
10
15
20
0
20
40
60
80
100
frequency
bandwidth = 0.208

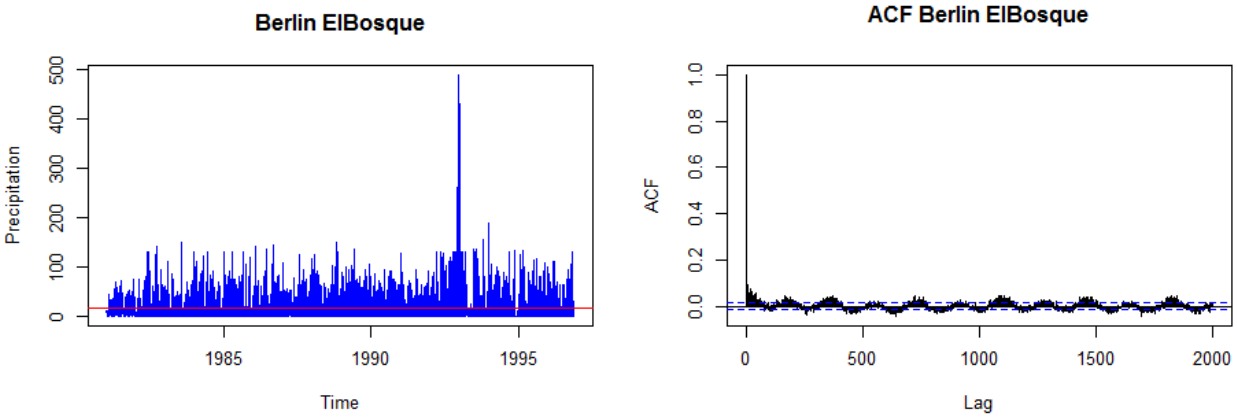
Berlin ElBosque
Precipitation
0
100
200
300
400
500
1985
1990
1995
Time

ACF Berlin ElBosque
ACF
0.0
0.2
0.4
0.6
0.8
1.0
0
500
1000
1500
2000
Lag

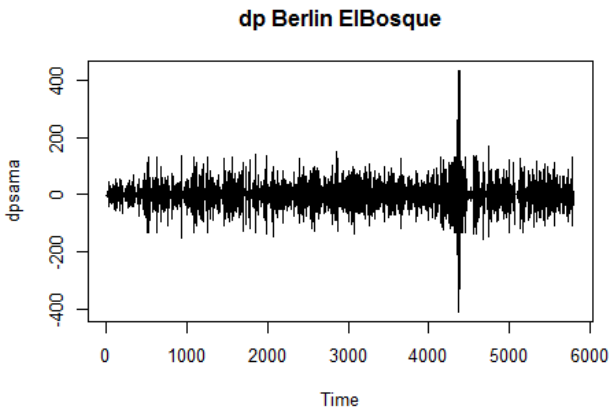
dp Berlin ElBosque
dpsama
-400
-200
0
200
400
0
1000
2000
3000
4000
5000
6000
Time

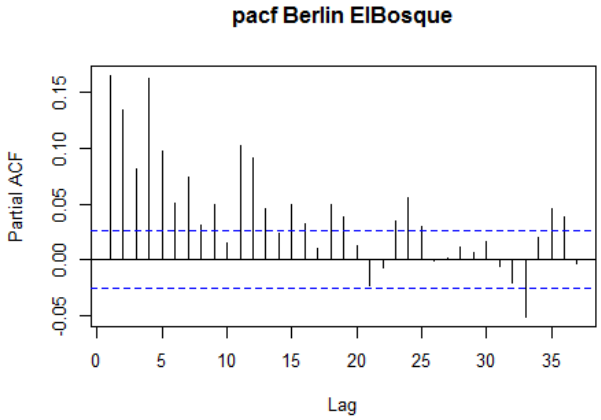
pacf Berlin ElBosque
Partial ACF
-0.05
0.00
0.05
0.10
0.15
0
5
10
15
20
25
30
35
Lag

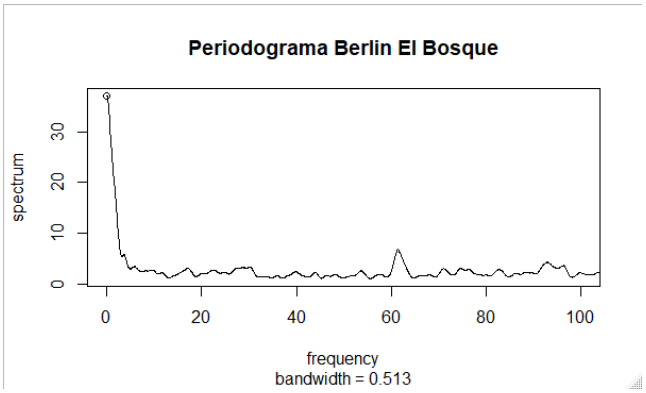
Periodograma Berlin El Bosque
spectrum
0
10
20
30
0
20
40
60
80
100
frequency
bandwidth = 0.513

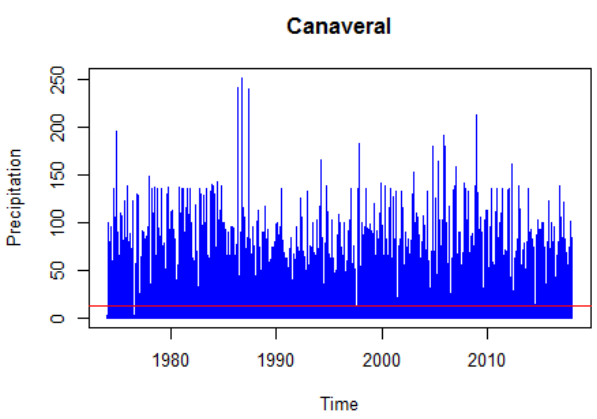
Canaveral
Precipitation
0
50
100
150
200
250
1980
1990
2000
2010
Time

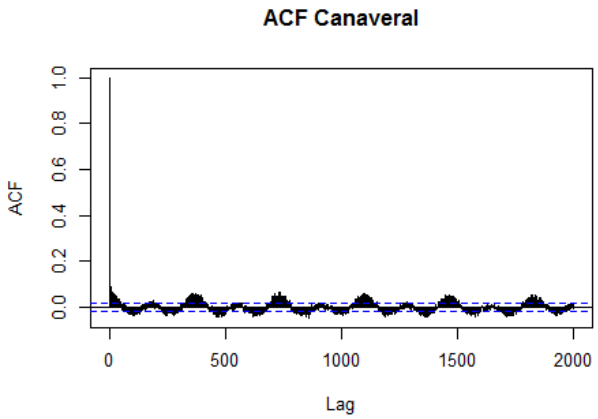
ACF Canaveral
ACF
0.0
0.2
0.4
0.6
0.8
1.0
0
500
1000
1500
2000
Lag

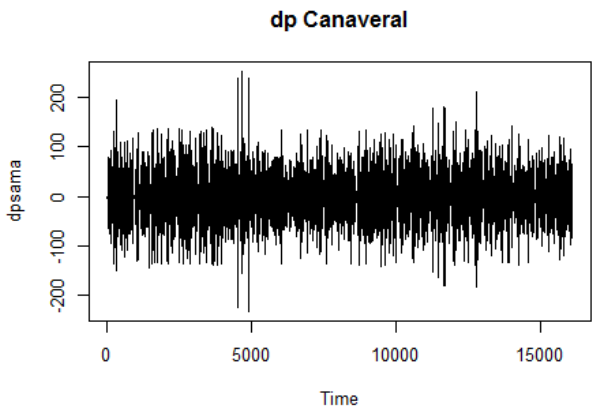
dp Canaveral
dpsama
-200
-100
0
100
200
0
5000
10000
15000
Time

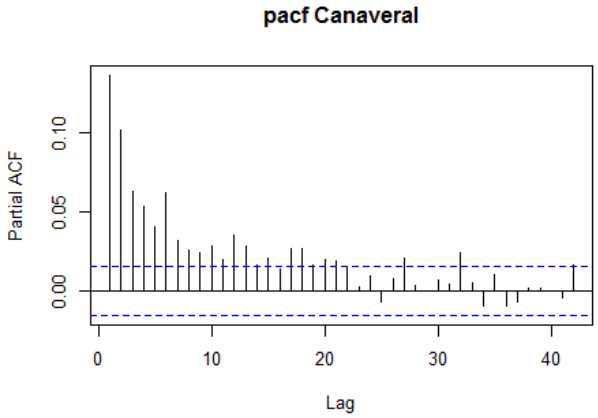
pacf Canaveral
Partial ACF
0.00
0.05
0.10
0
10
20
30
40
Lag

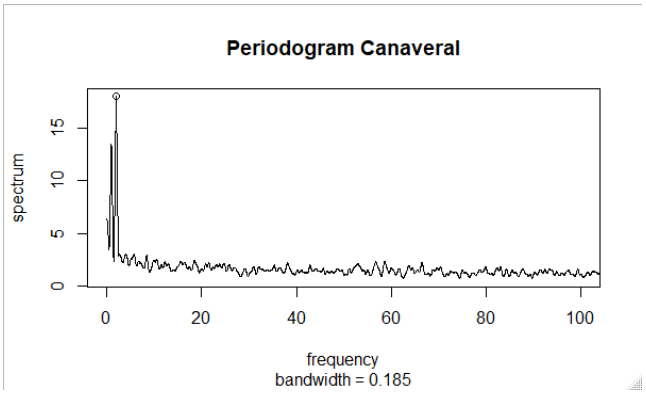
Periodogram Canaveral
spectrum
0
5
10
15
0
20
40
60
80
100
frequency
bandwidth = 0.185

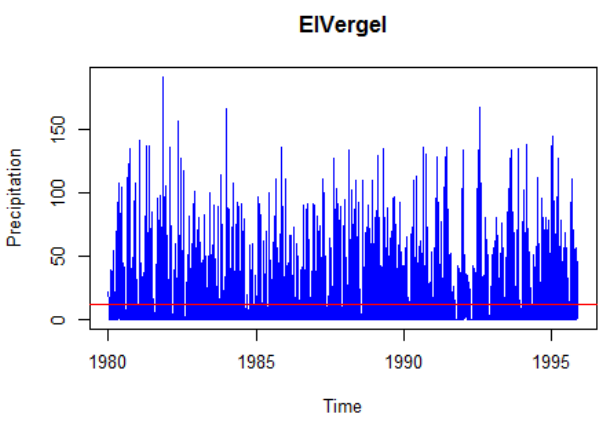
ElVergel
Precipitation
0
50
100
150
1980
1985
1990
1995
Time

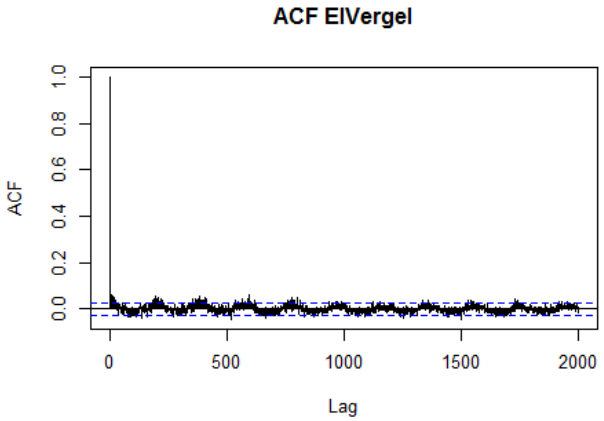
ACF ElVergel
ACF
0.0
0.2
0.4
0.6
0.8
1.0
0
500
1000
1500
2000
Lag

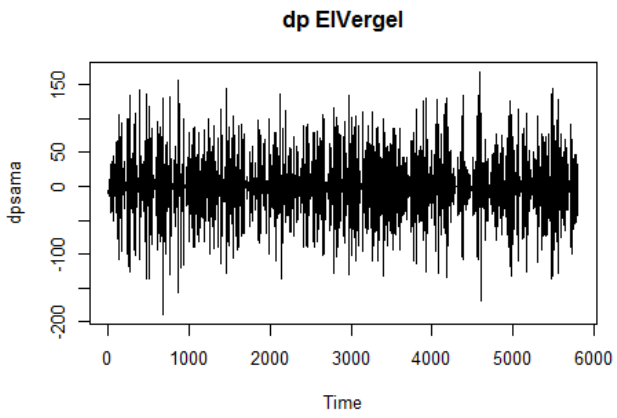
dp ElVergel
dpsama
-200
-100
0
50
150
0
1000
2000
3000
4000
5000
6000
Time

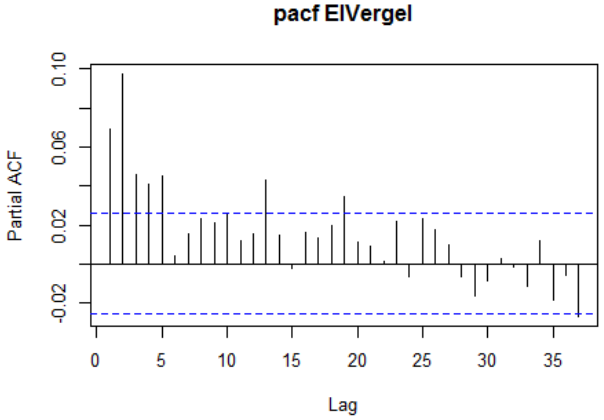
pacf ElVergel
Partial ACF
-0.02
0.02
0.06
0.10
0
5
10
15
20
25
30
35
Lag

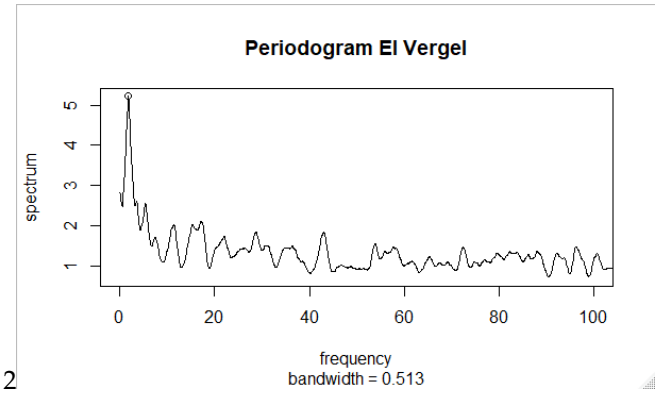
Periodogram El Vergel
spectrum
1
2
3
4
5
0
20
40
60
80
100
frequency
bandwidth = 0.513

2

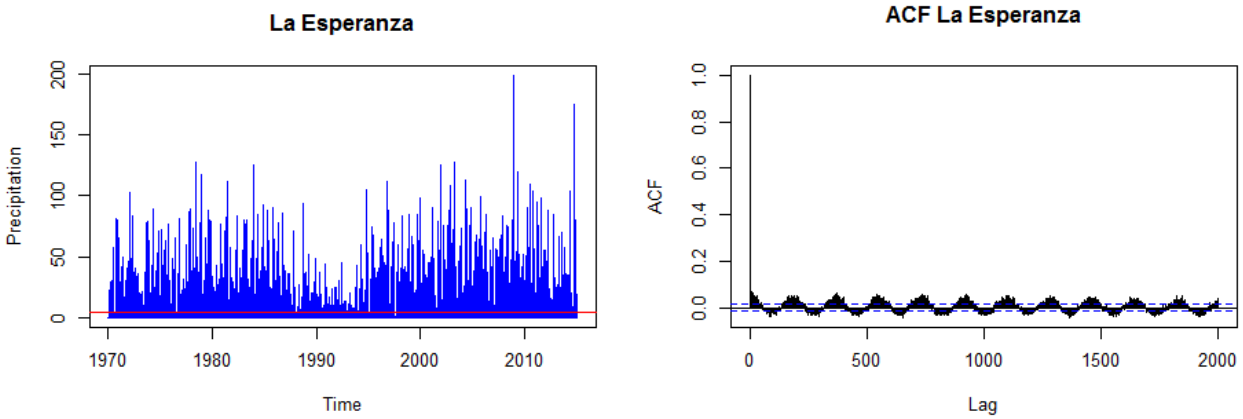
La Esperanza
Precipitation
0
50
100
150
200
1970
1980
1990
2000
2010
Time

ACF La Esperanza
ACF
0.0
0.2
0.4
0.6
0.8
1.0
0
500
1000
1500
2000
Lag

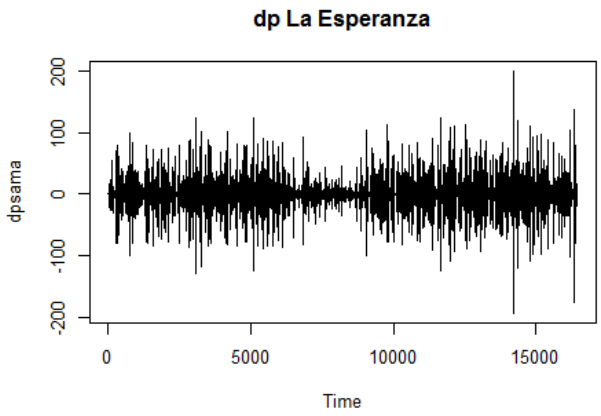
dp La Esperanza
dpsama
-200
-100
0
100
200
0
5000
10000
15000
Time

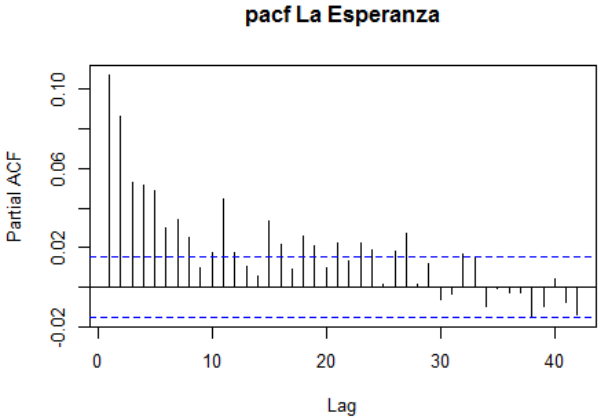
pacf La Esperanza
Partial ACF
-0.02
0.02
0.06
0.10
0
10
20
30
40
Lag

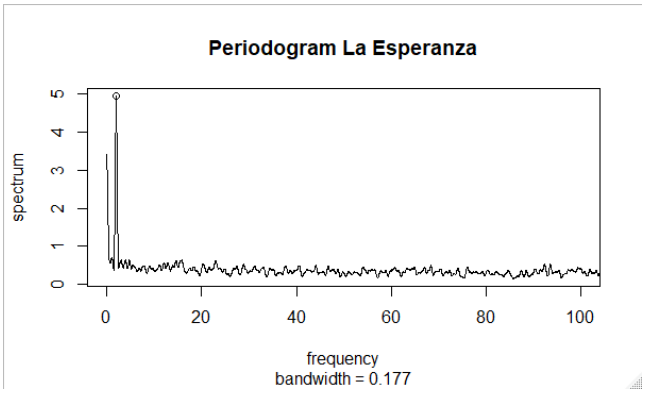
Periodogram La Esperanza
spectrum
0
1
2
3
4
5
0
20
40
60
80
100
frequency
bandwidth = 0.177

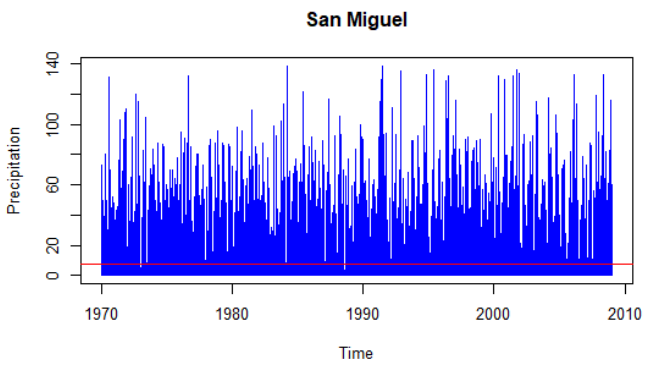
San Miguel
Precipitation
0
20
60
100
140
1970
1980
1990
2000
2010
Time

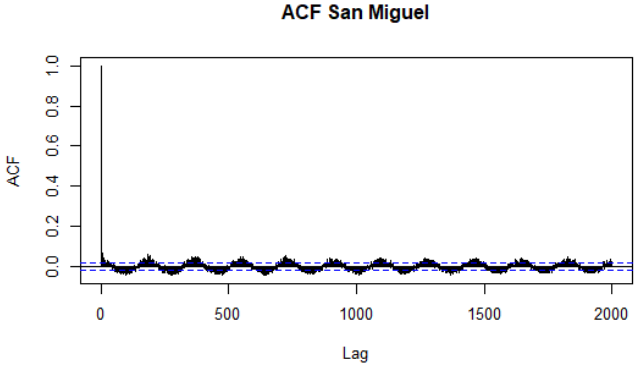
ACF San Miguel
ACF
0.0
0.2
0.4
0.6
0.8
1.0
0
500
1000
1500
2000
Lag

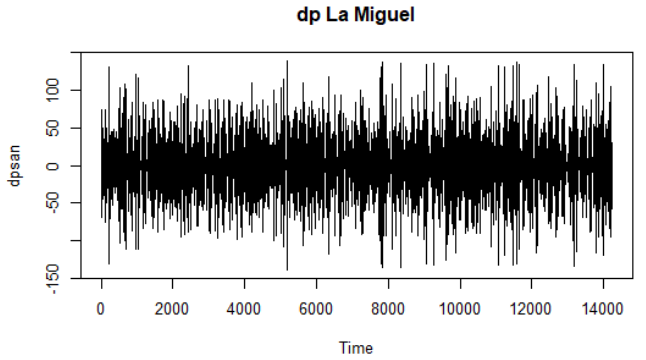
dp La Miguel
dpsan
-150
-50
0
50
100
0
2000
4000
6000
8000
10000
12000
14000
Time

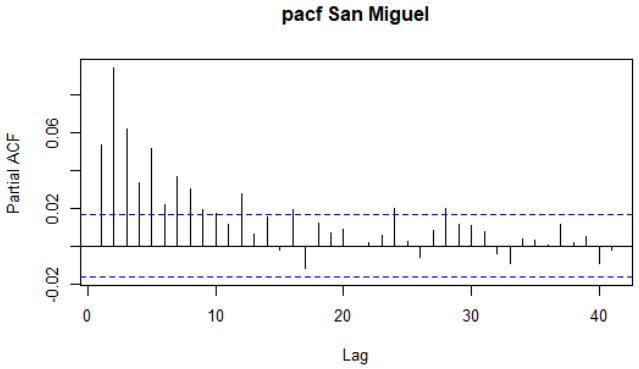
pacf San Miguel
Partial ACF
-0.02
0.02
0.06
0
10
20
30
40
Lag

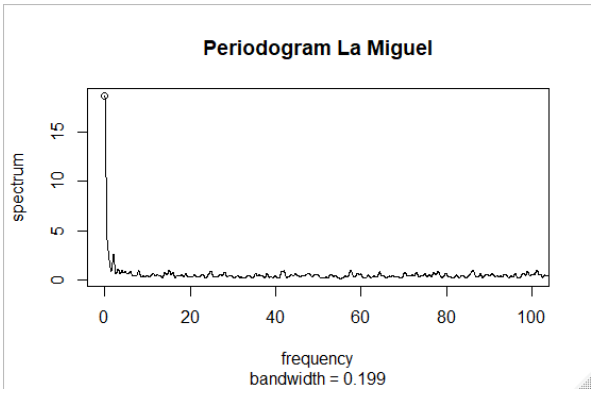
Periodogram La Miguel
spectrum
0
5
10
15
0
20
40
60
80
100
frequency
bandwidth = 0.199

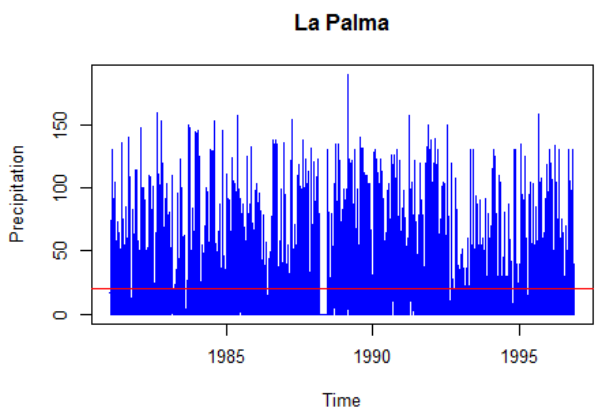
La Palma
Precipitation
0
50
100
150
1985
1990
1995
Time

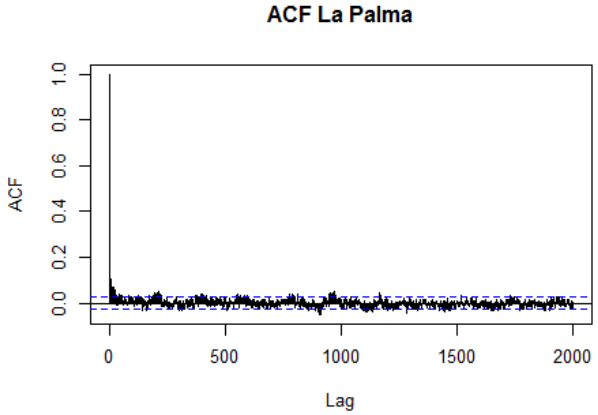
ACF La Palma
ACF
0.0
0.2
0.4
0.6
0.8
1.0
0
500
1000
1500
2000
Lag

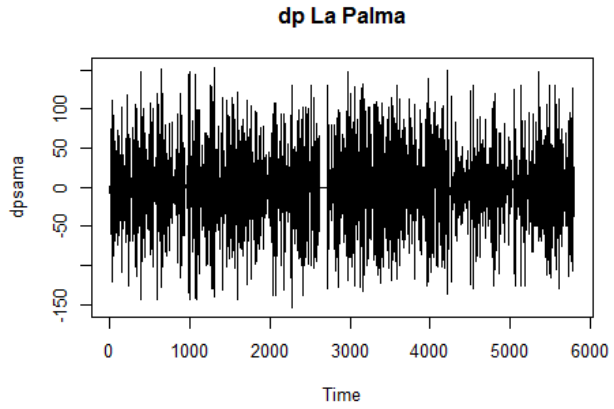
dp La Palma
dpsama
-150
-50
0
50
100
0
1000
2000
3000
4000
5000
6000
Time

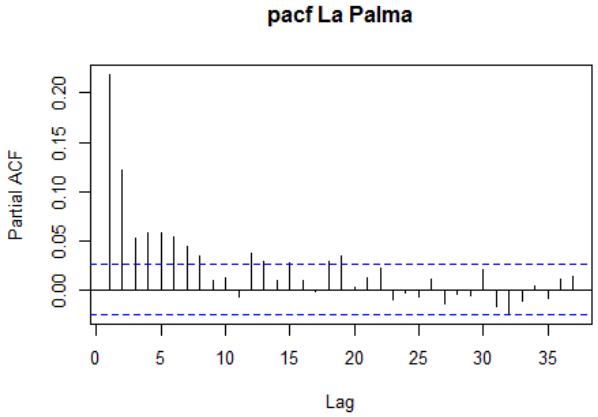
pacf La Palma
Partial ACF
0.00
0.05
0.10
0.15
0.20
0
5
10
15
20
25
30
35
Lag

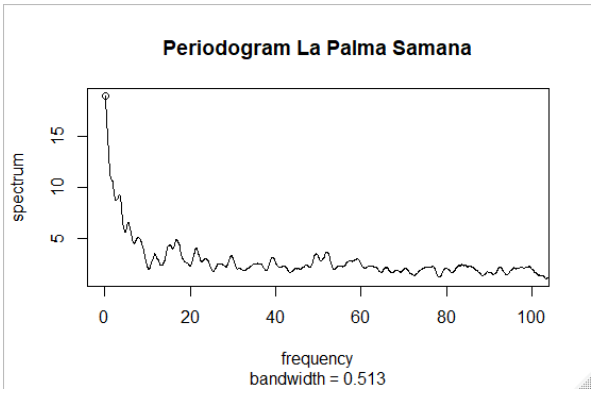
Periodogram La Palma Samana
spectrum
5
10
15
0
20
40
60
80
100
frequency
bandwidth = 0.513

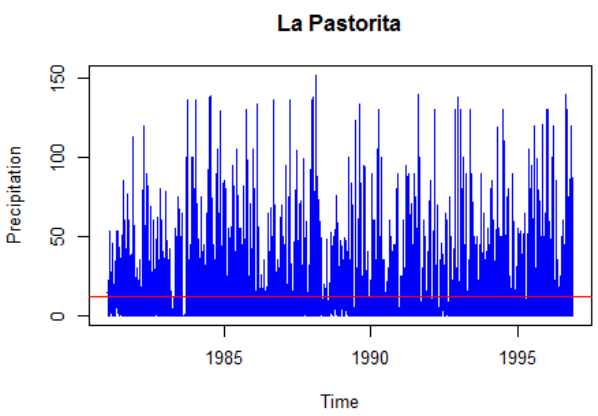
La Pastorita
Precipitation
0
50
100
150
1985
1990
1995
Time

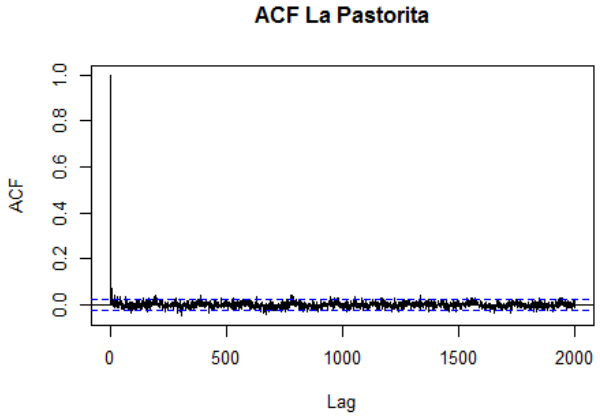
ACF La Pastorita
ACF
0.0
0.2
0.4
0.6
0.8
1.0
0
500
1000
1500
2000
Lag

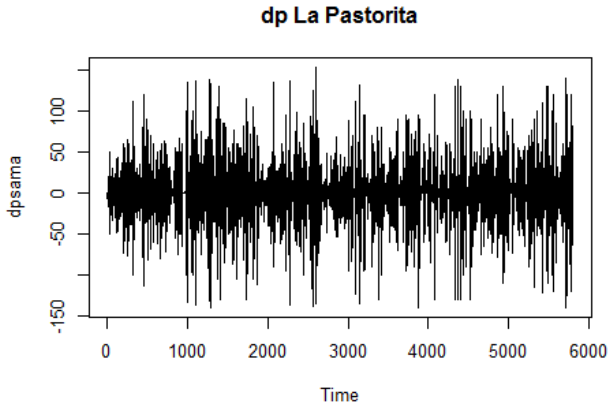
dp La Pastorita
dpsama
-150
-50
0
50
100
0
1000
2000
3000
4000
5000
6000
Time

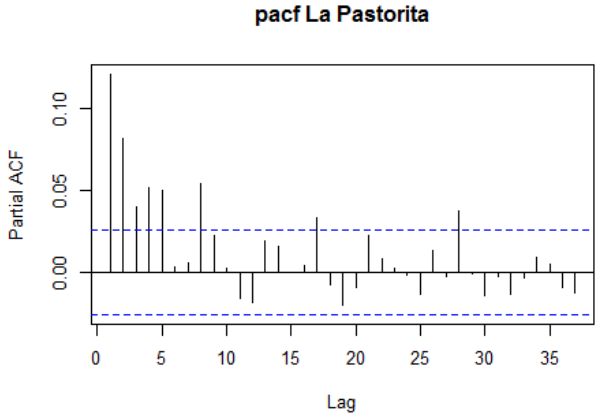
pacf La Pastorita
Partial ACF
0.00
0.05
0.10
0
5
10
15
20
25
30
35
Lag

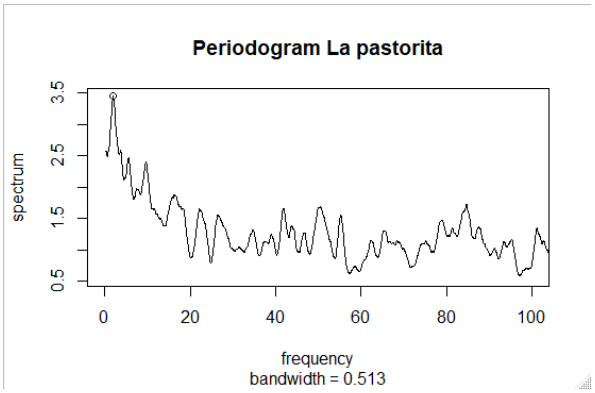
Periodogram La pastorita
spectrum
0.5
1.5
2.5
3.5
0
20
40
60
80
100
frequency
bandwidth = 0.513

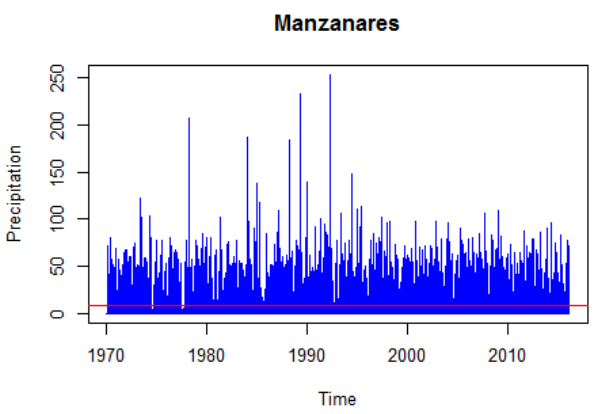
Manzanares
Precipitation
0
50
100
150
200
250
1970
1980
1990
2000
2010
Time

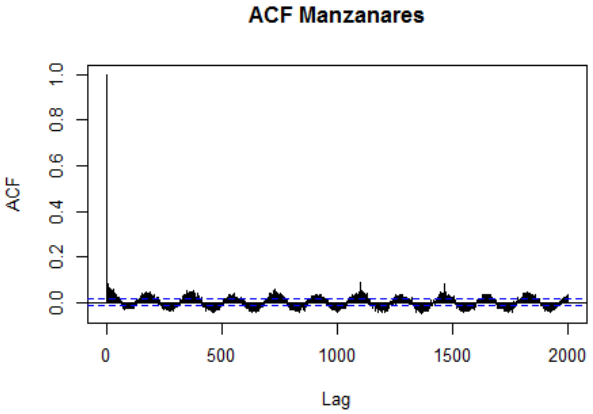
ACF Manzanares
ACF
0.0
0.2
0.4
0.6
0.8
1.0
0
500
1000
1500
2000
Lag

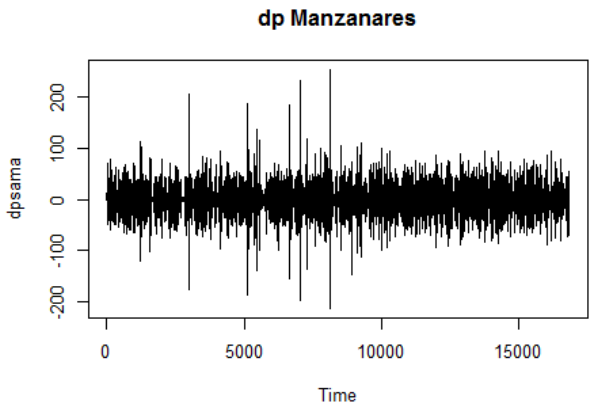
dp Manzanares
dpsama
-200
-100
0
100
200
0
5000
10000
15000
Time

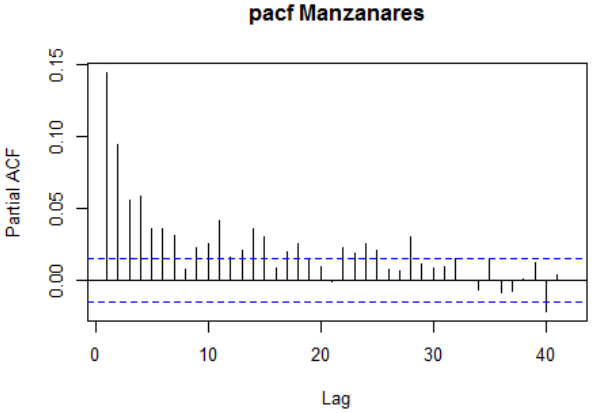
pacf Manzanares
Partial ACF
0.00
0.05
0.10
0.15
0
10
20
30
40
Lag

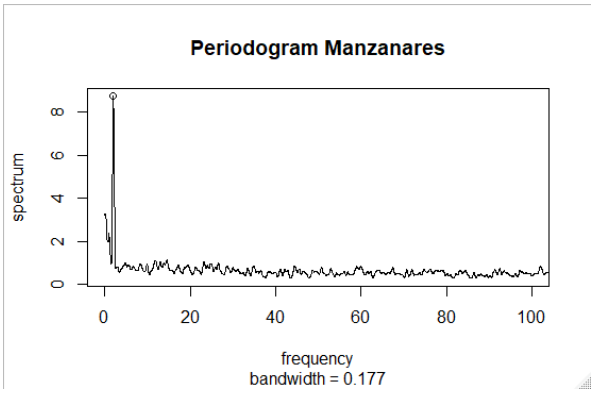
Periodogram Manzanares
spectrum
0
2
4
6
8
0
20
40
60
80
100
frequency
bandwidth = 0.177

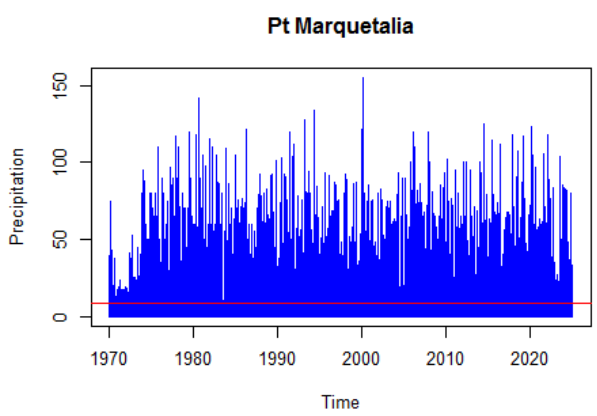
Pt Marquetalia
Precipitation
0
50
100
150
1970
1980
1990
2000
2010
2020
Time

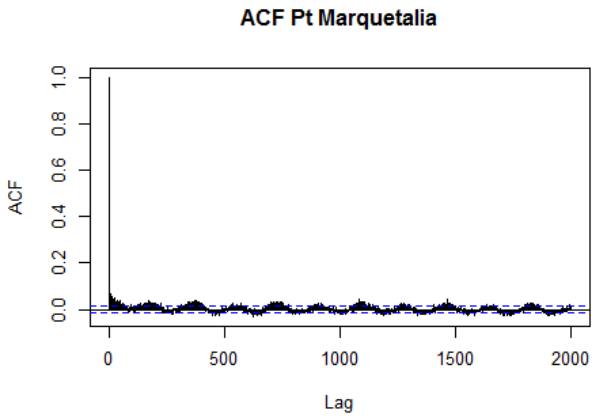
ACF Pt Marquetalia
ACF
0.0
0.2
0.4
0.6
0.8
1.0
0
500
1000
1500
2000
Lag

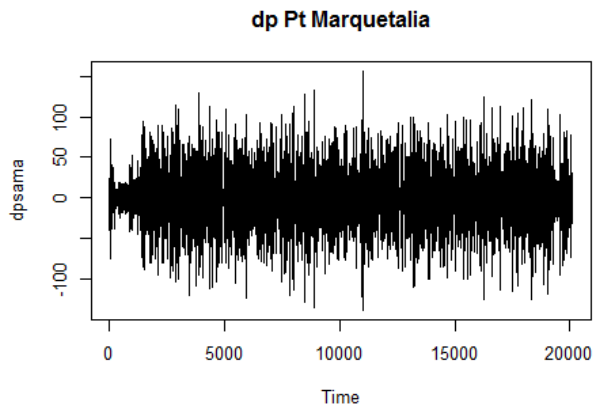
dp Pt Marquetalia
dpsama
-100
0
50
100
0
5000
10000
15000
20000
Time

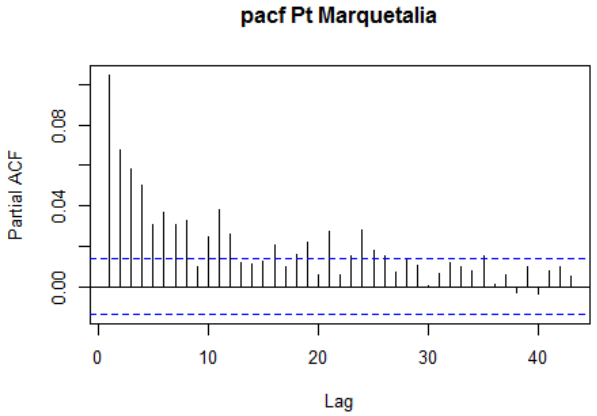
pacf Pt Marquetalia
Partial ACF
0.00
0.04
0.08
0
10
20
30
40
Lag

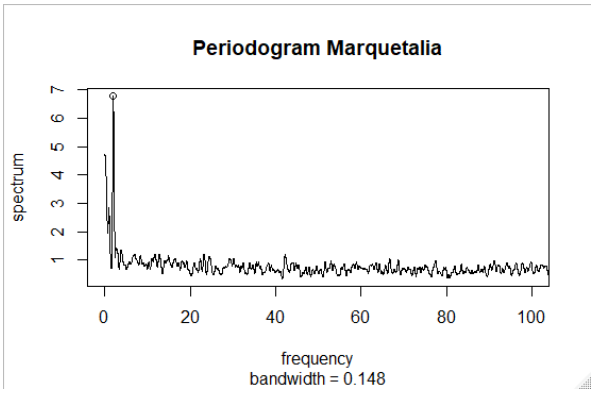
Periodogram Marquetalia
spectrum
1
2
3
4
5
6
7
0
20
40
60
80
100
frequency
bandwidth = 0.148

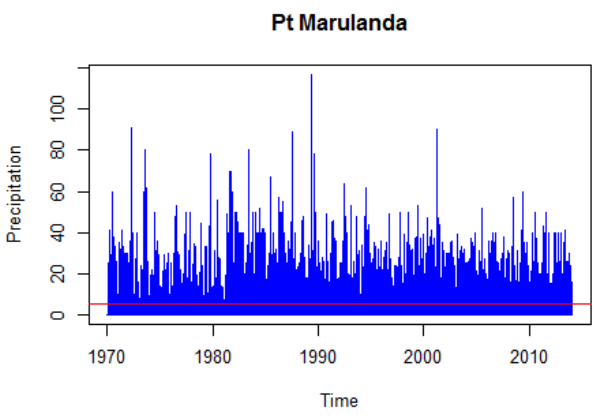
Pt Marulanda
Precipitation
0
20
40
60
80
100
1970
1980
1990
2000
2010
Time

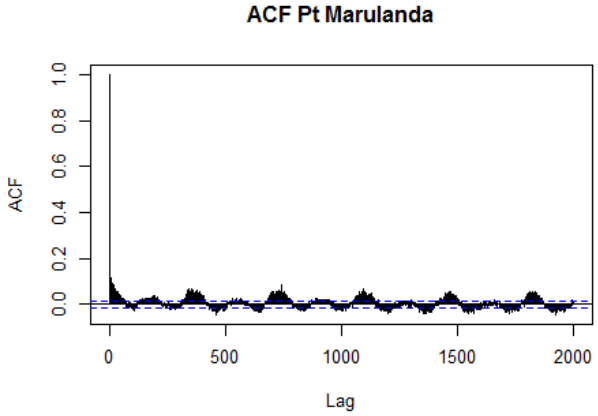
ACF Pt Marulanda
ACF
0.0
0.2
0.4
0.6
0.8
1.0
0
500
1000
1500
2000
Lag

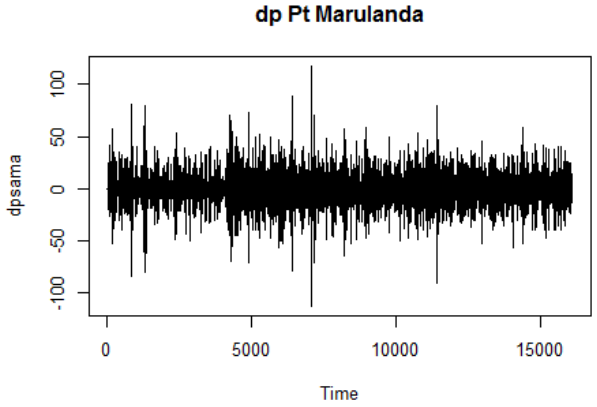
dp Pt Marulanda
dpsama
-100
-50
0
50
100
0
5000
10000
15000
Time

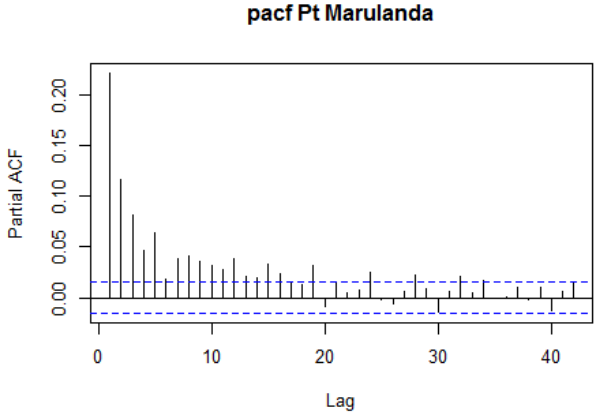
pacf Pt Marulanda
Partial ACF
0.00
0.05
0.10
0.15
0.20
0
10
20
30
40
Lag

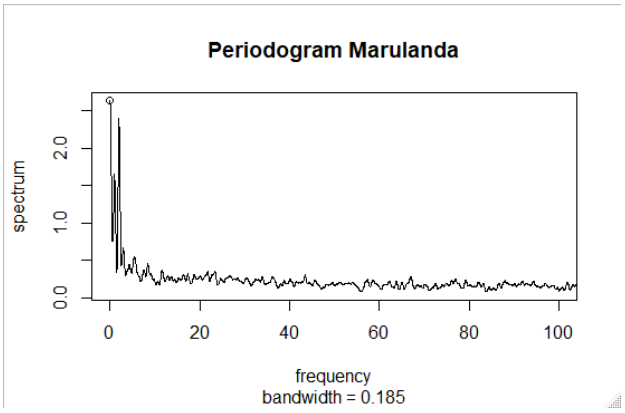
Periodogram Marulanda
spectrum
0.0
1.0
2.0
0
20
40
60
80
100
frequency
bandwidth = 0.185

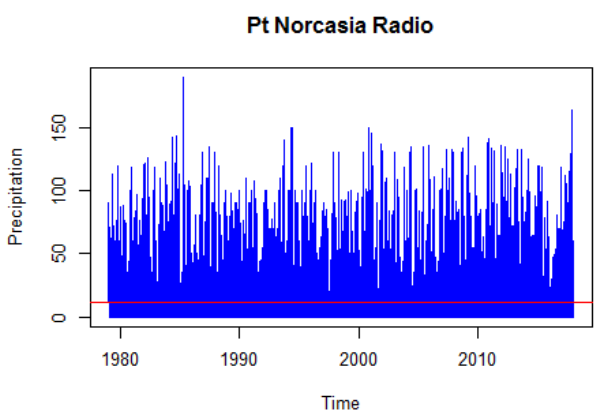
Pt Norcasia Radio
Precipitation
0
50
100
150
1980
1990
2000
2010
Time

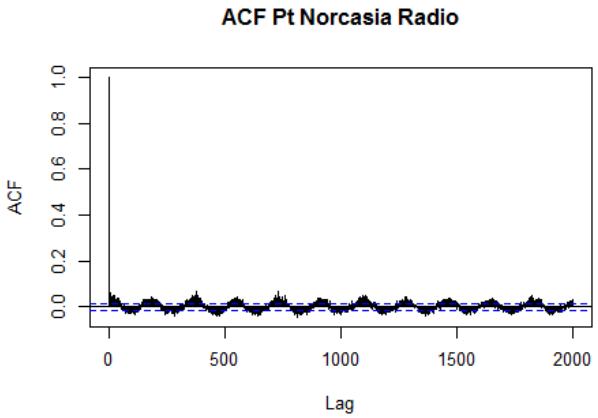
ACF Pt Norcasia Radio
ACF
0.0
0.2
0.4
0.6
0.8
1.0
0
500
1000
1500
2000
Lag

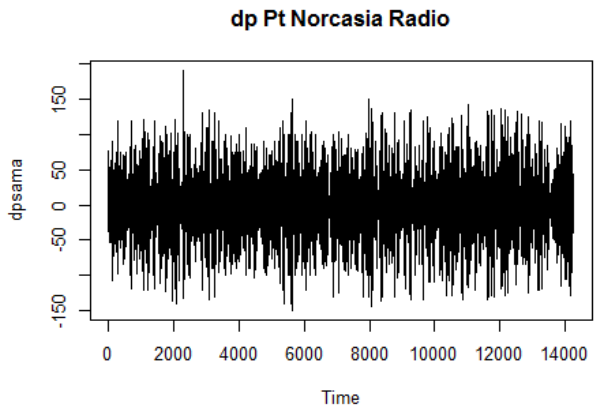
dp Pt Norcasia Radio
dpsama
-150
-50
0
50
150
0
2000
4000
6000
8000
10000
12000
14000
Time

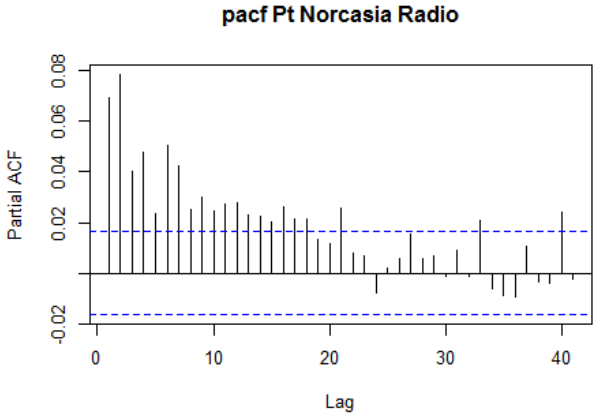
pacf Pt Norcasia Radio
Partial ACF
-0.02
0.02
0.04
0.06
0.08
0
10
20
30
40
Lag

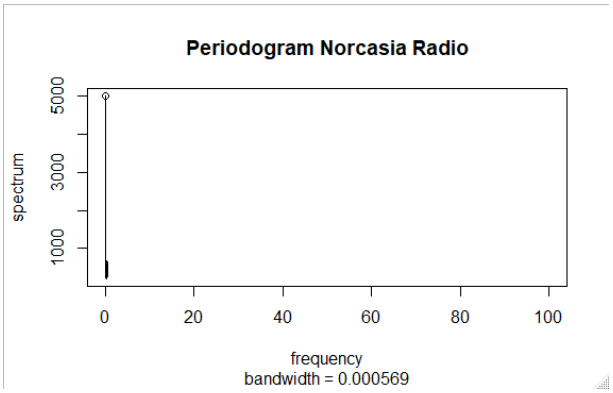
Periodogram Norcasia Radio
spectrum
1000
3000
5000
0
20
40
60
80
100
frequency
bandwidth = 0.000569

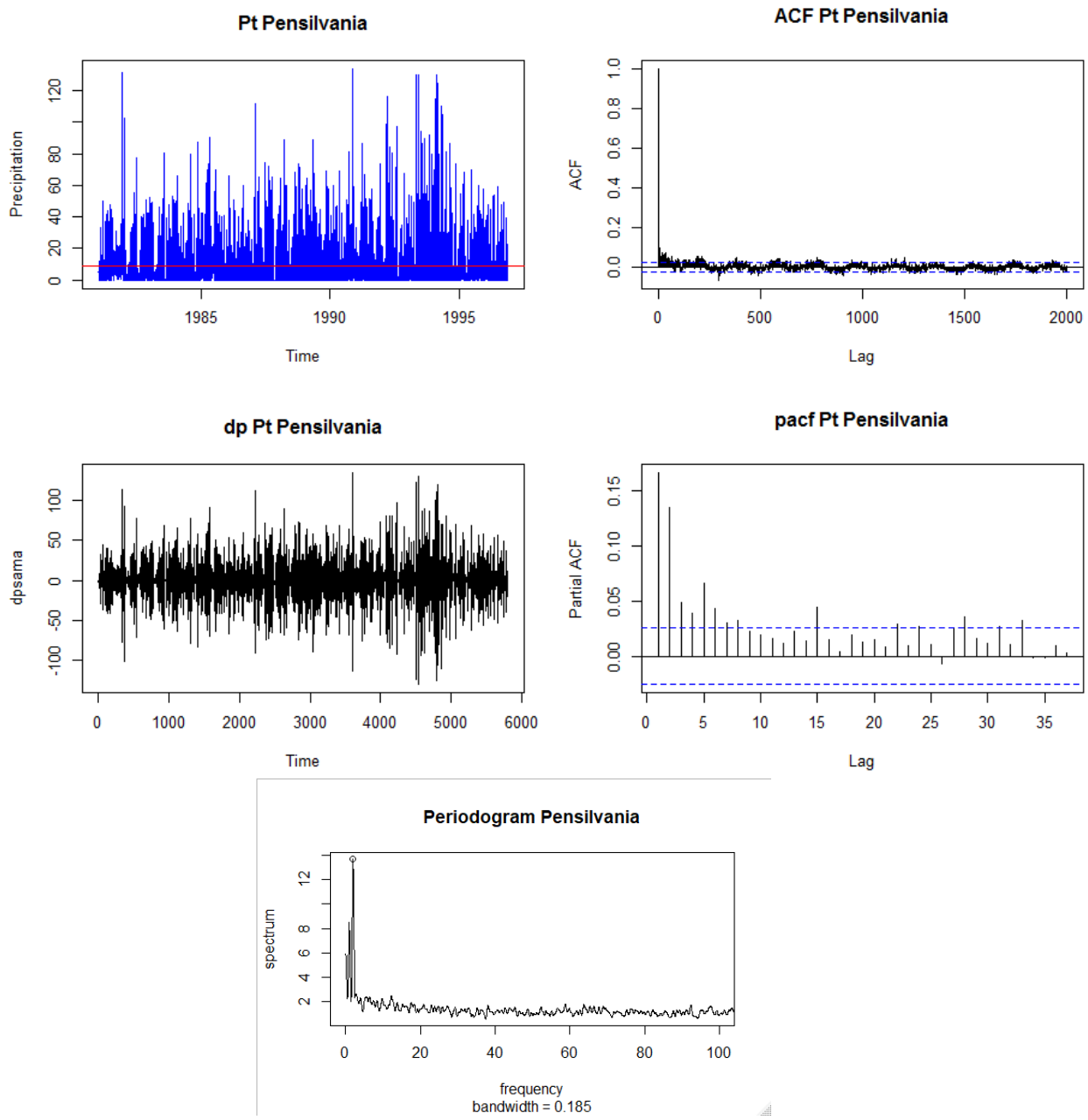
Pt Pensilvania
Precipitation
0
20
40
60
80
120
1985
1990
1995
Time
ACF Pt Pensilvania
ACF
0.0
0.2
0.4
0.6
0.8
1.0
0
500
1000
1500
2000
Lag
dp Pt Pensilvania
dpsama
-100
-50
0
50
100
0
1000
2000
3000
4000
5000
6000
Time
pacf Pt Pensilvania
Partial ACF
0.00
0.05
0.10
0.15
0
5
10
15
20
25
30
35
Lag
Periodogram Pensilvania
spectrum
2
4
6
8
12
0
20
40
60
80
100
frequency
bandwidth = 0.185

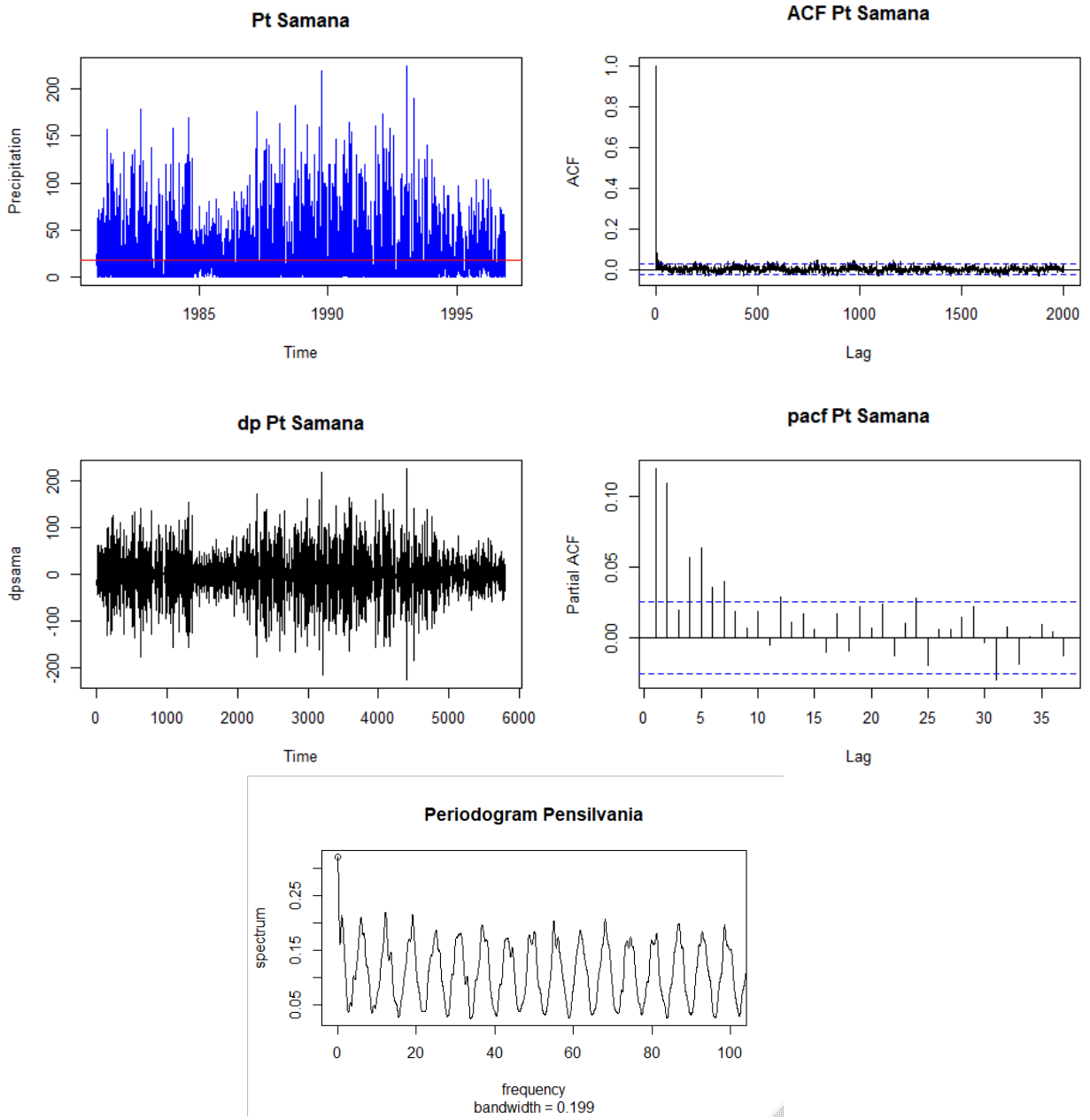
Pt Samana
Precipitation
0
50
100
150
200
1985
1990
1995
Time
ACF Pt Samana
ACF
0.0
0.2
0.4
0.6
0.8
1.0
0
500
1000
1500
2000
Lag
dp Pt Samana
dpsama
-200
-100
0
100
200
0
1000
2000
3000
4000
5000
6000
Time
pacf Pt Samana
Partial ACF
0.00
0.05
0.10
0
5
10
15
20
25
30
35
Lag
Periodogram Pensilvania
spectrum
0.05
0.15
0.25
0
20
40
60
80
100
frequency
bandwidth = 0.199

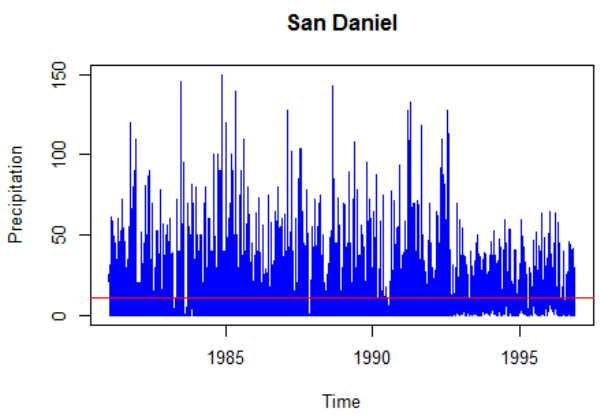
San Daniel
Precipitation
0
50
100
150
1985
1990
1995
Time

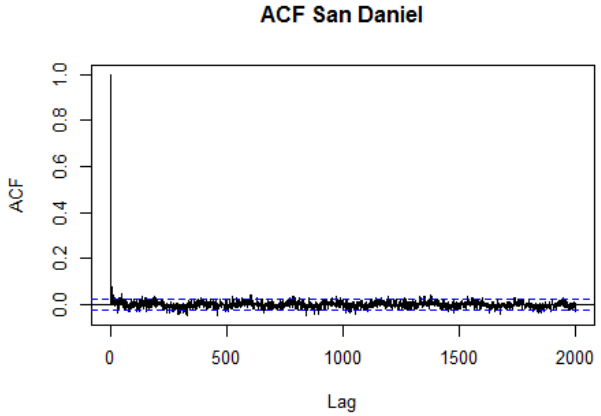
ACF San Daniel
ACF
0.0
0.2
0.4
0.6
0.8
1.0
0
500
1000
1500
2000
Lag

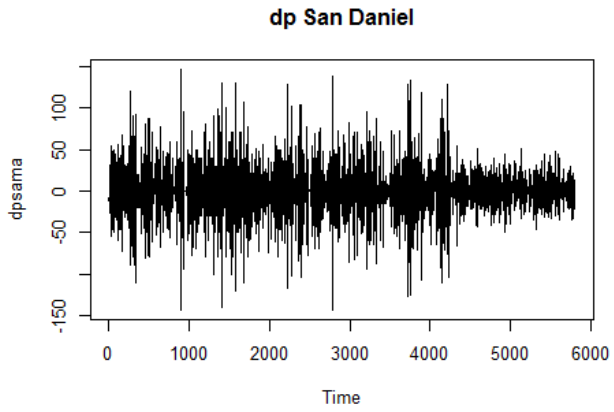
dp San Daniel
dpsama
-150
-50
0
50
100
0
1000
2000
3000
4000
5000
6000
Time

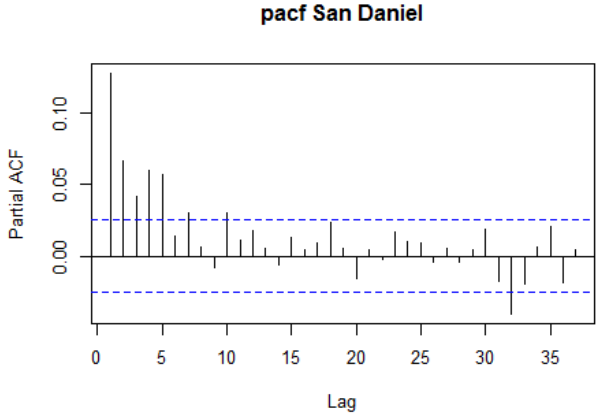
pacf San Daniel
Partial ACF
0.00
0.05
0.10
0
5
10
15
20
25
30
35
Lag

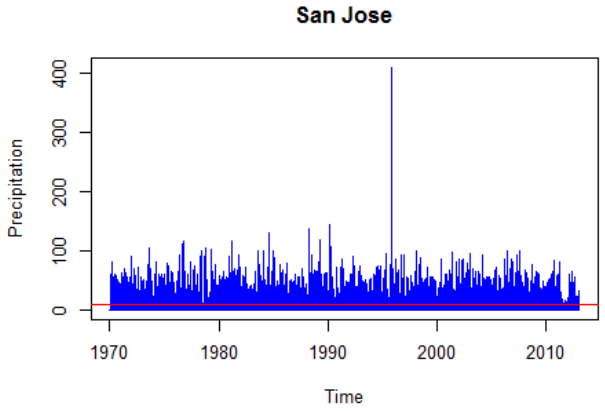
San Jose
Precipitation
0
100
200
300
400
1970
1980
1990
2000
2010
Time

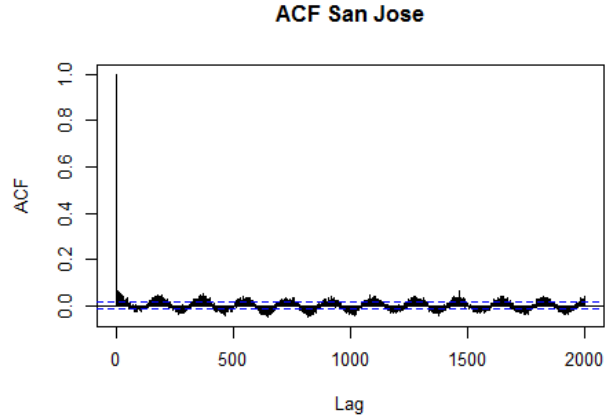
ACF San Jose
ACF
0.0
0.2
0.4
0.6
0.8
1.0
0
500
1000
1500
2000
Lag

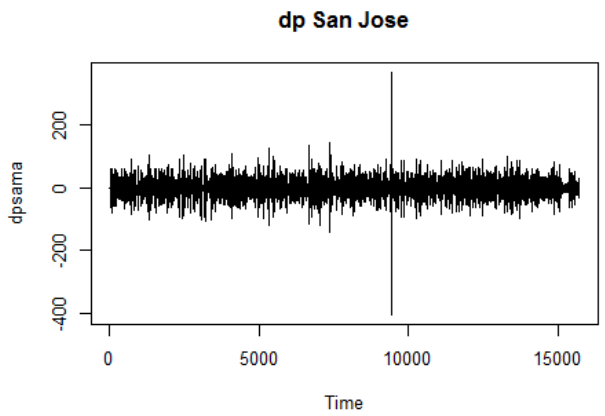
dp San Jose
dpsama
-400
-200
0
200
0
5000
10000
15000
Time

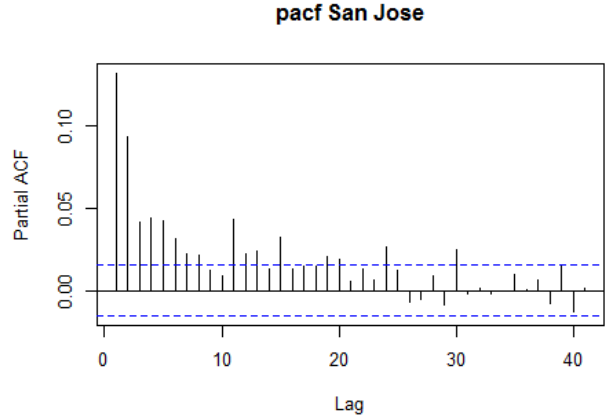
pacf San Jose
Partial ACF
0.00
0.05
0.10
0
10
20
30
40
Lag

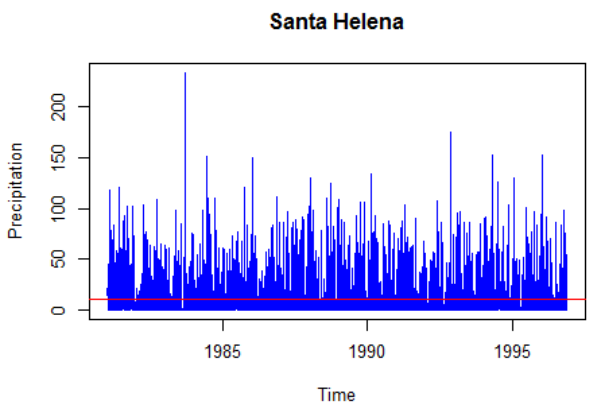
Santa Helena
Precipitation
0
50
100
150
200
1985
1990
1995
Time

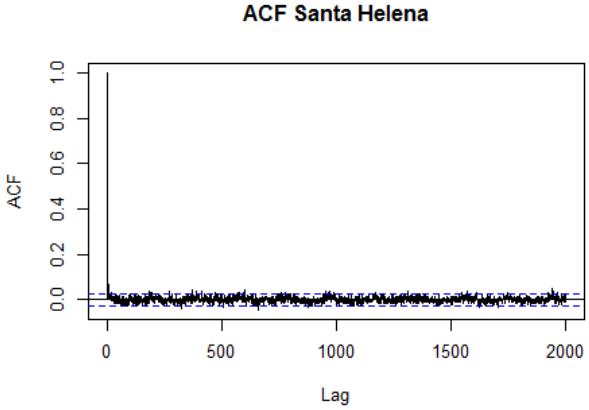
ACF Santa Helena
ACF
0.0
0.2
0.4
0.6
0.8
1.0
0
500
1000
1500
2000
Lag

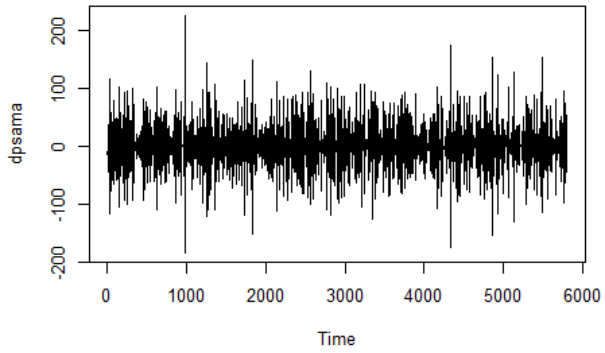
dp Santa Helena
dpsama
-200
-100
0
100
200
0
1000
2000
3000
4000
5000
6000
Time

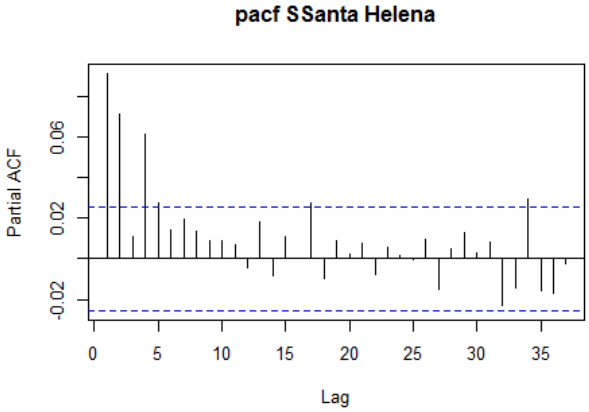
pacf SSanta Helena
Partial ACF
-0.02
0.02
0.06
0
5
10
15
20
25
30
35
Lag

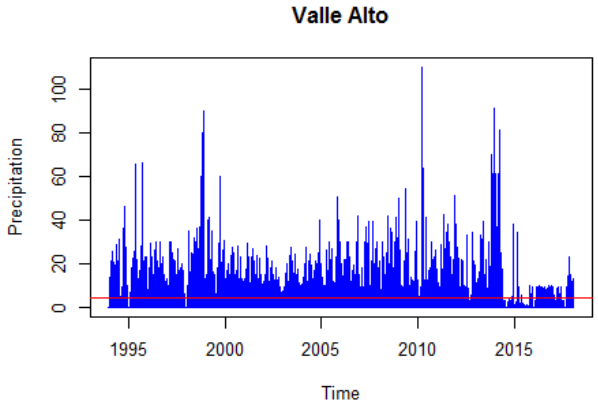
Valle Alto
Precipitation
0
20
40
60
80
100
1995
2000
2005
2010
2015
Time

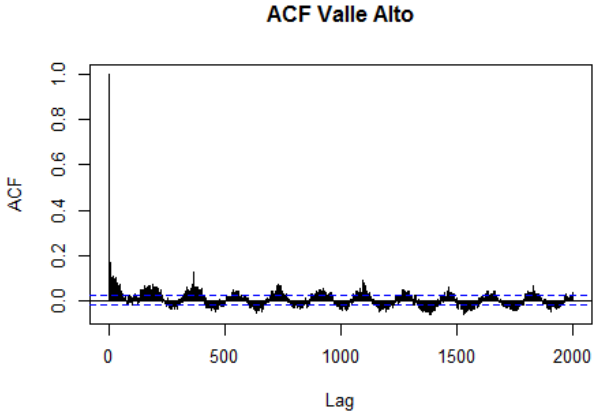
ACF Valle Alto
ACF
0.0
0.2
0.4
0.6
0.8
1.0
0
500
1000
1500
2000
Lag

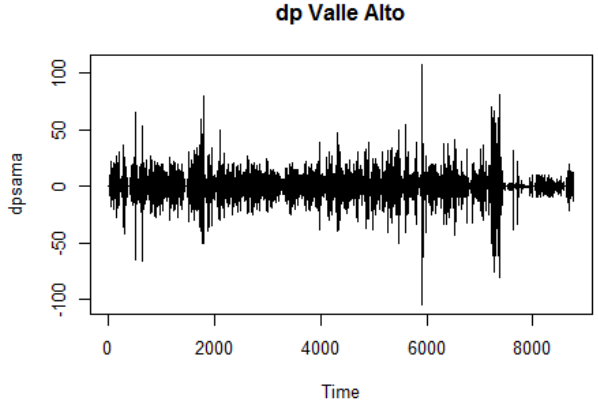
dp Valle Alto
dpsama
-100
-50
0
50
100
0
2000
4000
6000
8000
Time

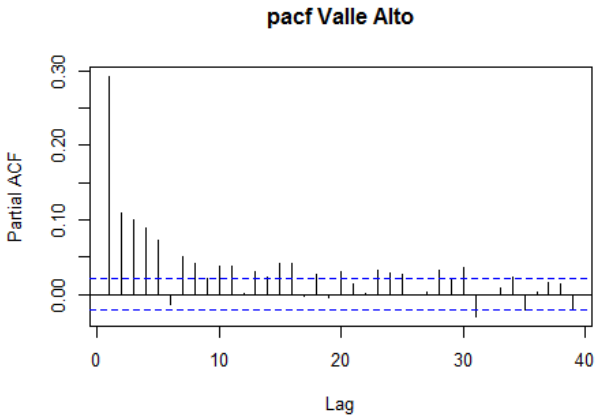
pacf Valle Alto
Partial ACF
0.00
0.10
0.20
0.30
0
10
20
30
40
Lag

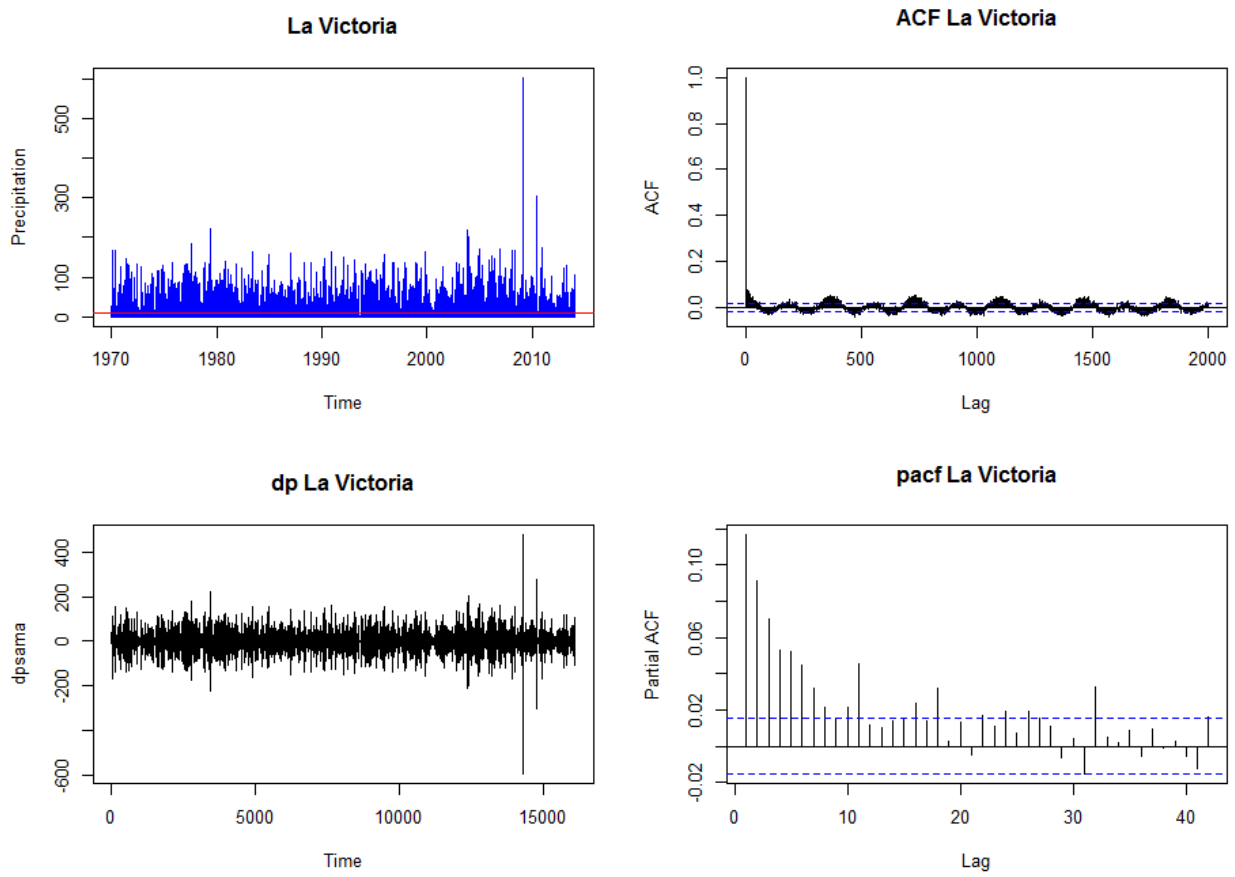
La Victoria
Precipitation
0
100
300
500
1970
1980
1990
2000
2010
Time
ACF La Victoria
ACF
0.0
0.2
0.4
0.6
0.8
1.0
0
500
1000
1500
2000
Lag
dp La Victoria
dpsama
-600
-200
0
200
400
0
5000
10000
15000
Time
pacf La Victoria
Partial ACF
-0.02
0.02
0.06
0.10
0
10
20
30
40
Lag

SST

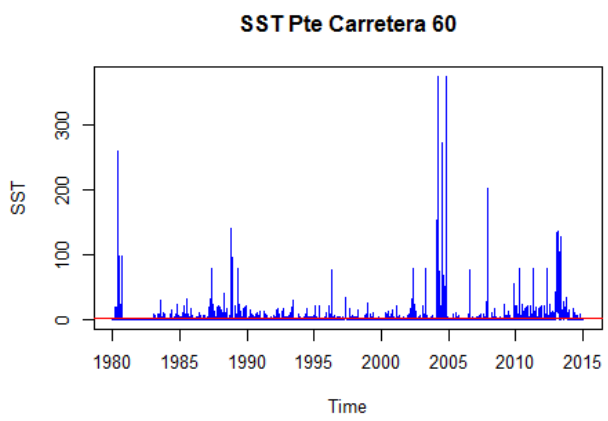
SST Pte Carretera 60
SST
0
100
200
300
1980
1985
1990
1995
2000
2005
2010
2015
Time

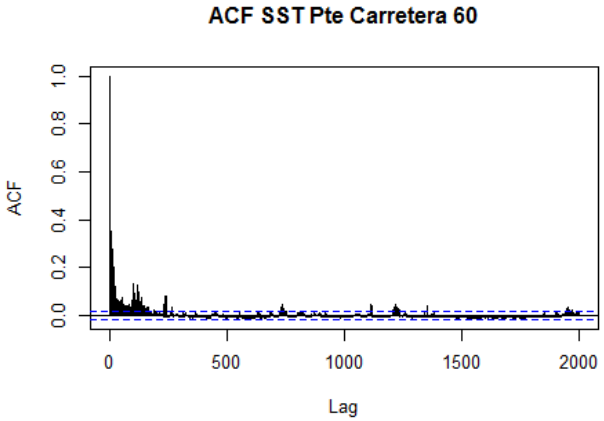
ACF SST Pte Carretera 60
ACF
0.0
0.2
0.4
0.6
0.8
1.0
0
500
1000
1500
2000
Lag

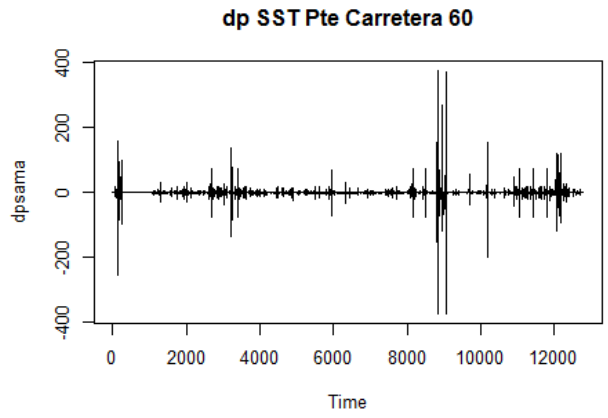
dp SST Pte Carretera 60
dpsama
-400
-200
0
200
400
0
2000
4000
6000
8000
10000
12000
Time

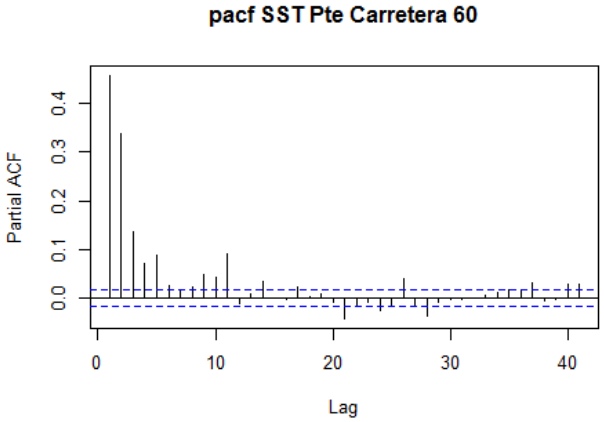
pacf SST Pte Carretera 60
Partial ACF
0.0
0.1
0.2
0.3
0.4
0
10
20
30
40
Lag

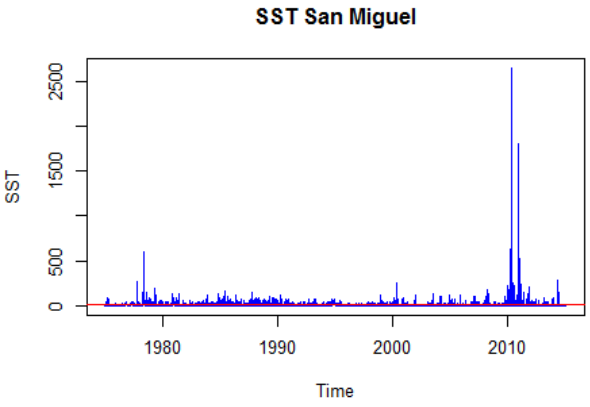
SST San Miguel
SST
0
500
1500
2500
1980
1990
2000
2010
Time

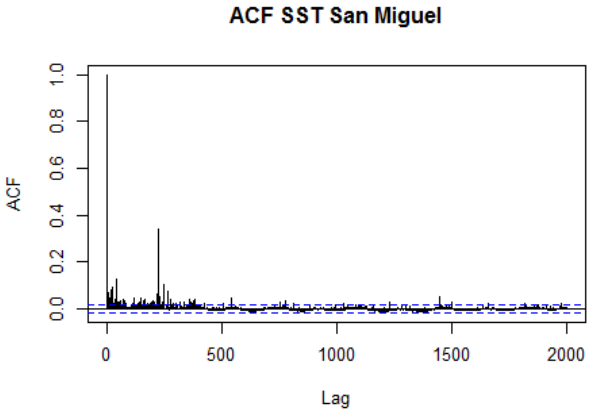
ACF SST San Miguel
ACF
0.0
0.2
0.4
0.6
0.8
1.0
0
500
1000
1500
2000
Lag

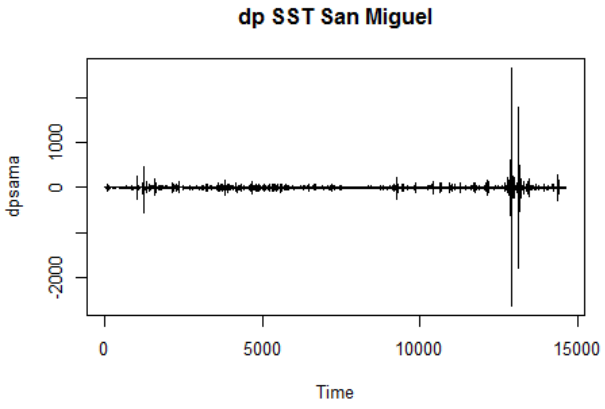
dp SST San Miguel
dpsama
-2000
0
1000
0
5000
10000
15000
Time

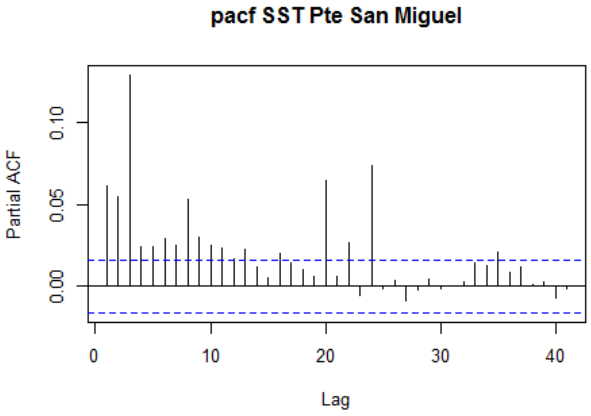
pacf SST Pte San Miguel
Partial ACF
0.00
0.05
0.10
0
10
20
30
40
Lag

Water quality data at different depth in the monitoring station

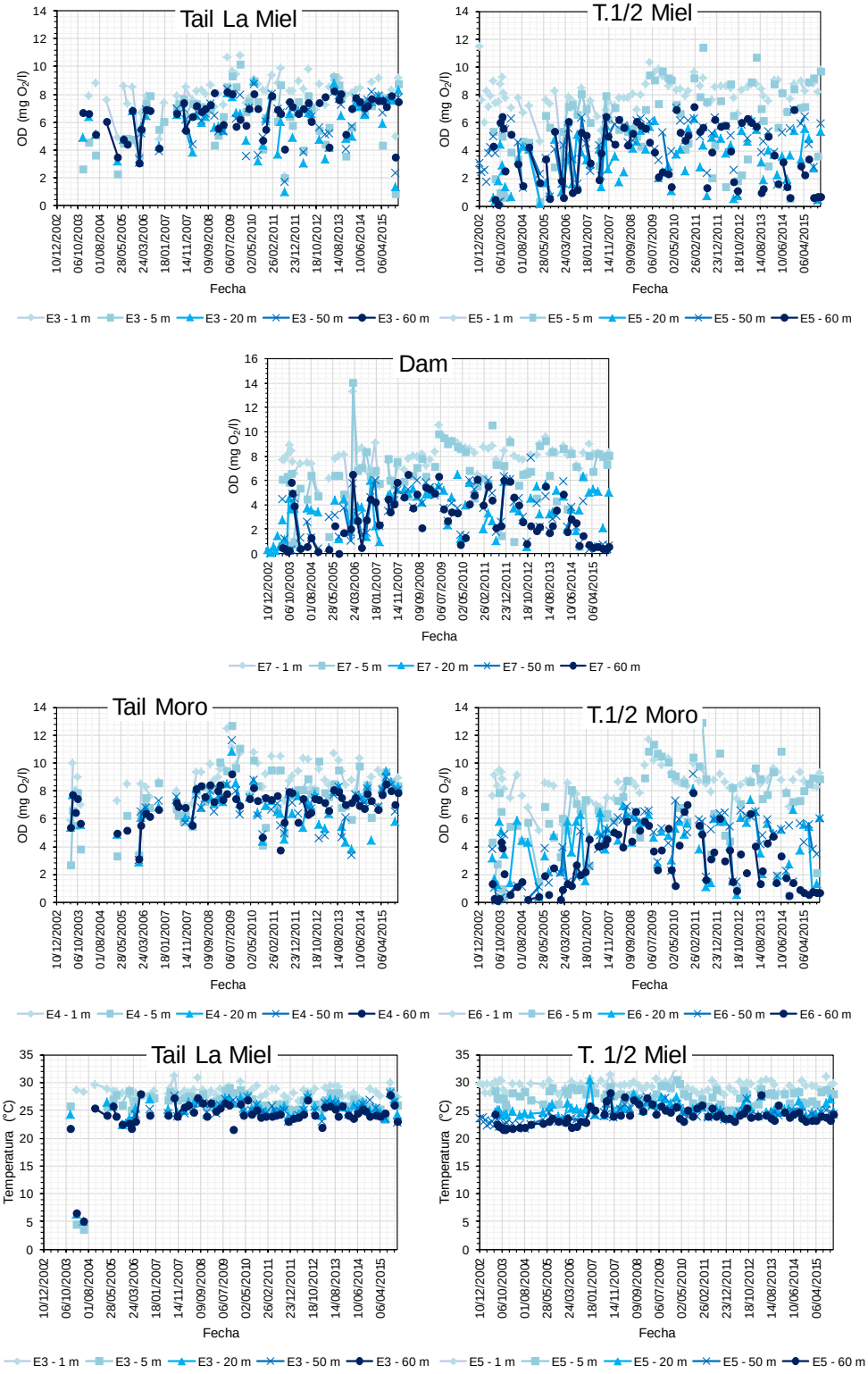

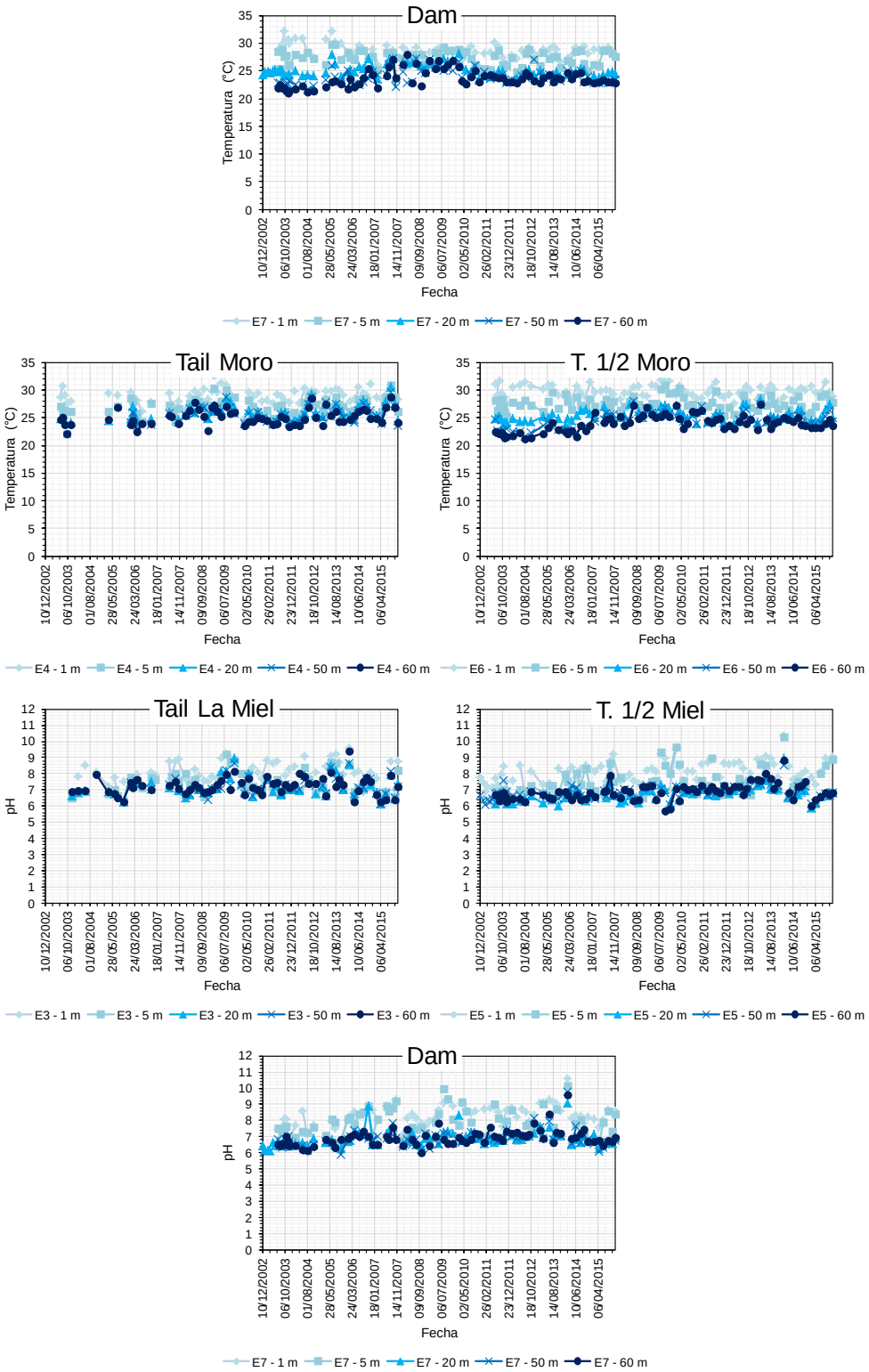
Dam
Temperatura (°C)
Fecha
E7 - 1 m
E7 - 5 m
E7 - 20 m
E7 - 50 m
E7 - 60 m
Tail Moro
T. 1/2 Moro
E4 - 1 m
E4 - 5 m
E4 - 20 m
E4 - 50 m
E4 - 60 m
E6 - 1 m
E6 - 5 m
E6 - 20 m
E6 - 50 m
E6 - 60 m
Tail La Miel
T. 1/2 Miel
pH
E3 - 1 m
E3 - 5 m
E3 - 20 m
E3 - 50 m
E3 - 60 m
E5 - 1 m
E5 - 5 m
E5 - 20 m
E5 - 50 m
E5 - 60 m
Dam
pH
Fecha
E7 - 1 m
E7 - 5 m
E7 - 20 m
E7 - 50 m
E7 - 60 m

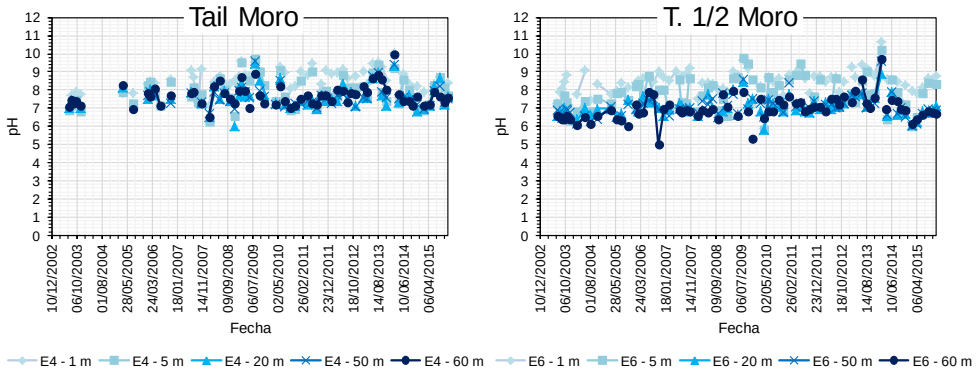
Tail Moro
T. 1/2 Moro
pH
Fecha
E4 - 1 m
E4 - 5 m
E4 - 20 m
E4 - 50 m
E4 - 60 m
E6 - 1 m
E6 - 5 m
E6 - 20 m
E6 - 50 m
E6 - 60 m

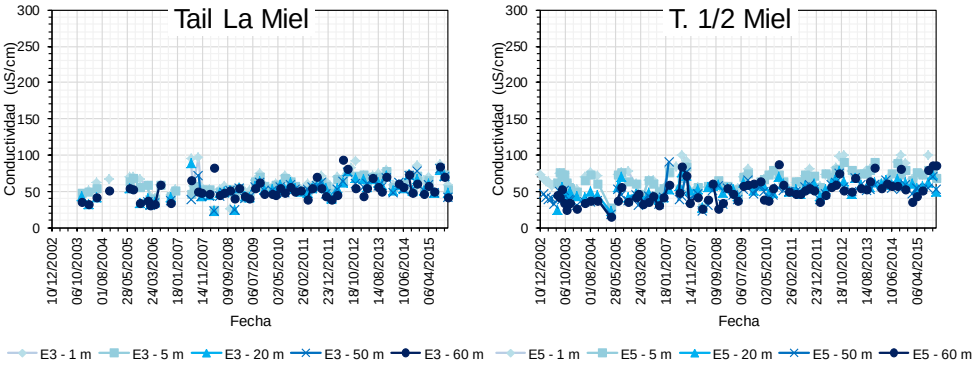
Tail La Miel
T. 1/2 Miel
Conductividad (uS/cm)
Fecha
E3 - 1 m
E3 - 5 m
E3 - 20 m
E3 - 50 m
E3 - 60 m
E5 - 1 m
E5 - 5 m
E5 - 20 m
E5 - 50 m
E5 - 60 m

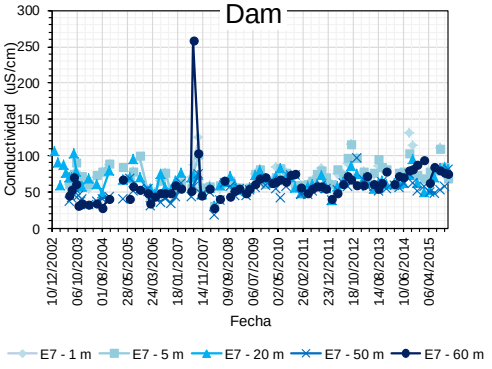
Dam
Conductividad (uS/cm)
Fecha
E7 - 1 m
E7 - 5 m
E7 - 20 m
E7 - 50 m
E7 - 60 m

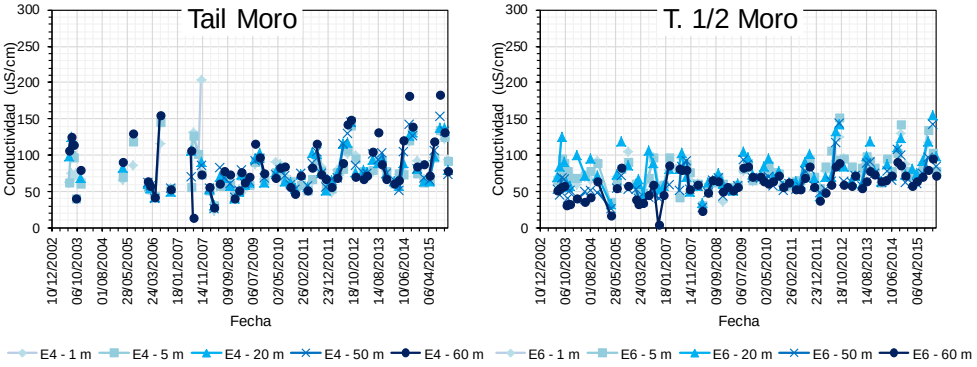
Tail Moro
T. 1/2 Moro
Conductividad (uS/cm)
Fecha
E4 - 1 m
E4 - 5 m
E4 - 20 m
E4 - 50 m
E4 - 60 m
E6 - 1 m
E6 - 5 m
E6 - 20 m
E6 - 50 m
E6 - 60 m

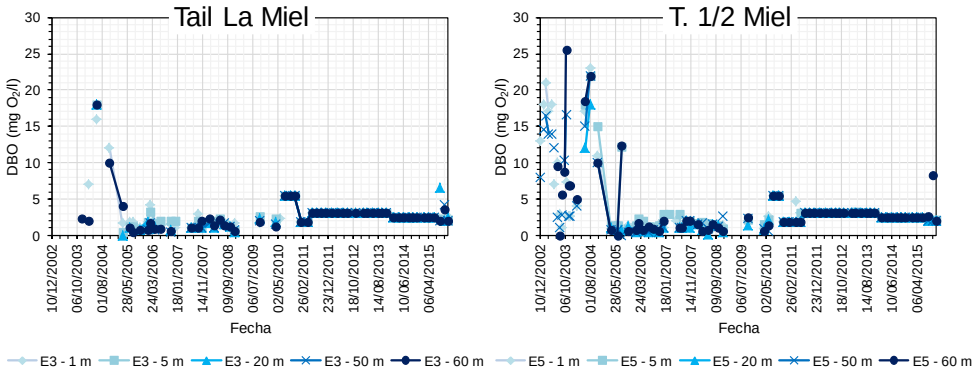
Tail La Miel
T. 1/2 Miel
DBO (mg O2/l)
Fecha
E3 - 1 m
E3 - 5 m
E3 - 20 m
E3 - 50 m
E3 - 60 m
E5 - 1 m
E5 - 5 m
E5 - 20 m
E5 - 50 m
E5 - 60 m

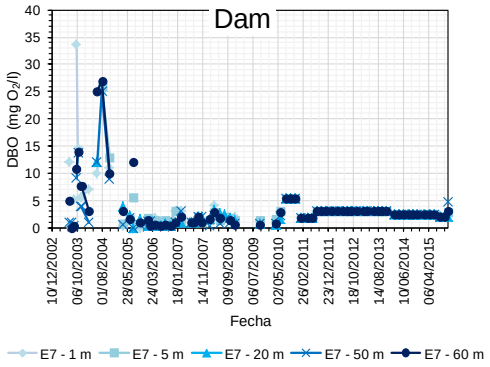
Dam
DBO (mg O2/l)
Fecha
E7 - 1 m
E7 - 5 m
E7 - 20 m
E7 - 50 m
E7 - 60 m

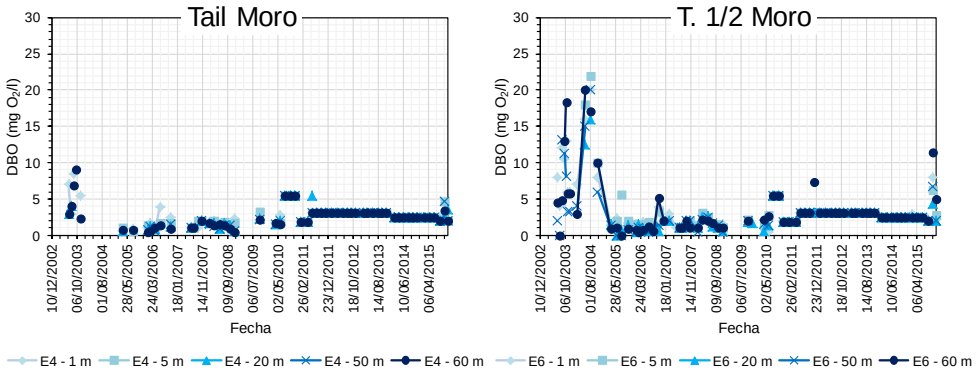
Tail Moro
T. 1/2 Moro
DBO (mg O2/l)
Fecha
E4 - 1 m
E4 - 5 m
E4 - 20 m
E4 - 50 m
E4 - 60 m
E6 - 1 m
E6 - 5 m
E6 - 20 m
E6 - 50 m
E6 - 60 m

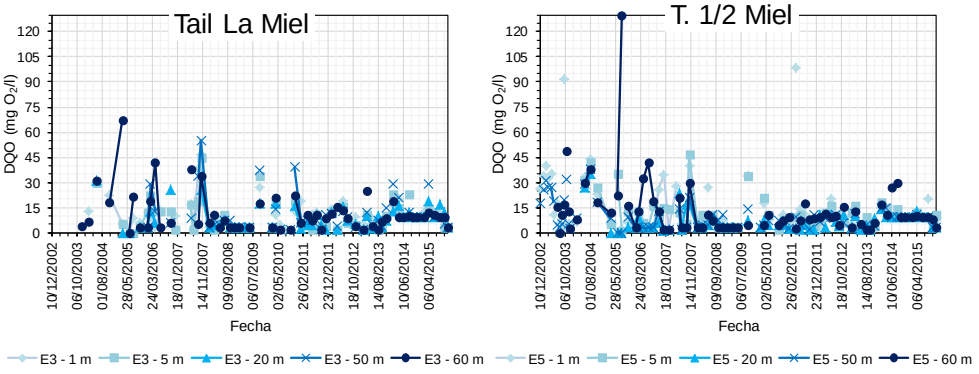
Tail La Miel
T. 1/2 Miel
DQO (mg O2/l)
Fecha
E3 - 1 m
E3 - 5 m
E3 - 20 m
E3 - 50 m
E3 - 60 m
E5 - 1 m
E5 - 5 m
E5 - 20 m
E5 - 50 m
E5 - 60 m

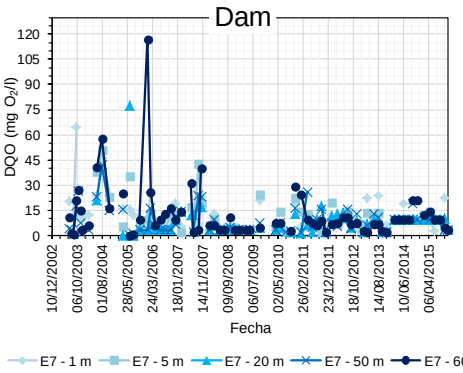
Dam
DQO (mg O2/l)
Fecha
E7 - 1 m
E7 - 5 m
E7 - 20 m
E7 - 50 m
E7 - 60 m

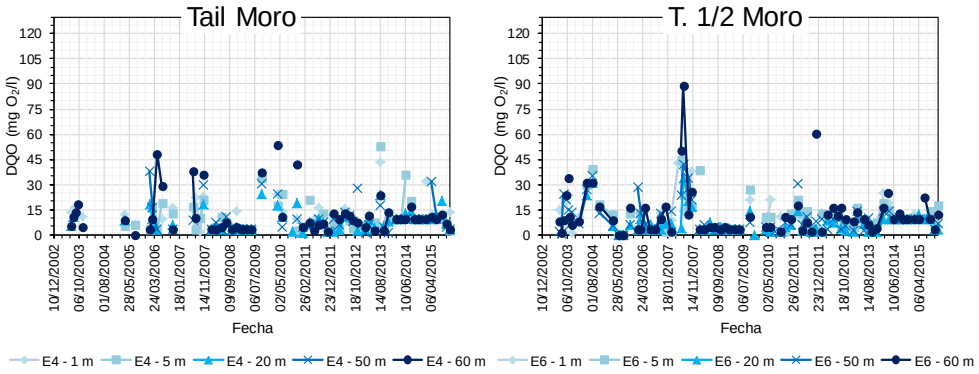
Tail Moro
T. 1/2 Moro
DQO (mg O2/l)
Fecha
E4 - 1 m
E4 - 5 m
E4 - 20 m
E4 - 50 m
E4 - 60 m
E6 - 1 m
E6 - 5 m
E6 - 20 m
E6 - 50 m
E6 - 60 m

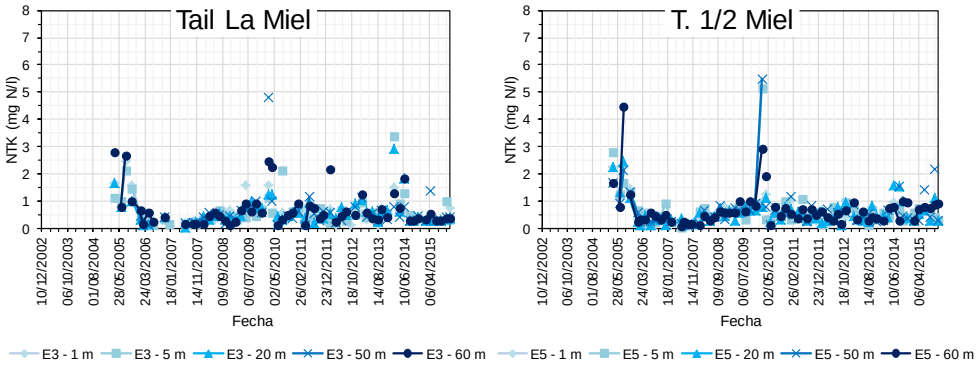
Tail La Miel
T. 1/2 Miel
NTK (mg N/l)
Fecha
E3 - 1 m
E3 - 5 m
E3 - 20 m
E3 - 50 m
E3 - 60 m
E5 - 1 m
E5 - 5 m
E5 - 20 m
E5 - 50 m
E5 - 60 m

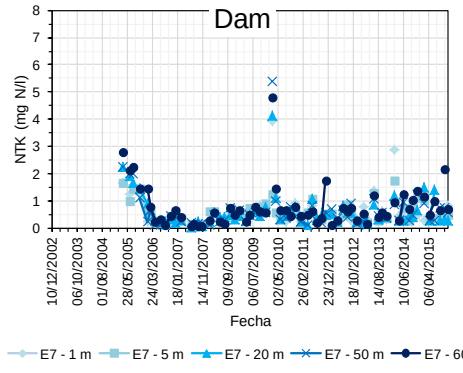
Dam
NTK (mg N/l)
Fecha
E7 - 1 m
E7 - 5 m
E7 - 20 m
E7 - 50 m
E7 - 60 m

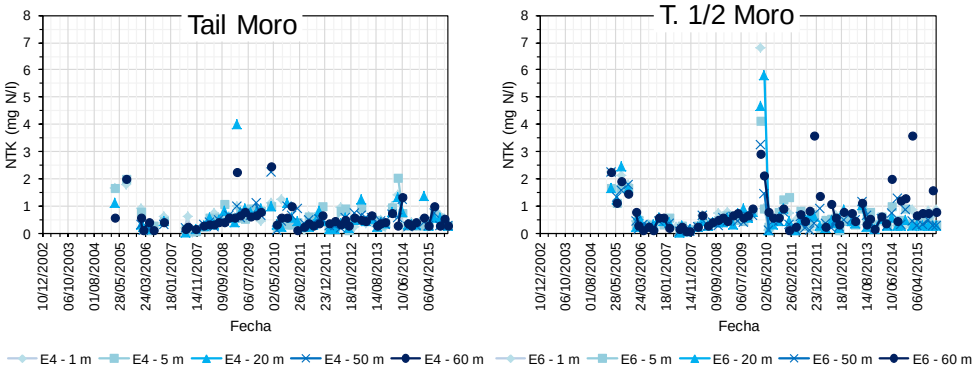
Tail Moro
NTK (mg N/l)
Fecha
T. 1/2 Moro
NTK (mg N/l)
Fecha
E4 - 1 m
E4 - 5 m
E4 - 20 m
E4 - 50 m
E4 - 60 m
E6 - 1 m
E6 - 5 m
E6 - 20 m
E6 - 50 m
E6 - 60 m

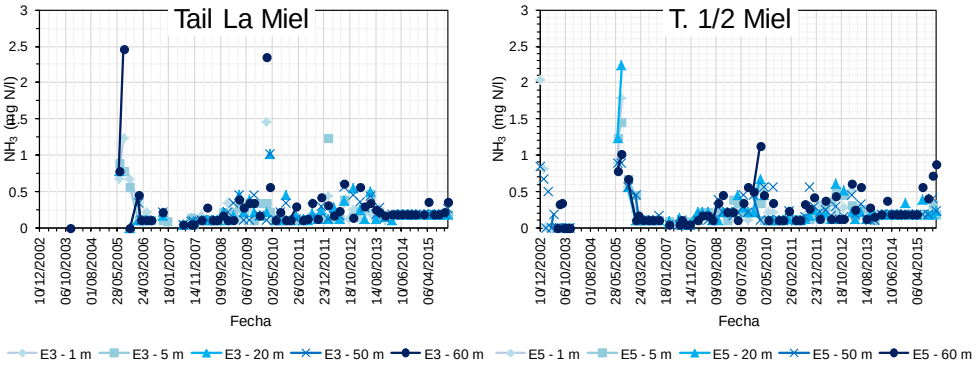
Tail La Miel
NH3 (mg N/l)
Fecha
T. 1/2 Miel
NH3 (mg N/l)
Fecha
E3 - 1 m
E3 - 5 m
E3 - 20 m
E3 - 50 m
E3 - 60 m
E5 - 1 m
E5 - 5 m
E5 - 20 m
E5 - 50 m
E5 - 60 m

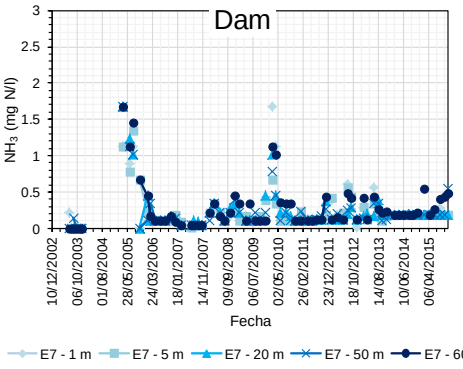
Dam
NH3 (mg N/l)
Fecha
E7 - 1 m
E7 - 5 m
E7 - 20 m
E7 - 50 m
E7 - 60 m

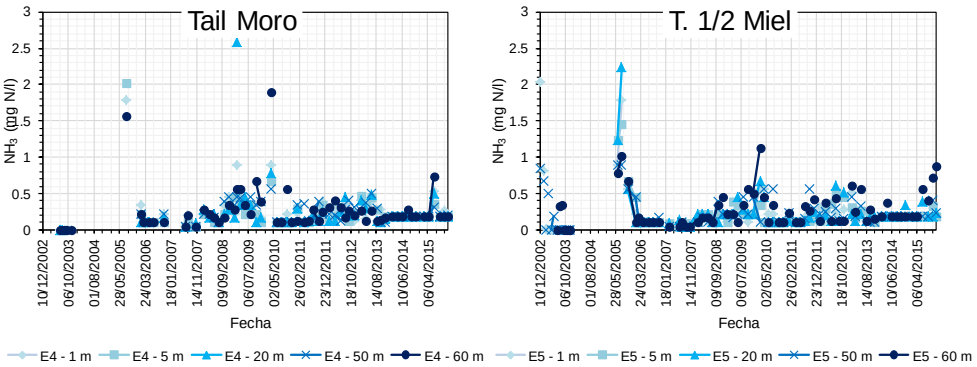
Tail Moro
NH3 (mg N/l)
Fecha
T. 1/2 Miel
NH3 (mg N/l)
Fecha
E4 - 1 m
E4 - 5 m
E4 - 20 m
E4 - 50 m
E4 - 60 m
E5 - 1 m
E5 - 5 m
E5 - 20 m
E5 - 50 m
E5 - 60 m

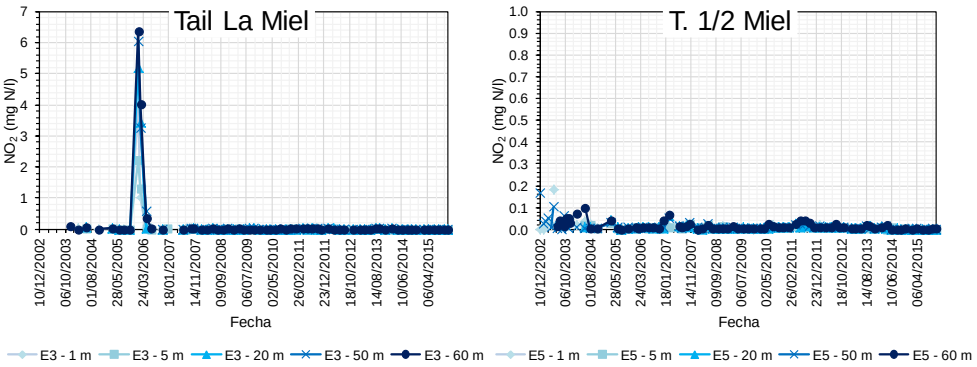
Tail La Miel
T. 1/2 Miel
NO2 (mg N/l)
Fecha
E3 - 1 m
E3 - 5 m
E3 - 20 m
E3 - 50 m
E3 - 60 m
E5 - 1 m
E5 - 5 m
E5 - 20 m
E5 - 50 m
E5 - 60 m

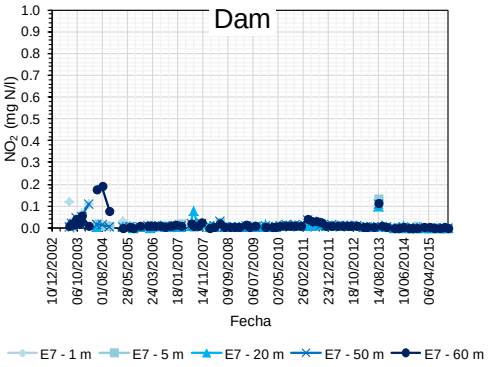
Dam
NO2 (mg N/l)
Fecha
E7 - 1 m
E7 - 5 m
E7 - 20 m
E7 - 50 m
E7 - 60 m

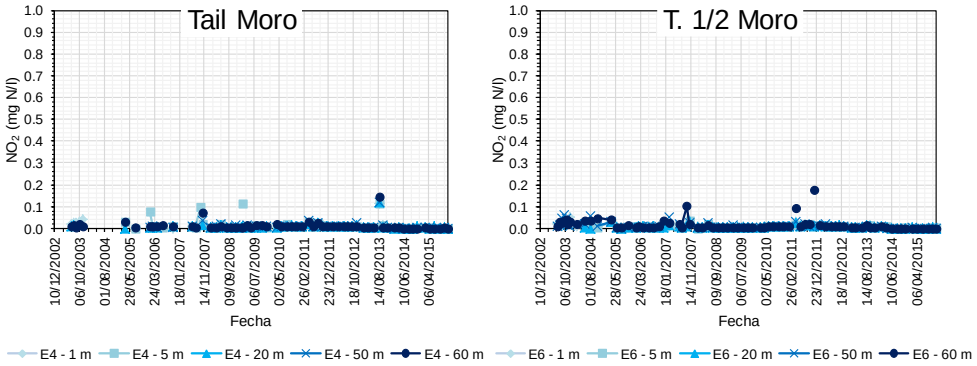
Tail Moro
T. 1/2 Moro
NO2 (mg N/l)
Fecha
E4 - 1 m
E4 - 5 m
E4 - 20 m
E4 - 50 m
E4 - 60 m
E6 - 1 m
E6 - 5 m
E6 - 20 m
E6 - 50 m
E6 - 60 m

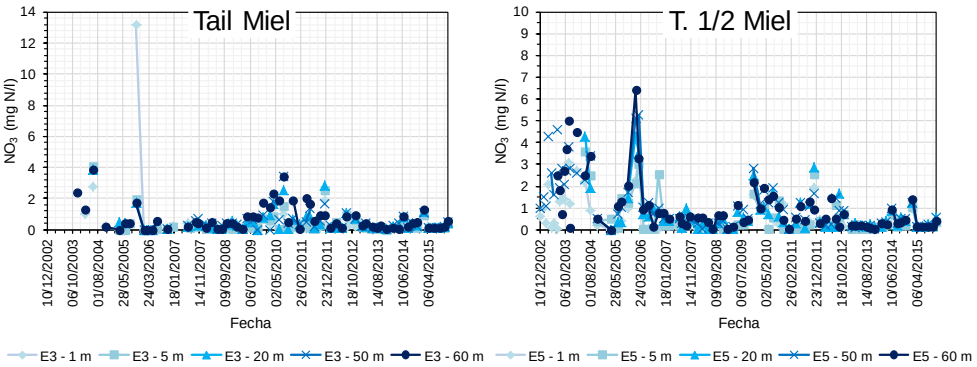
Tail Miel
T. 1/2 Miel
NO3 (mg N/l)
Fecha
E3 - 1 m
E3 - 5 m
E3 - 20 m
E3 - 50 m
E3 - 60 m
E5 - 1 m
E5 - 5 m
E5 - 20 m
E5 - 50 m
E5 - 60 m

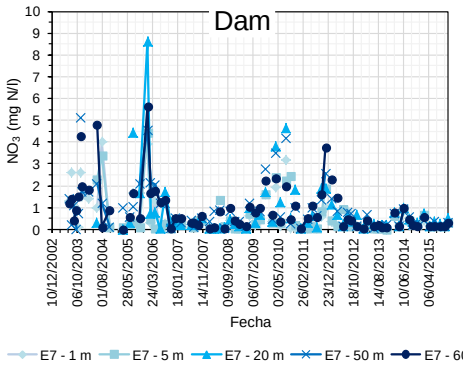
Dam
NO3 (mg N/l)
Fecha
E7 - 1 m
E7 - 5 m
E7 - 20 m
E7 - 50 m
E7 - 60 m

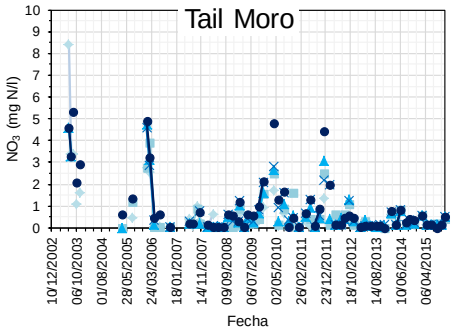
Tail Moro
NO3 (mg N/l)
Fecha

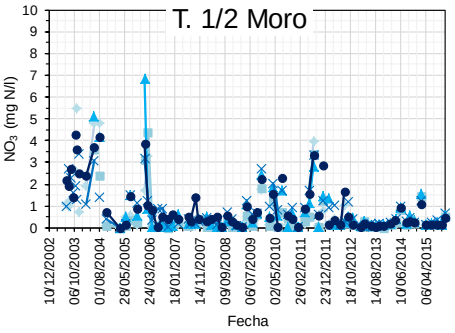
T. 1/2 Moro
NO3 (mg N/l)
Fecha

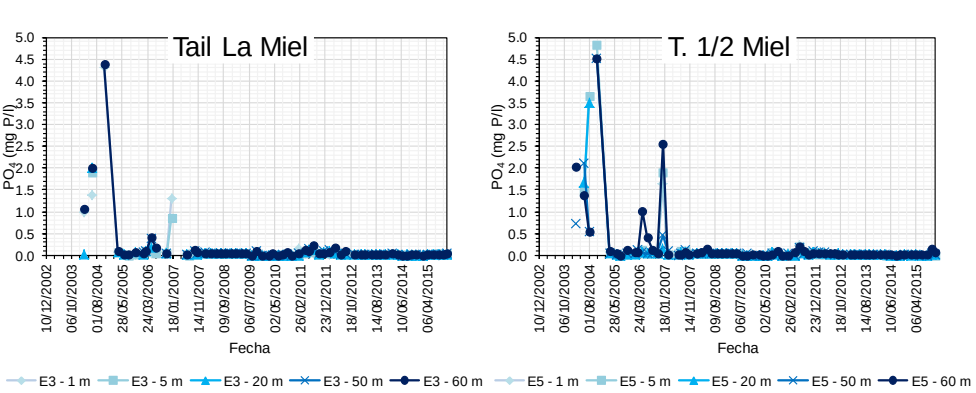
E4 - 1 m
E4 - 5 m
E4 - 20 m
E4 - 50 m
E4 - 60 m
E6 - 1 m
E6 - 5 m
E6 - 20 m
E6 - 50 m
E6 - 60 m

Tail La Miel
PO4 (mg P/l)
Fecha

T. 1/2 Miel
PO4 (mg P/l)
Fecha

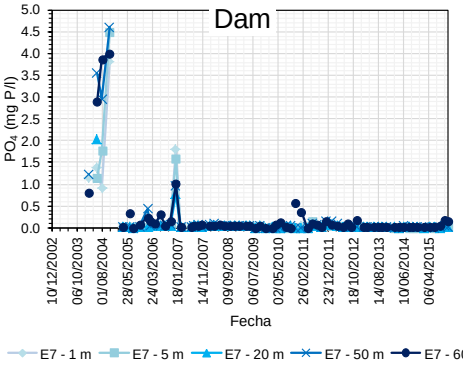
Dam
PO4 (mg P/l)
Fecha
E7 - 1 m
E7 - 5 m
E7 - 20 m
E7 - 50 m
E7 - 60 m

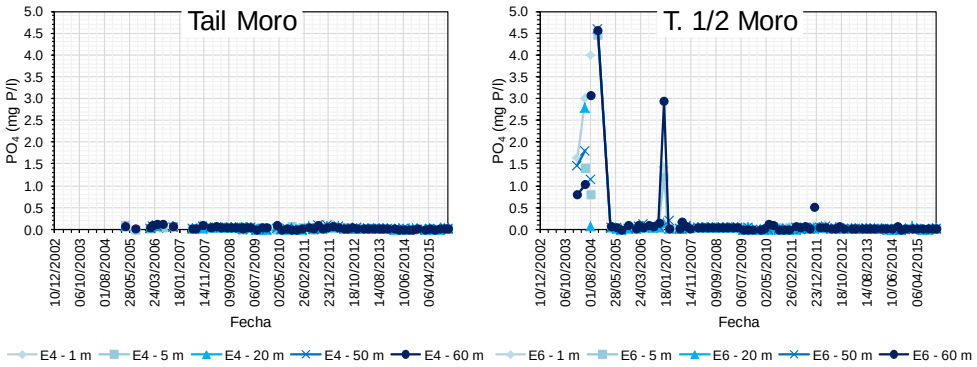
Tail Moro
T. 1/2 Moro
PO4 (mg P/l)
Fecha
E4 - 1 m
E4 - 5 m
E4 - 20 m
E4 - 50 m
E4 - 60 m
E6 - 1 m
E6 - 5 m
E6 - 20 m
E6 - 50 m
E6 - 60 m

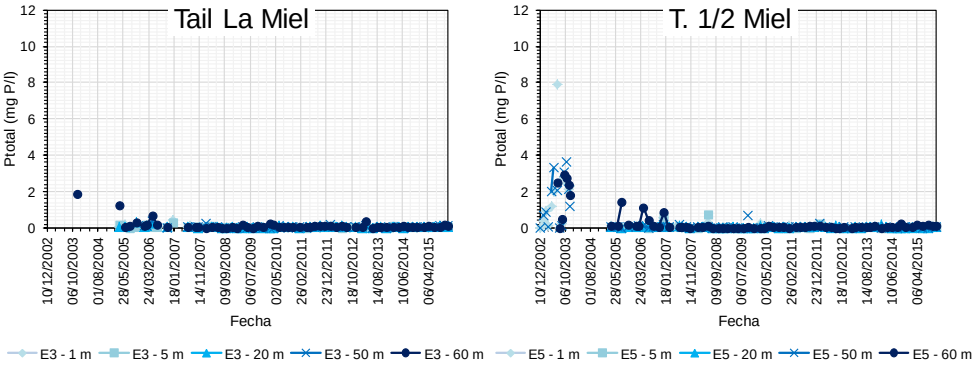
Tail La Miel
T. 1/2 Miel
Ptotal (mg P/l)
Fecha
E3 - 1 m
E3 - 5 m
E3 - 20 m
E3 - 50 m
E3 - 60 m
E5 - 1 m
E5 - 5 m
E5 - 20 m
E5 - 50 m
E5 - 60 m

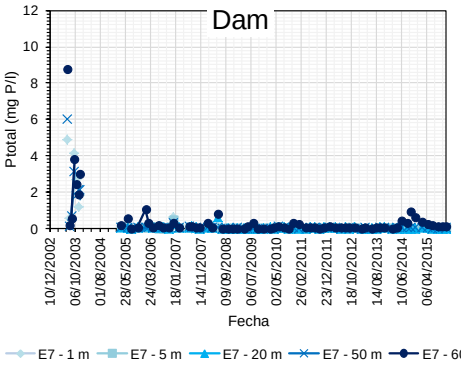
Dam
Ptotal (mg P/l)
Fecha
E7 - 1 m
E7 - 5 m
E7 - 20 m
E7 - 50 m
E7 - 60 m

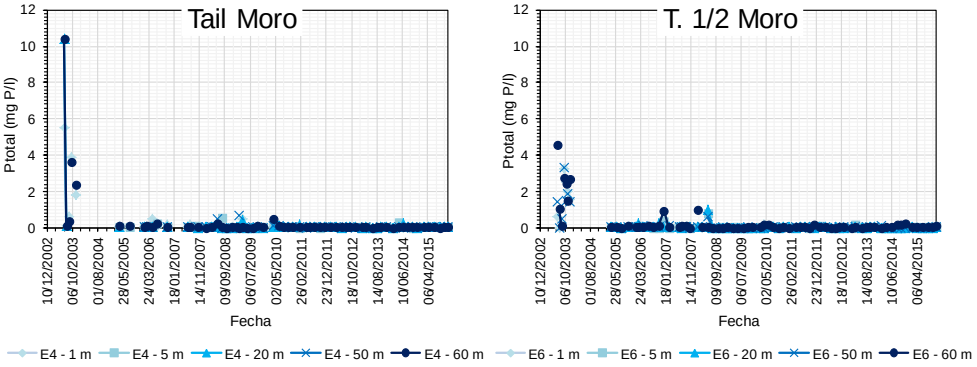
Tail Moro
T. 1/2 Moro
Ptotal (mg P/l)
Fecha
E4 - 1 m
E4 - 5 m
E4 - 20 m
E4 - 50 m
E4 - 60 m
E6 - 1 m
E6 - 5 m
E6 - 20 m
E6 - 50 m
E6 - 60 m

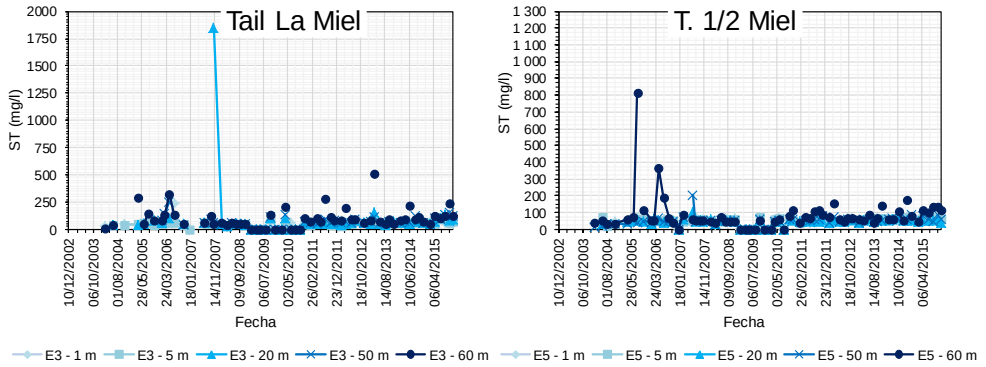
Tail La Miel
ST (mg/l)
Fecha
E3 - 1 m
E3 - 5 m
E3 - 20 m
E3 - 50 m
E3 - 60 m
E5 - 1 m
E5 - 5 m
E5 - 20 m
E5 - 50 m
E5 - 60 m

T. 1/2 Miel
ST (mg/l)
Fecha

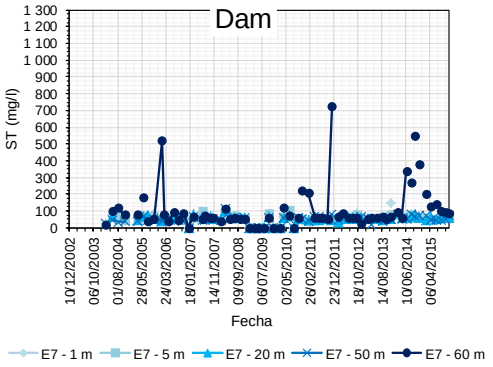
Dam
ST (mg/l)
Fecha
E7 - 1 m
E7 - 5 m
E7 - 20 m
E7 - 50 m
E7 - 60 m

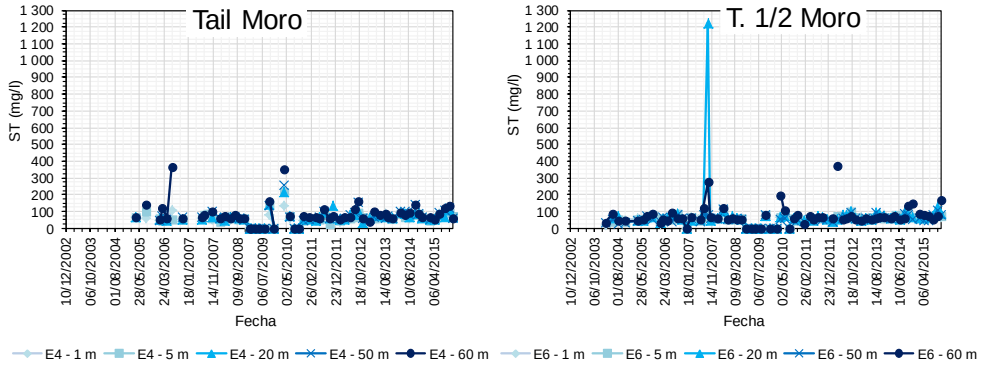
Tail Moro
ST (mg/l)
Fecha
E4 - 1 m
E4 - 5 m
E4 - 20 m
E4 - 50 m
E4 - 60 m
E6 - 1 m
E6 - 5 m
E6 - 20 m
E6 - 50 m
E6 - 60 m

T. 1/2 Moro
ST (mg/l)
Fecha

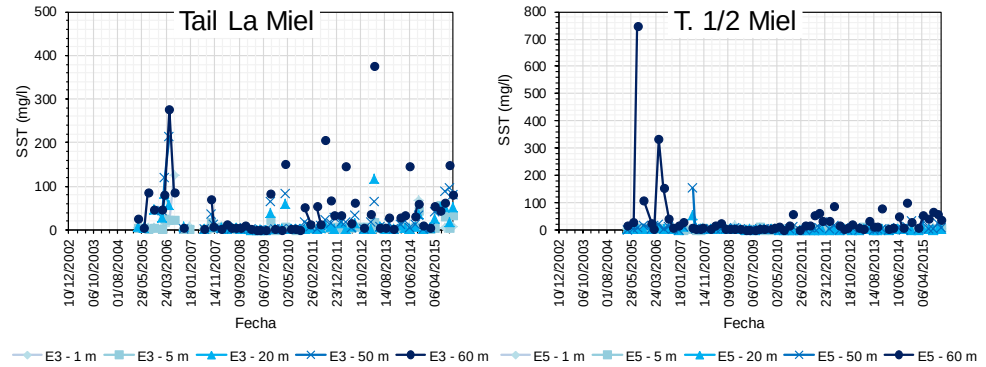
Tail La Miel
SST (mg/l)
Fecha
E3 - 1 m
E3 - 5 m
E3 - 20 m
E3 - 50 m
E3 - 60 m
E5 - 1 m
E5 - 5 m
E5 - 20 m
E5 - 50 m
E5 - 60 m

T. 1/2 Miel
SST (mg/l)
Fecha

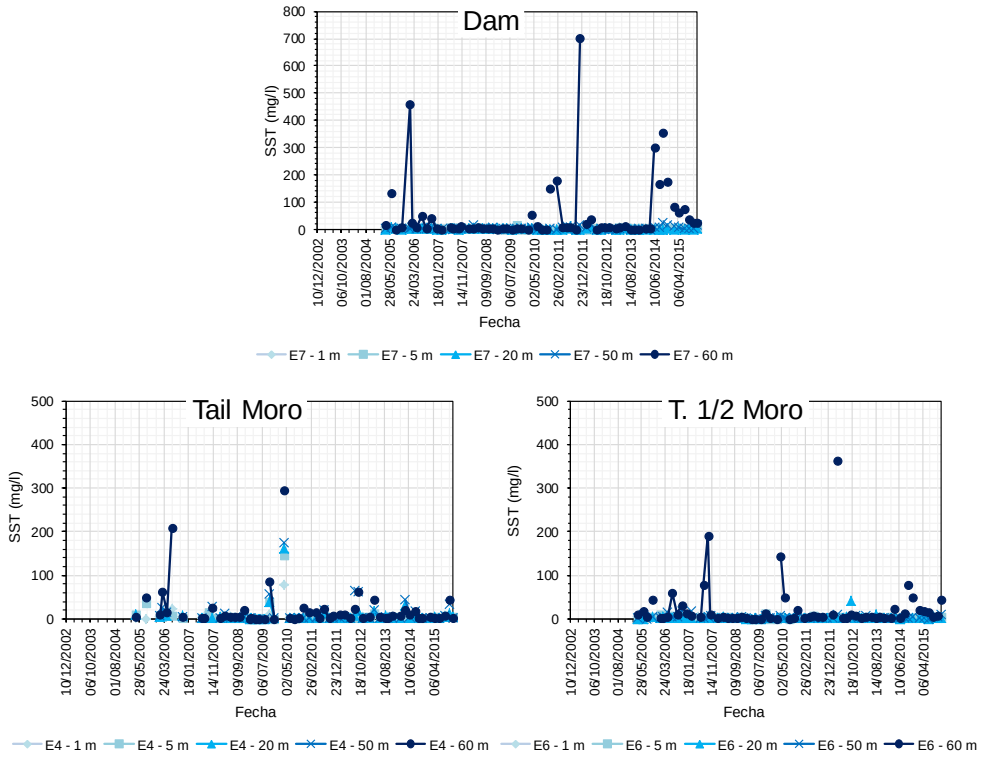
Dam
SST (mg/l)
800
700
600
500
400
300
200
100
0
10/12/2002
06/10/2003
01/08/2004
28/05/2005
24/03/2006
18/01/2007
14/11/2007
09/09/2008
06/07/2009
02/05/2010
26/02/2011
23/12/2011
18/10/2012
14/08/2013
10/06/2014
06/04/2015
Fecha
E7 - 1 m
E7 - 5 m
E7 - 20 m
E7 - 50 m
E7 - 60 m
Tail Moro
SST (mg/l)
500
400
300
200
100
0
Fecha
T. 1/2 Moro
SST (mg/l)
Fecha
E4 - 1 m
E4 - 5 m
E4 - 20 m
E4 - 50 m
E4 - 60 m
E6 - 1 m
E6 - 5 m
E6 - 20 m
E6 - 50 m
E6 - 60 m

A summary of the statistical results for the different time series is presented below.

Range, mean, and standard deviation of water quality parameters of "La Miel" reservoir for dry season

	Site E3			Site E4			Site E5			Site E6			Site E7		
Parameters	Range	Mean	SD	Range	Mean	SD	Range	Mean	SD	Range	Mean	SD	Range	Mean	SD
Conductivity	44.4 - 96.0	62.96	10.57	44.0 - 133.9	79.46	24.1	52.8 - 100.8	68.95	12.61	35.5 - 117.2	72.56	15.84	49.7 - 132.1	71.16	16.73
BOD	1.0 - 16.0	2.67	2.19	0.84 - 8.65	2.76	1.62	0.91 - 24.40	4.2	5.78	0.40 - 20.00	3.5	3.96	0.43 - 25.0	3.7	4.85
COD	2.0 - 30.0	10.13	5.34	2.94 - 43.20	12.03	8.9	1.60 - 47.00	13.44	11.83	0.99 - 43.00	11.57	9.34	2.49 - 46.00	11.97	9.12
NH4-N	0.050 - 1.46	0.28	0.33	0.0 - 1.79	0.26	0.33	0.00 - 1.79	0.28	0.36	0.000 - 1.680	0.26	0.32	0.00 - 1.68	0.28	0.35
NO2-N	0.00 - 3.96	0.12	0.61	0.0 - 0.112	0.01	0.02	0.00 - 0.048	0.01	0.01	0.001 - 0.050	0.01	0.01	0.00 - 0.12	0.02	0.03
NO3-N	0.005 - 2.80	0.3	0.45	0.024 - 8.400	0.64	1.47	0.024 - 2.72	0.5	0.69	0.024 - 4.80	0.76	1.23	0.002 - 4.00	0.7	1.01
NTK	0.127 - 2.46	0.61	0.52	0.129 - 1.79	0.58	0.37	0.10 - 2.24	0.57	0.42	0.112 - 6.83	0.78	1.24	0.10 - 3.92	0.68	0.84
pH	6.72 - 9.6	7.91	1.65	6.78 - 10.0	8.81	1.61	6.78 - 10.37	7.91	1.24	6.89 - 10.66	8.42	1.27	6.72 - 10.62	8.07	1.09
DO	2.15 - 10.8	8.06	0.78	3.52 - 12.55	8.53	0.82	3.40 - 10.39	8.1	0.78	3.43 - 11.70	8.52	0.7	3.16 - 10.57	8.36	0.71
PO4	0.004 - 1.39	0.13	0.34	0.004 - 0.112	0.03	0.03	0.003 - 1.65	0.09	0.3	0.004 - 4.00	0.3	0.87	0.004 - 1.81	0.17	0.43
TP	0.0 - 0.42	0.05	0.08	0.002 - 5.52	0.24	0.91	0.00 - 7.90	0.32	1.15	0.00 - 1.6815	0.11	0.31	0.00 - 4.90	0.24	0.79
TSS	1.24 - 125.0	8.93	23.67	0.00 - 23.00	4.19	4.76	0.60 - 17.00	3.25	2.44	0.00 - 7.00	3.14	1.69	1.00 - 9.00	3.17	1.82
Water Temp	23.4 - 30.9	28.34	1.21	26.1 - 31.3	29.08	1.2	28.0 - 32.8	29.59	0.93	27.7 - 31.8	30.09	1.04	26.10- 32.10	28.99	0.98

Range, mean, and standard deviation of water quality parameters of "La Miel" reservoir for wet season

	Site E3			Site E4			Site E5			Site E6			Site E7		
Parameters	Range	Mean	SD	Range	Mean	SD	Range	Mean	SD	Range	Mean	SD	Range	Mean	SD
Conductivity	25.5 - 97.0	61.81	15.25	22.6 - 203.0	78.52	30.01	26.7 - 100.4	68.97	14.82	30.2 - 129.2	74.71	19.23	28.2 - 125.0	72.23	18.30
BOD	1.0 - 16.0	2.90	2.56	0.58 - 8.9	2.63	1.39	0.72 - 27.55	3.57	4.46	0.40 - 16.00	3.05	2.58	0.43 - 24.15	3.21	3.44
COD	1.9 - 47.0	11.02	9.66	2.0 - 34.0	10.49	6.82	2.0 - 98.3	14.84	17.5	2.20 - 43.00	11.00	8.16	2.20 - 46.40	10.92	8.26

									3						
NH4-N	0.108 - 0.672	0.18	0.12	0.0 - 0.896	0.22	0.17	0.00 - 2.03	0.22	0.27	0.000 - 0.896	0.21	0.17	0.00 - 1.12	0.22	0.26
NO2-N	0.001 - 1.01	0.02	0.13	0.0 - 0.039	0.01	0.01	0.00 - 0.184	0.01	0.02	0.001 - 0.0345	0.01	0.01	0.00 - 0.051	0.01	0.01
NO3-N	0.002 - 13.2	0.68	2.31	0.02 - 2.57	0.44	0.53	0.002 - 3.13	0.48	0.67	0.002 - 4.80	0.48	0.91	0.002 - 2.05	0.42	0.55
NTK	0.12 - 1.68	0.56	0.39	0.05 - 1.68	0.52	0.38	0.09 - 2.24	0.54	0.45	0.09 - 2.24	0.58	0.46	0.14 - 1.68	0.57	0.35
pH	6.75 - 9.10	8.06	1.22	6.78 - 9.47	8.96	1.15	6.71 - 9.2	8.18	1.09	5.91 - 9.39	8.43	1.17	6.62 - 9.28	7.96	1.22
DO	4.8 - 10.8	8.01	0.59	6.09 - 12.55	8.39	0.56	4.7 - 11.5	8.14	0.59	5.20 - 11.7	8.40	0.66	4.94 - 13.30	8.26	0.65
PO4	0.006 - 4.3	0.19	0.76	0.004 - 0.11	0.03	0.03	0.004 - 0.218	0.03	0.04	0.004 - 4.500	0.21	0.84	0.004 - 3.82	0.16	0.67
TP	0.002 - 0.204	0.03	0.03	0.002 - 3.88	0.19	0.58	0.002 - 2.59	0.19	0.55	0.00 - 2.875	0.13	0.48	0.00 - 3.41	0.13	0.51
TSS	1.24 - 68.8	6.47	10.78	1.24 - 78.0	6.87	13.95	0.60 - 17.00	3.15	2.40	1.24 - 8.00	3.23	1.73	1.00 - 8.00	3.56	1.94
Water Temp	23.4 - 31.3	28.19	1.09	24.2 - 31.3	28.74	1.37	27.8 - 31.5	29.39	0.78	27.6 - 31.6	29.73	0.93	25.70 - 32.10	28.46	1.22

Change point detections and homogeneity test

Sites	Site E3		Site E4		Site E5		Site E6		Site E7	
Parameters	Mann Kendall	Pettitt Change	Mann Kendall	Pettitt Change	Mann Kendall	Pettitt Change	Mann Kendall	Pettitt Change	Mann Kendall	Pettitt Change
Conductivity	reject	2011-09-30	reject	2012-03-31	reject	2011-07-31	reject	2012-03-31	reject	2011-07-31
BOD	reject	2010-07-31	reject	2010-05-31	Fail to reject	2004-11-30	Fail to reject	2010-07-31	Fail to reject	2010-05-31
COD	Fail to reject	No-Change	Fail to reject	No-Change	reject	2004-11-30	Fail to reject	2007-12-31	reject	2006-04-30
NH4	Fail to reject	2011-07-31	reject	2008-09-30	reject	2008-09-30	reject	2010-01-31	reject	2010-01-31
NO2	reject	2012-12-31	reject	2013-11-30	reject	2012-12-31	reject	2012-12-31	reject	2012-12-31
NO3	Fail to reject	No-Change	Fail to reject	2006-04-30	reject	2006-04-30	Fail to reject	2006-04-30	reject	2006-06-30
NTK	Fail to reject	No-Change	Fail to reject	No-Change	Fail to reject	2008-11-30	Fail to reject	No-	Fail to reject	No-

								Change		Change
DO	reject	2009-05-31	reject	2008-03-31	reject	2009-03-31	reject	2009-03-31	reject	2009-03-31
pH	Fail to reject	2009-05-31	reject	2008-05-31	reject	2009-01-31	reject	2006-03-31	reject	2009-05-31
PO4	reject	2009-07-31	reject	2009-07-31	reject	2009-07-31	reject	2009-07-31	reject	2009-07-31
PT	reject	2008-05-31	reject	2008-07-31	reject	2008-07-31	reject	2007-11-30	reject	2008-07-31
TSS	reject	2009-11-30	Fail to reject	2010-05-31	reject	2009-11-30	reject	2010-05-31	reject	2010-03-31
Water Temp	reject	2011-07-31	reject	2008-05-31	Fail to reject	2010-05-31	Fail to reject	No-Change	reject	2005-11-30

Seasonal assessment applying Mann Whitney U test

Sites	E3		E4		E5		E6		E7	
Parameters	PValue	Hypothesis	Pvalue	Hypothesis	Pvalue	Hypothesis	Pvalue	Hypothesis	Pvalue	Hypothesis
Conductivity	0.43	Fail to reject	0.21	Fail to reject	0.31	Fail to reject	0.20	Fail to reject	0.16	Fail to reject
BOD	0.49	Fail to reject	0.16	Fail to reject	0.37	Fail to reject	0.11	Fail to reject	0.46	Fail to reject
COD	0.30	Fail to reject	0.37	Fail to reject	0.46	Fail to reject	0.07	Fail to reject	0.32	Fail to reject
NH4	0.27	Fail to reject	0.49	Fail to reject	0.31	Fail to reject	0.22	Fail to reject	0.44	Fail to reject
NO2	0.26	Fail to reject	0.43	Fail to reject	0.47	Fail to reject	0.48	Fail to reject	0.30	Fail to reject
NO3	0.37	Fail to reject	0.29	Fail to reject	0.25	Fail to reject	0.38	Fail to reject	0.26	Fail to reject
NTK	0.43	Fail to reject	0.22	Fail to reject	0.43	Fail to reject	0.41	Fail to reject	0.30	Fail to reject
DO	0.45	Fail to reject	0.40	Fail to reject	0.38	Fail to reject	0.48	Fail to reject	0.41	Fail to reject
pH	0.37	Fail to reject	0.46	Fail to reject	0.47	Fail to reject	0.27	Fail to reject	0.40	Fail to reject
PO4	0.42	Fail to reject	0.22	Fail to reject	0.38	Fail to reject	0.45	Fail to reject	0.44	Fail to reject
PT	0.43	Fail to reject	0.42	Fail to reject	0.44	Fail to reject	0.38	Fail to reject	0.50	Fail to reject
TSS	0.25	Fail to reject	0.48	Fail to reject	0.31	Fail to reject	0.30	Fail to reject	0.23	Fail to reject
Water Temp	0.24	Fail to reject	0.42	Fail to reject	0.20	Fail to reject	0.16	Fail to reject	0.31	Fail to reject

Seasonal assessment applying Levene test

Sites	E3		E4		E5		E6		E7	
Parameters	PValue	Hypothesis	Pvalue	Hypothesis	Pvalue	Hypothesis	Pvalue	Hypothesis	Pvalue	Hypothesis
Conductivity	0.19987978	Fail to reject	0.58747508	Fail to reject	0.48446544	Fail to reject	0.16704485	Fail to reject	0.25498194	Fail to reject
BOD	0.79035097	Fail to reject	0.59567107	Fail to reject	0.75505974	Fail to reject	0.93154885	Fail to reject	0.41398437	Fail to reject
COD	0.23752698	Fail to reject	0.51942649	Fail to reject	0.33658297	Fail to reject	0.94294444	Fail to reject	0.79845095	Fail to reject
NH4	0.02302163	reject	0.39136763	Fail to reject	0.6007208	Fail to reject	0.34638418	Fail to reject	0.35916077	Fail to reject
NO2	0.19998722	Fail to reject	0.2454728	Fail to reject	0.19688486	Fail to reject	0.83360921	Fail to reject	0.04023733	reject
NO3	0.22932757	Fail to reject	0.36102038	Fail to reject	0.73199182	Fail to reject	0.37550901	Fail to reject	0.10569138	Fail to reject
NTK	0.4603213	Fail to reject	0.81884872	Fail to reject	0.92233534	Fail to reject	0.19523751	Fail to reject	0.1036541	Fail to reject
DO	0.65558934	Fail to reject	0.76591617	Fail to reject	0.81844839	Fail to reject	0.97925672	Fail to reject	0.83875663	Fail to reject
pH	0.26084777	Fail to reject	0.56027261	Fail to reject	0.86263727	Fail to reject	0.75207525	Fail to reject	0.41010812	Fail to reject
PO4	0.68079831	Fail to reject	0.8628851	Fail to reject	0.15944621	Fail to reject	0.56225035	Fail to reject	0.85654746	Fail to reject
PT	0.42951799	Fail to reject	0.82794132	Fail to reject	0.09532077	Fail to reject	0.56457819	Fail to reject	0.40648524	Fail to reject
TSS	0.56806647	Fail to reject	0.28414679	Fail to reject	0.9879787	Fail to reject	0.8716762	Fail to reject	0.31777131	Fail to reject
Water Temp	0.82398201	Fail to reject	0.56760372	Fail to reject	0.32146597	Fail to reject	0.18127263	Fail to reject	0.72251298	Fail to reject

Spatial assessment between stations applying Kruskal-Wallis test

Sites	E3 - E5		E4 - E6		E3 - E7		E4 - E7	
Parameters	PValue	Hypothesis	Pvalue	Hypothesis	Pvalue	Hypothesis	Pvalue	Hypothesis
Conductivity	0.000116136	reject	0.398579043	Fail to reject	8.9175E-06	reject	0.08515564	Fail to reject
BOD	0.958406991	Fail to reject	0.794406494	Fail to reject	0.69872617	Fail to reject	0.67916794	Fail to reject
COD	0.449122525	Fail to reject	0.610289759	Fail to reject	0.5829174	Fail to reject	0.91186984	Fail to reject
NH4	0.732347224	Fail to reject	0.295817589	Fail to reject	0.40748817	Fail to reject	0.04560119	reject
NO2	0.91947213	Fail to reject	0.051488019	Fail to reject	0.27121027	Fail to reject	0.2460667	Fail to reject
NO3	0.021418808	reject	0.829377051	Fail to reject	0.01529233	reject	0.64531592	Fail to reject

NTK	0.461447375	Fail to reject	0.52879919	Fail to reject	0.82630379	Fail to reject	0.90830462	Fail to reject
DO	0.960433227	Fail to reject	0.002161122	reject	0.57819331	Fail to reject	8.3706E-09	reject
pH	0.299762392	Fail to reject	0.954638798	Fail to reject	0.00072827	reject	0.05496965	Fail to reject
PO4	0.284229557	Fail to reject	0.121484017	Fail to reject	0.66958757	Fail to reject	0.15448444	Fail to reject
PT	0.957196923	Fail to reject	0.026201212	reject	0.56593219	Fail to reject	0.0074867	reject
TSS	0.00034869	reject	0.212768433	Fail to reject	0.0168239	reject	0.36967806	Fail to reject
Water Temp	3.57384E-20	reject	1.17812E-09	reject	0.00183406	reject	0.03872747	reject

Tendency

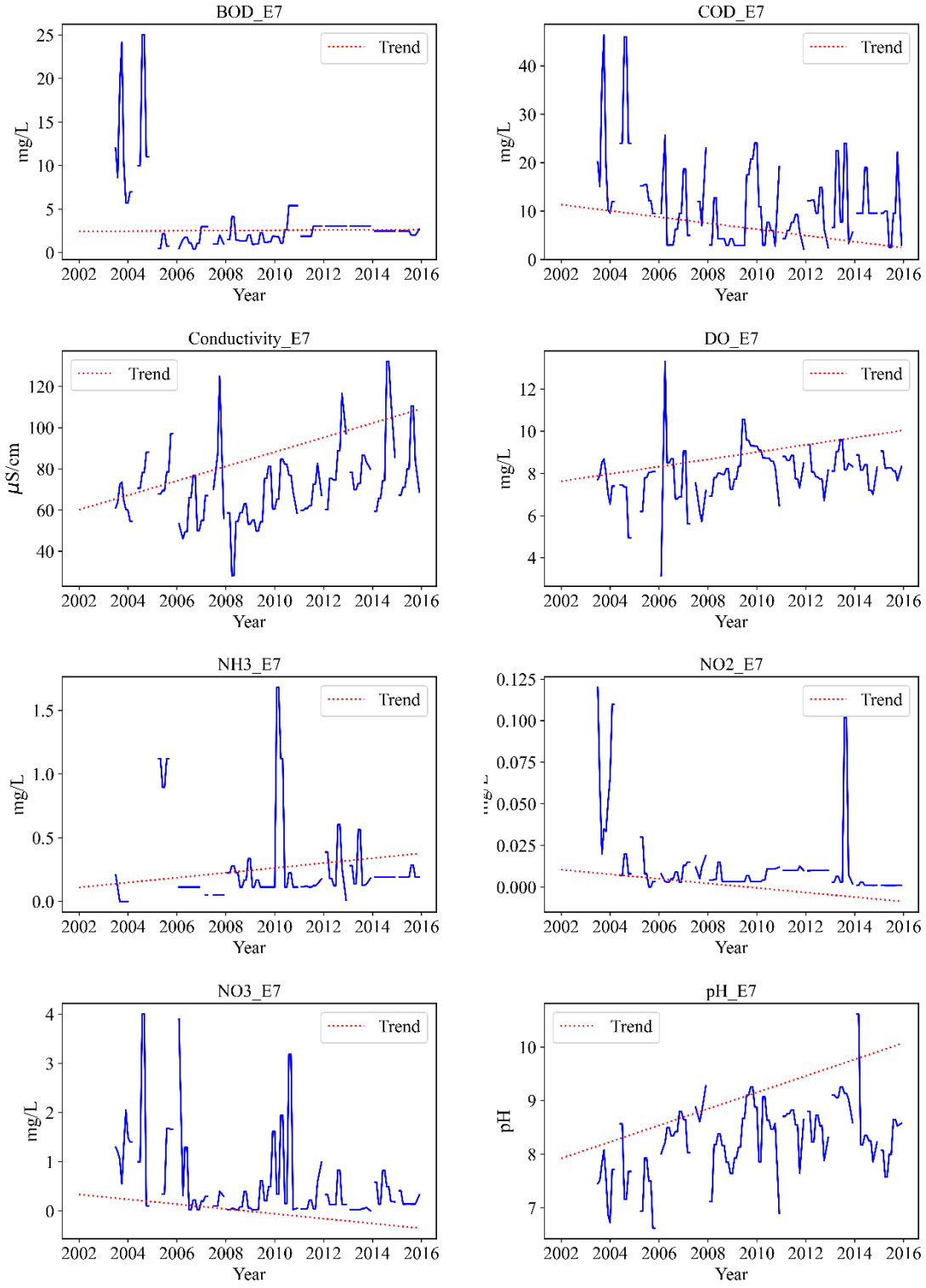
BOD_E7
Trend
mg/L
Year
COD_E7
Trend
mg/L
Year
Conductivity_E7
Trend
μS/cm
Year
DO_E7
Trend
mg/L
Year
NH3_E7
Trend
mg/L
Year
NO2_E7
Trend
Year
NO3_E7
Trend
mg/L
Year
pH_E7
Trend
pH
Year

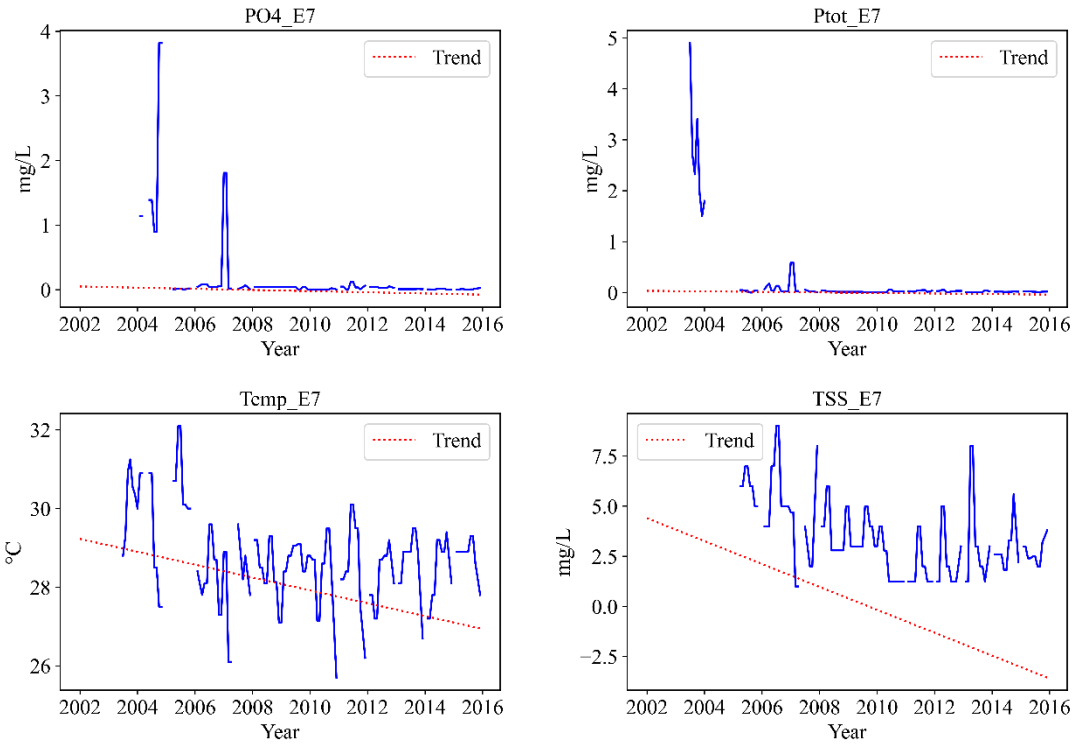

Fig. 1. Trend plots applying Mann-Kendall test

Correlations

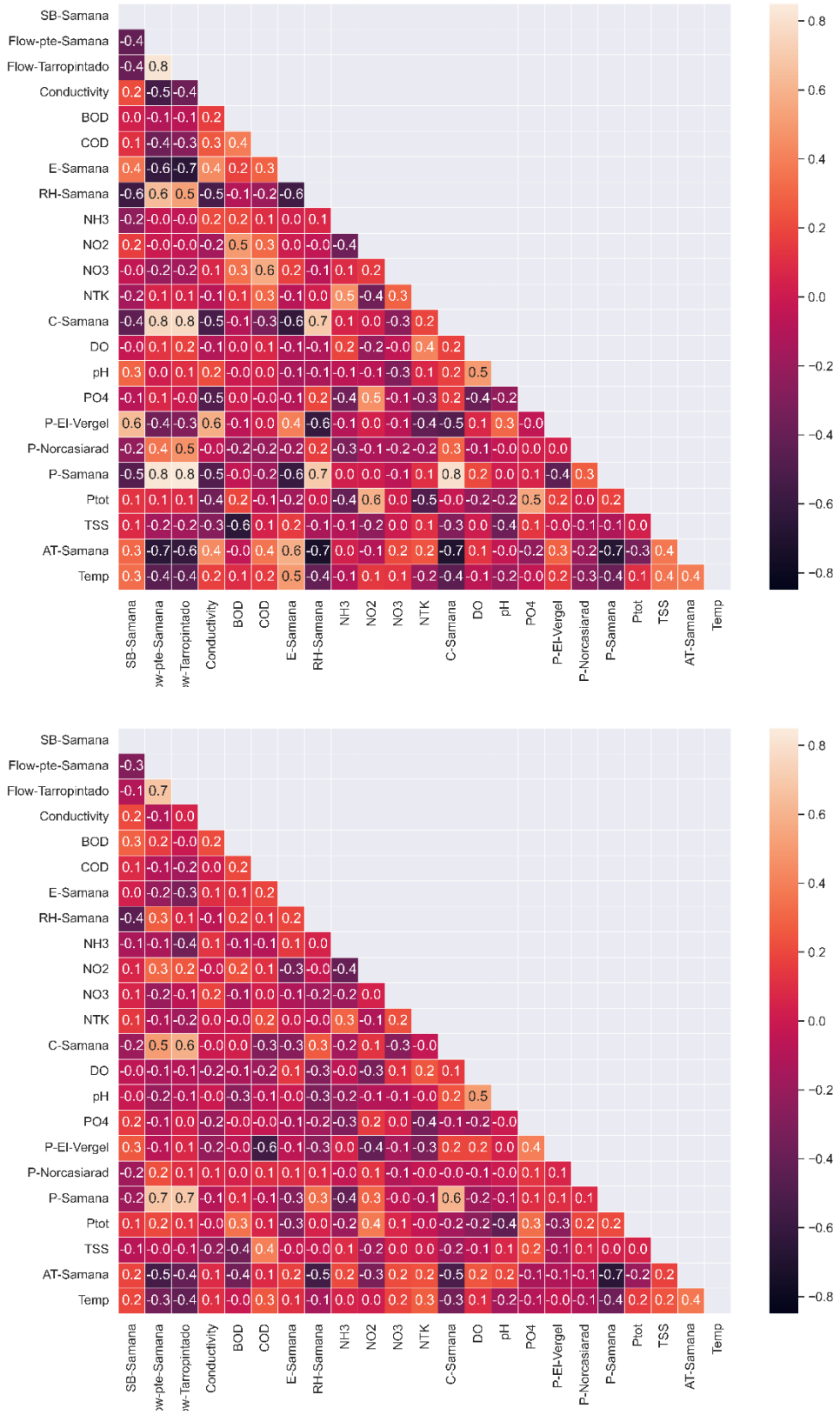

Fig. 2. Spearman correlation test results for station E7 during dry and wet season

Imputation results

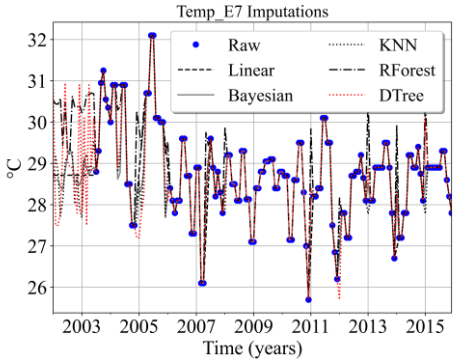

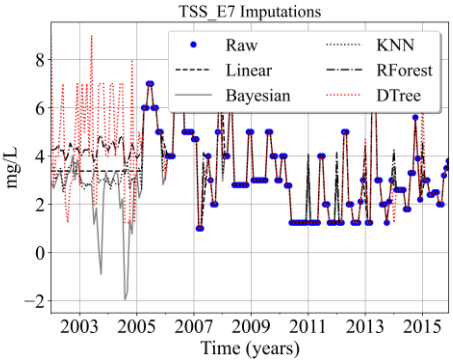

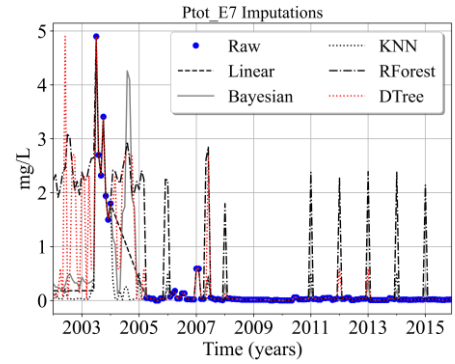

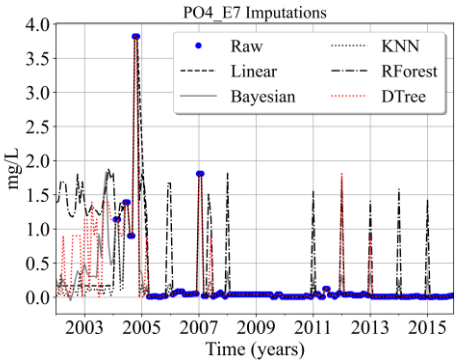

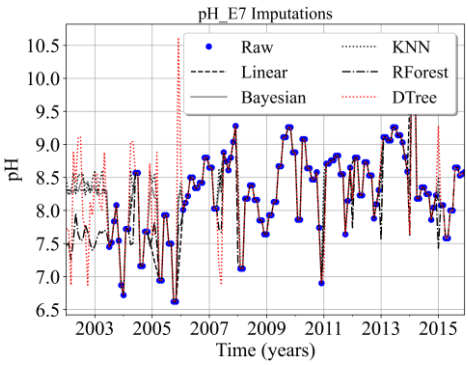

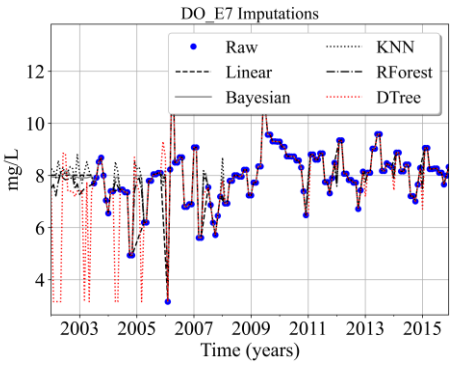

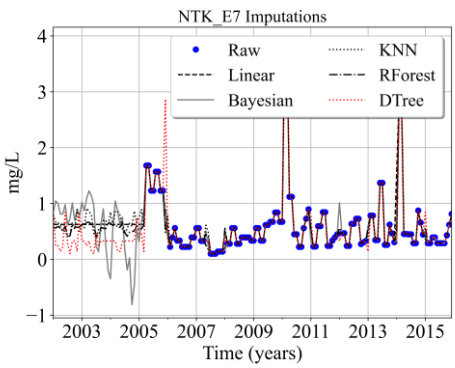

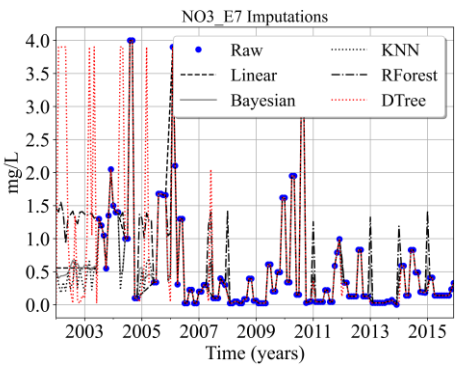

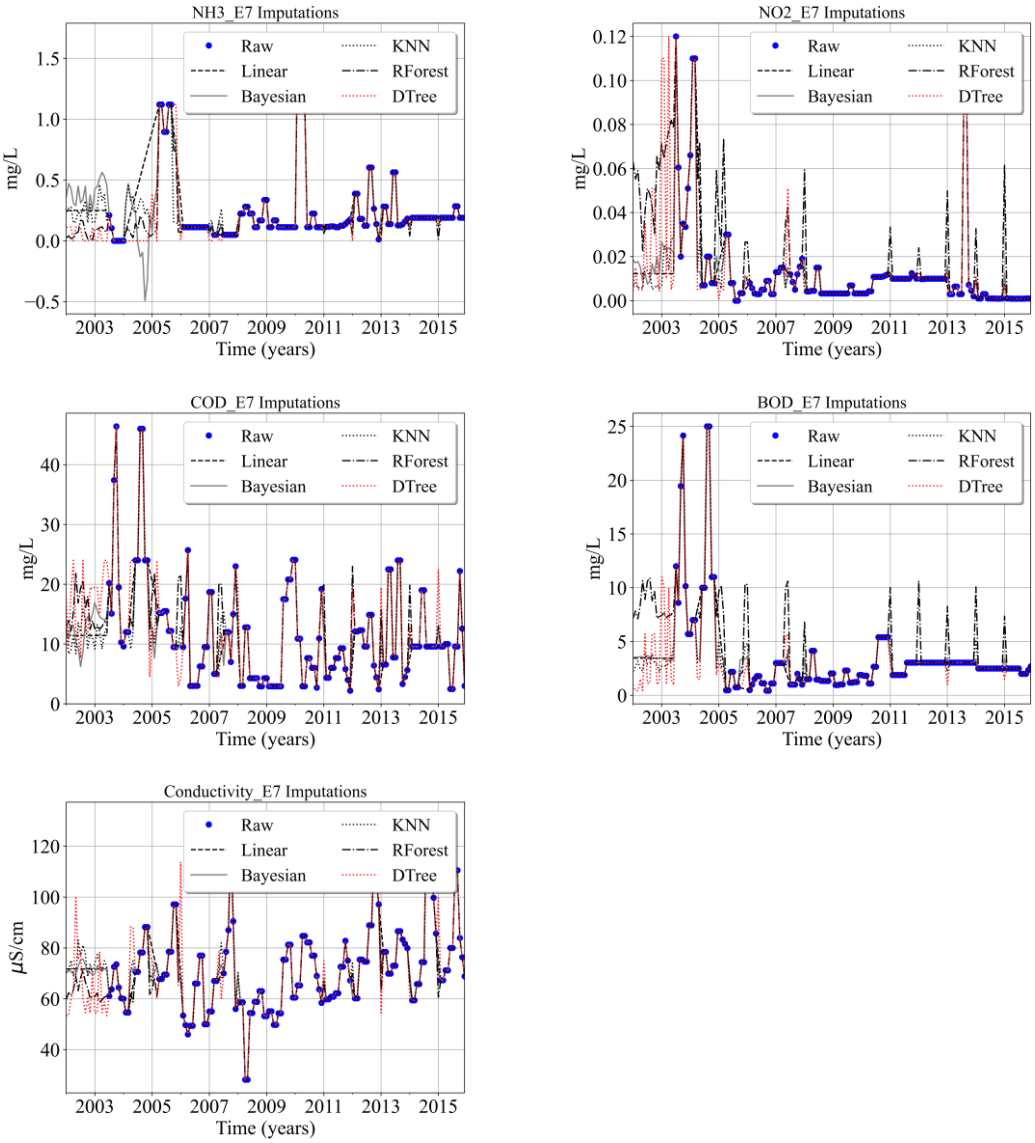

Fig.3. Graphical representation of the imputation techniques

Percentage of missing data

Conductivity_E3	29.17
BOD_E3	27.98
COD_E3	29.17
NH3_E3	32.74
NO2_E3	27.98
NO3_E3	27.98
NTK_E3	31.55
DO_E3	29.17
pH_E3	27.98
PO4_E3	27.98
Ptot_E3	32.74
TSS_E3	31.55
Temp_E3	27.98
Flow-pte-Samana	0.00
Conductivity_E7	20.24
BOD_E7	21.43
COD_E7	20.83
NH3_E7	27.38
NO2_E7	20.24
NO3_E7	21.43
NTK_E7	29.17
DO_E7	20.24
pH_E7	20.24
PO4_E7	24.40
Ptot_E7	25.00
TSS_E7	29.17
Temp_E7	20.24

B. Supplementary material to Chapter 3

This appendix provides the supplementary material to Chapter 3. For the numerical analysis of the telemac model, the following cases were run, in which the schematics and the mass losses in the system are verified.

Solvers and stability

Case	*Solver*	*Name*	*Preconditioning*		*Treatment of the Linear System*		*subroutine*	*time step*	*Simulation Duration*	*Rel error Vlm*	*Total Vlm Lost*	*Max Courant Num*	*Num Iteration*	*Stable*
1	2	Conjugate residual	Yes	Type=2	Not	N/A		0.1	1h:32m:29s	4.88E-09	1.6996	0.30787	23	yes
1B	2	Conjugate residual	Yes	Type=2	Yes	Type=2	rescjg	0.1	0h:35m:10s	-3.85E-10	-0.1341	0.30000	11	very
1CB	2	Conjugate residual	Not	N/A	Yes	Type=2		0.1	0h:50m:59s	8.25E-11	0.0288	0.30606	43	yes
2	7	Generalized Minimum Residual	Yes	Type=2	Not	N/A		0.1	1h:46m:26s	8.48E-09	2.9568	0.30000	16	yes
2B	7	Generalized Minimum Residual	Yes	Type=2	Yes	Type=2	gmres	0.1	0h:35m:10s	1.56E-11	0.0054	0.30606	4	very
2CB	7	Generalized Minimum Residual	Not	N/A	Yes	Type=2		0.1	1h:11m:14s	1.25E-10	0.0437	0.30606	35	yes
3	1	Conjugate Gradient	Yes	Type=2	Not	N/A		0.01	9h:18m:8s	-2.55E-08	-8.9044	0.03078	7	very
3B	1	Conjugate Gradient	Yes	Type=2	Yes	Type=2	gracjg	0.1	1h:30m:31s	-2.49E-10	-0.0870	0.30606	11	very
3CB	1	Conjugate Gradient	Not	N/A	Yes	Type=2		0.1	1h:49m:45s	7.64E-11	0.0266	0.30606	48	yes
4	3	Normal equation	Yes	Type=2	Not	N/A		0.1	4h:17m:21s	-2.88E-07	-100.5434	0.30786	65	failed
4B	3	Normal equation	Yes	Type=2	Yes	Type=2	equnor	0.1	0h:46m:36s	-2.59E-10	-0.0902	0.30606	30	yes
4CB	3	Normal equation	Not	N/A	Yes	Type=2		0.1	5h:47m:17s	1.60E-10	0.0557	0.30606	551	No
5B	4	minimal error	Yes	Type=2	Yes	Type=2	errmin	0.1	0h:47m:36s	3.66E-10	0.1277	0.30606	39	failed
6	6	CGS stabilized	Yes	Type=2	Not	N/A		0.1	2h:09m:19s	-9.59E-11	-0.0334	0.30786	24	failed
6B	6	CGS stabilized	Yes	Type=2	Yes	Type=2	cgstab	0.1	0h:35m:28s	9.40E-11	0.0328	0.30606	7	very
6CB	6	CGS stabilized	Not	N/A	Yes	Type=2		0.1	0h:58m:16s	9.43E-11	0.0329	0.30606	34	failed
7B	9	MUMPS direct solver	Yes	Type=2	Yes	Type=2	pre4_mumps	0.1	CASE NOT YET IMPLEMENTED FOR MUMPS					failed

2D configuration

Simulation	*Cases*	*Z Planes*	*Solver*	*Duration*	*time*	*Vol add by source*	*Mass Loss*	*Vol loss*	*Observation*
Comp1	2D Cte visc	1	GMRES	200	0h01m:22s	-4.40E+03		-3.98E-04	Source, Hydrostatic
Comp2	2D K-e	1	GMRES	200	0h02m:20s	-4.40E+03		5.26E-03	Source, Hydrostatic
Miel 1	3D Cte visc	2	GMRES	200	0h02m:13s		-4.40E+03		Source, Hydrostatic
Miel 2	3D K-e	2	GMRES	200	0h05m:34s		-4.40E+03		Source, Hydrostatic

Simulation	*Cases*	*Z Planes*	*Solver*	*Duration*	*time*	*Vol add by source*	*Mass Loss*	*Vol loss*	*Observation*
Miel 2A	3D K-e	2	GMRES	200	0h05m:23s		3.09E-04		No source, Hydrostatic
Miel 3	3D K-e	2	GMRES	1000	0h26m:29s		1.55E-03		No source, Hydrostatic
Miel 3A	3D K-e	2	GMRES	1000	0h27m:05s		-2.20E+04		Source, Hydrostatic
Miel 4	3D K-e	10	GMRES	100	0h33m:01s		-2.20E+03		Source, Hydrostatic
Miel T	3D K-e T	10	GMRES	100	3h23m:45s		-2.30E+04		Source, Non Hydrost
Miel T1	3D K-e T	10	GMRES	1000			-2.30E+04		Source, Non Hydrost

Verification velocities profiles

The orders of magnitude of the velocities at different points of the reservoir are verified, as well as the stability of the profiles in the different velocity components.

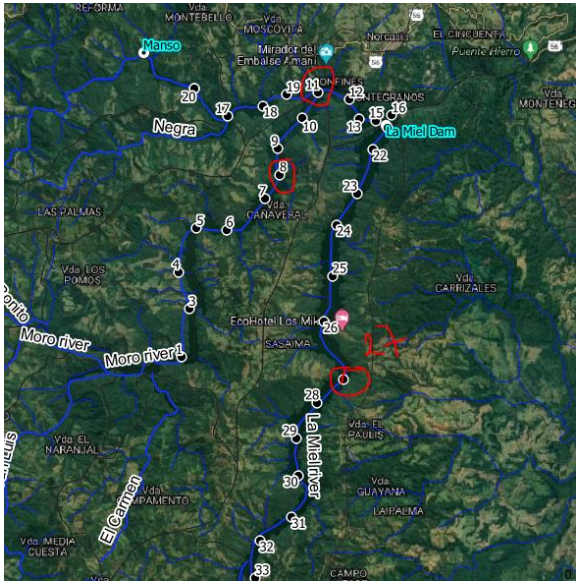

P8

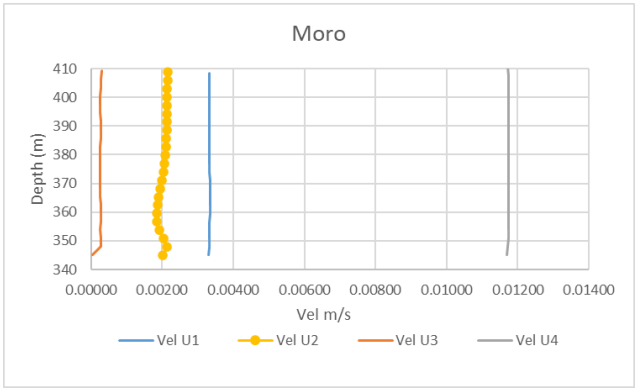
Moro
Depth (m)
410
400
390
380
370
360
350
340
0.00000 0.00200 0.00400 0.00600 0.00800 0.01000 0.01200 0.01400
Vel m/s
Vel U1
Vel U2
Vel U3
Vel U4

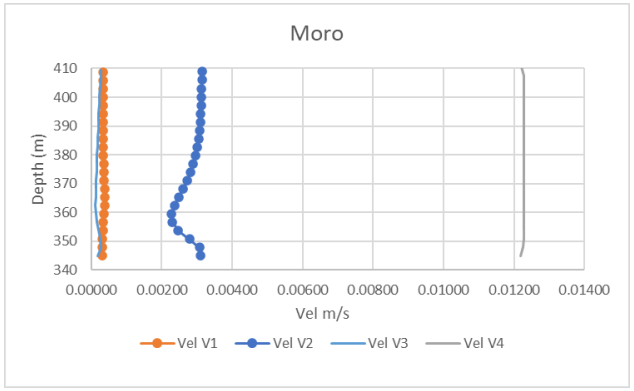
Moro
Depth (m)
410
400
390
380
370
360
350
340
0.00000 0.00200 0.00400 0.00600 0.00800 0.01000 0.01200 0.01400
Vel m/s
Vel V1
Vel V2
Vel V3
Vel V4

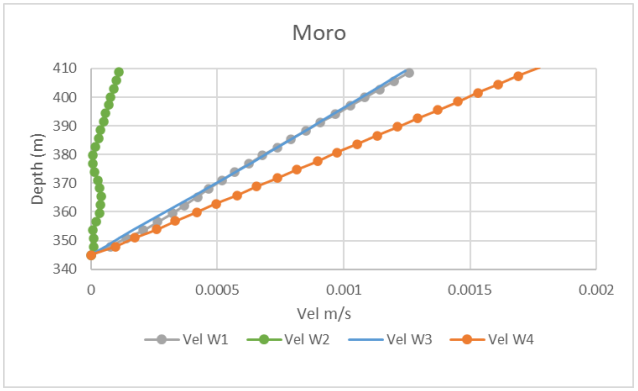
Moro
Depth (m)
410
400
390
380
370
360
350
340
0 0.0005 0.001 0.0015 0.002
Vel m/s
Vel W1
Vel W2
Vel W3
Vel W4

P11

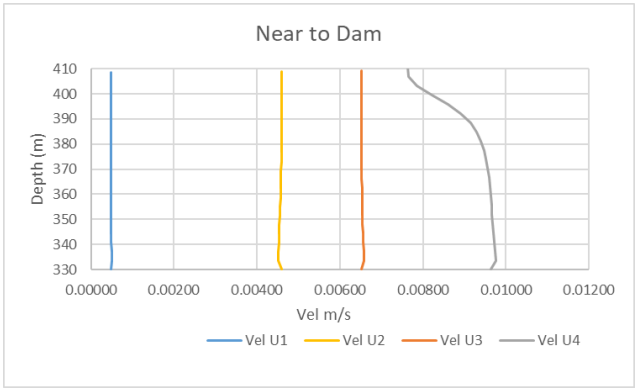
Near to Dam
Depth (m)
410
400
390
380
370
360
350
340
330
0.00000 0.00200 0.00400 0.00600 0.00800 0.01000 0.01200
Vel m/s
Vel U1
Vel U2
Vel U3
Vel U4

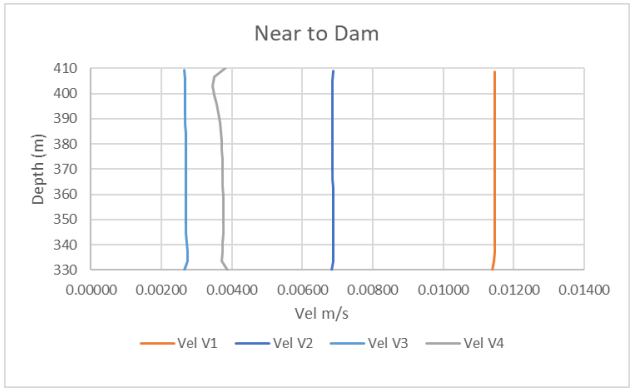
Near to Dam
Depth (m)
410
400
390
380
370
360
350
340
330
0.00000 0.00200 0.00400 0.00600 0.00800 0.01000 0.01200 0.01400
Vel m/s
Vel V1
Vel V2
Vel V3
Vel V4

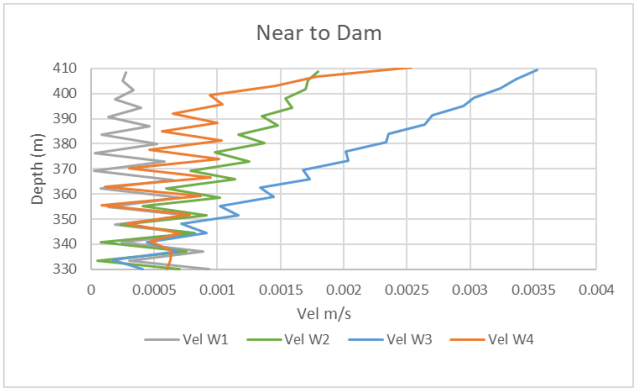
Near to Dam
Depth (m)
410
400
390
380
370
360
350
340
330
0 0.0005 0.001 0.0015 0.002 0.0025 0.003 0.0035 0.004
Vel m/s
Vel W1
Vel W2
Vel W3
Vel W4

P27

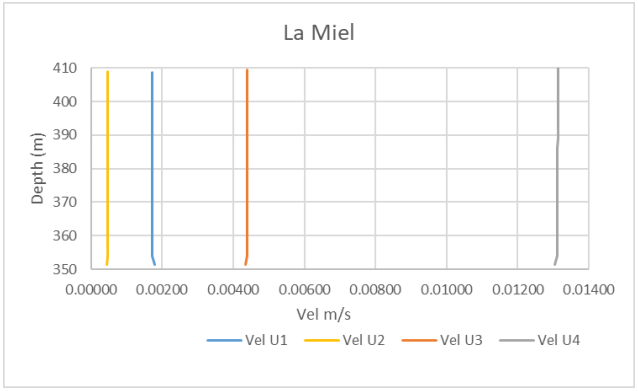
La Miel
Depth (m)
410
400
390
380
370
360
350
0.00000 0.00200 0.00400 0.00600 0.00800 0.01000 0.01200 0.01400
Vel m/s
Vel U1 Vel U2 Vel U3 Vel U4

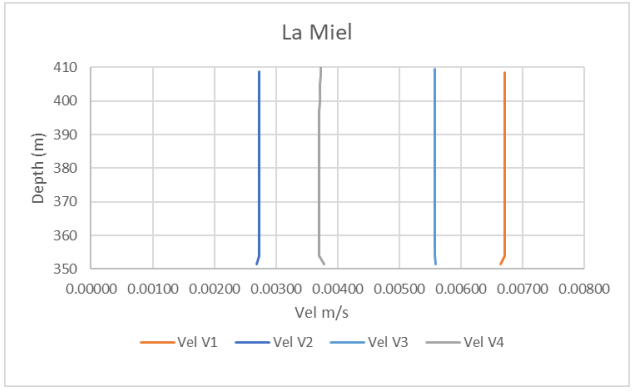
La Miel
Depth (m)
410
400
390
380
370
360
350
0.00000 0.00100 0.00200 0.00300 0.00400 0.00500 0.00600 0.00700 0.00800
Vel m/s
Vel V1 Vel V2 Vel V3 Vel V4

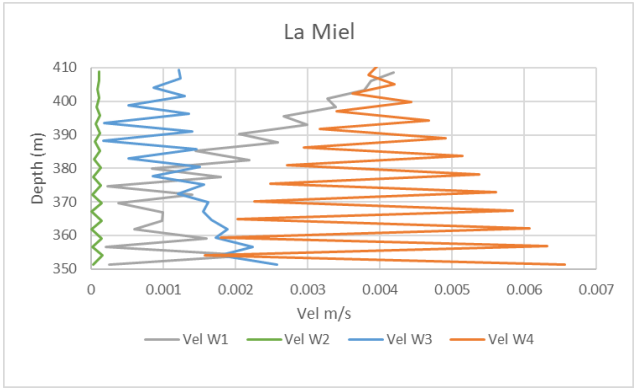
La Miel
Depth (m)
410
400
390
380
370
360
350
0 0.001 0.002 0.003 0.004 0.005 0.006 0.007
Vel m/s
Vel W1 Vel W2 Vel W3 Vel W4

P16

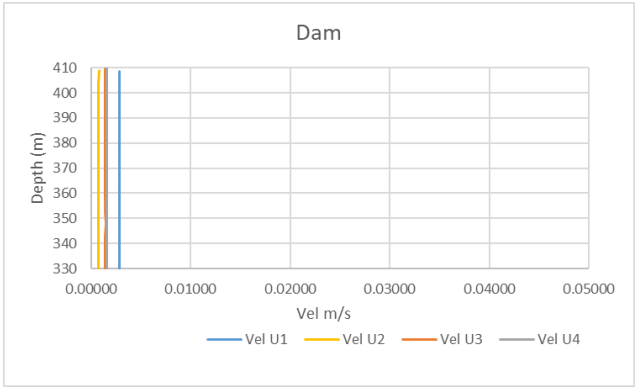
Dam
Depth (m)
410
400
390
380
370
360
350
340
330
0.00000 0.01000 0.02000 0.03000 0.04000 0.05000
Vel m/s
Vel U1 Vel U2 Vel U3 Vel U4

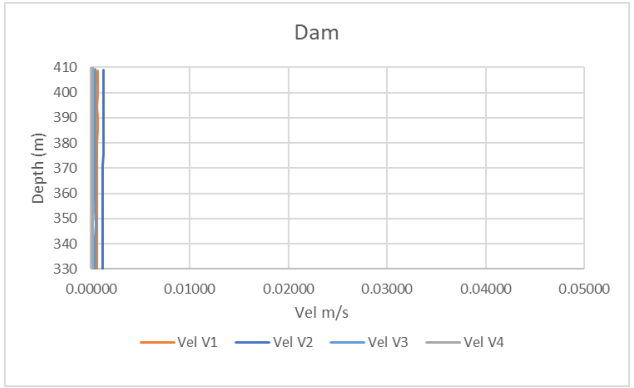
Dam
Depth (m)
410
400
390
380
370
360
350
340
330
0.00000 0.01000 0.02000 0.03000 0.04000 0.05000
Vel m/s
Vel V1 Vel V2 Vel V3 Vel V4

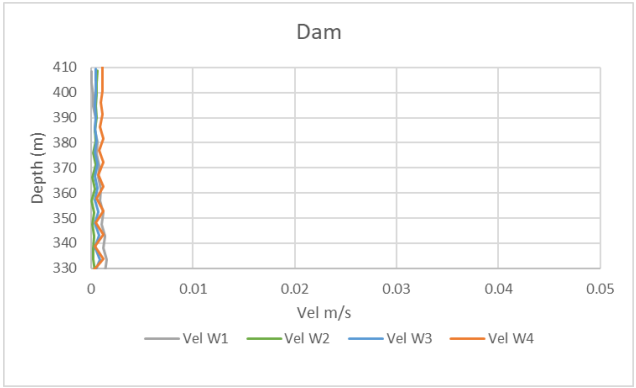
Dam
Depth (m)
410
400
390
380
370
360
350
340
330
0 0.01 0.02 0.03 0.04 0.05
Vel m/s
Vel W1 Vel W2 Vel W3 Vel W4

Steady state conditions hydrodynamics model

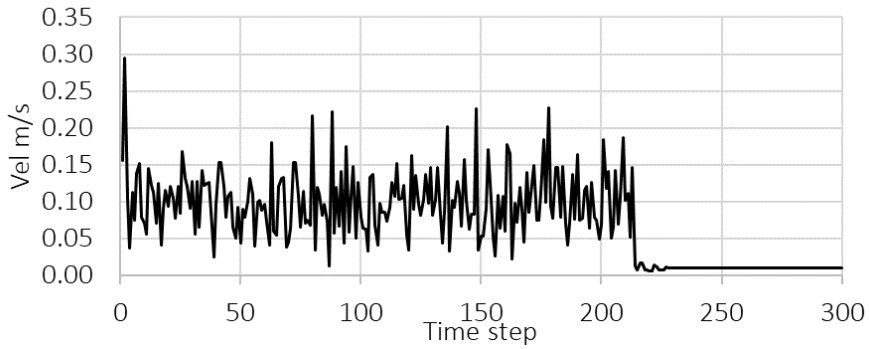

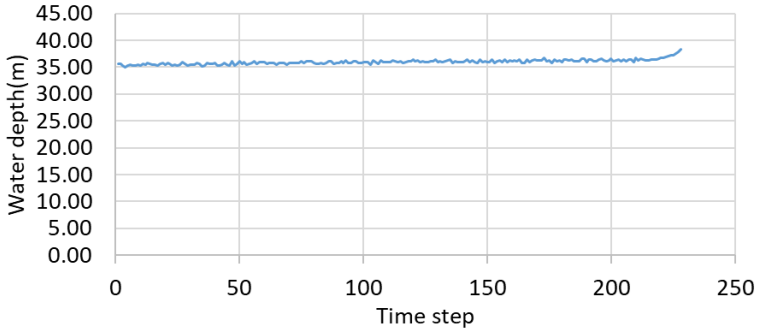

Time step configuration

Case	*Mesh*	*BC*	*HYD*	*Durations*	*time step*	*procesors*	*OBS*	*Time*		*TURB MOD*
MIEL1	Geo3	BC7 NO fraguas	Mesh 1	6000	0.1	24	Vel more instable 300m/s	NA	NA	Cte viscosity
MIEL2	Geo4	BC7 NO fraguas	Mesh 1	6000	0.1	24	Vel instable 300m/s	NA	NA	Cte viscosity
MIEL3	Geo4	BC5 more points	Mesh 1	2000	0.1	24	Vel instable 300m/s	NA	NA	Cte viscosity
MIEL4	Geo4	BC8 less points	Mesh 1	12000	0.1	24	Vel less instable 8m/s	18 hours		Cte viscosity
MIEL5	Geo4	BC8	Mesh 1	12000	0.1	24	Vel less instable 10m/s	18 hours	Continuity Miel4	Cte viscosity
MIEL6	Geo6	BC8	Mesh 1	21600	0.1	24	Vel stable 4m/s	1day16 h	Continuity Miel5	Cte viscosity
MIEL7	Geo6	BC8	Mesh 1	28800	0.1	24	Vel stable 4m/s	2day10 h	Continuity Miel6	Cte viscosity

Case	*Mesh*	*BC*	*HYD*	*Durations*	*time step*	*procesors*	*OBS*	*Time*		*TURB MOD*
MIEL8	Geo6	BC8	Mesh 1	28800	0.1	24	Vel stable 4.16m/s	2day5 h	Continuity Miel7	Cte viscosity
MIEL9	Geo6	BC8	Mesh 1	28800	0.1	24	Vel stable 4.16m/s		Continuity Miel8	Cte viscosity
MIEL9A	Geo6	BC8	Mesh 1	3600	1	24	Vel stable 4.68m/s	41mint		Cte viscosity
MIEL9B	Geo6	BC8	Mesh 1	3600	5 y 4	24	fail	NA		Cte viscosity
MIEL9B	Geo6	BC8	Mesh 1	3600	3	24		16mint		Cte viscosity
MIEL9C	Geo7	BC8	Mesh 1	3600	3	24	Vel stable 3.68m/s	15 mint	Continuity Miel8	Cte viscosity
MIEL9D	Geo7	BC8	Mesh 1	3600	5	24	fail	NA		Cte viscosity
MIEL9E	Geo7	BC8	Mesh 1	3600	2 y 1.5	24		22 mint		Cte viscosity
MIEL9E	Geo7	BC8	Mesh 1	28800	1	32		5 h		Cte viscosity
MIEL10	Geo7	BC8	Mesh 1	28800	1	32	Vel stable 3.6m/s	5 h	Continuity Miel9E1	Cte viscosity
MIEL11	Geo8	BC8	Mesh 1	57600	1	32	Vel stable 3.9m/s	9h:32m	Continuity Miel10E	Cte viscosity
MIEL12	Geo8	BC8	Mesh 1	108000	1	32	Vel stable 4.23m/s	18h	Continuity Miel11	Cte viscosity
MIEL13	Geo8	BC8	Mesh 1	216000	1	32	Vel stable 4.23m/s	1 days 12h	Continuity Miel12	Cte viscosity

Thermal cases configuration

For the numerical analysis of the thermal model, the following cases were run to verify the response of the thermal distribution to different configurations.

Simulation	*Case*	*Z Planes/ Mesh*	*Stratific*	*Duration*	*time*	*Mass Loss*	*Mass Loss Tracer*	*Setup*
Test case with hydro alone, and not dry zones	v8_1	10 Mesh1	N/A	1000	0h28m:05s	-9.32E-12	NA	Mesh 1, Turb H=4 Turb V=2 ML=5 Hydrodynamics, with Non Hydro assumption, advection =4
Test case with hydro alone, and not dry zones	v8_2	10 Mesh2	N/A	1000	0h26m:42s	-1.33E-11	NA	Mesh 2 IDEM
Test case with hydro alone, and not dry zones	v8_3	10 Mesh3		1000	0h45m:35s	-2.33E-12	NA	Mesh 3 IDEM
Test case with hydro and temperature	v8_4	10 Mesh2	yes	1000	0h56m:26s	-2.05E-11	97.59	IDEM, Initial conditions for temperature
Test case with hydro and temperature	v8_5	10 Mesh3	yes	1000	1h18m:29s	-4.19E-11	-55.41738	IDEM, Initial conditions for temperature
Test case with hydro, temperature	v8_6	10 Mesh3	yes	1000	0h56m:13s	-4.19E-11	-55.41738	IDEM, Initial conditions for temperature
Test case with hydro, temperature and waqtel (heat exchange at the atmosphere=0)	v8_7	10 Mesh1	yes	1000	2h22m:52s	-2.17E-11	(-564.7374)(-564.7374)	IDEM,compling sigma, not initial conditions
Test case with hydro, temperature and waqtel (heat exchange at the atmosphere=1)	v8_8	10 Mesh1	yes	1000	2.83E-12	-2.17E-11	(-0.154602)(-0.16988)	IDEM, PRESCRIBED TRACERS VALUES 0;18;0;0
Test case with hydro, temperature and waqtel (heat exchange at the atmosphere=2)	v8_9	10 Mesh1	yes	1000				IDEM, PRESCRIBED TRACERS VALUES 0;18;0;0
Test case with hydro, temperature and waqtel (heat exchange at the atmosphere=2)	v8_10	10 Mesh1	yes	1000	1h45m:35s	5.11E-12	(-0.11219)(-0.15944)	IDEM, PRESCRIBED TRACERS VALUES 18;18;0;0
Test case with hydro, temperature and waqtel (heat exchange at the atmosphere=2)	v8_11	10 Mesh2	yes	1000	2h14m:32s	-1.56E-11	(-161.1631)(-493.2484)	IDEM, PRESCRIBED TRACERS VALUES 18;18;0;0
Test case with hydro, temperature and waqtel (heat exchange at the atmosphere=2)	v8_12	10 Mesh3	yes	1000	2h11m:33s	-1.56E-11	(-161.1631)(-807.0426)	IDEM, PRESCRIBED TRACERS VALUES 18;18;0;0, Initial conditions
Test case with hydro, temperature and waqtel (heat exchange at the atmosphere=2)	v8_13	11 Mesh3						IDEM, PRESCRIBED TRACERS VALUES 18;18 Initial conditions

Thermic sensitivity analysis

Cases	*Duration*	*Time*	*Results*	*Observations*
0. Example defualt values	1200 seg	24 mint		
1. Less planes = 20 instaed 40	1200 seg	5 mint	Change thermocline	
2. without PPE	1200 seg	15 mint	No changes thermocline	
3. without Boussinesq	1200 seg	25 mint	Change thermocline	Wrong results
4. without WIND, processor 4	1200 seg	11 mint	Change thermocline	No mixing
5. with BC temp 26 only 2 points	1200 seg	31 mint	Change thermocline	
5B. with BC temp 100 more points	1200 seg	FAIL	Change thermocline	
5A. with BC temp 50 more points	1200 seg	17 mint	Change thermocline	
6. duration=21600	21600 seg	8 horas	Change thermocline	
7. Hor turbulence model k-e coef = 0 Y 0.01	1200 seg	17 mint	No changes thermocline	
8. Hor turbulence model k-e coef =1E-6	1200 seg	23 mint	Change thermocline	
9. Hor turbulence model smagorisky	1200 seg	13 mint	No changes thermocline	
10. Hor y vert turbulence model spalart	1200 seg	48 min	FAIL	
11. Hor turbulence model k-w coef = 0 Y 0.01	1200 seg	22 mint	No changes thermocline	
12. Vert turbulence model k-e coef = 0 Y 0.01	1200 seg	20 mint	No changes thermocline	
13. Ver turbulence model k-e coef =1E-6	1200 seg	15 mint	Change thermocline	
14. Vert turbulence model mixing leght prandt	1200 seg	12 mint	Change thermocline	
15. Ver turbulence model smagorisky	1200 seg	14 mint	No changes thermocline	
16. Ver turbulence model k-w	1200 seg	20 mint	Change thermocline	
17. COEFF. OF WIND INFLUENCE =0	1200 seg	11 mint	No changes thermocline	
18. friction coef , LAW= 3, COEF= 60	1200 seg	11 mint	No changes thermocline	
19 Coupled WAQTEL thermic, meteo	1200 seg	20 mint	Change thermocline	
20 Coupled WAQTEL meteo data only wind, meteo cero	1200 seg	21 mint	Change thermocline	
21 Coupled WAQTEL meteo data only wind, ray	1200 seg	22 mint	Change thermocline	
22 Coupled WAQTEL meteo data 0.0017	1200 seg	23 mint	Change thermocline	
23 Coupled WAQTEL meteo data 0.0035	1200 seg	24 mint	Change thermocline	
24 Coupled WAQTEL meteo data exchange =1	1200 seg	17 mint	Change thermocline	

C. Supplementary material to Chapter 4

This appendix provides the supplementary material to Chapter 4. Details of the model used to describe periphyton growth.

Periphyton biomass growth processes

When the resulting net growth rate or the difference between growth and removal rates is positive, biomass is gained (accumulated); when it is negative, biomass is lost. The challenge of the model is to describe and quantify the effects of each term in Equation 12 well enough to predict biomass with an acceptable level of precision. Therefore, the factors that mediate the growth of the periphyton and the associated processes will be described.

$$GPer = \mu max.\varphi T.\varphi I.\varphi N.\varphi P$$

Where,

μmax maximum growth rate of the periphyton. (1 day)

Effects of temperature and light (φT.φI)

Temperature and solar radiation drive photosynthesis and respiration, processes that convert carbon dioxide, nutrients, water, and energy in the form of sunlight into oxygen, biomass, and energy. Optimal light and temperature conditions can dampen or inhibit photosynthesis (DeNicola 1996, Hill 1996). In the model developed here, these effects are quantified by the following equations.

$$\varphi T = \frac{0.851}{P_S^B} * 1.066^{(T-20)}$$

Equation 1 effect of temperature on the periphyton

T: It is the water temperature °C

Ps: maximum rate of photosynthesis (1 /day)

In situations where the light conditions at the water surface (incident irradiance) are not approximately equal to those at the surface and bottom of the bed, the attenuation of light through the water column is simulated using Beer's Law- Lambert (Kuczynski, 2019), as in this case, therefore.

$$Ih = Io \exp(-keh)$$

Equation 2 flux density of solar radiation

Ih: the flux density of solar radiation at the bottom of the bed (W /m^2)

Io: the flux density of solar radiation at the surface. (W /m^2)

h: is the depth of the water from the surface to the bottom of the bed (m)

Ke: Extinction coefficient (m^{-1})

The extinction coefficient is calculated using the following expression, which was an empirical relationship of the data from the measurements on the Cauca River.

$$ke = (0.62 * Turbiedad)^{0.5} - 0.08$$

Equation 3 flux density of solar radiation

φI or limitation by light represents the effect of sunlight on algae growth; this dimensionless parameter ranges from 0 to 1.

$$\varphi I = \frac{1}{keh} \log\left(\frac{Io + \sqrt{IK^2 + Io^2}}{Ih + \sqrt{IK^2 + Ih^2}}\right)$$

Equation 4 Effect of light on the periphyton
IK is a calibration parameter (W / m^2), of *n* order of magnitude of 100.

Effect by nutrients (φN)

Assuming optimal light, temperature, and physical conditions, Periphyton growth is controlled by nutrient availability (Kuczynski, 2019).

The macronutrients that most frequently limit the growth of periphyton in freshwater and marine systems are bioavailable nitrogen (N) and phosphorus (P). Increases in freshwater N or P loads due to anthropogenic activity often result in eutrophication, that is, increases in periphyton production (Biggs 1988, 2000a, b) and large diurnal variations in DO and pH negatively affecting sensitive organisms). The bioavailable forms of N and P are dissolved inorganic N (DIN, that is, the sum of nitrate, NO3-N, nitrite, NO2-N and ammonium, NH4-N) and dissolved reactive P (DRP, mainly phosphates, PO4- P). Dissolved organic N and P fractions (DON and DOP) and N and P particles (PN and PP) can also become bioavailable when degraded by bacteria and enzymes (e.g., Hu et al. 2016, Lambert et al. .2015). The rates at which some forms of these nutrients are absorbed are variable, and nutrient absorption has been studied extensively in North America (Kilroy et al. 2018), but not in Colombia.

In this model, nutrient limitation (ϕN) will be quantified using Michaelis-Menten kinetics in which the growth rate increases with increasing concentration of a limiting nutrient (model input.

$$\varphi N = min\left(\frac{[PO4]}{KP + [PO4]}, \frac{[NO3]}{KN + [NO3]}\right)$$

Equation x Effect of nutrients on the periphyton

= semi-saturation constant of phosphate (mg / l) (around 0.005 mgP / l),
KN = semi-saturation constant of nitrate (mg / l) (around 0.03 mgN / l).

Periphyton Carry capacity (φP)

The term carrying capacity can be used to implicitly model the limitation of periphyton productivity by nutrient delivery through the biofilm. Said biomass limiting mechanism mathematically slows down exponential growth by decreasing the growth rate to zero with an expression that depends on a defined maximum sustainable biomass (Pmax), which results in an S-shaped biomass versus time curve. with a horizontal asymptote at Pmax. Conceptually, the carrying capacity is the maximum sustainable biomass in the system given the limitations related to biomass (Kuczynski, 2019).

It is possible to use the carrying capacity as a logistic growth saturation model, as shown below.
φP or carry capacity

$$Pper = \frac{Pmax - PER}{Pmax}$$

There is another model called a modified logistic model

$$Pper = 1 - \left(\frac{PER}{Pmax}\right)^2$$

And finally, the expression of Michaelis-Menten:

$$Pper = \frac{PER}{Kper + Per}$$

er: semi-saturation constant
Pmax: maximum carrying capacity of the periphyton in the ecosystem
Per: Periphyton concentration

With the field data, several experiments were carried out, and the model that best suited the Cauca

River was logistic growth.

$$Pper = \frac{Pmax - PER}{Pmax}$$

Equation xx effect of carrying capacity on the periphyton

Periphyton biomass loss processes

As previously introduced, the processes of periphyton loss or removal in this model include respiration R, grazing G, flow-induced shedding (shedding) S, and mortality and autogenous shedding M. Therefore, the factors that mediate the loss of biomass of the periphyton and the associated processes will be described.

Periphyton losses: Ls = R + G + S + Mper

Respiration (R)

Respiration occurs in both light and dark conditions and can be modeled as the sum of basal and light-enhanced respiration (eg, Canale and Auer 1982, Tomlinson et al. 2010). The magnitude of the respiratory rate is mediated by temperature and, in the case of light-enhanced respiration, by light. The maximum respiration rate is a model calibration coefficient.

$$R = Kr * (1.024)^{T-20}$$

Equation xx Effect of respiration on the periphyton

R periphyton respiration (1 / day)

Kr: Periphyton respiration rate (day ^{1})

Per: Periphyton concentration (μg C /m^2)

Grazing (G)

Grazing is a peripheral biomass loss mechanism (Feminella and Hawkins 1995; Steinman 1996; Hillebrand et al. 2002) that can limit a periphyton accumulation event even in the presence of high concentrations of nutrients (for example, Biggs et al. 1998, sturt et al. 2011).

In this model, it is taken with a coefficient, G grazing (day^{-1}), which is calibrated.

Detachment (S)

S is the process that represents the detachment of the periphyton, with optimal light and temperature, the productivity of the periphyton is controlled by hydraulics and geomorphology. Detachment is often modeled as a function of biomass, flow, velocity, or shear stress.

For the case study, detachment is modeled using a quadratic expression with a model adjustment parameter and the water velocity, considering the shear stress on the periphyton biofilm according to the following expression.

$$S = (d1 * PER) - (U - up)^2$$

Equation xx Effect of detachment on the periphyton

U: average speed in the study section (m /s)

up: shear speed (m /s)

d1: constant (s^2 /m^2)

Mortality

As the periphyton thickens and ages, its structural integrity is compromised. Autogenous shedding occurs when the periphyton biofilm thickens, ages, breaks down and falls off. This is the main mechanism of mortality of the periphyton.

In this model, Mper mortality is taken as a rate (day^{-1}) which is calibrated.

References

Abdi, H., & Williams, L. J. (2010). Principal Component Analysis. 2.

Agostinho, AA., Pelicice, FM., & Gomes, LC. (2008). Dams and the fish fauna of the Neotropical region: impacts and management related to diversity and fisheries. Brazilian Journal of Biology, 68(4 suppl), 1119–1132. https://doi.org/10.1590/S1519-69842008000500019

Alsaleh, M., & Abdul-Rahim, A. S. (2021a). Moving toward sustainable environment: The effects of hydropower industry on water quality in EU economies. Energy and Environment. https://doi.org/10.1177/0958305X211039452

Alsaleh, M., & Abdul-Rahim, A. S. (2021b). Do global competitiveness factors effects the industry sustainability practices? Evidence from European hydropower industry. Journal of Cleaner Production, 310, 127492. https://doi.org/10.1016/j.jclepro.2021.127492

Alzate-Gómez, J.-Andrea., Aguirre-Duran, Cesar., Escobar-Vargas, J. Alberto., Montoya-Jaramillo, L.-Javier., & Piedrahita-Escobar, C.-C. (2023). On the Spatial-Temporal Behavior, and on the Relationship Between Water Quality and Hydrometeorological Information to Predict Dissolved Oxygen in Tropical Reservoirs. Case Study: La Miel, Hydropower Dam. Air, Soil and Water Research, 16, 1–15. https://doi.org/10.1177/11786221221150189

Amorim, C. A., Dantas, Ê. W., & Moura, A. do N. (2020). Modeling cyanobacterial blooms in tropical reservoirs: The role of physicochemical variables and trophic interactions. Science of The Total Environment, 744, 140659. https://doi.org/10.1016/J.SCITOTENV.2020.140659

Amorim, L. F., Martins, J. R. S., Nogueira, F. F., Silva, F. P., Duarte, B. P. S., Magalhães, A. A. B., & Vinçon-Leite, B. (2021a). Hydrodynamic and ecological 3D modeling in tropical lakes. SN Applied Sciences, 3(4). https://doi.org/10.1007/s42452-021-04272-6

Amorim, L. F., Martins, J. R. S., Nogueira, F. F., Silva, F. P., Duarte, B. P. S., Magalhães, A. A. B., & Vinçon-Leite, B. (2021b). Hydrodynamic and ecological 3D modeling in tropical lakes. SN Applied Sciences, 3(4), 444. https://doi.org/10.1007/s42452-021-04272-6

Anderson Jr., J. D., Degroote, J., Degrez, G., Dick, E., Grundmann, R., & Vierendeels, J. (2009). Computational fluid dynamics: an introduction. Berlin: Springer.

Angelotti, N. ;, Vinçon-Leite, B. ;, & Carmigniani, R. (2021). Hydrodynamic modelling for early warning of sanitary risks in open swimming waters. https://hdl.handle.net/20.500.11970/108309

Aptech. (2021, July 26). Retrieved from https://www.aptech.com/blog/introduction-to-the-fundamentals-of-vector-autoregressive-models/

Azadi, F., Ashofteh, P.-S., & Loáiciga, H. A. (2019). Reservoir Water-Quality Projections

under Climate-Change Conditions. Water Resources Management, 33(1), 401–421. https://doi.org/10.1007/s11269-018-2109-z

Bach, P. M., Wolfgang, R., Mikkelsen, P. S., McCarthy, D. T., & Deletic, A. (2014). A critical review of integrated urban water modelling e Urban drainage and beyond. Environmental Modelling & Software, 88-107.

Barbarossa, V., Schmitt, R. J. P., Huijbregts, M. A. J., Zarfl, C., King, H., & Schipper, A. M. (2020). Impacts of current and future large dams on the geographic range connectivity of freshwater fish worldwide. Proceedings of the National Academy of Sciences of the United States of America, 117(7), 3648–3655. https://doi.org/10.1073/pnas.1912776117

Basso, M., Mateus, M., Ramos, T. B., & Vieira, D. C. S. (2021). Potential Post-Fire Impacts on a Water Supply Reservoir: An Integrated Watershed-Reservoir Approach. Frontiers in Environmental Science, 9. https://doi.org/10.3389/fenvs.2021.684703

Bedri, Z., Bruen, M., Dowley, A., & Masterson, B. (2013). Environmental consequences of a power plant shut-down: A three-dimensional water quality model of Dublin Bay. Marine Pollution Bulletin, 71(1–2), 117–128. https://doi.org/10.1016/j.marpolbul.2013.03.025

Boehrer, B., & Schultze, M. (2009). Density Stratification and Stability. In Encyclopedia of Inland Waters (pp. 583–593). Elsevier. https://doi.org/10.1016/B978-012370626-3.00077-6

Branco, C. W. C., Leal, J. J. F., Huszar, V. L. de M., Farias, D. da S., Saint'Pierre, T. D., Sousa-Filho, I. F., de Palermo, E. F. de A., Guarino, A. W. S., Gomes, A. R., & Kozlowsky-Suzuki, B. (2019). New lake in a changing world: the construction and filling of a small hydropower reservoir in the tropics (Rio de Janeiro, Brazil). Environmental Science and Pollution Research, 26(35), 36007–36022. https://doi.org/10.1007/s11356-019-06665-y

Brito, D., Ramos, T. B., Gonçalves, M. C., Morais, M., & Neves, R. (2018). Integrated modelling for water quality management in a eutrophic reservoir in south eastern Portugal. Environmental Earth Sciences (.

Calamita, E. (2020). Modelling the effects of large dams on water quality in tropical rivers [ETH Zürich]. https://doi.org/10.3929/ethz-b-000476521

Chai, T., & Draxler, R. R. (2014). Root mean square error (RMSE) or mean absolute error (MAE)? – Arguments against avoiding RMSE in the literature. Geoscientific Model Development, 7(3), 1247–1250. https://doi.org/10.5194/gmd-7-1247-2014

Chapman, D. (2021). Water Quality Assessments. CRC Press. https://doi.org/10.1201/9781003062103

Chen, K., Chen, H., Zhou, C., Huang, Y., Qi, X., Shen, R., Liu, F., Zuo, M., Zou, X., Wang, J., Zhang, Y., Chen, D., Chen, X., Deng, Y., & Ren, H. (2020). Comparative analysis of surface water quality prediction performance and identification of key water parameters using different machine learning models based on big data. Water Research, 171. https://doi.org/10.1016/j.watres.2019.115454

Chen, K., Zhou, H. C., Huang, Y., & Qi, X. (2020). Comparative analysis of surface water quality prediction performance and identification of key water parameters using different machine learning models based on big data. Water Research.

Chen, P., Li, L., & Zhang, H. (2015). Spatio-temporal variations and source apportionment of water pollution in Danjiangkou Reservoir Basin, Central China. Water (Switzerland), 7(6), 2591–2611. https://doi.org/10.3390/w7062591

Chen, Y. (2020). Numerical study of the hydrodynamics of Fangar Bay by using unstructured meshes - Analysis of diffusion by using salinity as a tracer with the TELEMAC 3D model.

Chuo, M., Ma, J., Liu, D., & Yang, Z. (2019). Effects of the impounding process during the flood season on algal blooms in Xiangxi Bay in the Three Gorges Reservoir, China. Ecological Modelling, 392, 236–249. https://doi.org/10.1016/j.ecolmodel.2018.11.017

Cooper, A. J. ;, & Spearman, J. (2017). Validation of a TELEMAC-3D model of a seamount (Vol. 17). www.opentelemac.org

Costi, J., Forster, A., Marques, W. C., Duarte, R. F. ;, & Arigony-Neto, J. (2019). Application of the TELEMAC-3D to simulate flooding and hydrodynamic patterns of Southern Brazilian wetlands. XXVIth TELEMAC-MASCARET User Conference.

Crowe, S. A., O'Neill, A. H., Katsev, S., Hehanussa, P., Haffner, G. D., Sundby, B., Mucci, A., & Fowle, D. A. (2008). The biogeochemistry of tropical lakes: A case study from Lake Matano, Indonesia. Limnology and Oceanography, 53(1), 319–331. https://doi.org/10.4319/lo.2008.53.1.0319

Curtarelli, M. P. ; A. E. H. ; R. C. D. ; S. J. L. (2013). Modeling the effects of cold front passages on the heat fluxes and thermal structure of a tropical hydroelectric reservoir. Hydrology & Earth System Sciences Discussions, 10, 8467–8850.

da Silva, M. C., de Paula Kirinus, E., Bendô, A. R. R., Marques, W. C., Vargas, M. M., Leite, L. R., Junior, O. O. M., & Pertille, J. (2021). Dynamic modeling of effluent dispersion on Mangueira bay — Patos Lagoon (Brazil). Regional Studies in Marine Science, 41. https://doi.org/10.1016/j.rsma.2020.101544

Dalu, T., & Wasserman, R. J. (2018). Cyanobacteria dynamics in a small tropical reservoir: Understanding spatio-temporal variability and influence of environmental variables. Science of the Total Environment, 643, 835–841. https://doi.org/10.1016/j.scitotenv.2018.06.256

de Oliveira, K. L., Ramos, R. L., Oliveira, S. C., & Christofaro, C. (2021). Spatial variability of surface water quality in a large Brazilian semiarid reservoir and its main tributaries. Environmental Monitoring and Assessment, 193(7). https://doi.org/10.1007/s10661-021-09194-9

Dongliang, L., Keqiang, L., Shengkang, L., & Guohong, L. W. (2016). A coastal three-dimensional water quality model of nitrogen in Jiaozhou Bay linking field experiments with modelling. Marine Pollution Bulletin.

Dordoni, M., Seewald, M., Rinke, K., Schmidmeier, J., & Barth, J. A. C. (2022). Novel evaluations of sources and sinks of dissolved oxygen via stable isotopes in lentic water bodies. Science of the Total Environment, 838. https://doi.org/10.1016/j.scitotenv.2022.156541

Duarte, B. ;, Amorim, L. ;, Martins, J. R., & Bernardino, J. C. (2021). Comparison of 1D and 3D hydrodynamic models on the assessement of climate change scenarios impact over a small tropical lake. EGU General Assembly 2021.

Elçi, Ş. (2008). Effects of thermal stratification and mixing on reservoir water quality. Limnology, 9(2), 135–142. https://doi.org/10.1007/s10201-008-0240-x

Fu, L., & Gan Wang, Y. (2012). Statistical Tools for Analyzing Water Quality Data. In Water Quality Monitoring and Assessment (pp. 143–168). InTech. https://doi.org/10.5772/35228

Gaeta, M. G., Samaras, A. G., & Archetti, R. (2020a). Numerical investigation of thermal discharge to coastal areas: A case study in South Italy. Environmental Modelling & Software, 124, 104596. https://doi.org/10.1016/j.envsoft.2019.104596

Gaeta, M. G., Samaras, A. G., & Archetti, R. (2020b). Numerical investigation of thermal discharge to coastal areas: A case study in South Italy. Environmental Modelling and Software, 124. https://doi.org/10.1016/j.envsoft.2019.104596

Gaeta, M. G., Samaras, A., Archetti, R., & Lamberti, A. (2015). NUMERICAL INVESTIGATION OF THERMAL DISCHARGE TO COASTAL AREAS USING TELEMAC-3D: A CASE STUDY FOR SOUTH ITALY. https://www.researchgate.net/publication/279758154

González, R. G. (2019). encyclopedia.com (CENGAGE). Retrieved from https://www.encyclopedia.com/social-sciences/applied-and-social-sciences-magazines/vector-autoregression#B

Gooseff, M. N., Strzepek, K., & Chapra, S. C. (2005). Modeling the potential effects of climate change on water temperature downstream of a shallow reservoir, lower madison river, MT. Climatic Change, 68(3), 331–353. https://doi.org/10.1007/s10584-005-9076-0

Goudsmit, G.-H., Burchard, H., Peeters, F., & Wüest, A. (2002). Application of k-ϵ turbulence models to enclosed basins: The role of internal seiches. Journal of Geophysical Research: Oceans, 107(C12), 23-1-23–13. https://doi.org/10.1029/2001JC000954

Gyimah, R. A. A., Gyamfi, C., Anornu, G. K., Karikari, A. Y., & Tsyawo, F. W. (2021). Multivariate statistical analysis of water quality of the Densu River, Ghana. International Journal of River Basin Management, 19(2), 189–199. https://doi.org/10.1080/15715124.2020.1803337

Halini Baharim, N., Ismail, R., & Hanif Omar, M. (2011). Effects of Thermal Stratification on the Concentration of Iron and Manganese in a Tropical Water Supply Reservoir. In Sains Malaysiana (Vol. 40, Issue 8).

Hernandez M, O. E. (2014). Development of a highly resolved 3-D computational model for applications in water quality and ecosystems. thesis, University of Iowa.

Hervouet, J. (2007). Hydrodynamics of Free Surface Flows. Wiley. https://doi.org/10.1002/9780470319628

Hinkelmann, R. (2005). Efficient Numerical Methods and Information-Processing Techniques for Modeling Hydro- and Environmental Systems (Vol. 21). Springer-Verlag. https://doi.org/10.1007/3-540-32379-1

Honek, D., Caletka, M., & Šulc Michalková, M. (2018). Retrospective analysis of published hydrological researches: models, trends and geographical aspects over the last two decades of hydrological modelling. Geographical Journal, 287-313.

Hurvich, C. M., & Tsai, C. L. (1991). Bias of the corrected aic criterion for underfitted regression and time series models. Biometrika, 78(3), 499–509. https://doi.org/10.1093/biomet/78.3.499

Huszar, V. L. M., Caraco, N. F., Roland, F., & Cole, J. (2006). Nutrient–chlorophyll relationships in tropical–subtropical lakes: do temperate models fit? Biogeochemistry, 79(1–2), 239–250. https://doi.org/10.1007/s10533-006-9007-9

Hwang, S.-J., Kim, K., Park, C., Seo, W., Choi, B.-G., Eum, H. S., Park, M.-H., Noh, H. R., Sim, Y. B., & Shin, J.-K. (2016). Hydro-meteorological Effects on Water Quality Variability in Paldang Reservoir, Confluent Area of the South-Han River-North-Han River-Gyeongan Stream, Korea. Korean Journal of Ecology and Environment, 49(4), 354–374. https://doi.org/10.11614/KSL.2016.49.4.354

Jerves-Cobo, R., Forio, M. A. E., Lock, K., Van Butsel, J., Pauta, G., Cisneros, F., Nopens, I., & Goethals, P. L. M. (2020). Biological water quality in tropical rivers during dry and rainy seasons: A model-based analysis. Ecological Indicators, 108(September 2019), 105769. https://doi.org/10.1016/j.ecolind.2019.105769

Jiang, B., Wang, F., & Ni, G. (2018). Heating Impact of a Tropical Reservoir on Downstream Water Temperature: A Case Study of the Jinghong Dam on the Lancang River. Water, 10(7), 951. https://doi.org/10.3390/w10070951

Justin-Brochet, E., Pham, C.-T. ;, & Vidal-Hurtado, J. ; (2021). Recent improvements for the Berre lagoon modelling with TELEMAC-3D. https://hdl.handle.net/20.500.11970/108311

Katsev, S., Crowe, S. A., Mucci, A., Sundby, B., Nomosatryo, S., Haffner, G. D., & Fowle, D. A. (2010). Mixing and its effects on biogeochemistry in the persistently stratified, deep, tropical Lake Matano, Indonesia. Limnology and Oceanography, 55(2), 763–776. https://doi.org/10.4319/lo.2010.55.2.0763

Killingtveit, Å. (2019). Hydropower. In Managing Global Warming (pp. 265–315). Elsevier. https://doi.org/10.1016/B978-0-12-814104-5.00008-9

Knapen, R., Janssen, S., Roosenschoon, O., Verweij, P., de Winter, W., Uiterwijk, M., & Wien, J.-E. (2013). Evaluating OpenMI as a model integration platform across disciplines. Environmental Modelling & Software, 274-282.

Kopmann, R., & Markofsky, M. (2000). Three-dimensional water quality modelling with TELEMAC-3D. Hydrological Processes, 14(13), 2279–2292. https://doi.org/10.1002/1099-1085(200009)14:13<2279::AID-HYP28>3.0.CO;2-7

Kumar Shrestha, N., Tolessa Leta, O., & Bauwens, W. (2017). Development of RWQM1-based integrated water quality model in OpenMI with application to the River Zenne, Belgium. Hydrological Sciences Journal, 774-799.

Labaj, A. L., Michelutti, N., & Smol, J. P. (2018). Annual stratification patterns in tropical mountain lakes reflect altered thermal regimes in response to climate change. Fundamental and Applied Limnology, 191(4), 267–275. https://doi.org/10.1127/fal/2018/1151

Laval, B. E., Imberger, J., & Findikakis, A. N. (2005). Dynamics of a large tropical lake: Lake Maracaibo. Aquatic Sciences, 67(3), 337–349. https://doi.org/10.1007/s00027-005-0778-1

Leta, O. T., Griensven, A. v., Shrestha, N. K., & Bauwens, W. (2014). Integrated Water Quality Modelling of the River Zenne (Belgium) Using OpenMI. Advances in Hydroinformatics.

Lewis, W. M. (1996). Tropical lakes: how latitude makes a difference.

Li, J., Yang, W., Li, W., Mu, L., & Jin, Z. (2018). Coupled hydrodynamic and water quality simulation of algal bloom in the Three Gorges Reservoir, China. Ecological Engineering, 97-108.

Li, X. zhu, Chen, Z. jun, Fan, X. chao, & Cheng, Z. jiang. (2018). Hydropower development situation and prospects in China. Renewable and Sustainable Energy Reviews, 82(August 2017), 232–239. https://doi.org/10.1016/j.rser.2017.08.090

Li, X., Guo, M., Duan, X., Zhao, J., Hua, Y., Zhou, Y., Liu, G., & Dionysiou, D. D. (2019). Distribution of organic phosphorus species in sediment profiles of shallow lakes and its effect on photo-release of phosphate during sediment resuspension. https://doi.org/10.1016/j.envint.2019.104916

Ligier, P.-Louis., & Okumura, Non. (2019). Three-dimensional hydrodynamic modelling in a bay of the Lake Mälaren to assess environmental impacts from a cooling and heating power plant production. XXVIth TELEMAC-MASCARET User Conference.

Lindenschmidt, K.-E., Carr, M. K., Sadeghian, A., & Morales-Marin, L. (2019). CE-QUAL-W2 model of dam outflow elevation impact on temperature, dissolved oxygen and nutrients in a reservoir. Scientific Data, 6(1), 312. https://doi.org/10.1038/s41597-019-0316-y

Lindim, C., Pinho, J. L., & Vieira, J. M. P. (2011). Analysis of spatial and temporal patterns in a large reservoir using water quality and hydrodynamic modeling. Ecological Modelling, 222(14), 2485–2494. https://doi.org/10.1016/j.ecolmodel.2010.07.019

Ling, T. Y., Gerunsin, N., Soo, C. L., Nyanti, L., Sim, S. F., & Grinang, J. (2017). Seasonal changes and spatial variation in water quality of a large young tropical reservoir and its downstream river. Journal of Chemistry, 2017. https://doi.org/10.1155/2017/8153246

Liqoarobby, R., Sunardi, Suparman, Y., & Fadilah, K. (2021). Aqueous Systems of Dissolved Oxygen in Reservoir. E3S Web of Conferences, 249, 03015. https://doi.org/10.1051/e3sconf/202124903015

Lisboa, P. V., & Fernandes, E. H. (2015). Anthropogenic influence on the sedimentary dynamics of a sand spit bar, Patos Lagoon Estuary, RS, Brazil. Revista de Gestão Costeira Integrada, 35–46. https://doi.org/10.5894/rgci541

Liu, C., Pan, C., Chang, Y., & Luo, M. (2021). An integrated autoregressive model for predicting water quality dynamics and its application in Yongding River. Ecological Indicators, 133. https://doi.org/10.1016/j.ecolind.2021.108354

Liu, C., Pan, C., Chang, Y., & Luo, M. (2021). An integrated autoregressive model for predicting water quality dynamics and its application in Yongding River. Ecological Indicators.

Lliev, I., & Hadjinikolova, L. (2013). Seasonal and vertical dynamics of the water temperature and oxygen content in Kardzhali reservoir, Bulgaria. Agricultural Science and Technology. https://www.researchgate.net/publication/305781610

Lobato, T. C., Hauser-Davis, R. A., Oliveira, T. F., Silveira, A. M., Silva, H. A. N., Tavares, M. R. M., & Saraiva, A. C. F. (2015). Construction of a novel water quality index and quality indicator for reservoir water quality evaluation: A case study in the Amazon region. Journal of Hydrology, 522, 674–683. https://doi.org/10.1016/j.jhydrol.2015.01.021

Mamun, M., Kim, J. Y., & An, K. G. (2021). Multivariate statistical analysis of water quality and trophic state in an artificial dam reservoir. Water (Switzerland), 13(2). https://doi.org/10.3390/w13020186

Mamun, M., Lee, S. J., & An, K. G. (2018). Temporal and spatial variation of nutrients, suspended solids, and chlorophyll in Yeongsan watershed. Journal of Asia-Pacific Biodiversity, 11(2), 206–216. https://doi.org/10.1016/j.japb.2018.02.006

Marcé, R., Rodríguez-Arias, M. À., García, J. C., & Armengol, J. O. A. N. (2010). El Niño Southern Oscillation and climate trends impact reservoir water quality. Global Change Biology, 16(10), 2857–2865. https://doi.org/10.1111/j.1365-2486.2010.02163.x

Marín-Ramírez, A., Gómez-Giraldo, A., & Román-Botero, R. (2020). Seasonal variability of advective and atmospheric heat fluxes and mean temperature in a tropical Andean reservoir. Revista de La Academia Colombiana de Ciencias Exactas, Fisicas y Naturales, 44(171), 360–375. https://doi.org/10.18257/raccefyn.1081

Marques, É. T., Gunkel, G., & Sobral, M. C. (2019). Management of tropical river basins and reservoirs under water stress: Experiences from northeast Brazil. Environments - MDPI, 6(6).

https://doi.org/10.3390/environments6060062

Matta, E., Selge, F., Gunkel, G., & Hinkelmann, R. (2017). Three-dimensional modeling of wind- and temperature-induced flows in the Icó-Mandantes Bay, Itaparica Reservoir, NE Brazil. Water (Switzerland), 9(10). https://doi.org/10.3390/w9100772

Merkel, U. H. (2019). Thermal Stratification in Small Lakes with TELEMAC-3D: Showcase "Lake Monsterloch." XXVIth TELEMAC-MASCARET User Conference. https://doi.org/10.5281/zenodo.3611576

Mesquita, J. B. de F., Lima Neto, I. E., Raabe, A., & de Araújo, J. C. (2020). The influence of hydroclimatic conditions and water quality on evaporation rates of a tropical lake. Journal of Hydrology, 590, 125456. https://doi.org/10.1016/J.JHYDROL.2020.125456

Moloney, V., Karunarathna, H., Murray, T., Rutt, I., Everett, A., & Reeve, D. (2016). Investigation of wind and tidal forcing on stratified flows in Greenland fjords with TELEMAC-3D. European Journal of Computational Mechanics, 25(3), 249–272. https://doi.org/10.1080/17797179.2016.1191121

Nadarajah, S., Wijenayake, W. M. H. K., & Amarasinghe, U. S. (2019). Influence of hydrology on water quality and trophic state of irrigation reservoirs in Sri Lanka. Lakes and Reservoirs: Research and Management, 24(3), 287–298. https://doi.org/10.1111/lre.12283

Pajares, S., Merino-Ibarra, M., Macek, M., & Alcocer, J. (2017). Vertical and seasonal distribution of picoplankton and functional nitrogen genes in a high-altitude warm-monomictic tropical lake. Freshwater Biology, 62(7), 1180–1193. https://doi.org/10.1111/fwb.12935

Piccioni, F. ;, Vinçon-Leite, B. ;, Le, M.-H. ;, & Casenave. (2021). Aquatic ecological modelling with TELEMAC3D: performance of the ecological library AED2 in a natural ecosystem. https://hdl.handle.net/20.500.11970/108308

Pimenta, A. M., Albertoni, E. F., & Palma-Silva, C. (2012). Characterization of water quality in a small hydropower plant reservoir in southern Brazil. Lakes & Reservoirs: Science, Policy and Management for Sustainable Use, 17(4), 243–251. https://doi.org/10.1111/lre.12007

Plec, D. F., Silva, T. F. das G., Vinçon-Leite, B., & Nascimento, N. (2021). Thermal functioning of a tropical reservoir assessed through three-dimensional modelling and high-frequency monitoring. RBRH, 26. https://doi.org/10.1590/2318-0331.262120200150

Politano, M., Haque, M. M., & Weber, L. J. (2008a). A numerical study of the temperature dynamics at McNary Dam. Ecological Modelling, 212(3–4), 408–421. https://doi.org/10.1016/J.ECOLMODEL.2007.10.040

Politano, M., Haque, M. M., & Weber, L. J. (2008b). A numerical study of the temperature dynamics at McNary Dam. Ecological Modelling, 212(3–4), 408–421. https://doi.org/10.1016/J.ECOLMODEL.2007.10.040

Rajwa, A., Bialik, R. J., Karpiński, M., & Luks, B. (2014). Dissolved Oxygen in Rivers: Concepts and Measuring Techniques (pp. 337–350). https://doi.org/10.1007/978-3-319-07599-0_19

Rajwa-Kuligiewicz, A., Bialik, R. J., & Rowiński, P. M. (2015). Dissolved oxygen and water temperature dynamics in lowland rivers over various timescales. Journal of Hydrology and Hydromechanics, 63(4), 353–363. https://doi.org/10.1515/johh-2015-0041

Rangel, LM., Silva, LHS., Arcifa, MS., & Perticarrari, A. (2009). Driving forces of the diel distribution of phytoplankton functional groups in a shallow tropical lake (Lake Monte Alegre, Southeast Brazil). Brazilian Journal of Biology, 69(1), 75–85. https://doi.org/10.1590/S1519-69842009000100009

Rangel-Peraza, J. G., De Anda, J., González-Farias, F., & Erickson, D. (2009). Statistical assessment of water quality seasonality in large tropical reservoirs. Lakes and Reservoirs: Research and Management, 14(4), 315–323. https://doi.org/10.1111/j.1440-1770.2009.00412.x

Ranković, V., Radulović, J., Radojević, I., Ostojić, A., & Čomić, L. (2012). Prediction of dissolved oxygen in reservoirs using adaptive network-based fuzzy inference system. Journal of Hydroinformatics, 14(1), 167–179. https://doi.org/10.2166/hydro.2011.084

Ricardo, P., Medeiros, P., Cavalcante, G. H., Brandini, N., & Knoppers, B. A. (2016). Inter-annual variability on the water quality in the Lower São Francisco River (NE-Brazil) Variabilidade inter-anual na qualidade da água no Baixo Rio São Francisco (NE-Brasil). Original Article Acta Limnologica Brasiliensia, 28, 5. https://doi.org/10.1590/S2179-975X3515

Rueda, F., Moreno-Ostos, E., & Armengol, J. (2006). The residence time of river water in reservoirs. Ecological Modelling, 191(2), 260–274. https://doi.org/10.1016/j.ecolmodel.2005.04.030

Samal, N. R., Mazumdar, A., Jöhnk, K. D., & Peeters, F. (2009). Assessment of ecosystem health of tropical shallow waterbodies in eastern India using turbulence model. Aquatic Ecosystem Health & Management, 12(2), 215–225. https://doi.org/10.1080/14634980902908589

Sanz-RamoS, M., Amengual, A., Bladé, E., Romero, R., & Roux, H. (2018). Flood forecasting using a coupled hydrological and hydraulic model (based on FVM) and high resolution meteorological model. E3S Web of Conferences.

Scanlon, T. ;, Moreau, J. ;, & Stickland. (2020). A Hydrodynamic Model of the West Coast of Scotland with Coupled Sea Lice Dispersion. https://hdl.handle.net/20.500.11970/108307

Schober, P., Boer, C., & Schwarte, L. A. (2018). Correlation Coefficients: Appropriate Use and Interpretation. Anesthesia-Analgesia Research Society.

Scott Winton, R., Calamita, E., & Wehrli, B. (2019). Reviews and syntheses: Dams, water quality and tropical reservoir stratification. Biogeosciences, 16(8), 1657–1671. https://doi.org/10.5194/bg-16-1657-2019

Semensatto, D., Labuto, G., Zorzal-Almeida, S., & McRae, D. V. (2021). Spatio-temporal changes in water quality in the Guarapiranga reservoir (São Paulo, Brazil): insights from a long-term monitoring data series. Environmental Monitoring and Assessment, 193(7). https://doi.org/10.1007/s10661-021-09167-y

Shrestha, N. K., Leta, O. T., & Bauwens, W. (2017). Development of RWQM1-based integrated water quality model in OpenMI with application to the River Zenne, Belgium. Hydrological Sciences Journal, 774–799.

Silva, S. N., & Castillo, J. Á. del. (2021). An Approach of the Hydropower: Advantages and Impacts. A Review. Journal of Energy Research and Reviews, June, 10–20. https://doi.org/10.9734/jenrr/2021/v8i130201

Singh, V. P. (2018). Hydrologic modeling: progress and future directions. Geoscience Letters.

Smolders, S., Maximova, T., & Vanlede, J. (2015). Salinity in the 3D TELEMAC model Scaldis (the Scheldt Estuary): tracer diffusion, dispersion and numerical diffusion. https://www.researchgate.net/publication/282973633

Spear, R., & Hornberger, G. (1980). Eutrophication in Peel Inlet – II. Identification of critical uncertainties via generalized. Water Res, 43–49.

TELEMAC-3D. (2020). TELEMAC-3D User Manual Version v8p2.

Tessema, N., Kebede, A., & Yadeta, D. (2021). Modelling the effects of climate change on streamflow using climate and hydrological models: the case of the Kesem sub-basin of the Awash River basin, Ethiopia. International Journal of River Basin Management, 19(4), 469–480. https://doi.org/10.1080/15715124.2020.1755301

Vaidya, R. A., Molden, D. J., Shrestha, A. B., Wagle, N., & Tortajada, C. (2021). The role of hydropower in South Asia's energy future. International Journal of Water Resources Development, 37(3), 367–391. https://doi.org/10.1080/07900627.2021.1875809

Varol, M. (2020a). Spatio-temporal changes in surface water quality and sediment phosphorus content of a large reservoir in Turkey. Environmental Pollution, 259, 113860. https://doi.org/10.1016/j.envpol.2019.113860

Varol, M. (2020b). Use of water quality index and multivariate statistical methods for the evaluation of water quality of a stream affected by multiple stressors: A case study. Environmental Pollution, 266, 115417. https://doi.org/10.1016/j.envpol.2020.115417

Vega, A. S., Lizama, K., & Pastén, P. A. (2018). Water Quality: Trends and Challenges. In Water Policy in Chile (pp. 25–51). https://doi.org/10.1007/978-3-319-76702-4_3

Vilas, M. P., Marti, C. L., Oldham, C. E., & Hipsey, M. R. (2018). Macrophyte-induced thermal stratification in a shallow urban lake promotes conditions suitable for nitrogen-fixing cyanobacteria. Hydrobiologia, 806(1), 411–426. https://doi.org/10.1007/s10750-017-3376-z

Vilas, M., Marti, C. L., Oldham, C. E., & Hipsey, M. R. (2018). Macrophyte-induced thermal stratification in a shallow urban lake promotes. Hydrobiologia, 411–416.

Vinçon-Leite, B., & Casenave, C. (2019). Modelling eutrophication in lake ecosystems: A review. Science of the Total Environment, 2985–3001.

VOUK, I., MURPHY, E., CHURCH, I., PILECHI, A., & CORNETT, A. (2019). THREE-DIMENSIONAL MODELLING OF HYDRODYNAMICS AND THERMOSALINE CIRCULATION IN THE SAINT JOHN RIVER ESTUARY, CANADA. 38th IAHR World Congress - "Water: Connecting the World," 38, 1866–1875. https://doi.org/10.3850/38wc092019-0895

W. Gassman, P., M. R. Reyes, C. H. Green, & J. G. Arnold. « The Soil and Water Assessment Tool: Historical Development, Applications, and Future Research Directions ». Transactions of the ASABE 50, no 4 (2007): 1211 50. https://doi.org/10.13031/2013.23637.

WAQTEL, (2021). Technical manual Version v8p3. http://wiki.opentelemac.org/doku.php?id=documentation_v8p4r0. Accessed in June 2023.

Weirich, C. A., Robertson, D. M., & Miller, T. R. (2019). Physical, biogeochemical, and meteorological factors responsible for interannual changes in cyanobacterial community composition and biovolume over two decades in a eutrophic lake. Hydrobiologia, 828(1), 165–182. https://doi.org/10.1007/s10750-018-3810-x

Whitehead, P. G. (2016). Water Quality Modeling Review. Wiley StatsRef: Statistics Reference Online.

Williams, G. P. (1963). Heat transfer coefficients for natural water surfaces. International Association of Scientific Hydrology, 62, 203–212.

Woldeab, B., Beyene, A., Ambelu, A., Buffam, I., & Mereta, S. T. (2018). Seasonal and spatial variation of reservoir water quality in the southwest of Ethiopia. Environmental Monitoring and Assessment, 190(3). https://doi.org/10.1007/s10661-018-6527-4

Yang, P., Fong, D. A., Lo, E. Y. M., & Monismith, S. G. (2019). Circulation patterns in a shallow tropical reservoir: Observations and modeling. Journal of Hydro-Environment Research, 27, 75–86. https://doi.org/10.1016/J.JHER.2019.09.002

Yang, X., Yuan, J., Yue, F.-J., Li, S.-L., Wang, B., Mohinuzzaman, M., Liu, Y., Senesi, N., Lao, X., Li, L., Liu, C.-Q., Ellam, R. M., Vione, D., & Mostofa, M. G. (2020). New insights into mechanisms of sunlight-and dark-mediated high-temperature accelerated diurnal production-degradation of fluorescent DOM in lake waters. https://doi.org/10.1016/j.scitotenv.2020.143377

Yaseen, Z., Ehteram, M., Sharafati, A., Shahid, S., Al-Ansari, N., & El-Shafie, A. (2018). The Integration of Nature-Inspired Algorithms with Least Square Support Vector Regression Models: Application to Modeling River Dissolved Oxygen Concentration. Water, 10(9), 1124. https://doi.org/10.3390/w10091124

Yassen, Z. M., Ehteram, M., Sharafati, A., Shahid, S., Al-Ansari, N., & El-Shafie, A. (2018). The Integration of Nature-Inspired Algorithms with Least Square Support Vector Regression Models: Application to Modeling River Dissolved Oxygen Concentratio. Water.

Zarfl, C., Berlekamp, J., He, F., Jähnig, S. C., Darwall, W., & Tockner, K. (2019). Future large hydropower dams impact global freshwater megafauna. Scientific Reports, 9(1), 1–10. https://doi.org/10.1038/s41598-019-54980-8

Zarfl, C., Lumsdon, A. E., Berlekamp, J., Tydecks, L., & Tockner, K. (2015). A global boom in hydropower dam construction. Aquatic Sciences, 77(1), 161–170. https://doi.org/10.1007/s00027-014-0377-0

Zhang, H., Huang, G. H., Wang, D., Zhang, X., Li, G., An, C., . . . Nie, X. (2012). An integrated multi-level watershed-reservoir modeling, system for examining hydrological and biogeochemical processes in small prairie watersheds. water r e s e arch, 1207-1224.

Zhang, R., Luz, ǀ, Cuartas, A., Luiz, ǀ, De, V., Carvalho, C., Reis, K., Leal, D., Mendiondo, E. M., Abe, N., Birkinshaw, S., Guilherme, ǀ, Mohor, S., Seluchi, M. E., Carlos, ǀ, Nobre, A., Doutor, E., & Bondesan, A. (2018). Season-based rainfall-runoff modelling using the probability-distributed model (PDM) for large basins in southeastern Brazil. 32, 2217–2230. https://doi.org/10.1002/hyp.13154

Zhang, W., Wang, Y., Peng, H., Li, Y., Tang, & Benjamin Wu, K. (2009). A Coupled Water Quantity–Quality Model for Water Allocation Analysis. Water Resour Manage.

Zhang, Y., P. F., M. P., & Thorburn, P. J. (2019). Applying Multi-Layer Artificial Neural Network and Mutual Information to the Prediction of Trends in Dissolved Oxygen. Frontiers in Environmental Science .

Ziaie, R., Mohammadnezhad, B., Taheriyoun, M., Karimi, A., & Amiri, S. (2019). Evaluation of Thermal Stratification and Eutrophication in Zayandeh Roud Dam Reservoir Using Two-Dimensional CE-QUAL-W2 Model. Journal of Environmental Engineering, 145(6). https://doi.org/10.1061/(ASCE)EE.1943-7870.0001529

List of Publications

ISI Journal Papers: submitted or under review

1. Jorge Escobar-Vargas, Nathaly Triviño Leon, Jhonatan Rodríguez, Nelson Obregón Neira, Nicolás Escobar-Castañeda, Sergio Castiblanco-Ballesteros, **Juliana Alzate**, Andrés Vargas-Luna, Juan Diego Giraldo-Osorio, Daniel Castillo, Sebastian Restrepo, Carlos Rivera, Saul Prada, Úrsula Jaramillo, María Constanza Rojas, Marcelo Barros, Ángela Zapata, Alejandra Neira, Mauricio Gonzalez, Felipe Peña-Heredia. A methodology for the development of integrated modelling tools to simulate socio-ecological systems.
2. **Juliana A. Alzate G**., Carlos A. Rivera-Rondón, Angela Zapata, Sergio A. Castiblanco, Alejandra Neira, Lina Triana, Nathaly Triviño, Jorge Escobar-Vargas, Saul Prada-Pedreros, Nelson Obregón. A model to describe the effects of low flow on benthic algae and nutrients in the Cauca River (Colombia)

ISI Journal Papers: published or accepted.

3. **Alzate-Gómez, J.-Andrea**., Aguirre-Duran, Cesar., Escobar-Vargas, J. Alberto., Montoya-Jaramillo, L.-Javier., & Piedrahita-Escobar, C.-C. (2023). On the Spatial-Temporal Behavior, and on the Relationship Between Water Quality and Hydrometeorological Information to Predict Dissolved Oxygen in Tropical Reservoirs. Case Study: La Miel, Hydropower Dam. Air, Soil and Water Research, 16, 1–15. https://doi.org/10.1177/11786221221150189

4. **Alzate-Gómez, J.-Andrea**., Roux Hélène., Cassan Ludovic., Bonometti Thomas., Escobar-Vargas, J. Alberto., Montoya-Jaramillo, L.-Javier. C.-C. (2023). Analysis of different hypotheses for modelling air-water exchange and temperature evolution in a tropical reservoir. Journal of Water and Climate Change.

In Proceedings of International Conferences

5. **Juliana A. Alzate G**., Carlos A. Rivera-Rondón, Angela Zapata, Sergio A. Castiblanco, Alejandra Neira, Lina Triana, Nathaly Triviño, Jorge Escobar-Vargas, Saul Prada-Pedreros, Nelson Obregón. A model to describe the effects of low flow on benthic algae and nutrients in the Cauca River (Colombia). Poster presentation *SIL 2021* Gwangju, Korea